VOLUME 76 JUNE 8, 1972 NUMBER 12

JPCHAx

THE JOURNAL OF PHYSICAL CHEMISTRY

PUBLISHED BIWEEKLY BY THE AMERICAN CHEMICAL SOCIETY

THE JOURNAL OF

PHYSICAL CHEMISTRY

AMERICAN CHEMICAL SOCIETY, *1155 Sixteenth St., N.W., Washington, D. C. 20036*

Books and Journals Division
JOHN K CRUM, *Director*
JOSEPH H. KUNEY, *Head, Business Operations Department*
RUTH REYNARD, *Assistant to the Director*

 Published biweekly by the American Chemical Society at 20th and Northampton Sts., Easton, Pa. 18042. Second-class postage paid at Washington, D. C., and at additional mailing offices.

All manuscripts should be sent to *The Journal of Physical Chemistry,* Department of Chemistry, University of Minnesota, Minneapolis, Minn. 55455.

Additions and Corrections are published once yearly in the final issue. See Volume 75, Number 26 for the proper form.

Extensive or unusual alterations in an article after it has been set in type are made at the author's expense, and it is understood that by requesting such alterations the author agrees to defray the cost thereof.

The American Chemical Society and the Editor of *The Journal of Physical Chemistry* assume no responsibility for the statements and opinions advanced by contributors.

Correspondence regarding accepted copy, proofs, and reprints should be directed to Editorial Production Office, American Chemical Society, 20th and Northampton Sts., Easton, Pa. 18042. Manager: CHARLES R. BERTSCH. Assistant Editor: EDWARD A. BORGER.

Advertising Office: Century Communications Corporation, 142 East Avenue, Norwalk, Conn. 06851.

Business and Subscription Information

Remittances and orders for subscriptions and for single copies, notices of changes of address and new professional connections, and claims for missing numbers should be sent to the Subscription Service Department, American Chemical Society, 1155 Sixteenth St., N.W., Washington, D. C. 20036. Allow 4 weeks for changes of address. Please include an old address label with the notification.

Claims for missing numbers will not be allowed (1) if received more than sixty days from date of issue, (2) if loss was due to failure of notice of change of address to be received before the date specified in the preceding paragraph, or (3) if the reason for the claim is "missing from files."

Subscription rates (1972): members of the American Chemical Society, $20.00 for 1 year; to nonmembers, $60.00 for 1 year. Those interested in becoming members should write to the Admissions Department, American Chemical Society, 1155 Sixteenth St., N.W., Washington, D. C. 20036. Postage to Canada and countries in the Pan-American Union, $5.00; all other countries, $6.00. Single copies for current year: $3.00. Rates for back issues from Volume 56 to date are available from the Special Issues Sales Department, 1155 Sixteenth St., N.W., Washington, D. C. 20036.

This publication and the other ACS periodical publications are now available on microfilm. For information write to: MICROFILM, Special Issues Sales Department, 1155 Sixteenth St., N.W., Washington, D. C. 20036.

Notice to Authors last printed in the issue of December 23, 1971

THE JOURNAL OF

PHYSICAL CHEMISTRY

Volume 76, Number 12 June 8, 1972

JPCHAx 76(12) 1669–1794 (1972)

COMMUNICATIONS TO THE EDITOR

AUTHOR INDEX

In papers with more than one author the name of the author to whom inquiries about the paper should be addressed is marked with an asterisk in the by-line.

THE JOURNAL OF
PHYSICAL CHEMISTRY
Registered in U. S. Patent Office

VOLUME 76, NUMBER 12 JUNE 8, 1972

Kinetic Isotope Effects in the Reaction of Methyl Radicals with Molecular Hydrogen[1]

by J. S. Shapiro and R. E. Weston, Jr.*

Chemistry Department, Brookhaven National Laboratory, Upton, New York 11973 *(Received December 22, 1971)*

Publication costs assisted by the Brookhaven National Laboratory

The photolysis of acetone and acetone-d_6 has been used as a source of CH_3 and CD_3 radicals, which subsequently abstract a hydrogen atom from acetone or from added hydrogen. Relative rate constants for abstraction from various isotopic species of hydrogen were determined over the temperature range of 398–718°K by carrying out the photolysis in the presence of H_2–D_2 mixtures or of HD. At each temperature, a series of experiments at different acetone/hydrogen ratios enables one to correct for hydrogen abstraction from the radical source. Mass spectrometric analysis of the resulting methane provides a measurement of the isotope effect. The experimental rate constant ratios are compared with those calculated on the basis of LEPS and BEBO models of the activated complex.

Introduction

The reaction between methyl radicals and molecular hydrogen has received little attention since the early quantitative studies by Steacie and coworkers[2,3] on the photolysis of acetone in the presence of hydrogen. The reactions in question are

$$CH_3COCH_3 \longrightarrow 2CH_3 + CO \quad (a)$$

$$CH_3 + CH_3COCH_3 \longrightarrow CH_4 + CH_2COCH_3 \quad (1)$$

$$CH_3 + H_2 \longrightarrow CH_4 + H \quad (2)$$

$$CH_3 + D_2 \longrightarrow CH_3D + D \quad (3)$$

$$H \text{ or } D + CH_3COCH_3 \longrightarrow H_2 \text{ or } HD + CH_2COCH_3 \quad (b)$$

The rate of reaction 2 was determined indirectly by measuring the total rate of methane production and subtracting the contribution from reaction 1. (This has been referred to by Majury and Steacie[2] as Method I.)

Since rate 1 is slightly faster than rate 2 over the temperature range generally studied (125–300°), a large fraction of the methane is produced in reaction 1, especially at the lower temperatures. Thus, a large error in the estimation of methane formed in reaction 2 results. Majury and Steacie[2] and Whittle and Steacie[3] have adopted an alternative procedure, *i.e.*, by reaction of methyl radicals with deuterium (reaction 3), or trideuteriomethyl radicals with hydrogen. Mass spectrometric analysis of the methane produced enables one to distinguish between CH_4 produced in reaction 1 and CH_3D produced in reaction 3. (This method has been referred to as Method II.) This method however excludes direct measurement of rate 2. Steacie and Whittle's measurements[3] of the activation energies E_2 (by Method I) and E_3 (by Method II) are reported with uncertainties of ±1 kcal/mol. Unfortunately, these errors are of the same magnitude as the expected differences in the activation energies for the isotopic reactions 2 and 3.

The only investigation in which the difference $E_2 - E_3$ has been determined directly is reported by Davison

(1) Research performed under the auspices of the U. S. Atomic Energy Commission.

(2) T. G. Majury and E. W. R. Steacie, *Can. J. Chem.*, **30**, 800 (1952).

(3) E. Whittle and E. W. R. Steacie, *J. Chem. Phys.*, **21**, 933 (1953).

and Burton[4] in the study of acetone photolysis in the presence of equimolar mixtures of H_2 and D_2. However, the validity of these experiments has been questioned by Steacie[5] because many runs were allowed to proceed to a stage where the decomposition of acetone was greater than 5%. Nevertheless, some of these data, when extrapolated to the early stages of the reaction, do lead to values of ~3 kcal/mol for $E_3 - E_1$ and ~1 kcal/mol for $E_3 - E_2$ which are in reasonable agreement with Steacie's results.[3]

Walker[6] has reviewed the current state of these and related investigations and has concluded that the activation energies measured by Steacie and Whittle[3] are too low by ~1 kcal/mol (where Method I is used). This conclusion is also stated in other earlier publications.[7,8]

In view of these uncertainties, and because of previous work in this laboratory on the kinetic isotope effect in related systems[9] (*e.g.*, $CF_3 + H_2$–D_2), it was considered worthwhile to reinvestigate this system with a different experimental approach.

Experimental Section

1. Materials. Acetone (Baker research grade) was purified by distillation from a trap at −88° to a trap at −196° to remove possible traces of biacetyl. Acetone-d_6 (Merck Sharp and Dohme) was purified in a similar manner with care being taken to avoid exchange of deuterium with hydrogen atoms. Both acetone and acetone-d_6 were stored in blackened reservoirs on the high-vacuum line. The purities of the acetone and acetone-d_6 were measured by mass spectrometry. Acetone-d_6 was found to contain 3.34% acetone-d_5, by direct analysis. In addition, photolysis of acetone-d_6 at 250° followed by collection of the methane fraction and its analysis by mass spectrometry led to a value of 0.037 for the ratio CHD_3/CD_4. This agrees with the direct analysis. Deuterium (Biorad Laboratories) of 99.9% D atom stated purity was used; analysis showed that it contained 1.2% HD. Both hydrogen and deuterium gases were introduced into reservoirs on the vacuum line by bubbling them slowly through a charcoal trap at −196° to remove residual traces of atmospheric O_2, N_2, and CO. Hydrogen deuteride was prepared by Dr. D. R. Christman of this laboratory. According to mass spectrometric analysis, it contained 1.2% H_2 and 1.0% D_2. Samples of deuterated methanes (CH_3D, CH_2D_2, CHD_3, CD_4), purchased from Merck Sharp and Dohme, were used in the determination of fragmentation patterns. Matheson research grade cylinders of hydrogen, methane, ethane, and carbon monoxide were used.

2. Apparatus. The basic vacuum line has already been described.[9] A few alterations allowed the apparatus to handle small quantities of products while allowing rapid pumping of hydrogen. Improved temperature measurements were made with a platinum resistance thermometer inserted in the cavity of the photolysis cell, a Müller bridge circuit, and a Leeds and Northrup null detector. Temperature regulation depended on a thermistor probe and proportional controller (Radio Frequency Laboratories). A temperature range of 398–718°K was covered.

A cylindrical quartz photolysis cell of 297 cm^3 was housed in the photolysis furnace. Between the entrance to the cell and the connection to the manifold a small tube (~2 cm^3) served to trap the acetone in solid form while hydrogen or hydrogen–deuterium mixtures were introduced. Mixtures of acetone and H_2–D_2 were well mixed by Toepler pumping prior to photolysis. Greaseless valves were used to isolate the reaction cell, the acetone condensation tube, and the acetone reservoirs from the vacuum system. A Hanovia medium-pressure lamp with a Corning 9700 filter was used as a source of 3130-Å radiation. The light beam was focussed through a quartz lens and collimated through a series of shield plates so as to fill the entire cell. Control experiments with H_2–D_2 mixtures showed no observable exchange at 200°. This proved the absence of mercury-sensitized decomposition, due to 2537-Å radiation in the presence of traces of mercury vapor, which was always present in the system.

Since no runs were allowed to proceed beyond 1–2% decomposition of acetone, careful separation of the relatively small $CH_3D + CH_4$ fraction from the reaction mixture was of utmost importance. Separation from the condensable material (acetone, ethane, and other high boiling products[10]) was readily achieved by passing the reaction mixture through two traps in series at −196°. Control experiments with mixtures of CH_3D–CH_4 of known composition have excluded the possibility of any loss of these gases in the solid matrix of condensables. Unreacted H_2–D_2 mixtures were removed by pumping these through a palladium thimble at about 350°. The thimble was sealed into a Pyrex tube which was heated externally with a heating tape, and the area of contact between the gas and the thimble was very small. Such a design is probably responsible for the absence of any observed exchange between C–H or C–D bonds in the methanes with the large excess of H_2–D_2 gas. A slight exchange has been reported in previous investigations.[2] The residual

(4) S. Davison and M. Burton, *J. Amer. Chem. Soc.*, **74**, 2307 (1952).

(5) E. W. R. Steacie, "Atomic and Free Radical Reactions," Vol. 2, Reinhold, New York, N. Y., 1954, pp 527–538.

(6) R. W. Walker, *J. Chem. Soc., A*, 2391 (1968). Kinetic data for these reactions are also reviewed by P. Gray, A. A. Herod, and A. Jones, *Chem. Rev.*, **71**, 247 (1971).

(7) J. F. Henderson and E. W. R. Steacie, *Can. J. Chem.*, **38**, 2161 (1960).

(8) H. O. Pritchard and G. O. Pritchard, *ibid.*, **41**, 3042 (1963).

(9) C. L. Kibby and R. E. Weston, Jr., *J. Chem. Phys.*, **49**, 4825 (1968).

(10) H. Shaw and S. Toby, *J. Phys. Chem.*, **72**, 2337 (1968).

noncondensable gas mixture (CH_4, CH_3D, CO, and some H_2, D_2, or HD) was finally transferred quantitatively with an automatic Toepler pump into sample tubes. Reactant pressures ranged from 30 to 120 Torr for acetone and from 35 to 130 Torr for hydrogen.

Isotopic analysis of the hydrogen isotopes and of the deuterated methanes was carried out with a modified CEC-103 mass spectrometer. All analyses were periodically checked against calibration curves of similar mixtures prepared manometrically. Occasional high-resolution analyses to check the purity of reagents or to isolate traces of isotopic methanes in a complex mixture were determined on a Hitachi–Perkin-Elmer RMU-7E instrument.

The CH_3D/CH_4 ratio was determined by comparison of *m/e* 17 (CH_3D^+) and *m/e* 15 (CH_3^+). By the use of fragmentation patterns, the peak at *m/e* 17 was corrected for the contribution of $^{13}CH_4^+$, and for $^{16}OH^+$ from small traces of water vapor. (The peak at *m/e* 18 was assumed to be the parent peak for H_2O^+.) The peak at *m/e* 15 was corrected for a contribution of CH_3^+ from CH_3D, based on the corrected height of the peak at *m/e* 17. This method was used in preference to a direct comparison of the parent CH_3D^+ and CH_4^+ peaks, which would require a large correction for O^+ from CO (3.3% of the parent CO^+ peak); also, this depends on the relative ionization sensitivities of CO and CH_4. The pressure of CO in the samples was usually equal to or greater than the CH_4 pressure. In the few cases where comparisons were made between analyses based on (*m/e* 17)/(*m/e* 15) and (*m/e* 17)/(*m/e* 16), the agreement was good. Analyses of CH_3D–CH_4 mixtures prepared by pressure measurement were found to be accurate to within 1%. The accuracy may be somewhat decreased in reaction mixtures containing carbon monoxide and hydrogen.

The CD_4/CD_3H ratio was determined by measurement of the parent peaks at *m/e* 19 (CD_3H^+) and *m/e* 20 (CD_4^+). The peak at *m/e* 20 was corrected for the small contribution from $^{13}CD_3H^+$, and the peak at *m/e* 19 was corrected for $^{13}CD_3^+$ from both CD_3H and CD_4. It is probable that the CD_4/CD_3H ratio in reaction mixtures, although less accurate than in mixtures of CD_4 and CD_3H alone, is more reliable than the CH_3D/CH_4 ratio, since it is determined directly from parent peaks.

Experimental Results

1. Photolysis of Acetone in the Presence of H_2–D_2 Mixtures. The principal reactions taking place in this system are given by reactions a, b, and 1–3. In addition, minor side reactions due to isotopic impurities are

$$CH_3 + HD \longrightarrow CH_4 + D \qquad (4)$$

and

$$CH_3 + DH \longrightarrow CH_3D + H \qquad (5)$$

Then, using the symbol R_x to designate the rate of production of product x, we have

$$\frac{R_{CH_4}}{R_{CH_3D}} = \frac{k_1(Ac) + k_2(H_2) + k_4(HD)}{k_3(D_2) + k_5(HD)} \qquad (A)$$

where (Ac) = (CH_3COCH_3). This can be put into the form

$$\frac{R_{CH_4}(D_2)(1 + C_1)}{R_{CH_3D}(Ac)(1 + C_2)} = \frac{k_1}{k_3(1 + C_2)} + \frac{k_2(H_2)}{k_3(Ac)} \qquad (B)$$

where $C_1 = k_5(HD)/k_3(D_2)$, and $C_2 = k_4(HD)/k_2(H_2)$. It then becomes possible to use a procedure similar to that described by McNesby[11] to separate the contributions of reactions 1 and 2. Experiments were carried out with various ratios of $(H_2)/(Ac)$, and a plot of corrected values of $R_{CH_4}(D_2)/R_{CH_3D}(Ac)$ against $(H_2)/(Ac)$ then yields an intercept $k_1/k_3(1 + C_2)$ and a slope k_2/k_3. The small (about 1%) corrections C_1 and C_2 were estimated from the analogous rate constants for CF_3 radicals.[9] Results at a series of temperatures are shown in Figure 1, and it is evident that eq B fits the experimental results. A linear least-squares procedure was used to obtain the slope and intercept at each temperature (Table I). From these, corrected values of the ratios k_1/k_3 and k_2/k_3 were obtained; the temperature dependence is shown in Figure 2. It was assumed that these rate constant ratios had the form

$$k_i/k_j = A \exp(B/RT) \qquad (C)$$

and values of A and B were obtained by a linear least-squares procedure. These are collected in Table II.

Table I: Rate Constant Ratios for the Acetone–(H_2–D_2) System

1000/T °K^{-1}	k_1/k_3[a]	σ[b]	k_2/k_3[c]	σ
1.392[d]	2.32	0.23	1.78	0.17
1.550	3.06	0.04	2.57	0.02
1.738	3.53	0.07	2.88	0.06
1.786	3.64	0.08	2.99	0.06
1.911	4.49	0.09	2.89	0.07
2.040	4.93	0.11	3.60	0.08
2.125	5.24	0.30	3.84	0.24
2.188	5.98	0.26	3.80	0.23
2.338	6.75	0.10	4.45	0.08
2.508	8.40	0.16	4.80	0.12

[a] From corrected intercept of eq B. [b] Standard deviation. [c] From slope of eq B. [d] Data at this temperature not used.

2. Photolysis of Acetone in the Presence of HD. The principal reactions in this system are (1), (4), and (5), with (2) and (3) as minor side reactions due to isotopic impurities in HD. The product ratio is again given by (A) which can be rearranged to

(11) J. R. McNesby, *J. Phys. Chem.*, **64**, 1671 (1960).

Table II: Temperature Dependence of Rate Constant Ratios, $k_i/k_j = A \exp(B/RT)$

Reaction	k_i/k_j	A	σ_A	A, Table VI	B, cal/mol	σ_B	B, Table VI
$CH_3 + H_2$–D_2	k_2/k_3	0.911	0.020	0.50	1327	24	2300
$CH_3 + HD$–DH	k_4/k_5	0.283	0.258	0.40	1929	690	600
$CD_3 + H_2$–D_2	k_7/k_8	1.592	0.124	4.0	588	70	−200
$CD_3 + HD$–DH	k_9/k_{10}	0.932	0.133	1.6	546	131	0
$CH_3 + Ac$–D_2	k_1/k_3	0.617	0.046	0.49	2028	75	2600
$CH_3 + Ac$–DH	k_1/k_5	2.30	0.92	1.0	821	370	1670
$CD_3 + Ac$-d_6–H_2	k_6/k_7	0.856	0.068	0.46	−1057	72	390
$CD_3 + Ac$-d_6–HD	k_6/k_9	1.47	0.13	1.8	−676	83	−790

$$\frac{R_{CH_4}(HD)(1 + C_1^{-1})}{R_{CH_3D}(Ac)(1 + C_2^{-1})} = \frac{k_1}{k_5(1 + C_2^{-1})} + \frac{k_4}{k_5}\frac{(HD)}{(Ac)} \quad (D)$$

The experimental data were analyzed in the same way as those for the $CH_3 + H_2$–D_2 reaction, and results are given in Figures 3 and 4, Table II, and Table III.

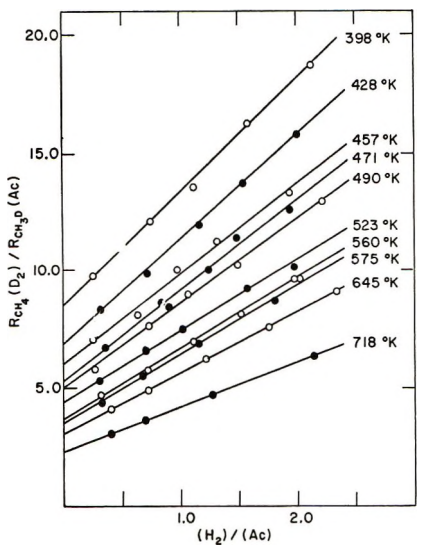

Figure 1. Basic data for the calculation of k_1/k_3 and k_2/k_3, plotted in the form of eq B.

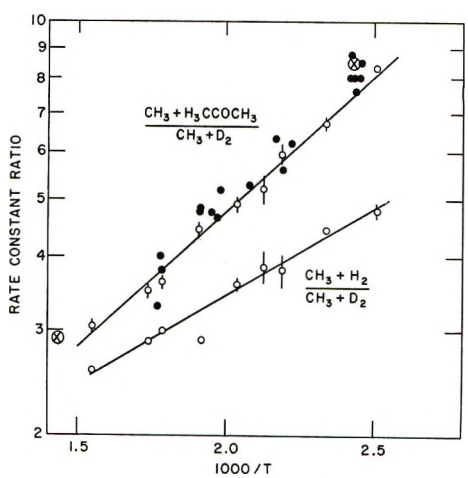

Figure 2. Temperature dependence of the rate constant ratios k_1/k_3 (upper line) and k_2/k_3. Other data for k_1/k_3: ⊗, McNesby, Gordon, and Smith;[13] ●, Whittle and Steacie.[3]

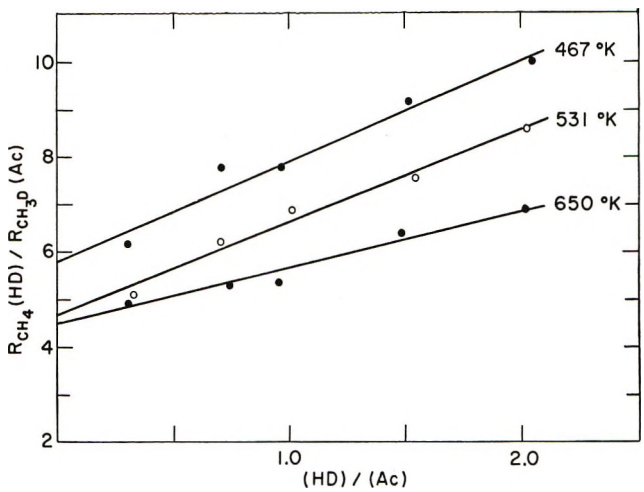

Figure 3. Basic data for the calculation of k_1/k_5 and k_4/k_5, plotted in the form of eq D.

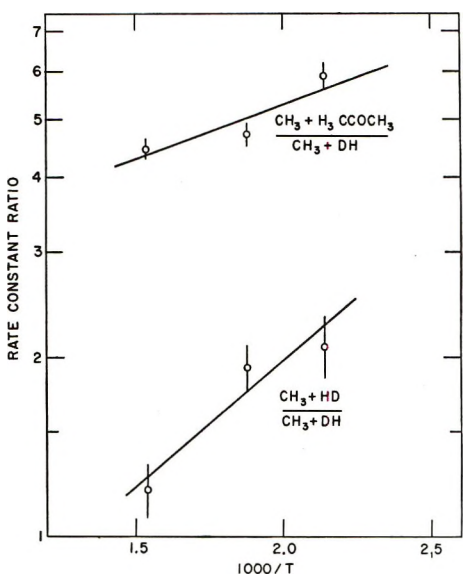

Figure 4. Temperature dependence of the rate constant ratios k_1/k_5 (upper line) and k_4/k_5.

3. Photolysis of Acetone-d_6 in the Presence of H_2–D_2 Mixtures. The principal reactions in this system are

$$CD_3COCD_3 + h\nu \longrightarrow 2CD_3 + CO \quad (c)$$

$$CD_3 + CD_3COCD_3 \longrightarrow CD_4 + CD_3COCD_2 \quad (6)$$

$$CD_3 + H_2 \longrightarrow CD_3H + H \quad (7)$$

$$CD_3 + D_2 \longrightarrow CD_4 + D \quad (8)$$

$$H \text{ or } D + CD_3COCD_3 \longrightarrow HD \text{ or } D_2 + CD_2COCD_3 \quad (d)$$

In addition, isotopic impurities in hydrogen contribute the reactions

$$CD_3 + HD \longrightarrow CD_3H + D \quad (9)$$

and

$$CD_3 + DH \longrightarrow CD_4 + H \quad (10)$$

The presence of acetone-d_5 as an impurity in the acetone used leads to reactions

$$CD_3COCD_2H + h\nu \longrightarrow CD_3 + CD_2H + CO \quad (e)$$

$$CD_3 + CD_3COCD_2H \longrightarrow CD_4 + CD_2COCD_2H \quad (11)$$

$$\longrightarrow CD_4 + CD_3COCDH \quad (12)$$

$$\longrightarrow CD_3H + CD_3COCD_2 \quad (13)$$

$$CD_2H + CD_3COCD_3 \longrightarrow CD_3H + CD_2COCD_3 \quad (14)$$

$$CD_2H + D_2 \longrightarrow CD_3H + D \quad (15)$$

Reactions involving two atoms of protium in the reactants can be disregarded. The expression for product composition is

$$\frac{R_{CD_4}}{R_{CD_3H}} = \frac{k_6(\text{Ac-}d_6) + k_8(D_2) + k_{10}(HD) + (k_{11} + k_{12})(\text{Ac-}d_5)}{k_7(H_2) + k_{13}(\text{Ac-}d_5) + k_9(HD) + \frac{(CD_2H)}{(CD_3)}[k_{14}(\text{Ac-}d_6) + k_{15}(D_2)]} \quad (E)$$

This can be rearranged into the form

$$\frac{R_{CD_4}(H_2)(1 + C_3)}{R_{CD_3H}(\text{Ac})(1 + C_4)} = \frac{k_6(1 - \rho) + (k_{11} + k_{12})\rho}{k_7(1 + C_4)} + \frac{k_8}{k_7}\frac{(D_2)}{(\text{Ac})} \quad (F)$$

where

$$(\text{Ac}) = (\text{Ac-}d_6) + (\text{Ac-}d_5)$$

$$\rho = (\text{Ac-}d_5)/(\text{Ac}) \cong (\text{Ac-}d_5)/(\text{Ac-}d_6)$$

$$C_3 = \frac{k_9(HD)}{k_7(H_2)} + \frac{k_{15}\rho(D_2)}{2k_7(H_2)} + \frac{\rho(\text{Ac})}{(H_2)}\left(\frac{k_{13}}{k_7} + \frac{k_{14}}{2k_7}\right)$$

and $C_4 = k_{10}(DH)/k_8(D_2)$.

In deriving this expression, we have assumed that $(CD_2H)/(CD_3) = \rho/2$. Values of k_9/k_7 and k_{10}/k_8 were assumed equal to the corresponding rate constant ratios for reactions of CF_3.[9] Reactions 11 and 12 involve secondary isotope effects only, and these were ignored. This leads to $k_{11}/k_6 = {}^3/_6$ and $k_{12}/k_6 = {}^2/_6$, so that the first term in (G) becomes $k_6(1 - \rho/6)/k_7(1 + C_4)$. It is also a reasonable approximation to neglect differences in rate constants for analogous reactions of CD_3 and CD_2H. With this assumption, $k_{15}/k_7 = k_8/k_7$, and an approximate value for this is obtained from the *uncorrected* data of these experiments. In the same way, k_{14}/k_7 is approximated by the uncorrected value of k_6/k_7 from these experiments.

The ratio k_{13}/k_7 is somewhat more difficult to evaluate. If we again ignore secondary effects due to isotopic substitution in both acetone and methyl radical, we can equate (k_{13}/k_7) with the previously determined (k_1/k_2) multiplied by a factor of ${}^1/_6$ to account for the single protium atom in CD_3COCD_2H. An alternative procedure, which still ignores secondary isotope effects, uses the ratio $k_1/6k_7$ from the work of Whittle and Steacie.[3] Since these corrections are small, the two alternatives lead to results that are identical, within experimental error. Values for k_6 and $(k_{13} + k_{14})$ have also been reported,[12] from which it would be possible to derive a correction. However, since these results (and those of Whittle and Steacie) do not come from experiments in which substrates compete for methyl radicals, we believe the best correction uses our values of (k_1/k_2).

The experimental results for this reaction system are shown in Figures 5 and 6, Table II, and Table IV.

Table III: Rate Constant Ratios for the Acetone–HD System

1000/T, °K^{-1}	k_1/k_6[a]	σ	k_4/k_6[b]	σ
1.537	4.43	0.17	1.19	0.13
1.881	4.67	0.22	1.92	0.17
2.140	5.84	0.30	2.08	0.24

[a] From corrected intercept of eq D. [b] From slope of eq D.

Table IV: Rate Constant Ratios for the Acetone-d_6–(H_2–D_2) System

1000/T, °K^{-1}	k_6/k_7[a]	σ	k_8/k_7[b]	σ
1.637	0.372	0.010	0.397	0.007
1.792	0.327	0.006	0.368	0.005
1.910	0.308	0.031	0.337	0.025
2.039	0.280	0.006	0.344	0.005
2.137	0.273	0.005	0.326	0.004
2.336	0.250	0.004	0.318	0.003
2.490	0.233	0.022	0.300	0.018

[a] From corrected intercept of eq F. [b] From slope of eq F.

4. Photolysis of Acetone-d_6 in the Presence of HD. The principal reactions in this system are (c), (d), (6),

(12) P. Gray and A. A. Herod, *Trans. Faraday Soc.*, **64**, 1568, 2723 (1968).

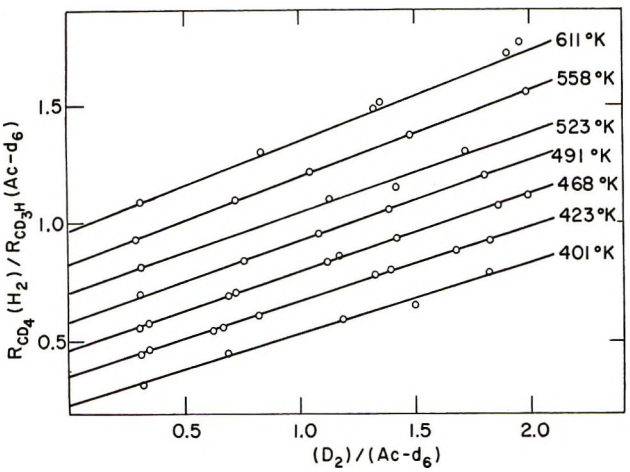

Figure 5. Basic data for the calculation of k_6/k_7 and k_8/k_7, plotted in the form of eq F.

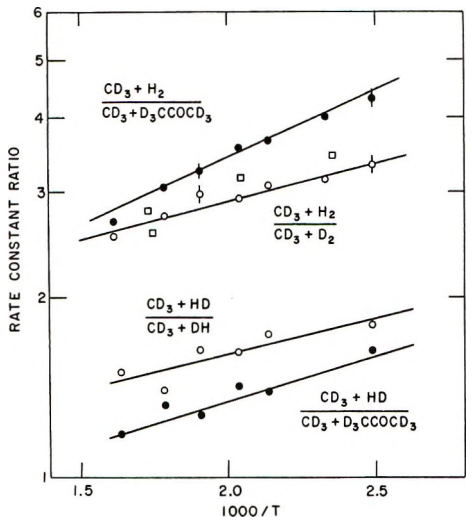

Figure 6. Temperature dependence of the rate constant ratios k_7/k_6 (upper filled circles), k_7/k_8 (upper open circles), k_9/k_{10} (lower open circles), and k_9/k_6. Other data for k_7/k_6: □, Whittle and Steacie.[3]

(9), and (10). Isotopic impurities lead to small contributions from (7), (8), (11), (12), (13), (14), and

$$CD_2H + DH \longrightarrow CD_3H + H \qquad (16)$$

The product ratio is given by eq E with the term $k_{15}(D_2)$ replaced by $k_{16}(HD)$. This expression can be rearranged to give

$$\frac{R_{CD_4}(HD)(1 + C_5)}{R_{CD_3H}(Ac)(1 + C_4^{-1})} = \frac{k_6(1 - \rho) + (k_{11} + k_{12})\rho}{k_9(1 + C_4^{-1})} + \frac{k_{10}(HD)}{k_9(Ac)} \qquad (G)$$

where

$$C_5 = \frac{k_7(H_2)}{k_9(HD)} + \frac{\rho k_{16}}{2k_9} + \frac{\rho(Ac)}{(HD)}\left(\frac{k_{13}}{k_9} + \frac{k_{14}}{2k_9}\right)$$

We have already discussed relative values of k_6, k_{11}, and k_{12}. For the ratio k_7/k_9, the corresponding ratio for CF_3 rate constants has again been used. Again with the neglect of secondary isotope effects, we approximate k_{16}/k_9 by k_{10}/k_9 obtained from the uncorrected data of this experiment. Similarly, the ratio k_{14}/k_9 is approximated by k_6/k_9. The ratio k_{13}/k_9 was estimated in two ways. The first method uses our values of k_1/k_5 and k_5/k_4 to obtain $k_1/6k_4$; again, this neglects secondary isotope effects between CD_3 and CH_3 and between acetone and acetone-d_6. A second approach uses the rate constants k_1 and k_4 determined by Whittle and Steacie.[3] Because the corrections derived by these two methods differ by as much as several per cent (when (Ac)/(HD) is large), a mean value was used in the final correction factor. Furthermore, because the correction factors $(1 + C_5)/(1 + C_4^{-1})$ are as large as 20%, in obtaining the least-squares fit to eq G we weighted points by the inverse of the correction term C_5. This led to slightly different values of the slope and intercept of the least-squares straight line than did the use of unweighted values. The experimental results for this system are contained in Figure 6 and 7, Table II, and Table V.

Table V: Rate Constants Ratios for the Acetone-d_6–HD System

$1000/T$, °K^{-1}	k_6/k_9[a]	σ	k_{10}/k_9[b]	σ
1.636	0.857	0.016	0.681	0.013
1.793	0.797	0.008	0.702	0.006
1.910	0.797	0.008	0.624	0.006
2.039	0.709	0.028	0.624	0.026
2.137	0.737	0.007	0.586	0.006
2.490	0.615	0.006	0.552	0.005

[a] From corrected intercept of eq G. [b] From slope of eq G.

Discussion

1. Comparison with Other Work. Because the errors in earlier work were of the same magnitude as the differences due to isotopic substitution, it is difficult to make meaningful comparisons. Some of the better data are collected in Table VI, and this table has been used to calculate A and B values given in Table II. The A values are probably not significant, but the B values agree with ours within 0.5 to 1.5 kcal/mol, which is about what one would expect. Our values for $CH_3 + HD/DH$ and $CH_3 + Ac/DH$ look unreasonable by comparison with the other data; this may result from the small number of experimental points we have for this particular system.

A direct comparison can be made with the value of 2300 cal/mole obtained by McNesby, Gordon, and Smith[13] for $E_{a3} - E_{a1}$; our value of 2030 is in good

(13) J. R. McNesby, A. S. Gordon, and S. R. Smith, *J. Amer. Chem. Soc.*, 78, 1287 (1956).

Table VI: Experimental Values of Rate Constant Parameters

Reaction	Reactants	Log A^a	E_a, kcal/mol	Ref
1	$CH_3 + CH_3COCH_3$	8.52	9.44	10
		8.35	9.53	*b*
		...	9.6	*c*
		8.53	9.63	*d*
		8.46	9.64	12
		8.6	9.7	*e*
		...	9.7	3
		8.62	9.82	*f*
		8.51	9.63	Mean
2	$CH_3 + H_2$	8.5	9.9	8
3	$CH_3 + D_2$	8.8	11.8	3
		8.4	11.9	13
		8.79	12.1	*g*
		...	12.6	4
		9.3	12.7	*h*
		8.8	12.2	Mean
4	$CH_3 + \mathbf{HD}^i$	8.1	10.0	3
			10.7	8
5	$CH_3 + \mathbf{DH}^i$	8.5	11.3	3
6	$CD_3 + CD_3COCD_3$	8.57	11.29	*b*
		8.66	11.44	*i*
		8.62	11.54	12
		8.77	11.56	*f*
		...	11.6	3
		8.66	11.49	Mean
7	$CD_3 + H_2$	9.0	11.1	3
8	$CD_3 + D_2$	8.4	10.9	3
9	$CD_3 + HD$	8.4	10.7	3
10	$CD_3 + DH$	8.2	10.7	3

[a] In units of M^{-1} sec^{-1}. [b] G. Greig and J. C. J. Thynne, *Trans. Faraday Soc.*, **62**, 379 (1966). [c] A. J. C. Nicholson, *J. Amer. Chem. Soc.*, **73**, 3981 (1951). [d] N. L. Arthur and P. Gray, *Trans. Faraday Soc.*, **65**, 424 (1969). [e] A. F. Trotman-Dickenson and E. W. R. Steacie, *J. Chem. Phys.*, **18**, 1097 (1950). [f] P. Gray and L. J. Leyshon, *Trans. Faraday Soc.*, **65**, 780 (1969). [g] J. Chanmugam and M. Burton, *J. Amer. Chem. Soc.*, **78**, 509 (1956). [h] R. E. Rebbert and E. W. R. Steacie, *Can. J. Chem.*, **32**, 113 (1954). [i] R. Shaw and J. C. J. Thynne, *Trans. Faraday Soc.*, **62**, 104 (1966). [j] The atom being abstracted is in bold-face type.

agreement. Their results for k_1/k_3 are also indicated in Figure 2. In addition, the data of Whittle and Steacie[3] can be used to obtain this rate constant ratio directly, although they did not do so. The results are shown in Figure 2, and the agreement with our data is good. A least-squares analysis of their data gives $k_1/k_3 = 0.505 \exp(2270/RT)$. Similarly, they present data which can be used to obtain a ratio $k_6/k_7 = 0.765 \exp(-820/RT)$, which again is in substantial agreement with our work. The individual points are shown in Figure 6. The data of Davison and Burton[4] obtained at low extents of reaction have been used by Steacie[5] to calculate a value of 2500 cal/mol for $E_{a3} - E_{a1}$. Davison and Burton also did experiments with mixtures of H_2 and D_2 from which they derived a value of 1100 cal/mol for $E_{a3} - E_{a2}$. Since this involved a

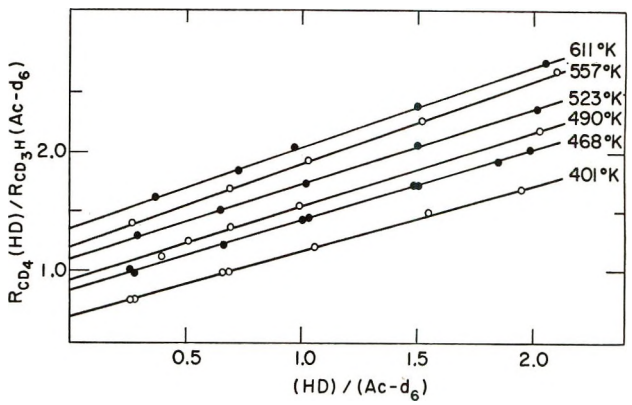

Figure 7. Basic data for the calculation of k_6/k_9 and k_{10}/k_9 plotted in the form of eq G.

correction for the contribution from reaction 1, it may be considered to be in good agreement with our result.

The mean value of 12.2 kcal/mol for E_{a3} can be combined with our value of 1.3 for $E_{a3} - E_{a2}$, giving a value of 10.9 kcal/mol for the activation energy of the $CH_3 + H_2$ reaction. This is slightly lower than the value suggested by Walker.[6] Taken together with the enthalpy of reaction 2 ($\Delta H = 1.0 \pm 1.5$ kcal/mol), this leads to a predicted activation energy for the reverse reaction of 9.9 ± 1.5 kcal mol. A direct measurement of this energy has been made by Kurylo and Timmons,[14] who found 11.8 ± 0.2. Thus, there is a discrepancy of almost 2 kcal/mol, which is probably not outside the combined errors in the energies used to predict this quantity.

2. Possible Sources of Error in Rate Constant Determination. Particularly because of the difference in isotope effects for reactions of CH_3 and CD_3, we were led to consider the possibility that methane was produced by reactions other than hydrogen atom abstraction, thus leading to errors in our reported rate constant ratios. The following mechanisms were considered.

(1) Radical–Atom Recombination Followed by Collisional Stabilization[4,8] of the Methane Formed; e.g.

$$CH_3 + H \rightleftharpoons CH_4^* \xrightarrow{M} CH_4 + M$$

Calculations of Rabinovitch and Setser[15] indicate that a substantial fraction of the methane thus formed would decompose at the temperatures and pressures used in our work. Then during acetone photolysis in the presence of D_2, the following reactions would occur

$$CH_3 + D_2 \longrightarrow CH_3D + D$$

$$CH_3 + D \longrightarrow CH_3D^* \longrightarrow CH_2D + H$$

$$CH_2D + D \longrightarrow CH_2D_2$$

(14) M. J. Kurylo and R. B. Timmons, *J. Chem. Phys.*, **50**, 5076 (1969).

(15) B. S. Rabinovitch and D. W. Setser, *Advan. Photochem.*, **3**, 1 (1964).

Analysis of the methane produced in such a photolysis at 250° (using high-resolution mass spectrometry to separate the m/e 18 peak due to CH_2D_2 from that of H_2O) gave a value of 0.06 for the ratio CH_2D_2/CH_3D.

Furthermore, Davison and Burton[4] found in this same system that equal amounts of HD and CH_3D were formed. This implies that reaction b is the most important path for the consumption of hydrogen atoms. We have confirmed these results by mass spectrometer analysis of the entire noncondensable fraction of a reaction mixture. The results of Whittle and Steacie[3] are also in agreement with this observation.

(2) *Direct Decomposition of Electronically Excited Acetone.*[10] If this were important in our reactions, the rate constant ratios should be sensitive to total pressure in the reaction cell, but this was not found. Runs carried out with a high pressure of added C_2F_6 did not give results different from normal runs. This is also evidence against the proposal of Henderson and Steacie[7] that methyl radicals abstract hydrogen from a vibrationally excited acetone molecule.

(3) *The Radical-Radical Disproportionation Reactions.*[16,17]

$$CH_3 + CH_3COCH_2 \longrightarrow CH_4 + CH_2COCH_2$$

or

$$CH_3 + CH_3CO \longrightarrow CH_4 + CH_2CO$$

It seems very unlikely that these reactions can be important at the high temperatures and low light intensities used in our work.

(4) *Reaction of Methyl Radicals with Acetone Adsorbed in the Walls of the Reaction Vessel.*[17,18] Again, the experiment with added C_2F_6 indicates that this is not important. Konstantatos and Quinn found wall reactions to be an important source of additional methane at acetone pressures of less than 8 Torr. This is about one-fourth of the lowest acetone pressure in the present work (see Experimental Section), so it seems unlikely that wall reactions are important in our work. We conclude that none of the above processes has a significant effect on our measurements of rate constant ratios.

3. *Calculation of Isotope Effects.* Ratios of rate constants k_{H_2}/k_{D_2} ($= k_2/k_3$ or k_7/k_8) and k_{HD}/k_{DH} ($= k_4/k_5$ or k_9/k_{10}) were calculated in the conventional way[19] from the expression

$$k_1/k_2 = (\nu_1^*/\nu_2^*)(f_m/f^{\pm})(\tau_1/\tau_2)$$

where ν^* is the imaginary frequency of the activated complex, and τ is a tunneling correction described below. The quantity f_m is the reduced partition function ratio of the hydrogen molecule; it is unity for the DH/HD ratio, whereas for H_2/D_2 it is given by

$$f_{D_2} = (m_D/m_H)^{1/2} \exp[(Z_{H_2} - Z_{D_2})/T]$$

In this expression, m is the atomic mass and Z is the sum of vibrational zero-point energy and a rotational correction. The data collected by Persky and Klein[20] were used for the calculation of f_{D_2}. A small correction (+2% at 333°K) would result from the additional zero-point energy term discussed by Wolfsberg;[21] however, in order to keep the present calculations comparable to those for the analogous CF_3 reactions, this correction was neglected.

The quantity $f^{\pm}$ is the reduced partition function ratio for the activated complex

$$f^{\pm} = \prod_{i=1}^{11} \frac{u_{2i}^{\pm} \sinh (u_{1i}^{\pm}/2)}{u_{1i}^{\pm} \sinh (u_{2i}^{\pm}/2)}$$

where $u_i = h\nu_i/kT$.

Vibrational frequencies of the activated complex were calculated with modifications of the Schachtschneider programs.[22] The geometry, internal coordinates, and vibrational potential energy function of the activated complex model are described in our earlier paper[9] on the $CF_3 + H_2$ system. Vibrational force constants for the methyl group in the free radical and in the activated complex were assumed to be the same as those in CH_4 (Table VII). These force constants have virtually no influence on the isotope effects, but they do have some effect on the calculated activation energy.

Table VII: Force Constants for the Methyl Group in CH_3 and H–H–CH_3

Force constant	Value[a]
F_d	5.50 mdyn/Å
F_{dd}	0.124 mdyn/Å
F_α	0.568 mdyn-Å
$F_{d\alpha}$	0.165 mdyn
All other interaction force constants are assumed to be zero	

[a] L. H. Jones and R. S. McDowell, *J. Mol. Spectrosc.*, **3**, 632 (1959).

Force constants for the H–H–C– part of the activated complex were determined from potential energies of the linear three-atom system, using either the BEBO or LEPS method as described below.

(16) B. de B. Darwent, M. J. Allard, M. F. Hartmann, and L. J. Lange, *J. Phys. Chem.*, **64**, 1847 (1960).

(17) P. Ausloos and E. W. R. Steacie, *Can. J. Chem.*, **33**, 47 (1955).

(18) J. Konstantatos and C. P. Quinn, *Trans. Faraday Soc.*, **65**, 2693 (1969).

(19) J. Bigeleisen and M. Wolfsberg, *Advan. Chem. Phys.*, **1**, 15 (1958).

(20) A. Persky and F. S. Klein, *J. Chem. Phys.*, **44**, 3617 (1966).

(21) M. Wolfsberg, *Advan. Chem. Ser.*, **No. 189**, 185 (1969).

(22) J. H. Schachtschneider and R. G. Snyder, *Spectrochim. Acta*, **19**, 117 (1963). We are indebted to Professor M. Wolfsberg for making available to us his modifications of these programs.

The force constant for the H(methyl)–C–H– bond (F_β) does not fit into either of the preceding categories, and therefore different values were tried, as discussed below.

All tunneling corrections were calculated for unsymmetrical Eckart barriers, with curvatures corresponding to the imaginary frequency of the 6-atom activated complex model. The barrier height in the forward direction is taken to be the calculated difference in potential energy between H_2 and the activated complex (V_a), less the zero-point energy of the appropriate isotopic modification of H_2. The barrier height in the reverse direction is the potential energy difference less the zero-point energy of C–H (or C–D).

4. Discussion of the BEBO Model. We first used the bond energy-bond order (BEBO) method of Johnston and Parr[23] to derive force constants for the –C–H–H part of the activated complex. The properties required for its use are given in Table VIII. A slightly lower value of $D_e(H_3C–H)$ has been used in other BEBO calculations.[24] To test the sensitivity of predicted isotope effects to this parameter, we made another set of calculations using 105.5 kcal/mol for D_e. This changes properties of the activated complex as shown in Table IX. The calculated rate constant ratios k_2/k_3 are quite insensitive to this change, whereas the k_4/k_5 ratios are decreased slightly by the force constants corresponding to a D_e value of 105.5. This effect becomes significant only at the lower end of the temperature range, when tunneling corrections are included.

Table VIII: Properties of Reactant and Product Bonds

	H–H	C–H
R_e, Å	0.742	1.09
D_0^0, kcal/mol	103.2	104.0[a]
ω, cm^{-1}	4395	2917[b]
D_e, kcal/mol	109.44	108.16
β, Å^{-1}	1.94	1.78
F, mdyn/Å	5.74	4.65
p	1.041	1.087

[a] J. A. Kerr, *Chem. Rev.*, **66**, 465 (1966); bond dissociation energy of $H_3C–H$. [b] $\nu_1(a_1)$ of $H_3C–H$.

Another parameter which influences the force constants of the activated complex is the stretching force constant of the C–H bond of the reactant. The value we used (4.65) is that of a hypothetical C–H diatomic molecule with a frequency of 2917 cm^{-1}, corresponding to $\nu_1(a_1)$ of CH_4. However, more elaborate force-field calculations for CH_4 indicate that this parameter could be as large as 5.0, the value used previously by Johnston[24] and by Kurylo and Timmons.[14] The force constants for the activated complex are changed slightly by this higher value of F(C–H), but the ratios k_2/k_3 and k_4/k_5 are virtually unaffected over the entire temperature range, with or without a tunneling correction.

Table IX: Results of BEBO and LEPS Calculations for H–H–C (Energies in kcal/mol, Force Constants in mdyn/Å)

	BEBO1[a]	BEBO2[b]	BEBO3[c]	LEPS1[d]	LEPS2[e]
V_a	14.59	13.46	13.46	13.24	10.63
n_{HH}	0.45	0.50	0.50	...	...
n_{CH}	0.55	0.50	0.50	...	...
R_{HH}, Å	0.95	0.92	0.92	0.96	0.95
R_{CH}, Å	1.25	1.27	1.27	1.29	1.28
F_{HH}	0.747	1.157	1.096	0.569	0.653
F_{CH}	1.451	1.157	1.096	0.789	0.930
F_{int}	1.744	1.879	1.818	1.649	1.597
$F_\phi/R_{HH}R_{CH}$	0.0413	0.0450	0.0416	0.0660	0.0657
E_a (500°K)	...	...	13.1[f]	10.8[f]	10.9[g]

[a] With input parameters F(C–H) = 4.65, D_e = 105.5. [b] F(C–H) = 5.00, D_e = 108.2. [c] F(C–H) = 4.65, D_e = 108.2. [d] With κ = 0.122. These values agree with those used in ref 14. [e] With κ = 0.148. [f] With F_β = 0.26 and correction for tunneling. [g] With F_β = 0.26, and no tunneling correction.

Another variable tested in the BEBO calculations was the geometry of the CH_3 part of the activated complex. Since the methyl radical is planar, one might expect the methyl group geometry in the activated complex to be intermediate between a planar and a tetrahedral configuration. The assumption of a planar geometry, with force constants unchanged, did lead to significant changes in vibrational frequencies, but the calculated isotope effects were changed by less than 1%.

In view of the above results, all further calculations with the BEBO model were carried out with the assumption of a tetrahedral configuration for the methyl group, and the parameters designated BEBO3 in Table IX.

As in the case of the $CF_3 + H_2$ system, we found that calculated isotope effects were sensitive to the choice of F_β, as shown in Figures 8 and 9. The lowest value of F_β (0.0001) is used for computational reasons as an approximation to zero; isotope effects calculated with this choice will be essentially those of a three-atom model with the same values of F_{CH},F_{HH},F_{int}, and F_ϕ. The value of 0.26 has been used by Sharp and Johnston[24] for the CF_3–H–CH_3 activated complex, and the value 0.568 is that of the corresponding force constant in methane.

When no correction is made for tunneling, the best fit to both k_2/k_3 and k_4/k_5 is provided by the calculations with F_β approximately zero, *i.e.*, the three-atom model. When tunneling corrections are included, all the above choices of F_β lead to values of k_{H_2}/k_{D_2} and k_{HD}/k_{DH} that are too high, except for the value F_β = 0.568, which

(23) H. S. Johnston and C. Parr, *J. Amer. Chem. Soc.*, **85**, 2544 (1963).

(24) H. S. Johnston, "Gas Phase Reaction Rate Theory," Ronald Press, New York, N. Y., 1966, Chapter 13 and Appendix.

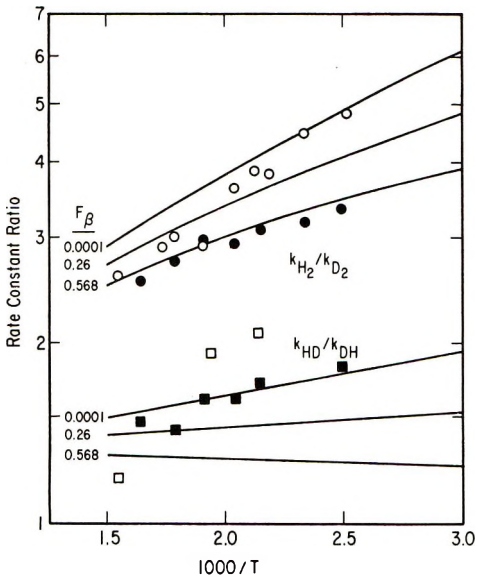

Figure 8. Solid lines, rate constant ratios calculated with BEBO3 parameters of Table IX, with no tunneling correction, and with various values of F_β. Experimental points: ○, k_2/k_3; □, k_4/k_5; ●, k_7/k_8; ■, k_9/k_{10}.

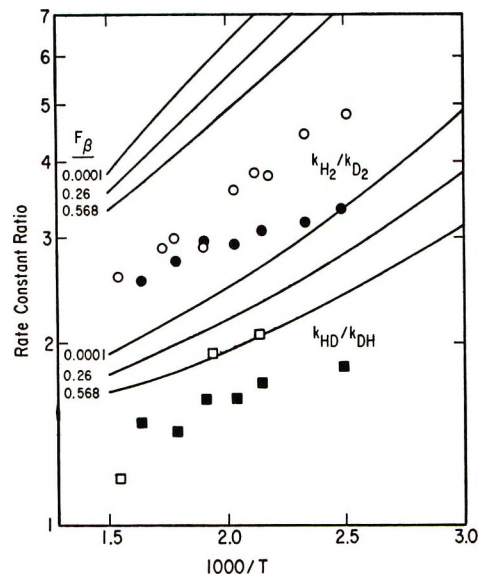

Figure 9. The same as Figure 8, except that the calculated rate constant ratios include a tunneling correction.

gives good agreement with the two best points for k_4/k_5. The situation here seems to be somewhat less satisfactory than it was for the analogous CF_3 isotope effects. All of the above choices of F_β lead to predicted isotope effects that are virtually identical for CH_3 and CD_3, contrary to the experimental results. This is discussed in greater detail below.

5. Discussion of the LEPS Model. In using the LEPS method,[24] it is necessary to fix the value of a parameter, κ, which appears in the potential energy expression. We followed the usual procedure of searching for a value of κ that gives agreement between

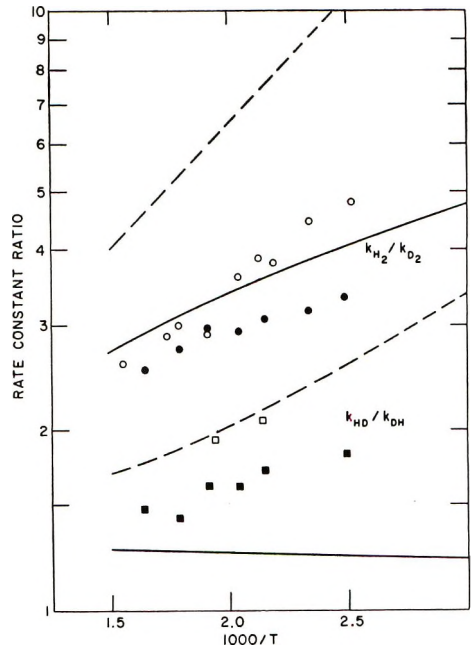

Figure 10. Solid lines, rate constant ratios calculated with LEPS2 parameters of Table IX, with no tunneling correction, and with F_β = 0.26 mdyn/Å. Dashed lines, similar calculations with LEPS1 parameters and tunneling corrections included. Experimental points as in Figure 9.

the calculated and observed activation energies. The appropriate values of κ and the resulting activated complex properties are given in Table IX. Since the force constants are much less sensitive to κ than is the potential energy of activation, V_a, both of the tabulated values of κ lead to identical isotope effects in the absence of tunneling (Figure 10). The sensitivity of k_{H_2}/k_{D_2} and k_{HD}/k_{DH} to the choice of the force constant F_β parallels that found in the BEBO case. With a value of 0.26 for F_β, the ratio k_{H_2}/k_{D_2} is virtually identical with that found in the analogous BEBO case, whereas the k_{HD}/k_{DH} ratio is considerably lower. This is true both with and without a tunneling correction. Again we found no significant differences in the calculated rate constant ratios for CD_3 compared with those for CH_3.

6. Comparison of Isotope Effects for CH_3, CD_3, and CF_3 Reactants. It is surprising that a significant difference is found between the rate constant ratios k_2/k_3 and k_7/k_8 and between k_4/k_5 and k_9/k_{10}. As we mentioned above, this is not predicted by either the BEBO or LEPS model when F_β is between zero and 0.568 mdyn/Å. A few sets of *ad hoc* force constants were tried, in an attempt to predict the observed difference. The calculated ratio $(k_2/k_3)/(k_7/k_8)$ will differ from unity only if *changes* in vibrational frequencies of the activated complex caused by substitution of -D-D for -H-H are influenced by the substitution of $-CD_3$ for $-CH_3$. This requires a coupling of vibrations in the two parts of the activated complex. Indeed, an in-

crease in F_β (which affects both the methyl bending frequency and the frequency of the linear C–H–H bend) does lead to differences in the rate constant ratios which are in the right direction. Tunneling corrections are very insensitive to the choice of F_β. However, since increasing this force constant also has the effect of increasing the value of $f^{\ddagger}$ (by raising vibrational frequencies), the ratios k_2/k_3 and k_4/k_5 are decreased below the observed values, even when tunneling corrections are included. It is not possible to find a value of F_β that meets these conflicting requirements simultaneously.

Another means of introducing a vibrational interaction between the methyl group and the rest of the activated complex is to add to the potential energy function a term $F_{dD}(\Delta d)(\Delta D)$. Here, F_{dD} is a force constant, ΔD is the displacement of the H atom being transferred, and Δd is the displacement of a methyl hydrogen. We find that an increase in F_{dD} has an effect which is similar to that of increasing F_β, and again there are conflicting requirements on the rate constant ratios which cannot be met.

The difference between isotope effects in the CD_3 and CH_3 reactions is even more surprising when it is noted that CF_3 and CH_3 give very similar values for k_{H_2}/k_{D_2} and k_{HD}/k_{DH} (Figure 11). This is in agreement with predictions of the BEBO calculations, from which it is found that $k_{H_2}/k_{D_2}(CH_3)$ is slightly higher than $k_{H_2}/k_{D_2}(CF_3)$, whereas $k_{HD}/k_{DH}(CH_3)$ is slightly lower than the corresponding ratio for CF_3. The LEPS results coincide even more closely, which is expected from the nearly equal values of F_{HH}, F_{CH}, and F_{int} for H–H–CF_3 and H–H–CH_3.

It is also interesting to consider the rate constant ratio $k(H + CH_4)/k(D + CH_4)$ determined by Kurylo and Timmons.[14] This is an intramolecular isotope effect resulting from differences in vibrational properties of the two activated complexes H–H–CH_3 and D–H–CH_3, which are the same as those for $CH_3 + H_2$ and $CH_3 + HD$. The relation between rate constants for these reactions is

$$\frac{k(H + CH_4)}{k(D + CH_4)} = \frac{k_2 f(HD/H_2)}{k_4}$$

Unfortunately, we do not have direct experimental data for the ratio k_2/k_4. However, Kurylo and Timmons have shown that both the LEPS and BEBO methods give calculated ratios of $k(H + CH_4)/k(D + CH_4)$ that are in good agreement with their experimental ratios.

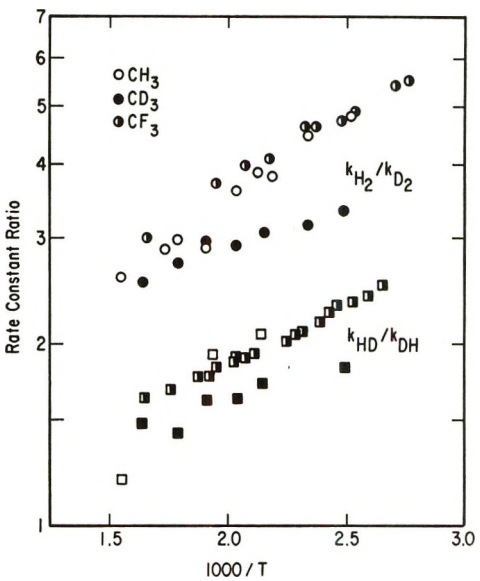

Figure 11. Comparison of experimental rate constant ratios in hydrogen abstraction reactions: ◑, $CF_3 + H_2$–$CF_3 + D_2$ (ref 9); ◨, CF_3 + HD–CF_3 + DH (ref 9); ○, $CH_3 + H_2$–$CH_3 + D_2$; □, CH_3 + HD–CH_3 + DH; ●, $CD_3 + H_2$–$CD_3 + D_2$; ■, CD_3 + HD–CD_3 + DH.

Our final conclusions are similar to these stated in an earlier paper.[9]

(1) Reasonably good predictions of kinetic isotope effects can be based on activated complex models which combine force constants for stable molecules with those obtained from the LEPS or BEBO three-atom method.

(2) The LEPS and BEBO methods lead to similar predictions. Neither method adequately accounts for the observed difference between isotope effects for CH_3 and CD_3 as reactants.

(3) It is not possible, on the basis of the observed effects and the model used, to decide if tunneling through the potential energy barrier is important.

Pyrolysis of 1,1-Difluoroethane[1]

by Barbara Noble, Halbert Carmichael,* and Carl L. Bumgardner

Department of Chemistry, North Carolina State University, Raleigh, North Carolina 27607 *(Received April 29, 1971)*

Publication costs borne completely by The Journal of Physical Chemistry

The static pyrolysis of 1,1-difluoroethane was studied between 430 and 530° and at pressures from 0.165 to 320 Torr in Pyrex vessels. The formation of HF and CH_2CHF was shown to be homogeneous and unimolecular with an activation energy of 63.4 ± 1.1 kcal/mol and a frequency factor of $10^{13.6\pm0.3}$ sec^{-1}. Minor side reactions producing methane, ethane, ethylene, CH_2CF_2, and hydrogen were observed. All the side products except ethylene were shown to arise from radical processes. The low-pressure rate constants are fitted by the RRK theory with 11 effective oscillators. Application of the RRKM theory to heterolytic and homolytic models of the activated complex resulted in calculated rate constants that are experimentally indistinguishable within the uncertainty of necessary assumptions.

Introduction

The pyrolytic dehydrochlorination of some chloroethanes was shown to be homogeneous and unimolecular 20 years ago.[2] Since that time a large body of experimental data had been built up on the unimolecular dehydrohalogenation of chlorine and bromine compounds.[3] Dehydrofluorination of fluorinated ethanes has been observed in several cases of chemical activation,[4,5] and an extensive series of studies of the dehydrofluorination of chemically activated fluorinated ethanes has shown a distinct trend toward less reaction for more highly fluorinated ethanes.[6-8]

This effect could be caused by either higher critical energies for the more highly fluorinated compounds or larger numbers of effective oscillators. Chemically activated 1,1-difluoroethane was formed and the amount of dehydrofluorination was measured over a range of temperature.[9] In another study 1,1-difluoroethane was formed with different energy content by two different chemical activation paths.[10] Both these studies compared their observations with the predictions of the RRK theory for different values E^* and s assuming values of E, the energy of the chemically activated molecules. The first successful study of direct pyrolytic dehydrofluorination was reported for a flow system.[11] Two studies of the dehydrofluorination of 1,1-difluoroethane have been carried out in shock tubes,[12,13] and the results are consistent with the flow system studies.

This work extends the pyrolysis of 1,1-difluoroethane to lower temperatures and pressures using the static pyrolysis technique that has been shown to be satisfactory for studying the homogeneous unimolecular dehydrofluorination of ethyl fluoride.[14] Pyrolysis allows a direct measure of E^*, and low-pressure studies allow direct determination of the RRK s parameter for reaction 1. A study of the predictions of the RRKM theory as applied to different models of the activated complex allows one to test the sensitivity of the calculations to details of structure.

$$CH_3CHF_2 \longrightarrow CH_2CHF + HF \qquad (1)$$

Experimental Section

All gases were obtained from the Matheson Co. The 1,1-difluoroethane contained no vinyl fluoride or other impurity detectable by gas chromatography and was used after degassing at −196°.

The pyrolysis cells were constructed of heavy-wall Pyrex and were closed with Teflon needle valves which were kept near room temperature. Two different cells were used. One with a volume of 55.9 cm^3 and a surface area of 157 cm^2 is referred to as the small cell. Most of the reported data were obtained in the large cell, which had a volume of 1956 cm^3 and a surface area of 1033 cm^2. The small cell was heated in a

(1) Abstracted in part from the thesis submitted by Barbara Noble Padnos in partial fulfillment of the requirements for the Ph.D. degree.

(2) D. H. R. Barton and K. E. Howlett, *J. Chem. Soc.*, 165 (1949).

(3) A. Maccoll, *Chem. Rev.*, **69**, 33 (1969).

(4) (a) G. O. Pritchard, M. Venugopalan, and T. F. Graham, *J. Phys. Chem.*, **68**, 1786 (1964); (b) R. D. Giles and E. Whittle, *Trans. Faraday Soc.*, **61**, 1425 (1965).

(5) J. A. Kerr, A. W. Kirk, B. V. O'Grady, and A. F. Trotman-Dickenson, *Chem. Commun.*, 365 (1967).

(6) G. O. Pritchard and R. L. Thommarson, *J. Phys. Chem.*, **71**, 1674 (1967).

(7) G. O. Pritchard and J. T. Bryant, *ibid.*, **72**, 1603 (1968).

(8) G. O. Pritchard and M. J. Perona, *Int. J. Chem. Kinet.*, **1**, 413 (1969).

(9) J. T. Bryant and G. O. Pritchard, *J. Phys. Chem.*, **71**, 3439 (1967).

(10) J. A. Kerr, D. C. Phillips, and A. F. Trotman-Dickenson, *J. Chem. Soc. A*, 1806 (1968).

(11) D. Sianesi, G. Nelli, and R. Fontanelli, *Chim. Ind. (Milan)*, 40 (1968).

(12) E. Tschuikov-Roux, W. J. Quiring, and J. M. Simmie, *J. Phys. Chem.*, **74**, 2449 (1970).

(13) P. Cadman, M. Day, A. W. Kirk, and A. F. Trotman-Dickenson, *J. Chem. Soc. D*, 203 (1970).

(14) M. Day and A. F. Trotman-Dickenson, *J. Chem. Soc. A*, 233 (1969).

tube furnace. The temperature varied by 3° within the cell and drifted by a similar amount during some pyrolyses. The large cell was mounted in a stainless-steel block furnace. Except for the external lead, the temperature throughout the cell varied by less than 1°. The observed temperature varied by less than 0.2° during any one pyrolysis. The temperature did vary from run to run and some data were corrected to constant temperatures using the Arrhenius parameters reported in this paper.

After pyrolyzing for a measured time, mixtures were analyzed by gas chromatography using a thermal conductivity detector. All quantitative work was done on a 6-ft silica gel column at 70°. Some samples were separated by low-temperature distillation and analyzed on a molecular sieve column for qualitative studies. All runs in the small cell involved a single aliquot taken by gas expansion after a measured time. With the large cell, a series of aliquots could be removed for analysis at various times. About 8% of the material in the pyrolysis cell was removed with each aliquot. The rate constants for reaction 1 were obtained by plotting the ratio difluoroethane/(vinyl fluoride and difluoroethane) for the series of samples from any one pyrolysis mixture against time. A single rate constant was determined using four to eight measurements. For low-pressure studies, the entire contents of the large cell was removed by pumping through a trap at −196°. This trap was warmed and aliquots were expanded into the chromagraph sampling loop. Either samples were stored 16 hr for mixing or repeat samples were taken to assure uniform analysis.

Results

When 1,1-difluoroethane is pyrolyzed, vinyl fluoride accounts for more than 95% of the total products. Small amounts of hydrogen, 1,1-difluoroethylene, ethylene, and methane and traces of ethane are formed. The observed rate of 1,1-difluoroethane disappearance matches the rate of appearance of products until more than half the starting material is consumed. After that, significant quantities of material are not recovered in the fractions that we analyzed. A small amount of telomeric material is deposited in the cooler parts of the pyrolysis cell, but material balances show that this accounts for only an insignificant fraction of the total material in all runs for which data are reported.

It had been previously suggested that α elimination or molecular hydrogen elimination could account for the presence of hydrogen or certain isotopically labeled ethylenes.[15] Addition of 10% NO to the pyrolysis decreases hydrogen, methane, and 1,1-difluoroethylene yields by as much as tenfold and entirely eliminates ethane. The work of Scott and Jennings[16] suggests the following mechanism for the formation of these products.

$$CH_3CHF_2 \longrightarrow CH_3\cdot + CHF_2\cdot \quad (2)$$

$$CH_3\cdot + CH_3CHF_2 \longrightarrow CH_4 + CH_3CF_2\cdot \quad (3)$$

$$2CH_3CF_2\cdot \longrightarrow CH_3CHF_2 + CH_2CF_2 \quad (4)$$

$$2CH_3\cdot \longrightarrow C_2H_6 \quad (5)$$

The formation of ethylene is more difficult to explain. The possibility of a surface reaction seems to be ruled out by the fact that our pyrolysis products contained 2% ethylene at all temperatures, with or without scavenger, in both cells, and for all the conversions studied. Similar amounts of ethylene were observed in shock tube studies at considerably higher temperatures.[12]

As had been observed by earlier workers,[14] both pyrolysis cells give reproducible results only after they had been aged with 1,1-difluoroethane. If the hot cell is exposed to air, a definite enhancement of the pyrolysis rate occurs, but reproducible results can be obtained by reaging the cell. All the data reported are for thoroughly aged cells.

The surface-to-volume ratio of the large cell is one-sixth that of the small cell, but the observed rate constants for the large cell are larger by a factor of 2 for the same nominal temperature. This effect can be explained by the known temperature gradients in the small cell, where the recorded temperature was for the hottest part of the cell.

Figure 1 shows the Arrhenius plot for reaction 1 between 430 and 535° for pressures between 30 and 300 Torr. The activation energy is 63.4 ± 1.1 kcal/mol and log A is 13.6 ± 0.3 in units of seconds. Figure 2 shows the rate constants measured between 0.165 and 9 Torr at 525° relative to the high-pressure rate con-

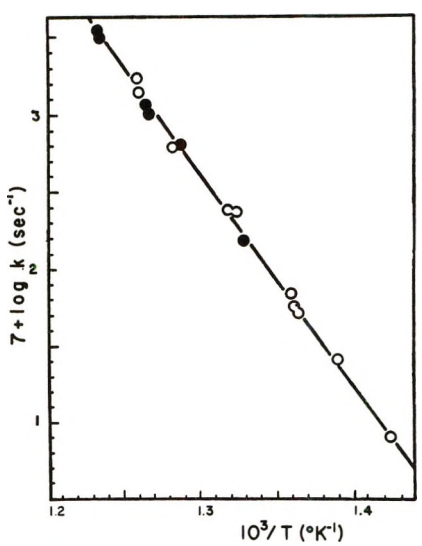

Figure 1. Arrhenius plot for dehydrofluorination of 1,1-difluoroethane: (○) single run, (●) replicate runs.

(15) M. J. Perona, J. T. Bryant, and G. O. Pritchard, *J. Amer. Chem. Soc.*, 90, 4782 (1968).

(16) P. M. Scott and K. R. Jennings, *J. Phys. Chem.*, 73, 1513 (1969).

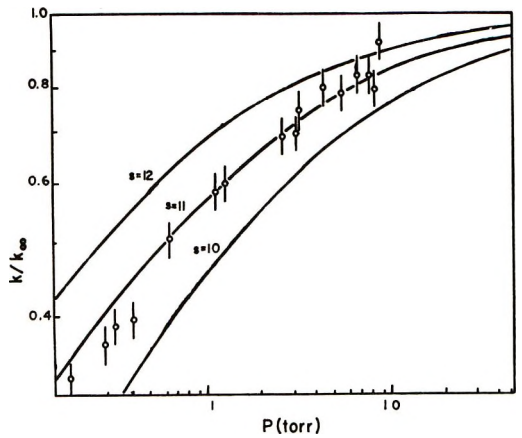

Figure 2. Low-pressure rate constants for dehydrofluorination of 1,1-difluoroethane. Bars represent the experimental uncertainty in k, lines are calculated from the RRK equation for $E^* = 63.4$ kcal/mol and $\log k^{\ddagger} = 13.6$.

stant. The aliquot method was used for pressures as low as 6 Torr, and the total sample method was used for pressures as high as 9 Torr. In the region where both methods were used, comparable results were obtained. The beginning of the falloff was observed with the aliquot method.

Discussion

The Arrhenius parameters found in this work for reaction 1 are within experimental uncertainty the same as those found at higher temperatures in both flow systems[11] and shock tubes.[12,13] This consistency over a temperature range of 600° indicates that all three techniques are observing the same elementary reaction. On the other hand, the activation energies reported in all pyrolysis studies are several kilocalories above those calculated from fitting early chemical activation experiments to the RRK theory.[9,10]

While no previous pyrolysis results on dehydrohalogenation reactions have been carried to sufficiently low pressures to give clearly defined falloff, data for both ethyl fluoride[14] and ethyl chloride[17] give strong indications of falloff in the same region observed here.

To examine the conditions necessary for the parameters of the RRK theory to be transferable from chemical activation to pyrolysis and *vice versa*, we calculated k/k_∞, the ratio of the rate constant to its high-pressure limit using[18]

$$k/k_\infty = \frac{1}{(s-1)!}\int_{x=0}^{\infty} \frac{x^{s-1}e^{-x}dx}{1 + \dfrac{k^{\ddagger}}{\lambda Z[A]}\left(\dfrac{x}{b+x}\right)^{s-1}} \qquad \text{(I)}$$

where $x = (E - E^*)/RT$, $b = E^*/RT$, λ is the collisional deactivation efficiency, Z is the collision number, and s is a variable parameter. For our calculation λ is assumed to be unity and Z is calculated from collision theory assuming a cross section of 5.0 A. Since the high-pressure limit of the RRK theory gives $k = k^{\ddagger}\cdot \exp(E^*/RT)$, the same form as the Arrhenius equation, $k^{\ddagger}$ is taken as the Arrhenius preexponential factor and E^* is taken as the Arrhenius activation energy. The curves in Figure 2 were calculated from eq I for $s = 10$, 11, and 12.

Figure 2 shows that the experimental data are best fitted by the curve for $s = 11$. Using this s, E^*, and $k^{\ddagger}$, the rate constants for reaction 1 can be calculated for different total energies E, from

$$k = k^{\ddagger}\left(\frac{E - E^*}{E}\right)^{s-1} \qquad \text{(II)}$$

Using the data at 500°K in ref 9 and the same λ and Z for deactivation, it is possible to calculate k for chemical activation

$$k_{\text{elim}} = \frac{[CH_2CHF]}{[CH_3CHF_2]}\lambda Z[A] \qquad \text{(III)}$$

The rate constant calculated from experimental data is 1.3×10^9 sec^{-1}, corresponding to $E = 98$ kcal/mol in Table I.

Table I: Rate Constants Calculated for Reaction 1 for Total Energy E

E, kcal/mol	$E - E^*$	Log k, sec^{-1}, $s = 11$	Log k, sec^{-1}, $s = 12$
80.0	16.6	6.8	6.1
85.0	21.6	7.65	7.1
90.0	26.6	8.3	7.75
95.0	31.6	8.8	8.35
100.0	36.6	9.25	8.8
105.0	41.6	9.6	9.2

This E is well above that used by earlier workers in fitting their chemical activation data to obtain values of E^*,[9] but is only slightly larger than the value that would be predicted for the formation of C–C bonds in partially fluorinated ethanes using recent thermochemical data,[19,20] while the E used by Bryant and Pritchard is 6 kcal/mol less.

The discrepancy in calculated rate constants is not caused by our arbitrary use of $\lambda = 1$. If $\lambda = 0.5$, the pressure corresponding to a calculated k/k_∞ is doubled. This shifts the calculated curve for $s = 12$ onto our experimental data. It is strictly fortuitous that a factor of 2 makes a one unit change in the continuous parameter s. For $s = 12$, $E^* = 63.4$, $k^{\ddagger} = 10^{13.6}$, and $\lambda = 0.5$, the results in the chemical activation experiments

(17) K. E. Howlett, *J. Chem. Soc.*, 3695 (1952).

(18) K. J. Ladler, "Chemical Kinetics," 2nd ed, McGraw-Hill, New York, N. Y., 1965, p 153.

(19) P. N. Clough, J. C. Polanyi, and R. T. Taguchi, *Can. J. Chem.*, **48**, 2919 (1970).

(20) H. W. Chang and D. W. Setser, *J. Amer. Chem. Soc.*, **91**, 7648 (1969).

are matched by equation III using E = 103 kcal/mol, even larger than for $\lambda = 1$. It can be concluded that our pyrolysis data and the chemical activation data are consistent with the RRK theory only if the energy, E, of the chemically activated ethanes is considerably higher than had been estimated by previous workers.

If the pyrolysis data allow a test of the consistency of the empirical RRK parameters found from pyrolysis and chemical activation, could the RRKM theory be used to distinguish between different models of the activated complex? The two complexes to be considered are a homolytic, or four-centered model, where the H–F bond is formed at the same time the C–F bond is broken, and a heterolytic model in which the C–F bond stretches without affecting C–H bonds. These models are shown as A and B. In each model the bonds

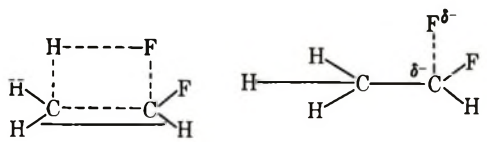

A, homolytic model B, heterolytic model

shown as dotted lines are arbitrarily taken as being half-order bonds in the activated complex. This is halfway between reactant and product bond orders. The vibration frequencies are then found by assuming that vibration frequencies change with the square root of the bond order.

All but one of the vibration frequencies of the reactant molecule have been measured.[21] The torsional frequency is assumed to be 250 cm^{-1}. In going to the four-centered complex, the following shifts result from the above assumptions. Each of four frequencies is decreased by a factor of $2^{1/2}$. These are nominally a C–H stretch, a C–F stretch, a CCH bend, and a CCF bend. A second CCH bend is taken as the reaction coordinate. The C–C stretch increases by a factor of $2^{1/4}$ because that bond is becoming a double bond. This model is very similar to the model used by Kerr and Timlin[22] in their treatment of the dehydrofluorination of chemically activated CH_2FCH_2F, except that we have not increased the torsional frequency. Our calculations repeated with their frequencies lead to results that are indistinguishable from those given here. For the heterolytic model, one CCF bending mode and one FCF bending mode are decreased by a factor of $2^{1/2}$. The torsional motion is taken as decreasing by a factor of 2 because a molecule with threefold symmetry on each end of the center bond is changing into one with threefold opposite twofold symmetry. A C–F stretch is taken as the reaction coordinate. All other activated complex frequencies are taken as being unchanged from the reactant molecule. All rotations are treated as being adiabatic.

In the limit of high pressure, the first-order rate constant is

$$k = \sigma \frac{kTQ_r^{\ddagger}Q_v^{\ddagger}}{hQ_r^{*}Q_v^{*}} e^{-E_c/RT} = Ae^{-E_a/RT} \quad \text{(IV)}$$

where σ is the reaction path degeneracy (see below for a discussion of the values used), Q_r is the rotational partion function without symmetry numbers, Q_v is the vibrational partition function, E_c is the critical energy, and E_a is the Arrhenius activation energy. The superscript asterisk refers to a property of the energized molecule and the double dagger refers to a property of the activated complex. From eq IV we find that

$$A = \sigma \frac{kTQ_r^{\ddagger}Q_v^{\ddagger}}{hQ_r^{*}Q_v^{*}} e^{-(E_c - E_a)/RT} \quad \text{(V)}$$

By taking temperature derivatives of the logarithms of eq IV

$$E_c - E_a = (E - E_0)^{*} - (E - E_0)^{\ddagger} - RT \quad \text{(VI)}$$

$E - E_0$ is the thermal energy of the vibrations at 800°K. Table II shows the total zero-point vibrational energy, E_z, and the vibrational parameter, $\langle \nu^2 \rangle / \langle \nu \rangle^2$, for the molecule and the two activated complex models. It also shows the critical energies corresponding to the measured activation energy and the calculated log A for both models.

Table II: Input Parameters and Results for RRKM Calculations

	$\langle \nu^2 \rangle / \langle \nu \rangle^2$	E_z kcal/mol	E_c	Log A, sec^{-1}
Molecule	1.393	37.10		
Heterolytic complex	1.457	34.33	61.7	14.8
Homolytic complex	1.434	32.90	61.5	14.6

Table II shows that the vibrational parameters are very similar for the two complexes, and our calculations show that the observable quantities are not sensitive to differences of the size shown. The calculations are affected by the changes in the zero-point energies that are shown in Table II. No significant effect is introduced by the small change in critical energies. Both models predict larger A factors than are seen experimentally. The rotational partition function ratios contribute factors of 1.49 and 1.39 for the heterolytic and homolytic models, respectively. The exponential terms contribute factors of 2.80 and 3.28. Since neither rotational nor exponential terms seem to be exceptionally large, the error must lie in the vibrational partition functions. To significantly decrease the ratio of vibrational partition functions in eq V would require that several of the low-frequency vibrations of both the

(21) D. C. Smith, R. A. Saunders, J. R. Nielsen, and E. E. Ferguson, *J. Chem. Phys.*, **20**, 847 (1952).

(22) J. A. Kerr and D. M. Timlin, *Trans. Faraday Soc.*, **67**, 1376 (1971).

activated complexes be increased. As our calculations with the Kerr and Timlin model show, changing a single frequency would not change the calculated falloff pressure. In any case, both the models would have to be changed by similar amounts.

If all rotations are assumed to be adiabatic, the RRKM theory gives the following expression for the rate constant relative to the high-pressure limit of the rate constant.[23]

$$k/k_\infty = \frac{1}{R'} \times \int_0^\infty \frac{\sum_{E_v^\ddagger < E^\ddagger} P^\ddagger(E_v^\ddagger) e^{-E^\ddagger/RT}\, dE^\ddagger}{1 + \frac{Q_r^\ddagger/Q_r^*}{\lambda Z[A] h N^*(E_c + E^\ddagger)} \sum_{E_v^\ddagger < E^\ddagger} P^\ddagger(E_v^*)} \quad \text{(VII)}$$

If the sums are evaluated by the method of Whitten and Rabinovitch,[24] the expression becomes

$$k/k_\infty = \frac{1}{R} \int_0^\infty \frac{(x + ax_z)^{s-1} e^{-x}\, dx}{1 + M\left(\frac{x + ax_z}{x + b}\right)^{s-1}} \quad \text{(VIII)}$$

x is $E^\ddagger/RT$, x_z is $E_z^\ddagger/RT$, and b is $(E_z^* + E_c)/RT$. The number of active vibrations, s, is 18 for difluoroethane. R is the value of the integral for $M = 0$. The empirical formulas given in Table III of ref 24 were used to evaluate a. M is given by

$$M = \frac{\sigma Q_r^\ddagger \prod^s \nu^*}{\lambda Z[A] Q_r^* \prod^{s-1} \nu^\ddagger} \quad \text{(IX)}$$

Z is the collision number and ν^* and $\nu^\ddagger$ are the vibration frequencies of the molecule and complex.

A computer program was written for a Hewlett-Packard 9100B computer to evaluate the integrals for arbitrary values of M (*i.e.*, different values of $[A]$). If the calculated values of k/k_∞ are plotted against log M, they can be matched with the observed values of k/k_∞ plotted against log $[A]$ by shifting one plot along the abscissa. In this way corresponding values of M and $[A]$ can be found. We can now solve for λ using eq VIII. This was done for the two activated complex models described, using the experimental data for 800°K and calculating Z from collision theory with 5.0-Å diameters.

There is some uncertainty in the value to use for σ. If free rotation about the C–C bond is allowed, σ should be 6 as used by previous workers.[10] However, the four-centered model and the use of the torsional motion as a vibrational degree of freedom imply that σ should be 4; each of two fluorines can react with either of the two hydrogens to which it is gauche. Since the high total energy content of the reacting molecules makes the assignment of the torsion motion as a vibration questionable, the choice is not clearcut.[25] In these calculations, σ was taken to be 4 for the homolytic model. Since there are only two carbon–fluorine bonds and these react with the hydrogens only after passing through the transition state in the heterolytic model, σ was taken as 2 for that model.

The values of λ which give agreement between calculated falloff and the observed falloff are 0.48 for the heterolytic and 0.76 for the homolytic model. Both these values of λ are reasonable and are experimentally indistinguishable, so we cannot favor either model on the basis of these calculations. That two activated complex models as different as these seem indistinguishable should emphasize that matching experimental and calculated rate constants leaves a great deal of uncertainty in the geometry of the activated complex.

(23) K. A. Laidler, "Theories of Chemical Reaction Rates," McGraw-Hill, New York, N. Y., 1969, p 128.

(24) G. Z. Whitten and B. S. Rabinovitch, *J. Chem. Phys.*, **38**, 2466 (1963).

(25) J. C. Hassler and D. W. Stezer, *ibid.*, **45**, 3246 (1966).

Photochemistry of Azoisopropane in the 2000-Å Region[1]

by M. Louis Arin and Colin Steel*

Department of Chemistry, Brandeis University, Waltham, Massachusetts 02154 *(Received August 23, 1971)*

Publication costs assisted by the National Science Foundation

The photochemistry of azoisopropane (AIP) using light in the 2000-Å region (n → π^* excitation) has been studied and compared with the n → π^* photochemistry. The data are consistent with the formation of vibrationally excited isopropyl radicals which, unless collisionally deactivated, undergo unimolecular elimination of either H·, reaction 6, or CH_3·, reaction 7. The pressure–wavelength data are fitted by $A_6 = A_7 = 10^{14}$ sec^{-1}, $E_6^0 = 41$ kcal mol^{-1}, and $E_7^0 = 46$ kcal mol^{-1}. The mean energy of the isopropyl radicals is ~35 kcal mol^{-1}, but they are formed with a wide energy spread of ~40 kcal mol^{-1}. The various radical reactions involving H·, CH_3·, and C_3H_7· in the system have been studied and compared with the literature values. The ratio of hydrogen abstraction from AIP by H· to addition of H· to AIP, k_{10}/k_{11}, has the value of 0.10. The quantum yield of decomposition = 0.97 ± 0.08 and is independent of wavelength or intensity in the 2000-Å region; it is also independent of pressure up to at least 400 Torr.

Introduction

Azoalkanes exhibit a weak n → π^* absorption band ($S_0 \rightarrow S_1$) centered in the region 340–360 nm (ϵ ~10 M^{-1} cm^{-1}) and a stronger absorption ($S_0 \rightarrow S_2$) in the 200-nm region (ϵ ~1000 M^{-1} cm^{-1}). The nature of the latter band has been the subject of some discussion. A recent spectroscopic investigation assigns it to an $n_+ \rightarrow \sigma^*$ transition.[2] Prior investigations into the photodecomposition of azoalkanes were carried out using n → π^* excitation. For such excitation at room temperature, the reactions involved in the photodecomposition of azoisopropane (AIP) may be written[3]

$$\text{AIP} \xrightarrow{h\nu} \longrightarrow \text{AIP}^+ \quad (1)$$

$$\text{AIP}^+ + \text{X} \longrightarrow \text{AIP} + \text{X} \quad (2)$$

$$\text{AIP}^+ \longrightarrow 2\text{C}_3\text{H}_7\cdot + \text{N}_2 \quad (3)$$

$$2\text{C}_3\text{H}_7\cdot \longrightarrow \text{C}_3\text{H}_6 + \text{C}_3\text{H}_8 \quad (4)$$

$$2\text{C}_3\text{H}_7\cdot \longrightarrow \text{C}_6\text{H}_{14}\ \text{(diisopropyl)} \quad (5)$$

At higher temperatures abstraction and addition reactions of the radicals have also to be considered.[3] Two questions arise. First, in view of the known ability of cyclic azoalkanes to yield vibrationally excited cyclic hydrocarbons,[4-6] can acyclic azoalkanes be used as a source of vibrationally excited radicals? Second, what is the state represented by AIP^+?

The possible unimolecular reactions of vibrationally excited isopropyl radicals (C_3H_7·*) are

$$\text{C}_3\text{H}_7\cdot{}^* \longrightarrow \text{C}_3\text{H}_6 + \text{H}\cdot \quad (6)$$

$$\text{C}_3\text{H}_7\cdot{}^* \longrightarrow \text{C}_2\text{H}_4 + \text{CH}_3\cdot \quad (7)$$

The critical energies E_6^0 and E_7^0 for these reactions are about 41 and 46 kcal mol^{-1} (see Discussion). Radicals possessing sufficient energy to carry out these unimolecular reactions we call "hot." The reaction AIP → $2C_3H_7$· + N_2 is endothermic by 15.2 kcal mol^{-1}.[7,8] Thus it is not surprising that light of wavelength 355 nm, which corresponds to the absorbance maximum of the n → π^* band and has an energy of 80.5 kcal einstein^{-1}, does not cause the formation of "hot" C_3H_7· radicals. This, however, should not be a limitation at 200 nm. Of course, even at this wavelength, although it is energetically feasible, there may be mechanistic restrictions to the production of "hot" radicals. Vibrationally excited isopropyl radicals have been produced by thermal and by chemical activation.[9-14] The results from several laboratories for reaction 6 have been summarized by Frey and Walsh[15] and compared with a calculated value (*viz.*, $A_6 = 10^{13.4}$ sec^{-1} and $E_6^0 = 41.7$ kcal mol^{-1}). There are also

(1) Abstracted from Ph.D. Thesis of M. L. Arin, Brandeis University, 1971.

(2) M. B. Robin, R. R. Hart, and N. A. Keubler, *J. Amer. Chem. Soc.*, **89**, 1564 (1967).

(3) R. H. Riem and K. O. Kutschke, *Can. J. Chem.*, **38**, 2332 (1960); R. W. Durham and E. W. R. Steacie, *ibid.*, **31**, 377 (1953).

(4) T. F. Thomas, C. I. Sutin, and C. Steel, *J. Amer. Chem. Soc.*, **89**, 5107 (1967).

(5) P. Cadman, H. M. Meunier, and A. F. Trotman-Dickenson, *ibid.*, **91**, 7640 (1969).

(6) F. H. Dorer, E. Brown, J. Do, and R. Rees, *J. Phys. Chem.*, **75**, 1640 (1971); H. M. Frey and I. D. R. Stevens, *J. Chem. Soc.*, 4700 (1964).

(7) J. G. Calvert and J. N. Pitts, Jr., "Photochemistry," Wiley, New York, N. Y., 1966, p 819.

(8) G. E. Coates and L. E. Sutton, *J. Chem. Soc.*, 1187 (1948).

(9) C. A. Heller and A. S. Gordon, *J. Phys. Chem.*, **62**, 709 (1958).

(10) K. S. Konar, R. M. Marshall, and J. H. Purnell, *Trans. Faraday Soc.*, **64**, 405 (1968).

(11) J. A. Kerr and A. F. Trotman-Dickenson, *ibid.*, **55**, 921 (1959).

(12) R. A. Back and S. Takamuku, *J. Amer. Chem. Soc.*, **86**, 2558 (1964).

(13) W. M. Jackson and J. R. McNesby, *J. Chem. Phys.*, **36**, 2272 (1962).

(14) W. E. Falconer, B. S. Rabinovitch, and R. J. Cvetanović, *ibid.*, **39**, 40 (1963).

(15) H. M. Frey and R. Walsh, *Chem. Rev.*, **69**, 103 (1969).

many reports on reaction 7, with E_7^0 ranging from 20 to 35 kcal mol^{-1} and A_7 from $10^{8.5}$ to $10^{15.2}$ sec^{-1}.[9-12] Nevertheless, although E_7^0 is reported as being less than E_6^0, Falconer, *et al.*,[14] were unable to find any evidence for (7) when $C_3H_7\cdot$ * was produced by chemical activation, while Jackson and McNesby[13] found that in the range 745–823°K an upper limit for k_7/k_6 was 0.06. Frey and Walsh have suggested that the only reasonable route for (7) is *via* the *n*-propyl radical, and on this basis have calculated as a lower limit for E_7^0 the value 43 ± 4 kcal mol^{-1}, with $A_7 = 10^{13\pm1}$ sec^{-1}.

Cyclic azoalkanes are known to be able to dissociate from both their first singlet (S_1) and triplet (T_1) states.[16-18] There is little convincing evidence for the involvement of vibrationally excited ground states (S_0^{vib}) in their photochemistry. In contrast, although it was not generally clearly stated, the implication in the early literature on the photochemistry of acyclic azo compounds was that dissociation occurred from S_0^{vib}. More recently, however, there have been suggestions that a triplet state may be the one from which dissociation occurs.[17,18]

Experimental Section

Materials. The preparation and purification of AIP have been described previously.[19] The impurities found in AIP were primarily C_3 and C_6 hydrocarbons and acetone. The impurities were reduced to less than 0.01% on a preparatory gc column consisting of 10 ft of 0.375-in. o.d. aluminum tubing packed with Chromosorb W (60/80 mesh) coated with Dow Silicone 710. The level of the impurities slowly increased with time, although samples were stored at Dry Ice temperature.[20] It was therefore necessary to occasionally repurify the samples. Available commercial sources of carbon dioxide were found to contain traces of C_1 and C_2 hydrocarbons which were removed by trap-to-trap vacuum distillation. Prepurified nitrogen was used without further purification.

Samples for photolysis were vaporized into photolysis vessels on a greaseless, mercury-free vacuum line which had been evacuated to less than 10^{-5} Torr before filling. The photolysis vessel consisted of a quartz cylindrical optical cell (l = 5 cm) fitted with a bellows high-vacuum valve. Mixtures of AIP and an added gas were made up by first filling the reaction vessel to the desired azo pressure, then quickly expanding a higher pressure of the added gas into the vessel. Pressures were measured by means of a Texas Instrument quartz spiral pressure gauge calibrated throughout the range 2×10^{-3} to 5×10^2 Torr.

Light Sources. Most samples were photolyzed by collimated light from a deuterium arc (Sylvania DE-50A). In the first experiments this light was passed through a monochromator (Bausch and Lomb high intensity) to isolate the 200-nm region. But since this resulted in a large loss of intensity and since the results were not significantly different from those in which the monochromator was not employed, the latter was only used in the quantum yield determinations (*vide infra*). In fact, we found that the simplest way to change the effective wavelength of photolysis was to interpose a filter consisting of a quartz 1-cm cell filled with an appropriate gaseous olefin in the pressure range 40–200 Torr. The relative intensities of different frequencies from the lamp incident on the filter, $I(\bar{\nu})$, were estimated from the published arc spectrum,[22] the measured transmission of the quartz used in fabricating the envelope of the lamp, and the measured absorption spectrum of oxygen at the pressure and pathlength equivalent to the air gap between the lamp and the cell.[23] If $F_i(\bar{\nu})$ is the fraction of light of frequency $\bar{\nu}$ transmitted by filter i and $P_{azo}(\bar{\nu})$ is the probability of absorption by azoisopropane, then the rate of decomposition when filter i is used is given by

$$R_i = \int_0^\infty I(\bar{\nu})F_i(\bar{\nu})P_{azo}(\bar{\nu})\Phi_{dec}(\bar{\nu})d\bar{\nu} \qquad (8)$$

where $\Phi_{dec}(\bar{\nu})$ is the decomposition yield at frequency $\bar{\nu}$. If $\Phi_{dec}(\bar{\nu})$ is frequency independent, then

$$R_i = \Phi_{dec}\int_0^\infty I(\bar{\nu})F_i(\bar{\nu})P_{azo}(\bar{\nu})d\bar{\nu}$$

The effective frequency of photolysis, $\bar{\nu}_{eff}$, for filter i is defined by

$$\frac{\int_0^{\nu_{eff}} I(\bar{\nu})F_i(\bar{\nu})P_{azo}(\bar{\nu})d\bar{\nu}}{\int_0^\infty I(\bar{\nu})F_i(\bar{\nu})P_{azo}(\bar{\nu})d\bar{\nu}} = 0.5$$

Typical curves are shown in Figure 1. Effective photolysis frequencies, cm^{-1} (wavelengths, nm) were as follows: no filter, 51,300 (195); ethylene filter, 50,000 (200); propylene filter, 49,020 (204); *trans*-butene-2 filter, 47,620 (210); cyclohexene filter, 46,300 (216). It is not practical to use any longer wavelength filters since the $S_0 \rightarrow S_2$ absorption of AIP only commences

(16) W. D. K. Clark and C. Steel, *J. Amer. Chem. Soc.*, **93**, 6347 (1971); B. S. Solomon, T. F. Thomas, and C. Steel, *ibid.*, **90**, 2249 (1968); P. Scheiner, *ibid.*, **90**, 988 (1968); S. D. Andrews and A. C. Day, *Chem. Commun.*, 667 (1966); P. S. Engel, *J. Amer. Chem. Soc.*, **89**, 5731 (1967).

(17) I. I. Abram, G. S. Milne, B. S. Solomon, and C. Steel, *ibid.*, **91**, 1220 (1969).

(18) S. Collier, D. Slater, and J. Calvert, *Photochem. Photobiol.*, **7**, 737 (1968).

(19) R. Renaud and L. C. Leitch, *Can. J. Chem.*, **32**, 545 (1954).

(20) The infrared spectrum of a thin liquid film of AIP which had not been rigorously purified showed a weak absorption at 1572 cm^{-1}. This has been assigned to a –N=N– stretching frequency.[21] Gas chromatography showed the presence of acetone, which has an absorption at 1572 cm^{-1}. After careful purification, a liquid layer of AIP as thick as 0.05 mm gave no absorption in this region.

(21) R. J. LeFèvre, M. F. O'Dwyer, and R. L. Werner, *Aust. J. Chem.*, **14**, 315 (1961).

(22) K. Watanabe and C. Inn, *J. Opt. Soc. Amer.*, **43**, 32 (1953).

(23) J. R. McNesby and H. Okabe, *Advan. Photochem.*, **3**, 174 (1964).

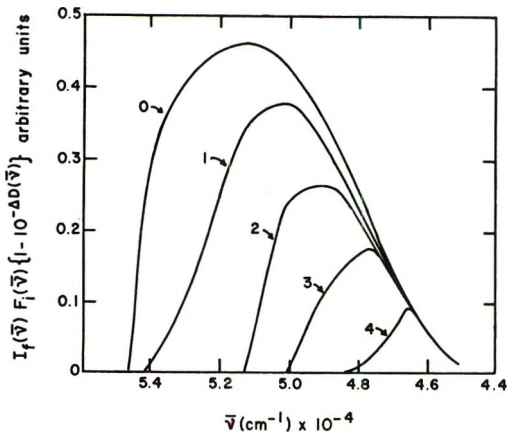

Figure 1. Product of light intensity incident on photolysis cell, $I_f(\bar{\nu})F_i(\bar{\nu})$, and fraction of light absorbed by AIP, $(1 - 10^{-\Delta D(\bar{\nu})})$, *vs.* frequency for various hydrocarbon filters. $F_i(\bar{\nu})$ is the fraction of the light transmitted by the filter i: $i = 0$, no filter; $i = 1$, ethylene; $i = 2$, propylene; $i = 3$, *trans*-butene-2; $i = 4$, cyclohexene.

at 220 nm. A typical light intensity was such that when the arc was used without an olefin filter 2×10^{12} photons/(cm^3 sec) were absorbed by 0.25 Torr of AIP. When the monochromator was used in the quantum yield experiments, the intensity was reduced so that about 2×10^{10} photons/(cm^3 sec) were absorbed by the same pressure of AIP. Photolyses in the 355-nm region ($n \rightarrow \pi^*$) were carried out as described previously.[24]

Quantum Yields. In the measurement of quantum yields, the monochromator was used to isolate appropriate wavelength regions. The absolute intensity of 254-nm light issuing from the monochromator was determined by ferrioxalate actinometry,[25] while the intensity at 200 nm relative to that at 254 nm was determined using a sodium salicylate screen as photon counter.[26] This enables the absolute intensity of light at 200 nm to be determined. In determining the effect of wavelength on the quantum yield, the rates of decomposition for different gaseous filters were calculated using eq 8, on the assumption that $\Phi_{dec}(\bar{\nu})$ = constant. The calculated and experimental results are shown in Table I. Considering the uncertainty in the estimation of $I(\bar{\nu})$, the agreement may be considered satisfactory. There is certainly no evidence for a significant wavelength dependence for Φ_{dec} in the 200-nm region. Unless specifically stated otherwise in the text, photolyses were carried out using the full arc.

Product Analyses. AIP and C_3 and C_6 hydrocarbons were analyzed by flame ionization gas chromatography using a 25 ft $\times$ $^1/_8$ in. column of 10% SF-96 on Chromosorb W. C_1–C_4 hydrocarbons were separated on a 10 ft $\times$ 0.175 in. column of activated alumina coated with 1% SF-96. Oxygenated hydrocarbons were separated on a 25 ft $\times$ 0.175 in. column of 10% Ucon Polar on Chromosorb W. Hydrogen and nitrogen analyses were carried out by thermal conductivity gas chromatography using Molecular Sieve 13X. The concentration of AIP was also determined spectrophotometrically using a Cary 14.

Table I: Calculated and Experimental Rates of AIP Photolysis Using Different Filters

Effective photolysis wavelength, nm	Filter	$R_i/R_{ethylene}$ Exptl	$R_i/R_{ethylene}$ Calcd
200	Ethylene	1.0	1.0
204	Propylene	0.60	0.52
210	*trans*-Butene-2	0.33	0.26
216	Cyclohexene	0.079	0.077

The percentage decomposition was measured in the following ways: (a) change in absorbance of AIP, (b) nitrogen evolution, (c) change in AIP concentration measured by gas chromatography, and (d) total hydrocarbon formation. In the latter method which is essentially a "carbon count," we use the fact that 1 mol of $C_6N_2H_{14}$ (AIP) is equivalent to 6 mol of CH_4, 3 mol of C_2H_4, and so on, in calculating the number of moles of AIP consumed. The hydrocarbons observed were CH_4, C_2H_4, C_2H_6, C_3H_8, C_3H_6, i-C_4H_{10}, and C_6H_{14} (diisopropyl). Some data are shown in Table II. The good agreement among the methods indicates that all the products are being observed and that there is no significant loss due to side reactions such as polymerization, for example.

Table II: Percentage Decomposition in AIP Photolysis Measured by Different Methods

Run	Type	Method of analysis a	b	c	d
183	$n \rightarrow \pi^*$	51.9			54.6
184	$n \rightarrow \pi^*$	62.8			64.6
186	$n \rightarrow \pi^*$	59.4	60.4		
187	$n \rightarrow \pi^*$	38.9	37.0		
175	$n \rightarrow \sigma^*$	13.3	10.4	13.5	12.8
177	$n \rightarrow \sigma^*$	58.1	61.5	59.2	60.3
178	$n \rightarrow \sigma^*$	52.9			52.1
180	$n \rightarrow \sigma^*$	50.4	49.1		
196	$n \rightarrow \sigma^*$	30.2	29.1		

Effect of Extent of Photolysis on Product Distribution. A series of photolyses was carried out to different extents of completion to determine the effect of prolonged photolysis on the rate of AIP consumption and on the product concentrations.

If a product P_i is formed at a rate proportional to the consumption of AIP, then throughout the range we

(24) G. S. Milne and C. Steel, *J. Phys. Chem.*, 72, 3754 (1968).

(25) C. G. Hatchard and C. A. Parker, *Proc. Roy. Soc., Ser. A*, 235, 518 (1956).

(26) F. S. Johnson, K. Watanabe, and R. Tousey, *J. Opt. Soc. Amer.*, 41, 702 (1951).

should have $[P_i]/\Delta[AIP] = K_i$, where K_i is a constant and $\Delta[AIP]$ is the change in AIP concentration. In the range 0–95% completion, we obtain such a constant for diisopropyl, but this was not true for the other products. For propylene, K_i tended to decrease slightly as the photolysis proceeded, while the K_i's for the other products increased. This can be seen from the data given in Table III, where we tabulate the product concentration normalized on C_6 (diisopropyl) at 5 and 50% decomposition. Because of this effect photolyses were generally carried out to <5% completion. In the range 1–5% completion, we could observe no significant trend in the product ratios.

Table III: Hydrocarbon Ratios in Photolysis of 0.25 Torr of AIP with Unfiltered Arc

% Decomp	$[C_3H_6]/[C_6]$	$[C_3H_8]/[C_6]$	$[i\text{-}C_4H_{10}]/[C_6]$	$[C_2H_4]/[C_6]$	$[CH_4]/[C_6]$	$[C_2H_6]/[C_6]$
5	1.70	0.75	0.133	0.120	0.033	0.004
50	1.63	0.80	0.230	0.142	0.062	0.007

Homogeneity of Reaction. It is generally accepted that reactions 4 and 5 are gas-phase radical reactions. However, since additional products are formed in the $n \rightarrow \sigma^*$ photolysis, the question arises as to the homogeneity of all the reactions in this case. In particular, one may ask if there is any photolysis of AIP molecules adsorbed on the end windows of the photolysis cell or if any of the radicals formed undergo reactions on the walls. The first question can be answered by carrying out photolyses in cylindrical vessels of the same diameter but with different path lengths (l = 1 and 5 cm). For such vessels, the calculated ratios of rates of product formation (moles per cubic centimeter per second) on the basis of two extreme mechanisms, (a) 100% decomposition in the gas phase and (b) 100% decomposition by surface adsorbed AIP molecules, differ markedly. The experimental values agreed exactly with those calculated on the basis of mechanism a. Information with respect to the second question can be obtained by carrying out photolyses using a wide range of light intensities. Reactions such as (4) and (5) are second order in radical concentration, while the rate at which radicals diffuse to the walls will be first order. It may therefore be expected that if there is a significant amount of surface reaction the product ratios should vary *inter alia* as the light intensity, and hence the steady-state concentration of radicals, is varied. However, even over a 400-fold variation in light intensity we were not able to detect any significant variation in the hydrocarbon ratios given in Table III.

Results and Discussion

(*1*) *General Reaction Scheme.* When AIP at 22° and in the pressure range 0.093 to 15.6 Torr is photolyzed using 355-nm light ($n \rightarrow \pi^*$ excitation), the only significant products (besides N_2) are C_3H_6, C_3H_8 and C_6H_{14}; see reactions 1–5. The ratio of the rate constant of disproportionation to that of combination, k_4/k_5, found in these studies was 0.57 ± 0.05, in good agreement with the average of the values obtained by several investigators.[2,11,27] However, when AIP was photolyzed using 200-nm light, H_2, CH_4, C_2H_4, $i\text{-}C_4H_{10}$, and a trace of C_2H_6 were found in addition to C_3H_6, C_3H_8, and C_6H_{14}. A typical hydrocarbon analysis is given in Table III, while H_2 analyses are shown in Figure 4.

A simple explanation for the appearance of these new products is that with 200-nm irradiation "hot" isopropyl radicals ($C_3H_7\cdot$) are being generated.

$$C_3H_7\cdot{}^* \longrightarrow C_3H_6 + H\cdot \quad (6)$$

$$C_3H_7\cdot{}^* \longrightarrow C_2H_4 + CH_3\cdot \quad (7)$$

$$C_3H_7\cdot{}^* + X \longrightarrow C_3H_7\cdot + X \quad (9)$$

$$H\cdot + AIP \longrightarrow H_2 + \dot{C}_3H_6N_2C_3H_7 \quad (10)$$

$$H\cdot + AIP \longrightarrow C_3H_7\dot{N}{-}N{-}C_3H_7 \quad (11)$$
$$\qquad\qquad\qquad\qquad\qquad\quad |$$
$$\qquad\qquad\qquad\qquad\qquad\quad H$$

$$CH_3\cdot + C_3H_7\cdot \longrightarrow i\text{-}C_4H_{10} \quad (12)$$

$$CH_3\cdot + C_3H_7\cdot \longrightarrow CH_4 + C_3H_6 \quad (13)$$

$$CH_3\cdot + CH_3\cdot \longrightarrow C_2H_6 \quad (14)$$

In comparison with the $n \rightarrow \pi^*$ photolysis, there are now two additional sources of propylene, reactions 6 and 13. The concentration of the "excess" propylene so generated is given by

$$[C_3H_6]_{xs} = [C_3H_6]_{tot} - k_4/k_5[C_6H_{14}] \quad (15)$$

The last term in (15) represents the propylene formed by reaction 4 and accounts for all the propylene in the $n \rightarrow \pi^*$ photolysis. Using the fact that $k_4/k_5 = 0.57$ and the data given in Table III, it can be seen that $[C_3H_6]_{xs}/[C_6H_{14}] = 1.1$, while $[CH_4]/[C_6H_{14}] = 0.03$. Therefore, essentially all the excess propylene should be generated by reaction 6 and $[C_3H_6]_{xs}$ should be a measure of the number of H atoms released into the system.

(*2*) *Inhibition of Product Formation by Oxygen.* We used oxygen as a radical scavenger because it is known to react very rapidly with free radicals,[28] has a low extinction coefficient in the 200-nm region,[23] and had already been used for scavenging studies in the $n \rightarrow \pi^*$ photolysis.[24] It should also be mentioned that, just as in the $n \rightarrow \pi^*$ photolysis, the oxygen had no effect on the overall rate of photodecomposition and there was no evidence for direct reaction of oxygen with electroni-

(27) C. A. Heller and A. S. Gordon, *J. Phys. Chem.*, **60**, 1315 (1956).
(28) D. P. Dingledy and J. G. Calvert, *J. Amer. Chem. Soc.*, **85**, 856 (1963).

cally excited AIP molecules. If the above mechanism is correct, oxygen should inhibit the formation of H_2, CH_4, i-C_4H_{10}, C_2H_6, C_3H_6, C_3H_8, and C_6H_{14}, leaving only C_3H_6 and C_2H_4 which originate from the decomposition of isopropyl radicals whose lifetime is sufficiently short that they are not intercepted by oxygen. In these experiments the AIP pressure was kept constant at 0.25 Torr, while the pressure of oxygen was varied from 1 to 400 Torr. Even at the lowest oxygen pressure, no H_2, CH_4, i-C_4H_{10}, C_2H_6, C_3H_8, or C_6H_{14} could be detected ($P < 2 \times 10^{-6}$ Torr), the only hydrocarbons present being C_2H_4 and C_3H_6. It is known that the oxidation of isopropyl radicals yields acetaldehyde, acetone, 2-propanol, and propylene.[24] Because of the latter compound, a correction was applied to the propylene concentration found in the 200-nm photolysis. This was done by photolyzing AIP at 355 nm under the same conditions of pressure and intensity as the photolysis at 200 nm and by subtracting this propylene concentration from that found at 200 nm. In Figures 2 and 3 we plot $[C_3H_6]_{xs}/\Delta[AIP]$ and $[C_2H_4]/\Delta[AIP]$ for experiments carried out both in the absence and in the presence of added oxygen (1 Torr). $\Delta[AIP]$ refers to the change in concentration of the AIP. The fact that the plots in the presence and absence of oxygen are identical strongly suggests that C_2H_4 and $C_3H_{6_{xs}}$ are arising by nonscavengable processes and that as pressure increases the relative importance of these processes decreases.

(3) Production and Scavenging of Hydrogen Atoms. In contrast to olefins, there are few reliable data for the activation energies of addition and abstraction reactions of H· with azo compounds. But by comparison with the known activation energies of the reactions of methyl radicals and of hydrogen atoms with olefins[29] and the activation energy of methyl radical attack on azo compounds,[30] an activation energy of 2.5 ± 0.5 kcal mol^{-1} ($=E_{11}^0$) may be estimated for reaction 11. This value is in agreement with the work of Henkins and Taylor,[31] who estimated an upper limit of 4 kcal mol^{-1} for the activation energy of the addition of hydrogen atoms to azomethane. The A factors for the metathetical reactions of H atoms tend to be large ($\sim 10^{14}$ cm^3 mol^{-1} sec^{-1}).[32] Using such an A factor and the above activation energy, it may be readily shown that under typical experimental conditions in which $[C_3H_7\cdot]_{\text{steady state}} = 5 \times 10^{-14}$ mol cm^{-3}, reaction 11 should proceed 5000 times more rapidly than the reaction of H· with $C_3H_7\cdot$, even assuming the latter to be collision controlled.

Moreover, since the percentage decomposition was generally limited to <5%, the reactions of H· with the hydrocarbon products were minimized. The ratio of abstraction to addition is given by $k_{10}/k_{11} = [H_2]/\{[C_3H_6]_{xs} - [H_2]\}$. This ratio, which should be pressure insensitive, is shown in Figure 4. The data yield the value 0.10 ± 0.015 for k_{10}/k_{11}.

The reaction of the hydrazino radicals which we have indicated should be formed by (11) are not known.

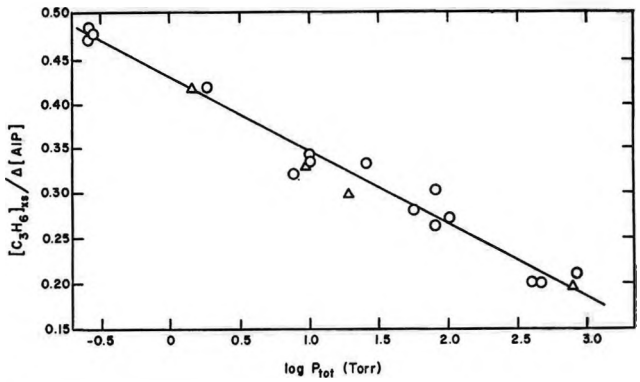

Figure 2. Excess propylene yields in the presence and absence of oxygen. $[C_3H_6]_{xs}$ is the concentration of "excess" propylene (see text for definition), $\Delta[AIP]$ is the change in AIP concentration: (○) no oxygen, P_{tot} = 0.25 Torr of AIP + P_{CO_2}; (△) oxygen, P_{tot} = 0.25 Torr of AIP + 1.0 Torr of O_2 + P_{CO_2}.

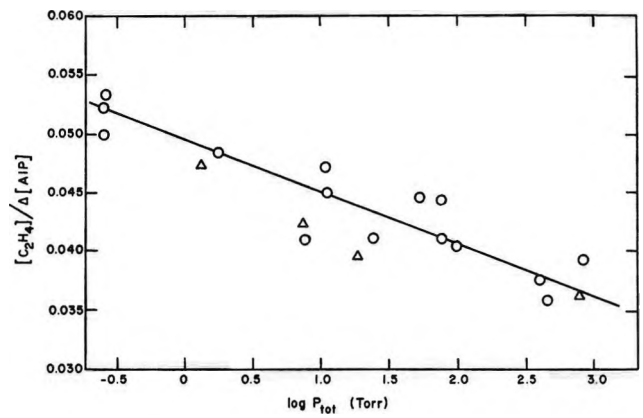

Figure 3. Ethylene yields in the presence and absence of oxygen. ○ and △ have the same meanings as in Figure 2.

One might have suspected that in this system they would have been mainly consumed by radical combination and disproportionation reaction with $C_3H_7\cdot$. Although we did have evidence from gas chromatographic retention times that hydrazines such as R_2N–NHR were formed, the yields were very much less than expected. However, the reactions of H atoms with olefins have been carefully investigated. Moreover, if ethylene is used, it may be estimated[33] that the vibrationally excited $C_2H_5\cdot$ radicals first formed will be collisionally stabilized before redissociating. We should therefore have

(29) R. J. Cvetanović and R. S. Irwin, *J. Chem. Phys.*, **46**, 1694 (1967); B. A. Thrush, *Progr. React. Kinet.*, **3**, 83 (1965).

(30) J. C. J. Thynne, *Trans. Faraday Soc.*, **60**, 2207 (1964); S. Toby and J. Nimoy, *J. Phys. Chem.*, **70**, 867 (1966); S. Toby and K. O. Kutschke, *Can. J. Chem.*, **37**, 672 (1959).

(31) H. Henkins and H. A. Taylor, *J. Chem. Phys.*, **8**, 1 (1940).

(32) A. F. Trotman-Dickenson and G. S. Milne, "Table of Bimolecular Gas Reactions," NSRDSNBS 9, National Bureau of Standards, U. S. Government Printing Office, Washington, D. C., 1967.

(33) B. S. Rabinovitch and D. W. Setser, *Advan. Photochem.*, **3**, 64 (1964).

$$H\cdot + C_2H_4 \longrightarrow C_2H_5\cdot \quad (16)$$

$$C_2H_5\cdot + C_3H_7\cdot \begin{cases} \longrightarrow C_5H_{12} & (17) \\ \longrightarrow C_2H_6 + C_3H_6 & (18) \\ \longrightarrow C_2H_4 + C_3H_8 & (19) \end{cases}$$

Reaction 17 gives isopentane, a product not formed in AIP photolysis in the absence of ethylene or in the photolysis of ethylene alone.[34] Since $[C_3H_7\cdot] \gg [C_2H_5\cdot]$, ethyl–ethyl dimerizations and disproportionations can be neglected as a major fate of $C_2H_5\cdot$ radicals. Using the literature value[29] for the rate constant of (16) and the values given above for A_{11} and E_{11}^0, we calculate that for $P_{AIP} = 0.29$ Torr and $P_{C_2H_4} = 16.0$ Torr, 83% of the hydrogen atoms should be consumed by (16). The literature value[35] of $k_{17}/k_{17} + k_{18} + k_{19} = 0.72$; thus, the calculated value of $[C_5H_{12}]/[C_3H_6]_{xs}$ is (0.83)(0.72) = 0.60. Unfortunately, C_3H_6 could not be measured directly, since the large C_2H_4 peak swamped the C_3H_6 peak on the gas chromatogram. We had to estimate its value indirectly by carrying out two experiments, one with C_2H_4 as the added gas and the second with the same pressure of CO_2 as added gas. In the second experiment, the ratio $[C_3H_6]_{xs}/[N_2]$ was found to be 0.232. This, together with the known pressure of N_2 produced in the first experiment, allowed us to estimate the pressure of $C_3H_{6_{xs}}$ produced in the first experiment as 0.0151 Torr. The observed pressure of C_5H_{12} was 0.00804 Torr. Thus the experimental value of $[C_5H_{12}]/[C_3H_6]_{xs} = 0.00804/0.0151 = 0.53$, in good agreement with the calculated value of 0.60.

Because ethylene is in such large excess, it did photolyze to a small extent during the photolysis of AIP–ethylene mixtures even though the photolyses were carried out using the propylene filter. The pertinent data are given in Table IV. It will be seen that after correction for the H_2 produced by direct photolysis of C_2H_4 there is little, if any, H_2 produced by the photolysis of AIP in presence of excess ethylene, which is to be expected if most of the H atoms are now reacting by (16).

(4) Production of Methyl Radicals. According to the proposed mechanism methyl radicals are produced by

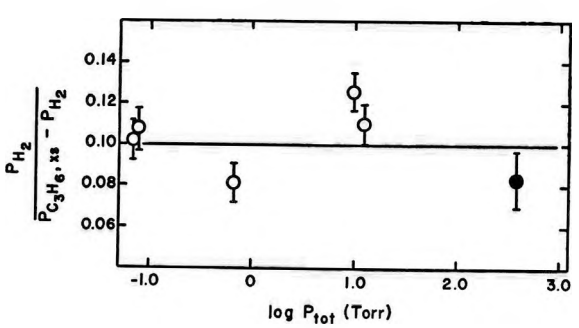

Figure 4. Relative yields of hydrogen and excess propylene, at various pressures, in the photolysis of AIP: (○) AIP alone, (●) P_{tot} = 0.27 Torr of AIP + 392 Torr of CO_2.

Table IV: Photolysis of AIP in the Presence and Absence of Ethylene and Carbon Dioxide

Irradiation time, hr	P_{AIP} × 10², Torr	P_x, Torr	P_{N_2} × 10², Torr	P_{H_2} × 10⁴, Torr
19.2	25.0	45.6 (C_2H_4)	8.4	14.3
19.0	0	45.4 (C_2H_4)	0	15.0
17.8	24.1	39.5 (CO_2)	8.8	9.2
18.5	22.1	41.2 (CO_2) 2.2 (O_2)	8.7	9.5

(7); these should then react with isopropyl radicals by combination and disproportionation reactions 12 and 13. The literature values of k_{13}/k_{12} are close to 0.20.[36] In this study, we found (see Table II for example) $k_{13}/k_{12} = [CH_4]/[i\text{-}C_4H_{10}] = 0.24 \pm 0.03$. The cross combination ratio, C, for methyl and isopropyl radicals is defined by

$$C = \frac{R_{i\text{-}C_4H_{10}}}{\{R_{C_2H_6}R_{C_6H_{14}}\}^{1/2}} = \frac{k_{12}}{\{k_{14}k_5\}^{1/2}} \quad (20)$$

Several such cross-combination ratios have been found for different radical pairs—the value being close to two in each case.[37] In this study we found $C = 1.9 \pm 0.1$. However, we should also have $[C_2H_4] = [C_4H_{10}] + [CH_4]$, while we always found that the right-hand side of this equation was about 35% greater than the left-hand side, indicating that there is a source of CH_3 other than (7). We know that acetone is an impurity in AIP (see Experimental Section). Therefore, samples were carefully purified by gas chromatography so that the acetone was <0.01% and the samples so prepared were used immediately. Nevertheless, the discrepancy remained. Although we have been unable to resolve this problem, it will be noted from Table III that $[i\text{-}C_4H_{10}]$ and $[CH_4]$ account for only a small fraction of the overall reaction.

There is another unresolved problem in the detailed accounting for the products in the n → σ^* photolysis. In the n → π^* photolysis the ratio $[C_3H_8]/[C_6H_{14}] = 0.57$. In the case of the n → σ^* photolysis, although this ratio is always less than $[C_3H_6]/[C_6H_{14}]$, it has a value greater than the value obtained in the n → π^* photolysis (see Table III). Nevertheless, all the propane has a radical origin since its formation could be totally inhibited by adding oxygen. From the known steady-state concentrations of H· and C_3H_7· in a typical run it could be estimated that the reaction H· +

(34) H. Okabe and J. R. McNesby, *J. Chem. Phys.*, **36**, 601 (1962).

(35) J. A. G. Dominguez, J. A. Kerr, and A. F. Trotman-Dickenson, *J. Chem. Soc.*, 3357 (1962).

(36) J. C. J. Thynne, *Trans. Faraday Soc.*, **58**, 1394 (1962); J. A. Kerr and A. F. Trotman-Dickenson, *J. Chem. Soc.*, 1609 (1960).

(37) A. J. C. Nicholson, *Trans. Faraday Soc.*, **50**, 1067 (1954); J. R. McNesby and A. S. Gordon, *J. Amer. Chem. Soc.*, **80**, 261 (1958); P. Ausloos and E. Murad, *ibid.*, **80**, 5929 (1958).

$C_3H_7\cdot \rightarrow C_3H_8$ was not of sufficient importance to account for the excess propane observed. One possibility is that because a significant fraction of the isopropyl radicals may be formed with high vibrational and/or translational energies (see section 6) a high cross section for hydrogen abstraction by hot isopropyl radicals may be the source of the excess propane. It is known, for example, that the metathesis between D_2 and H_2S and other similar reactions occur with significant probability only when the D_2 is vibrationally excited.[38] Also, translationally excited H atoms are known to have much higher cross sections for displacement and abstraction reactions than have their thermal counterparts.[39] Unfortunately, similar information is not yet available for the reaction of alkyl radicals. Another possible source of propane is the reaction $C_3H_7\dot{N}\text{–}NH(C_3H_7) + C_3H_7\cdot \rightarrow AIP + C_3H_8$.

In summary, the results presented in sections 1–4 indicate that the main aspects of the product pattern in the n $\rightarrow \sigma^*$ photolysis can be accounted for by reactions 6 and 7, together with the subsequent reactions of the H atoms and the methyl radicals formed in these reactions.

(5) *Quantum Yields.* The measurement of the quantum yield of decomposition, Φ_{dec}, for a photolysis wavelength of 200 nm is described in the Experimental Section. The value so obtained was 0.97 ± 0.08. We also report there data showing that Φ_{dec} is insensitive to wavelength in this region. In experiments using the full arc and neutral density filters, we showed that the rate of photolysis was directly proportional to the fraction of light transmitted by the filter, and so we were able to conclude that Φ_{dec} was independent of intensity when the latter was decreased from its normal value (see Experimental Section) to a value at least 200 times smaller. We also found that Φ_{dec} was invariant as we changed the pressure from 0.25 to 400 Torr by adding CO_2 (see Figure 5). We shall discuss the significance of the absence of any pressure effect on Φ_{dec} later. Although the overall decomposition is independent of wavelength in the n $\rightarrow \sigma^*$ region the same is not true for the product composition. We now discuss a possible model to explain these effects.

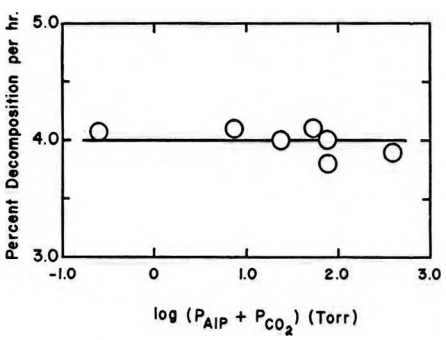

Figure 5. Rate of AIP decomposition *vs.* pressure for photolysis of AIP. In all experiments P_{AIP} = 0.25 Torr and the light intensity was constant.

(6) *Pressure and Wavelength Dependence of Products.* If excess propylene and ethylene are produced by reactions 6 and 7, then the rate of production of excess propylene is given by

$$R_{C_3H_{6xs}} = \sum_i \frac{k_6(E_i)}{k_6(E_i) + k_7(E_i) + \omega(p)} R_{C_3H_7}(E_i)$$

where $R_{C_3H_7}(E_i)$ is the rate of production of isopropyl radicals with energy E_i and $k_6(E_i)$ and $k_7(E_i)$ are the rate constants for reaction of radicals with energy E_i. $\omega(p)$ is taken to be the collision frequency; that is, every collision is assumed to be deactivating. Two isopropyl radicals are formed for the decomposition of every AIP molecule, and since $\Phi_{dec} = 1.0$, $2I_{abs} = \Sigma_i R_{C_3H_7}(E_i)$. Thus

$$\frac{[C_3H_6]_{xs}}{2\Delta[AIP]} = \sum_i \frac{k_6[E_i)}{k_6(E_i) + k_7(E_i) + \omega(p)} f(E_i) \quad (21)$$

where $f(E_i)$ equals $R_{C_3H_7}(E_i)/\Sigma_i R_{C_3H_7}(E_i)$ and therefore gives a measure of the spread of energies with which the radicals are formed. Similarly

$$\frac{[C_2H_4]}{2\Delta[AIP]} = \sum_i \frac{k_7(E_i)}{k_6(E_i) + k_7(E_i) + \omega(p)} f(E_i) \quad (22)$$

Lifetime and rate constants may be determined using the RRMK equation[40]

$$\frac{1}{\tau(E_i)} = k(E_i) = A\left(\frac{E_i - E^0 + a^+E_{zp}^+}{E_i + aE_{zp}}\right)^{s-1} \quad (23)$$

In this expression, a^+ and a may be obtained by the methods given by Whitten and Rabinovitch,[41] s is the total number of vibrational modes, E^0 is the critical energy and is equated with the high-pressure activation energy, while A is identified with the frequency factor. E_{zp} and E_{zp}^+ are the zero-point energies of the normal molecule and of the activated complex, respectively. Again, methods have been reported for estimating these values.[42] For A_6 and E_6^0, we used the values 10^{14} sec^{-1} and 41 kcal mol^{-1} which is close to the average of the experimental values and the values calculated by Frey and Walsh.[15] As was pointed out in the Introduction, there is considerable uncertainty about the values for A_7 and E_7^0. We find that our data are best fitted by $A_7 = 10^{14}$ sec^{-1} and $E_7^0 = 46$ kcal mol^{-1} which are in good agreement with the values calculated by Frey and Walsh. This high activation energy also indicates why Falconer, *et al.*,[14] could not

(38) A. Burcat, A. Lifshitz, D. Lewis, and S. H. Bauer, *J. Chem. Phys.*, **49**, 1449 (1968).

(39) R. Wolfgang, *Progr. React. Kinet.*, **3**, 99 (1965).

(40) D. W. Setser, B. S. Rabinovitch, and E. G. Spittler, *J. Chem. Phys.*, **35**, 1840 (1961).

(41) G. Z. Whitten and B. S. Rabinovitch, *ibid.*, **38**, 2466 (1963).

(42) S. W. Benson, "Thermochemical Kinetics," Wiley, New York, N. Y., 1968, p 30 ff.

observe (7). The reaction used by them to generate vibrationally excited isopropyl radicals was $H\cdot + C_3H_6 \rightarrow C_3H_7\cdot$ which is exothermic by only 39.7 kcal mol^{-1}.

The various models used to generate functions for $f(E_i)$ *vs.* E_i have been summarized by Cadman, *et al.*[5] Following these authors and considering the reaction $ABC^*(E_{vib}) \rightarrow A + B + C$, we write

$$F(E_i, E_j, E_k) = \frac{N_A(E_i)N_B(E_j)N_C(E_k)}{\sum_{E_i}\sum_{E_j} N_A(E_i)N_B(E_j)N_C(E_k)} \quad (24)$$

for the fraction of the processes which produce A with energy E_i, B with energy E_j, and C with energy E_k. N_A, N_B, and N_C are the energy level densities of the A, B, and C parts of ABC. E_i, E_j, and E_k are subject to the restriction $E_i + E_j + E_k = E_{vib}$. E_{vib} is the total vibrational energy which is free to be distributed amongst the vibrational modes. We may expect, if dissociation occurs from state D, that

$$E_{vib} < h\nu - E_D^0 \quad (25)$$

where $h\nu$ is the photon energy and E_D^0 is the critical energy for dissociation from state D. The less than sign follows because some of the excitation energy may ultimately go into E_{trans} and E_{rot}, the exact amount depending upon the detailed kinematics of the dissociation process.

The fraction of reactions which produces A with a specific energy E_i is

$$f_A(E_i) = \frac{N_A(E_i)\sum_{E_j} N_B(E_j)N_C(E_k)}{\sum_{E_i}\sum_{E_j} N_A(E_i)N_B(E_j)N_C(E_k)}$$

The energy level density N is calculated using the semiclassical expression

$$N(E) = \frac{(E + E_{zp})^{s-1}}{\Gamma(s)\prod_i^s h\nu_i}$$

In the model we let $S_A = S_C$ = the number of vibrational modes of the isopropyl radical, while we took S_B = the number of modes of AIP $- (S_A + S_C)$. That is, S_B, besides including an N=N stretching mode, includes vibrations that ultimately go into translation and rotation. We took $E_{zp}(A) = E_{zp}(C) = 54$ kcal mol^{-1} and $E_{zp}(B) = 25$ kcal mol^{-1}. $f(E_i)$ curves for isopropyl radicals for different values of E_{vib} are shown in Figure 6. In particular one should observe the wide dispersion of energies predicted from the model. If we consider the reaction as occurring in a stepwise fashion, $ABC^* \rightarrow AB + C \rightarrow A + B + C$, then the energy dispersion curves $f_A(E_i)$ and $f_C(E_k)$ are no longer identical, but the overall dispersion is quite similar to that obtained for the concerted rupture. In Figures 7 and 8 we compare the experimental results with the calculated functions using the above model.

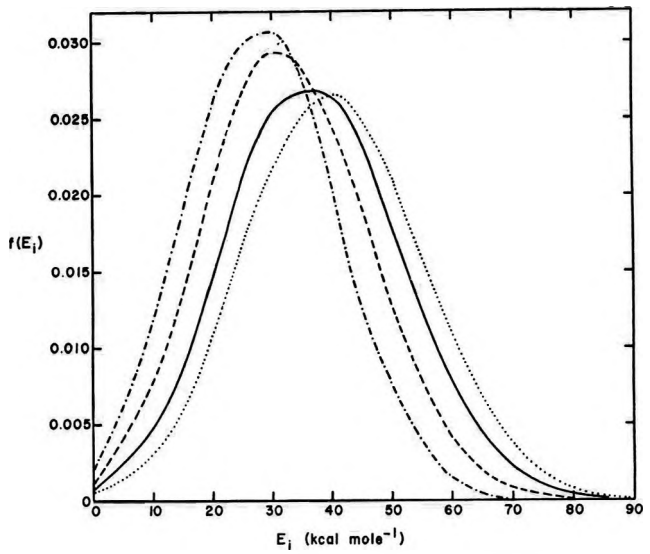

Figure 6. Dispersion of vibrational energies for isopropyl radicals formed in photolysis of AIP. $f(E_i)dE_i$ is the probability of producing a radical in the energy range $(E_i, E_i + dE_i)$. The total vibrational energies E_{vib} are (. . . .) 100, (——) 90, (- - -) 80, and (-·-·) 70 kcal mol^{-1}.

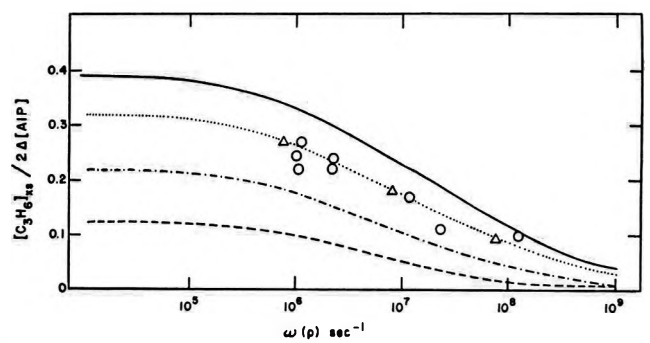

Figure 7. Variation in the yield of excess propylene with collision frequency. The curves are generated using the model discussed in the text: (○) experimental points, (△) values calculated allowing for nonmonochromaticity of source (see text); calculated curves for E_{vib} = 100 (——) 90 (· · · ·), 80 (-·-·), 70 kcal mol^{-1} (- - -). 1 Torr of AIP corresponds to a collision frequency, $\omega(p)$, of 1.64×10^7 sec^{-1}.

The wavelength 195 nm corresponds to a photon energy of 147 kcal $einstein^{-1}$, while the activation energy, $E_{S_0}^0$, for the thermal decomposition of ground state AIP is 41 kcal mol^{-1}.[43] Therefore, if photodecomposition does occur from S_0^{vib}, we may expect from eq 25, $E_{vib} < (147\text{–}41)$ kcal mol^{-1}. On the other hand, if, for example, dissociation occurred from T_1 we would have the uncertainty of not knowing $E_{T_1}^0$, the critical energy of dissociation from this state. In Figure 9 we plot the ratio $[C_2H_4]/[C_3H_6]_{xs}$ as a function of the collision frequency. The fact that the calculated

(43) G. Geiseler and J. Hoffmann, *Z. Phys. Chem.* (*Frankfurt am Main*), 57, 318 (1968).

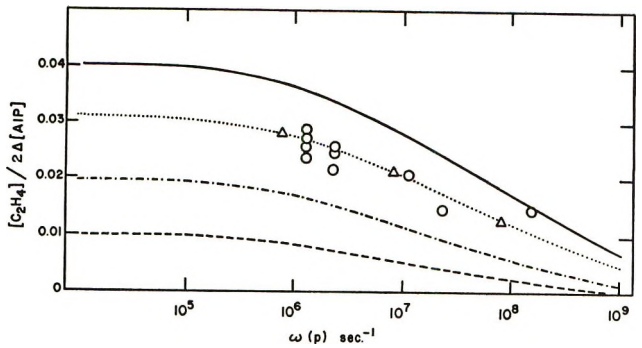

Figure 8. Variation in the yield of ethylene with collision frequency. The symbols have the same meanings as those in Figure 7.

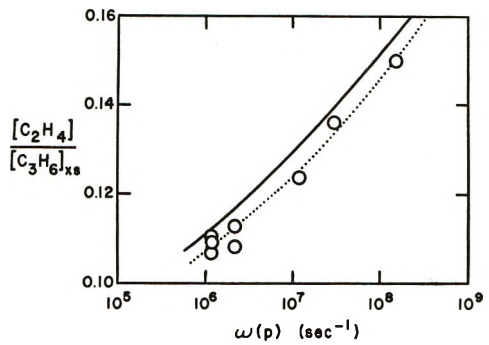

Figure 9. Variation in the ratio of ethylene to excess propylene with collision frequency: (O) experimental points; calculated curves for E_{vib} = 100 kcal mol^{-1} (——), 90 kcal mol^{-1} (· · · ·).

values increase with increasing frequency stems directly from the choice $E_7^0 > E_6^0$, and the good agreement with experiment is further evidence that the activation energy of reaction 7 cannot be less than that of reaction 6.

Corresponding to the different gaseous olefin filters, we have different "effective" photolysis wavelengths and hence possibly different values of E_{vib}. In Figures 10 and 11 we have plotted $[C_3H_6]_{xs}/2\Delta[AIP]$ and $[C_2H_4]/2\Delta[AIP]$ against the photon energy for the different filters. The full-line curve is that calculated by setting E_{vib} = 90 kcal mol^{-1} for λ_{eff} 195 nm, while the dashed curve is obtained by setting E_{vib} = 100 kcal mol^{-1} for the same wavelength.

Because of the very wide dispersion in energy of the radicals, the fact that nonmonochromatic light was used has little effect on the results. In Figures 7 and 8 we have also shown the results when allowance was made for nonmonochromaticity. This was done by weighting the $f(E)$ curves for E_{vib} = 100, 90, and 80 kcal mol^{-1} by the appropriate values of $I(\bar{\nu})P_{azo}(\bar{\nu})$ at 182, 195, and 208 nm, respectively, and generating a new $f[E]$ curve. It can be seen that the results do not differ significantly from those assuming monoenergetic excitation.

There remains a puzzling aspect of the pressure-dependence studies. Exactly the same effects as are

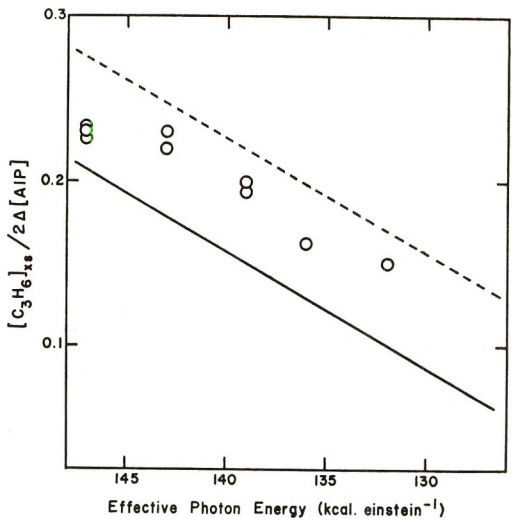

Figure 10. Variation in the yield of excess propylene *vs.* photon energy. The AIP pressure was kept constant at 0.25 Torr: (O) experimental points. The full and dashed lines were calculated by setting E_{vib} = 90 and 100 kcal mol^{-1}, respectively, when the effective photolysis wavelength was 195 nm (147 kcal einstein^{-1}).

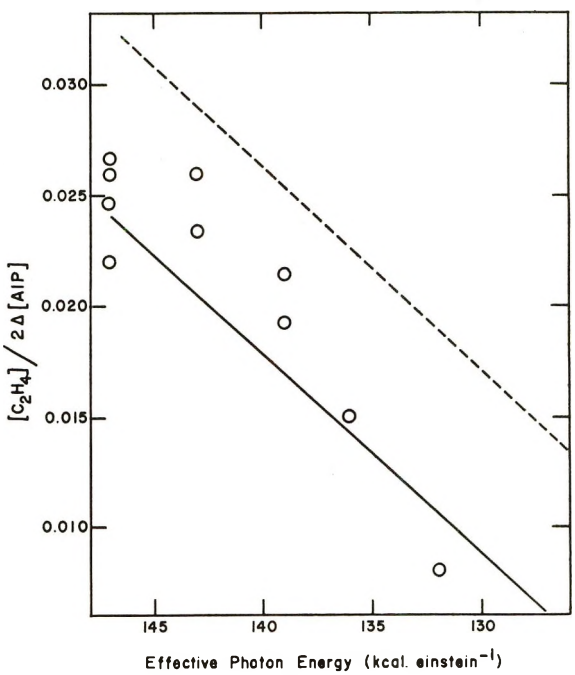

Figure 11. Variation in the yield of ethylene *vs.* photon energy. The symbols have the same meanings as those in Figure 10.

caused by varying the AIP pressure can be produced by using a constant AIP pressure and varying the pressure of CO_2 which acts as an "inert" gas. However, when the deactivation efficiency is estimated on a per collision basis, it turns out that CO_2 is only 0.04 times as effective as AIP. From previous work, one might have expected a value almost 10 times greater.[44]

(44) B. Stevens, "Collision Activation in Gases," Pergamon Press, Oxford, 1967, Chapter 6; G. H. Kohlmaier and B. S. Rabinovitch, *J. Chem. Phys.*, 38, 1709 (1963).

(7) *The Dissociative State.* In the previous section we saw that the data were consistent witn isopropyl radicals being formed with a mean energy of ~35 kcal mol^{-1} and a significant energy spread (σ ~40 kcal mol^{-1}). Also, the data were not inconsistent with decomposition originating from the ground state. If the bulk of the dissociation in the photolysis of AIP does occur from S_0^{vib}, then it should be possible to estimate, using unimolecular theory, the lifetime of the parent AIP molecule. One complication is that because of cis–trans isomerization[17,45] dissociation could originate from both *trans*-AIP (S_0^{vib}) and *cis*-AIP-(S_0^{vib}). Preliminary evidence indicates that, for a given excess energy, the trans isomer has the longer lifetime.[46] We may use a formula such as eq 23 to estimate the lifetime of *trans*-AIP(S_0^{vib}). For E_t = 80.5 kcal mol^{-1} (n $\rightarrow$ π^* excitation), we get τ_{trans} = 0.2 $\times$ 10^{-6} sec.[47] However, the variation in Φ_{dec} with pressure does not indicate such a long-lived species.[46,48] The data indicate that the longest lived species in the n $\rightarrow$ π^* photolysis of AIP has a lifetime of about 0.8 $\times$ 10^{-9} sec. Moreover, from the observed curvature of the $1/\Phi_{dec}$ *vs.* pressure plot it may be inferred that species with a range of lifetimes are involved.[48] In their study of the photolysis of azoethane, Worsham and Rice[49] were also unable to rationalize their Φ_{dec} data in terms of decomposition from the ground state, and Wu and Rice[48] observed curvature in the $1/\Phi_{dec}$ *vs.* pressure plots for the photodecomposition of hexafluoroazomethane. Of course, there is always the possibility that the formula given in eq 23 is not valid for representing the lifetimes of vibrationally excited azoalkanes, which would occur, for example, if the energy was not randomized before dissociation, or, if the formula is valid, that we have not chosen the correct values of the parameters A, E_0, a, a^+, E_{zp}, and $E_{zp}{}^+$.

In the same vein, we find that for E_t = 147 kcal mol^{-1} (λ_{irr} 195 nm), τ_{trans} = 3.5 $\times$ 10^{-9} sec. But, as can be seen from Figure 5, we were unable to detect any diminution of the decomposition rate up to pressures for which the time between collisions was 1.0 $\times$ 10^{-10} sec. Thus, although the data do not fit well with dissociation occurring from S_0^{vib}, the evidence for dissociation from another state is really by default. The observation of cis–trans isomerization certainly indicates that triplet states are involved in the overall photochemistry, but these need not be the states from which dissociation occurs, and we know so little about the properties of the upper states that we cannot apply any meaningful tests to the data except to rule out dissociation from S_1.[17,18]

The lack of pressure dependence for Φ_{dec} obtained for n $\rightarrow$ σ^* excitation, as opposed to the observed dependence for n $\rightarrow$ π^* excitation, indicates that in the former case the dissociative lifetime is considerably shorter. Therefore, if dissociation originates from a common state(s), its lifetime must decrease markedly as the vibronic energy is increased. Even for irradiation in the n,π^* band, Worsham and Rice[49] found that the lifetime of the dissociative state decreased by a factor of 2 as the exciting wavelength was decreased from 378 to 352. In principle, by carrying out very careful quantum yield measurements of all the processes involved in the photochemistry of both the cis and the trans isomers, it should be possible to resolve some of these problems and to make a more definite statement as to the nature of the dissociative state. We shall report on these studies later.[46]

Acknowledgment. We are grateful to the National Science Foundation (Grant GP-18808) for support of this work.

(45) R. F. Hutton and C. Steel, *J. Amer. Chem. Soc.*, **86**, 745 (1964).

(46) A. Rennert and C. Steel, unpublished results; ref 17 is a preliminary communication on the subject.

(47) The values of A and E_0 were taken from ref 42, *viz.*, 0.5 $\times$ 10^{14} sec^{-1} and 40.8 kcal mol^{-1}, E_{zp} and $E_{zp}{}^+$ were assigned the values 130 and 127 kcal mol^{-1} and a and a^+ the values 0.95 and 0.90.

(48) E. C. Wu and O. K. Rice, *J. Phys. Chem.*, **72**, 542 (1968).

(49) W. C. Worsham and O. K. Rice, *J. Chem. Phys.*, **46**, 2021 (1967).

Competitive Thermal Unimolecular Reactions of *trans*-Cyclopropane-d_2. Collisional Energy Transfer[1a]

by E. V. Waage[1b] and B. S. Rabinovitch*[1c]

Department of Chemistry, Illinois State University, Normal, Illinois 61701 and Department of Chemistry, University of Washington, Seattle, Washington 98195 *(Received January 3, 1972)*

Publication costs assisted by the National Science Foundation

trans-Cyclopropane-d_2 isomerization has been studied at low pressure as an example of a thermal, collisionally activated, competitive unimolecular reaction system. The competitive structural and geometric isomerizations have been studied in a 230-l. reactor at 480° in the pressure range near 10^{-3} Torr. At the lowest pressure, the ratio of the geometric to structural rate constant, k_g/k_p, declines to $k_g/k_p \simeq 7$. The fall-off behavior is in good agreement with earlier work at higher pressures. In the presence of He bath gas, k_g/k_p is 10% higher than for the pure substrate, when compared at identical values of k_p. At low pressures the relative amounts of the competing structural and geometric processes can provide information about vibrational energy transfer on collision, although this particular system has some limitations. The kinetic expressions for this complex, reversible isomerization system are formulated. Strong collider RRKM calculations are presented.

Introduction

Information about vibrational energy collisional transfer probabilities has been derived recently from inert gas studies in thermal unimolecular reactions. Relative efficiencies of various inert activators have been measured and correlated with molecular parameters; some information regarding the form of the transition probabilities has also been obtained.[2] A feature which limits the power of this method is the requirement for an independent measurement of collision cross sections.[3]

One technique which can circumvent this requirement involves the study of a unimolecular reaction which can proceed by two or more different reaction channels having different critical energies. At low pressures, the relative amounts of reactant molecules which have been collisionally excited to the various levels above the several critical threshold energies may be determined by measuring the relative rates of product formation. Quantitative information about the collisional transition probabilities can be obtained with use of a stochastic model. An unsuccessful illustration of such an experiment was first given by Chow and Wilson.[4]

We have applied the technique to the isomerization of *trans*-cyclopropane-d_2 to give the *cis* isomer (reversibly) and propylene (irreversibly). The competitive reaction has been characterized earlier in this laboratory at pressures down to 0.3 Torr where analytical difficulties were encountered.[5a] It is desirable, however, to obtain results at much lower pressure so that the reaction is closer to the limiting low pressure second-order region. In the present work, rate constants were measured to pressures of 10^{-3} Torr in a 230-l. vessel. Below this pressure, collisions with the wall became important.

Results are reported for both pure cyclopropane-d_2 and for He added as an inert activator. As will be shown, this system is not an ideal one for the intended purpose, but the results do yield qualitative information and insights into the nature of collisional excitation and vibrational energy transfer processes.

Experimental Section

Materials. Cyclopropane-d_2 was the same as that used previously;[5a] its composition was 94% *trans*-cyclopropane-d_2 (T) and 6% *cis*-cyclopropane-d_2 (C); 6% cyclopropane-d_1 was present but did not interfere. The freeze–pump–thaw method was used to remove traces of air and a distillation from a Dry Ice–acetone bath removed traces of water and mercury. Chromatographic analysis revealed that propylene was present at 5 ppm and other impurities at ~60 ppm.

Helium was Airco assayed reagent and was used without further purification.

Cyclopropane was Matheson tank grade quality and was used only for seasoning the vessel and for calibrating the gas chromatograph. Gas chromatographic

(1) (a) This work was supported in part by the National Science Foundation. (b) Illinois State University. (c) University of Washington.

(2) Y. N. Lin and B. S. Rabinovitch, *J. Phys. Chem.*, **72**, 1726 (1968).

(3) S. C. Chan, J. T. Bryant, L. D. Spicer, and B. S. Rabinovitch, *ibid.*, **74**, 2058 (1970).

(4) N. Chow and D. J. Wilson, *ibid.*, **66**, 342 (1962).

(5) (a) E. W. Schlag, Ph.D. Thesis, University of Washington, 1958; E. W. Schlag and B. S. Rabinovitch, *J. Amer. Chem. Soc.*, **82**, 5996 (1960). (b) This equation differs by the quantity $-k_p$, from ref 5a. This difference would affect the values of k_g in ref 5a by only 5%.

analysis revealed traces of impurities. After outgassing by the freeze–pump–thaw method, it was used without further purification.

Propylene was Phillips research grade and was used for standardizing the gas chromatograph. It was purified and checked in the same manner as for cyclopropane-d_0.

Apparatus and Method. A conventional vacuum rack was employed for gas handling. Mercury was excluded from the system. The vacuum system was pumped by an oil diffusion pump. Rate measurements were made in a static 230-l. Pyrex spherical reactor which was heated in a stirred air furnace. The temperature was measured with eight calibrated chromel–alumel thermocouples. The average thermal gradient was ±0.4° at 480°. The temperature was constant to ±0.2° during the course of a run. The reactor was connected to the rest of the system by a gallium cut-off valve.

We encountered a problem of water outgassing from the walls of the vessel at 480°. This general phenomenon was first called to our attention by D. F. Swinehart.[6] It was overcome by exposing the vessel to a cryogenic trap at −105° in order to freeze out water vapor during a run, while still leaving the reactants and products uncondensed at the low reaction pressures used.

The reactor was pumped with an ion pump and a molecular sieve 5-A cryogenic pump cooled with liquid nitrogen. The vessel was pumped to a nominal pressure of 2×10^{-7} Torr before each run, as measured on the ion pump. Large diameter tubing (32 and 60 mm) led from the vessel to the pumps. Dead space was 3.3 l.

A sample was measured out and admitted to the vessel with the cryogenic trap in place. Reaction times varied between 1 and 18 hr. The cryogenic trap was then replaced with liquid nitrogen to trap the reaction mixture. The pressure in the vessel was checked with a Hastings gauge to ensure that trapping had been complete. Products were transferred to a sample tube containing glass beads and were mechanically mixed to cancel the effects of fractionation. Aliquots were taken for gas chromatographic analysis and the bulk of the sample was transferred to a microcell for the ir analysis.

Analysis. Propylene and cyclopropane-d_2 were analyzed by gas chromatography with a flame detector. The column was 15% dinonyl phthalate on 50-mesh acid-washed firebrick. T and C have almost identical retention times and the sum of the two was found. The error was ±1%.

The ratio of cis- to trans isomers was determined with a Beckman IR-5 spectrometer furnished with a beam condenser and a microcell of volume 0.05 cm³. The error was ±2–5% depending on the amount of sample.

Results

Derivation of Rate Constants. The reaction scheme is

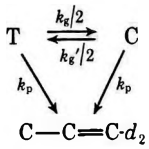

Since both *trans*- and *cis*-cyclopropane-d_2 yield propylene with the same[5a] rate constant k_p, the structural isomerization can be treated independently of the geometric isomerization. Then, $k_p = dP/dt\ 1/(T + C)$, where P is propylene-d_2 and concentrations of the species are implicit in these rate expressions. Since[5a] $k_g = k_g'$, then

$$\frac{dT}{dt} = -k_g(T - C)/2 - k_pT$$

and

$$\frac{dC}{dt} = k_g(T - C)/2 - k_pC$$

By subtraction[5b]

$$k_p + k_g = -\frac{d(T - C)}{dt}\frac{1}{(T - C)}$$

Treatment of the Data. The constant k_p is given by the usual first-order expression. For k_g, the integrated rate expression is

$$k_g = 2.303t^{-1} \log [(T - C)_0/(T - C)_t] - k_p$$

All rate constants were corrected to a common temperature of 476° with an Arrhenius activation energy of 60 kcal mol^{-1}.[5a] A dead space correction of 1.4% was not made since only relative rates were needed.

Rate Data. The range of pressure over which the reaction could be studied without added inert gas was restricted. Pressures above 3×10^{-3} Torr required excessive amounts of a limited supply of T, while at pressures below 10^{-3} Torr collisions with the wall predominated. With helium added, the partial pressure of T was maintained between 1.7×10^{-4} and 1.1×10^{-3} Torr while the partial pressure of He was varied between 1.9×10^{-2} and 3.7 Torr.

Experimental values of k_g and k_p are shown in Figure 1. The leveling off of k_g and k_p below 10^{-3} Torr for the pure substrate reflects heterogeneous wall effect. The wall can collisionally activate the molecules[7] but may also catalyze the reaction. Measurements in the lowest pressure region were also affected by the largest experimental error.

The mole ratio of He to cyclopropane-d_2 ranged between 46 and 3340 with a median around 130. On a

(6) D. F. Swinehart, private communication.

(7) K. M. Maloney and B. S. Rabinovitch, *J. Phys. Chem.*, **72**, 4483 (1968).

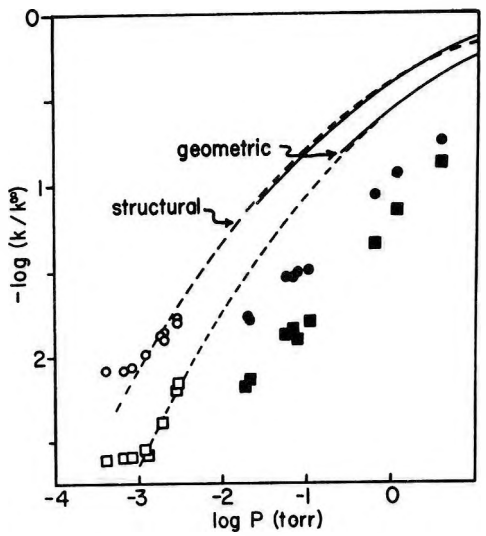

Figure 1. A comparison of theoretical and experimental fall-off data: ○, k_p; □, k_g for pure cyclopropane-d_2; ●, k_p; ■, k_g with He added. Dotted lines are theoretical curves; solid lines are best lines through the results in ref 5a.

collision basis,[8] this median dilution rises to ~200 if cross sections used previously are employed. From calculational studies[9] on collisional energy transfer at low pressure, it is known that the above dilution corresponds in practice to the infinite dilution case even though, as is shown below, He is $\sim 1/25$ as efficient as cyclopropane.

The ratio k_g/k_p is shown in Figure 2 as a function of k_p/k_p^∞ for both cyclopropane-d_2 and He activation. The curves are taken from the best lines through the data of Figure 1. In the region of overlap between the curves, the ratio k_g/k_p is 10% higher for He.

Relative Efficiency of He on a Conventional Basis. The average relative efficiency, $\bar{\beta}_p$, of He on a conventional pressure basis[2,8] is $\bar{\beta}_p \simeq 0.05$. This value compares with an earlier result of $\bar{\beta}_p = 0.060$ for k_p with light cyclopropane[10] which was obtained at much larger values of k_p/k_p^∞. The average relative efficiency on a collision basis[8] is $\bar{\beta}_c \simeq 0.037$.

Discussion

Interpretation of Results. The results shown in Figure 2 indicate that at $k_p/k_p^\infty = 2 \times 10^{-2}$, $k_g/k_p \simeq 9$ for cyclopropane-d_2 as the heat bath molecule, and $k_g/k_p \simeq 10$ for He. This represents a decline from a high pressure value[5a] of 24. The decline is qualitatively correct but is less than anticipated, as based on the degree of fall-off and the reported[5a] activation energy difference between the geometric and structural reactions, $E_A{}^p - E_A{}^g = 1$ kcal mol^{-1}; for a critical energy difference, $\Delta E_0 = E_0{}^p - E_0{}^g = 1$ kcal mol^{-1}, the calculations described below predict that for a strong collider $k_g/k_p = 1.0$ at $k_p/k_p^\infty = 2 \times 10^{-2}$. A larger ΔE_0 is therefore indicated.

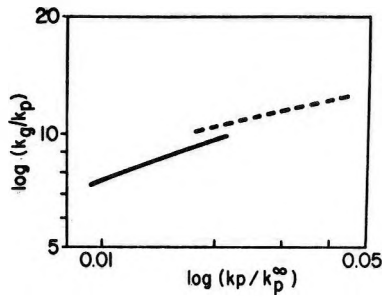

Figure 2. Plot of log (k_g/k_p) *vs.* log (k_p/k_p^∞). The lines represent the smoothed data of Figure 1; the dashed line is helium data and solid line is pure cyclopropane-d_2 data.

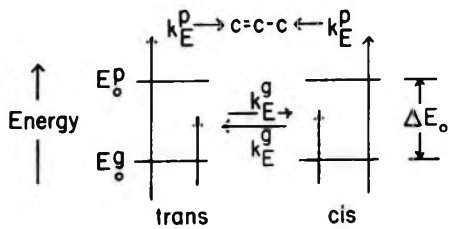

Figure 3. Schematic energy level relationships with activation to regions above $E_0{}^g$ and $E_0{}^p$, reversible geometric isomerization below $E_0{}^p$, and essentially irreversible structural isomerization above $E_0{}^p$.

This reaction system does not fully satisfy the requirement of two competitive reaction channels which each deplete the population of excited molecules. In the second-order region, all reactant molecules which are collisionally activated above $E_0{}^p$ decompose to give propylene, while those which are activated to the region $E_0{}^g$ to $E_0{}^p$ give only cis–trans isomerization (Figure 3). The depletion of excited molecules due to the structural reaction is independent of the cis–trans reaction which affects the difference $(T - C)$ but not $(T + C)$. Nonetheless, this system provides a crucial result: that k_g/k_p is larger for He than for cyclopropane-d_2 as the heat bath molecule, at the same values of k_p/k_p^∞; this last condition means that the net reaction flux (k_p) of molecules above $E_0{}^p$ is the same for both cases. How can this behavior be interpreted?

Since He is 25 times less efficient than cyclopropane-d_2, the weak collider population destribution curve above a reaction threshold declines relatively faster than for a strong collider. It follows that the average energy of reacting molecules $\langle E_{react} \rangle$ is smaller[9] for the weaker collider and the reactant population at threshold $E_0{}^p$ is higher in this case, *for identical values of* k_p. Steady-state population functions of molecules above each of the critical energies (Appendix I) are sketched

(8) F. J. Fletcher, B. S. Rabinovitch, K. W. Watkins, and D. J. Locker, *J. Phys. Chem.*, **70**, 2823 (1966).

(9) D. C. Tardy and B. S. Rabinovitch, *J. Chem. Phys.*, **45**, 3720 (1966); **48**, 1282 (1968).

(10) H. O. Pritchard, R. G. Sowden, and A. F. Trotman-Dickinson, *Proc. Roy. Soc. Ser. A*, **217**, 563 (1953).

in Figure 4 for both a stronger collider (sc) and a weaker collider (wc). The value of k_g for pure cyclopropane-d_2 is smaller, relative to He, since the steady-state population difference curve for the stronger collider cuts across the interval E_g^0 to E_p^0 and extends more strongly above E_0^p; of course, the shaded area so designated in Figure 4 cannot contribute to k_g^{sc} since only structural isomerization product can be isolated above E_0^p (in the low-pressure limit). Thus $k_g^{sc} < k_g^{wc}$, for $k_p^{wc} = k_p^{sc}$, as observed.

Calculations. The ratio k_g/k_p was calculated with use of RRKM theory (Appendix I). The models for the activated complex and the molecule are given in Appendix II. Initially, calculations were made with $\Delta E_0 = 0.9$ kcal mol^{-1}, but a low ratio of $k_g/k_p = 1.0$ at $k_p/k_p^\infty = 2 \times 10^{-2}$ resulted. Then E_0^g was lowered by 2.8 kcal mol^{-1}, or $\Delta E_0 = 3.7$ kcal mol^{-1}, and the resulting ratio becomes $k_g/k_p = 9$; since lowering E_0^g must not alter the observed geometric rate constants, k_g^∞ was kept constant by tightening the activated complex, *i.e.*, decreasing the preexponential factor tenfold.

A good fit was also obtained between the experimental data for the pure cyclopropane-d_2 system and the strong collider theoretical curves as shown in Figure 1. The curves were displaced 0.5 log unit to lower pressure to match the experimental falloff. Thus, the competitive rate expressions developed in Appendix I provide a reasonable explanation of the results.

Conclusions

This reaction system has provided some qualitative results concerning the efficiency of a weak collider as opposed to a strong collider. It also appears that the critical energy difference for the geometric and structural isomerizations may be somewhat larger than previously reported.

Finally, this work demonstrates that activation competitive reactions can yield novel information about collisional energy transfer as compared with conventional single channel unimolecular reactions.

Appendix I

Derivation of the Ratio k_g/k_p for a Strong Collider Bath Gas. The simple phenomenological reaction expression described in the text for k_g is derived here in terms of the microscopic rate constants. The same assumptions are made as in the Lindemann–RRK theory.[11] The development given here is an extension of the RRKM[12] formulation to the case of a reversible reaction with a competing irreversible reaction.

The populations of cyclopropane-d_2 molecules are divided up into discrete states by an imposed scheme of graining. Consider a normalized vector of such states which are in complete equilibrium, $\mathbf{N}^{eq}$. Let n_i^{eq} be an element of that vector which is the number of T and C molecules at energy i. Since T and C have almost identical thermodynamic properties,[13] it may

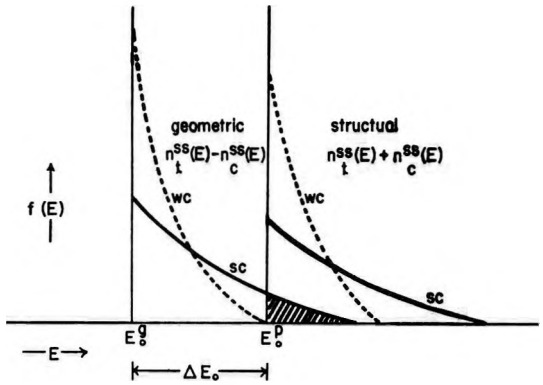

Figure 4. Schematic diagram of the depletion of states above the critical energies for a weak collider and a strong collider. f(E) is the steady-state distribution function and is proportional to steady-state quantities, expressions for which are derived in Appendix I. For geometric isomerization f(E) represents $(n_t^{ss}(E) - n_c^{ss}(E))$; for structural isomerization f(E) represents $(n_t^{ss}(E) + n_c^{ss}(E))$.

be assumed that the fractions of n_i^{eq} for both isomers are identical. Consider a mixture of T and C in thermal, but not chemical equilibrium, and define $n_{ti}^{eq} = [T/(T + C)]n_i^{eq}$, and $n_{ci}^{eq} = [C/(T + C)]n_i^{eq}$. Now consider the reaction scheme for the ith level

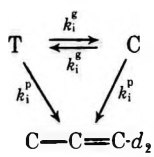

Here k_i is the microscopic geometric rate constant at energy i and k_i^p is the corresponding structural quantity. With the strong collision steady-state assumption, then

$$\frac{dn_{ti}^{ss}}{dt} = \omega n_{ti}^{eq} - k_i^g n_{ti}^{ss} + k_i^g n_{ci}^{ss} - k_i^p n_{ti}^{ss} - \omega n_{ti}^{ss} = 0$$

$$\frac{dn_{ci}^{ss}}{dt} = \omega n_{ci}^{eq} - k_i^g n_{ci}^{ss} + k_i^g n_{ti}^{ss} - k_i^p n_{ci}^{ss} - \omega n_{ci}^{ss} = 0$$

where ss denotes steady-state quantities and ω is the specific collision rate and is independent of energy i.

On subtraction and gathering terms

$$(n_{ti}^{ss} - n_{ci}^{ss}) = \frac{\omega}{2k_i^g + k_i^p + \omega}(n_{ti}^{eq} - n_{ci}^{eq})$$

(11) L. S. Kassel, "Kinetics of Homogeneous Gas Reactions," Chemical Catalog Co., New York, N. Y., 1932.

(12) R. A. Marcus, *J. Chem. Phys.*, **20**, 359 (1952); **43**, 2658 (1965).

(13) There are two optical isomers of *trans*-cyclopropane-d_2, each with a symmetry number of 2, so that these statistical factors cancel for a racemic mixture; for the cis isomer, there is no optical activity and the symmetry number is 1. The experimental equilibrium constant between cis and trans isomers is unity (see ref 5a).

Let $n_i^{ss} = n_{ti}^{ss} + n_{ci}^{ss}$; then $dn_i^{ss}/dt = \omega n_i^{eq} - k_i^p n_i^{ss} - \omega n_i^{ss} = 0$, and $n_i^{ss} = \omega n_i^{eq}/(\omega + k_i^p)$. The total rate of structural isomerization is

$$R_p = k_p(T + C) = \sum_i \frac{\omega k_i^p}{\omega + k_i^p} n_i^{eq}$$

The net geometric isomerization rate of T is the sum of the rate of deactivation of C product molecules and the rate of propylene production from excited C molecules, and corrected for the activation flux of stable C molecules. Then

$$R_g = {}^1/_2 k_g(T - C) = \sum_i (\omega n_{ci}^{ss} + k_i^p n_{ci}^{ss} - \omega n_{ci}^{eq})$$

and, on simplification

$$= \sum_i \frac{\omega k_i^g (n_{ti}^{eq} - n_{ci}^{eq})}{(1 + k_i^p/\omega)(\omega + 2k_i^g + k_i^p)}$$

Consider three limiting cases: (a) $k^p \to 0$ (which is the usual reversible rate equation)

$$R_g = \sum_i \frac{\omega k_i^g (n_{ci}^{eq} - n_{ci}^{eq})}{\omega + 2k_i^g}$$

(b) $\omega \to \infty$, which is the same limit for all $k^p \geq 0$

$$R_g = \sum_i k_i^g (n_{ti}^{eq} - n_{ci}^{eq})$$

(c) $\omega \to 0$

$$R_g = \sum_i \frac{\omega^2 k_i^g (n_{ti}^{eq} - n_{ci}^{eq})}{k_i^p (2k_i^g + k_i^p)}$$

which depends on ω^2 as opposed to ω.

In terms of the experimental rate constant

$$k_g = \frac{2R_g}{(T - C)} = \sum_i \frac{2k_i^g \omega (n_{ti}^{eq} - n_{ci}^{eq})(T - C)^{-1}}{(2k_i^g + k_i^p + \omega)(1 + k_i^p/\omega)}$$

and for continuous summation

$$k_g = \int_{E_0^g}^{\infty} \frac{2k_E^g \omega B(E)\, dE}{(2k_E^g + k_E^p + \omega)(1 + k_E^p/\omega)}$$

where $B(E)$ is the Boltzmann distribution function and k_E^g and k_E^p are the geometric and structural RRKM microscopic rate constants at energy $E = E^+ + E_0^g$. Since $E_0^p > E_0^g$, then $k^p = 0$ for $E^+ < E_0^p - E_0^g$.

In the above usage, k_E^g is the net microscopic rate constant for trans to give cis and, for a ring opening mechanism, is half the rate of such openings.

Appendix II

Vibration Frequency Assignments. There are three activated complex models for three possible reactions: (a) geometric isomerization; (b) structural isomerization with H transfer as the reaction coordinate; (c) same as (b) but with D transfer. The frequencies (in cm^{-1}) and degeneracies (in brackets) are listed in Table I.

Table I

Molecule	Activated complex		
	Geometric	Structural-H	Structural-D
3073 (4)	2973 (4)	3040 (3)	3050 (4)
2223 (2)	2160 (4)	2206 (2)	2190 (1)
1268 (5)	1260 (4)	1230 (5)	1230 (5)
1001 (4)	869 (5)	880 (3)	880 (3)
870 (2)	702 (3)	710 (6)	712 (6)
755 (3)	+ 2 internal rotors	510 (1)	510 (1)
633 (1)			
I_r^+ [a]	3.9	9.68	4.84
d	3	8	4
E_0, kcal mol^{-1}	61.8[b]	62.7	64.0

[a] $I_r^+ = d(I_A{}^+ I_B{}^+ I_C{}^+/I_A I_B I_C)^{1/2}$; d is the reaction path degeneracy, and I^+, I are the moments of inertia of the complex and the molecule along one of the principal axes. [b] For the actual calculation, this value was lowered by 2.6 kcal mol^{-1}.

The Reactions of Electrons in Glycerol

by Takashi Kajiwara and J. K. Thomas*

Department of Chemistry and the Radiation Laboratory,[1] University of Notre Dame, Notre Dame, Indiana 46556
(Received September 13, 1971)

Publication costs assisted by the U. S. Atomic Energy Commission

Nanosecond pulse radiolysis and laser photolysis techniques have been used to study the spectral and kinetic properties of electrons in glycerol. The spectra of solvated electrons show a blue shift with decreasing temperature although a time-dependent spectral shift due to relaxation of the solvent around the electron is not observed as in simpler alcohols. Solutes that react with $k \simeq 10^{10}\ M^{-1}\ \text{sec}^{-1}$ with e_s^- in simple alcohols or water react much more slowly ($\sim 1/40\times$) with e_s^- in glycerol. Decreasing the viscosity of glycerol by addition of water increases the rate constant. The data show that increasing viscosity dramatically reduces the mobility of e_s^- although the correlation is not linear. At high concentrations of acetone the yield of e_s^- is reduced, due to scavenging of the precursor of e_s^- by the solute. There is little effect of temperature from $+32$ to $-197°$ on this process. Cadmium ions also show this effect, while at the same time Cd^+ is produced. A discussion of the above data is presented.

Introduction

Recent pulse radiolysis techniques have enabled the physical chemist to study in detail the reactions and properties of electrons in various solvents. The data and conclusions have been reported in many reviews and a recent book.[2] The electron may be relatively freely bound or quasifree in liquids of low dielectric constant such as alkanes at room temperature,[3] resulting in very high mobilities about 10^4 larger than normal ions in these liquids. In more polar liquids or alkanes at lower temperatures[4] the electron has a mobility more nearly approaching that of a standard ion in these solvents.[2] Here it is suggested that the electron produced by the act of radiolysis loses energy and finally attains thermal equilibrium with the surroundings as a quasifree electron. A chance orientation of the solvent molecules provides a site of lower potential energy for the electron, where it is trapped. Subsequently the strong electric field of the electron orientates the molecules into a more suitable arrangement, deepening the traps and providing a strongly solvated electron in the liquid. These processes probably occur within 10^{-11} sec in a liquid at room temperature, but may be observed in the microsecond time region in liquids at low temperature or in polar glasses at $-197°$.[5]

The solvated electron reacts with many solutes with rate constants approaching a diffusion-controlled limit. Indeed activation energies for the reaction[2] of the hydrated electron with many solutes are about 3.5 kcal, *i.e.*, of the same order as the activation energy for diffusion of a water molecule in liquid water. It has been suggested recently[6] that at high solute concentrations the electron may react with the solute before solvation occurs.

The aim of the present work is to investigate the effect of high viscosities on the above processes; for example, glycerol has a viscosity some 500-fold larger than other alcohols at room temperature. This may affect the absolute rate of reaction of the solvated electron with a solute, if diffusion of the solvated electron is important as indicated above. A slower rate of reaction of the solvated electrons will enable us to work at high solute concentrations and facilitate the observation of the reaction of electrons with the solute prior to solvation.

Experimental Section

Water was triply distilled from a barnsted still, alkaline permanganate, and acid dichromate solutions. Acetone, chloroacetic acid, cadmium sulfate, and perchloric acid were analytical grade quality chemicals; benzyl alcohol was commercial grade and was distilled; glycerol was obtained from J. T. Baker Co. and for some experiments was purified by crystallization[7] and drying. No effect of purification was observed. The level of impurities capable of reacting with solvated electrons was estimated by irradiating a mixture of 50% glycerol, 50% water, viscosity 4.247 cP at 30°. The viscosity of this mixture is comparable to water and rate constants of e_s^- with reactive solutes of $10^{10}\ M^{-1}\ \text{sec}^{-1}$ are

(1) The Radiation Laboratory of the University of Notre Dame is operated under contract with the U. S. Atomic Energy Commission. This is AEC Document No. COO-38-804.

(2) M. Anbar and E. J. Hart, "The Hydrated Electron," Wiley, New York, N. Y., 1970; J. K. Thomas, *Radiat. Res. Rev.*, 1, 183 (1968); S. Arai and M. C. Sauer, *J. Chem. Phys.*, 44, 2297 (1966); M. C. Sauer, S. Arai, and L. Dorfman, *ibid.*, 42, 708 (1965).

(3) R. H. Minday, L. D. Schmidt, and H. T. Davis, *ibid.*, 50, 1473 (1969).

(4) L. B. Magnusson, J. T. Richards, and J. K. Thomas, *Int. J. Radiat. Chem. Phys.*, in press.

(5) J. T. Richards and J. K. Thomas, *J. Chem. Phys.*, 53, 218 (1970).

(6) (a) W. H. Hamill, *ibid.*, 53, 473 (1970); (b) R. K. Wolff, M. J. Bronskill, and J. W. Hunt, *ibid.*, 53, 4211 (1970).

(7) "Glycerol," C. S. Miner, Ed., ACS Publication No. 117, Reinhold, New York, N. Y., 1953.

expected. The decay of the solvated electron in these mixtures has a half-life $t_{1/2}$ of 2.5 μsec which is comparable to that obtained in water alone. The impurity level in pure glycerol is hence $<10^{-4}$ M. In subsequent experiments solute concentrations were greater than 10^{-2} M, and any effects of impurities in glycerol are thus negligible.

Samples were prepared by sealing the solution under vacuum in 1-cm square suprasil tubing or by the syringe technique[8] which has been described.

The Notre Dame 7 MeV Arco linear accelerator was used as the radiation source in the pulse radiolysis experiments. Usually 10-nsec pulses of 4 to 5 A were used producing about 2×10^{-5} M hydrated electrons in a water sample of 1-cm optical path length, *i.e.*, 4×10^{20} eV $l.^{-1}$ $pulse^{-1}$. The actual dosimetry was carried out by observing at the end of the pulse the hydrated electron in water at 600 mμ where the extinction coefficient is 10,600 M^{-1} cm^2 and the G value is 3.4 electrons/100 eV of energy absorbed.[12] The samples were either sealed in 1-cm square suprasil cells or introduced into a fixed 1-cm cell by a syringe. The absorption spectra of the transitory species were observed by passing a light beam from a 450-W XBO xenon lamp through the cell and over 80 ft out of the irradiation area to the accelerator control room. The light was focused onto the slits of a Bausch & Lomb f 3.5 monochromator, and the exit light monitored by a IP28 or similar photomultiplier, which was designed for a 2-nsec response time.[9] The signal from the IP28 was monitored on a Tektronix 7404 oscilloscope, the traces of which were photographed on 10,000 ASA Polaroid film. The response time of the system was less than 3 nsec. To improve the signal-to-noise ratio of the system, the xenon lamp was pulsed to a 20-fold increase in light level over the dc level for 1 msec. The intensity of the light pulse, I_0, was observed on a storage scope by bleeding a small portion of the signal from the photomultiplier to this scope. Absorption or emission spectra could be observed from 2500 to 9000 Å on this pulse radiolysis system.

A Korad K1Q ruby laser was used for the photolysis experiments. This laser after frequency doubling gave a 15-nsec pulse of 3471-Å light at 100-mJ energy output. The optical detection system in the laser experiments was similar to that used in the pulse radiolysis experiments. In both the Linac and laser experiments the oscilloscope traces were photographed on the Polaroid film, which were subsequently measured on an XY recorder which converted the axis into voltages. The voltages were then fed to a Univac computer which calculated the optical densities of the traces at different times and plotted the data in spectral or kinetic form.[10]

Results

Pure Glycerol. The pulse radiolysis of deaerated glycerol leads to a short-lived transitory absorption

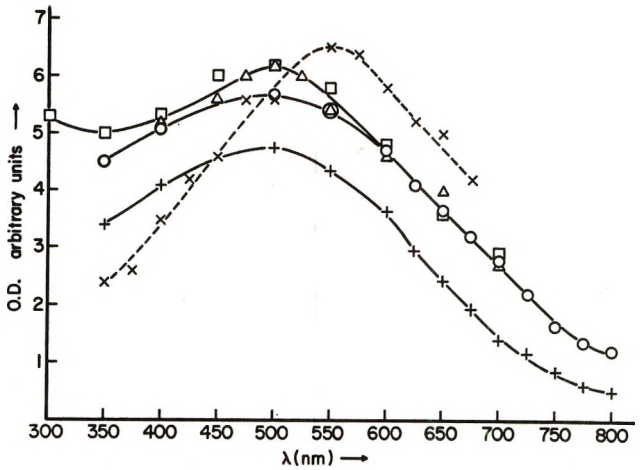

Figure 1. Spectra of e_s^- in glycerol at different temperatures: ⊡, 197°, γ radiolysis measured minutes after irradiation; ◬, 197°, pulse radiolysis at end of pulse; ×, 32°, pulse radiolysis at end of pulse; ⊙, −78°, pulse radiolysis at end of pulse; +, −78°, pulse radiolysis 500 nsec after pulse.

spectrum covering the visible region of the spectrum. The spectra at room temperature, +30, −78, and −197° are shown in Figure 1, together with the spectrum obtained in glycerol at −197° after irradiation on a ^{60}Co γ source. The ^{60}Co γ ray and 7-MeV electron spectra, which are measured at 10 min and 10 nsec following irradiation, are in agreement to within experimental error. The spectrum has a broad peak with a maximum at about 500 nm. The overall spectral properties and the reduction of the intensity of the spectrum by electron scavengers suggest that the spectrum is indeed due to solvated electrons.

The spectrum at room temperature is also shown in Figure 1, and it has a maximum at 550 mμ. This spectrum is somewhat narrower than that observed at −197°; the spectral and kinetic behavior again suggest that the spectrum is that of solvated electrons in glycerol. The red shift of the spectrum with increasing temperature is normally observed for spectra of solvated electrons,[11] and again this is in accord with the assignment of the spectra in Figure 1 to the solvated electrons in glycerol.

Kinetics of Decay of e_s^-. The spectra at −78° show a time dependence in the red portion of the spectrum. In the blue part of the spectrum about 20% of the e_s^- signal decays over a time period from the end of the pulse to 500 nsec after the pulse. In the red part of the spectrum up to 50% decays over this time period, an effect that is not observed at the two other temperatures.

(8) J. K. Thomas, S. Gordon, and E. J. Hart, *J. Phys. Chem.*, 68, 1525 (1964).

(9) J. W. Hunt and J. K. Thomas, *Radiat. Res.*, 32, 149 (1967).

(10) T. Gangwer, unpublished work, University of Notre Dame.

(11) J. Jortner, *Radiat. Res.*, 4, 24 (1964).

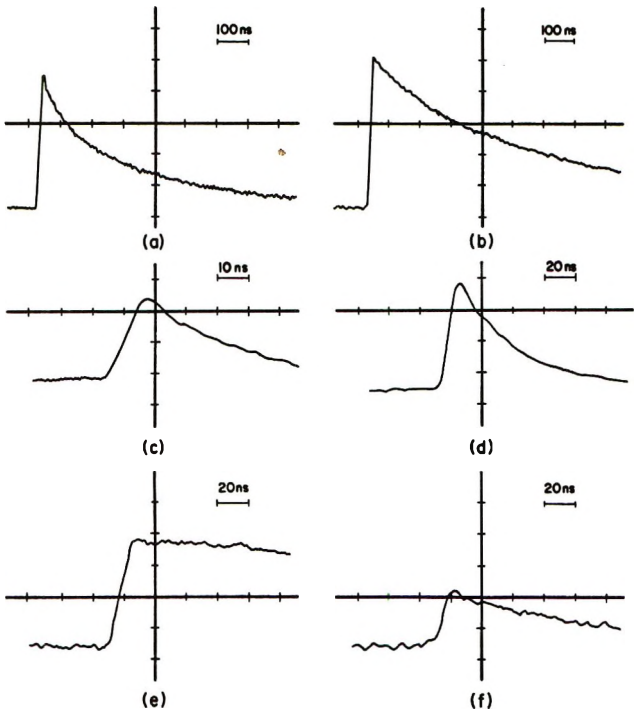

Figure 2. Decay of e_s^- in glycerol under different conditions at λ 550 nm: (a) pure deaerated glycerol, 32°, sweep 100 nsec/cm; (b) 0.5 *N* NaOH in glycerol, 32°, sweep 100 nsec/cm; (c) 0.3 *M* acetone, 32°, sweep 10 nsec/cm; (d) 10^{-2} *N* $HClO_4$, 32°, sweep 20 nsec/cm; (e) pure glycerol, 0°, sweep 20 nsec/cm; (f) 0.5 *M* acetone, 0°, sweep 20 nsec/cm.

The decay of the electron in glycerol is not a simple first- or second-order process as illustrated by the oscilloscope traces in Figure 2 which show the decay of the electron in glycerol under various experimental conditions. Pure glycerol in Figure 2a shows a sharp initial decay over several hundred nanoseconds which slowly gives way to a much slower decay. This type of kinetic decay has been observed in other alcohols[12] where it has been attributed to a geminate recombination of the electron and positive ion. The complex kinetics have been quantitatively explained for alcohols,[13] good agreement being obtained between the pulse data and scavenging steady-state experiments. Alkali slows down the decay of the electron as shown in Figure 2b for 0.5 *M* NaOH, 4% water in glycerol. This is also in agreement with the concept that the decay of the solvated electron is due to neutralization with the concomitant positive ion.

The *G* value of the electron in pure glycerol measured at the end of the pulse is 2.27/100 eV in pure glycerol and 2.91/100 eV in 0.5 *M* NaOH in glycerol. This was obtained by assuming an extinction coefficient for the e_s^- at 550 nm of 12,000 M^{-1} cm^{-1}, a number in keeping with that measured for e_s^- in other alcohols.[2]

Reactions of e_s^- with Solutes. Several solutes increase the rate of decay of the e_s^- in glycerol, typical data are shown in Figure 2c for the decay of e_s^- in 10^{-1} *M* acetone and in Figure 2d in 10^{-2} *M* $HClO_4$.

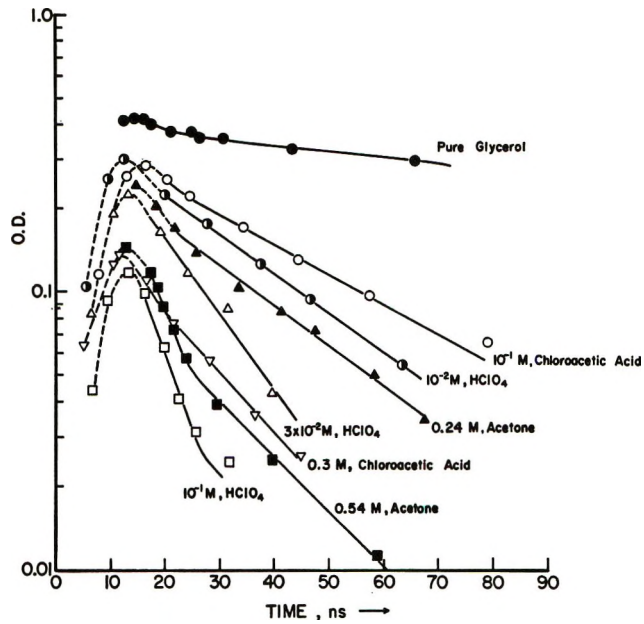

Figure 3. Decay of e_s^- in the presence of various solutes at 32°.

Except for the highest solute concentrations the rates of decay of e_s^- are first order over at least two to three half-lives as shown in Figure 3. As the rate of decay

Table I

Solute concn, *M*	*k*, M^{-1} sec^{-1}	Viscosity, cP	*k* in water, M^{-1} sec^{-1}
Acetone			
0.24	1.3×10^8	710	5.6×10^9
0.54	1.2×10^8	560	
Acetone–(10% water)		154	
0.024	2.4×10^8	(Glycerol–	5.6×10^9
0.047	2.8×10^8	10% water)	
Acetone–(25% water)		26.5	
0.012	0.9×10^9	(Glycerol–	5.6×10^9
0.028	1.2×10^9	25% water)	
$HClO_4$			
0.01	2.3×10^9		
0.03	1.8×10^9		2.2×10^{10}
0.01	1.2×10^9		
Chloroacetic acid			
0.1	1.9×10^8		1.2×10^9
0.3	1.4×10^8		
Benzyl alcohol			
0.1	5.5×10^7		
0.3	3.8×10^7		1.3×10^8
1.0	4.0×10^7		
Cd^{2+}			
0.036	5.6×10^8	404	5.2×10^{10}

(12) J. K. Thomas and R. V. Bensasson, *J. Chem. Phys.*, **46**, 4147 (1967).

(13) S. J. Rzad and J. H. Fendler, *ibid.*, **52**, 5395 (1970).

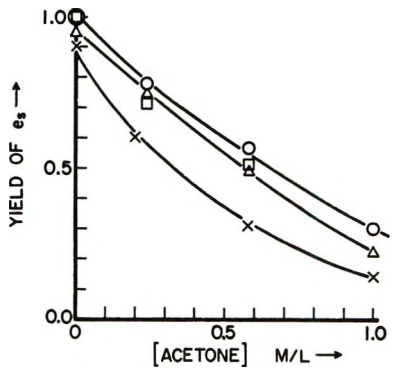

Figure 4. Yield of e_s^- in the presence of acetone. The curves are offset on the ordinate for clarity. ⊡, 32°, vertical offset 0; ⊙, 0°, vertical offset 0; △, −78°, vertical offset −0.5; ×, −197°, vertical offset −1.0.

of e_s^- in pure glycerol also approximates to first-order kinetics over the same time range, it is possible to correct for the natural decay of e_s^- and hence to obtain the rate constant for e_s^- with the solute. The rate constants for several solutes are given in Table I and are compared to the corresponding rate constants in water. The effect of viscosity on the rate constant is also shown in Table I, the viscosity being changed by addition of water.

Yield of e_s^- in the Presence of Solutes. The addition of solutes to glycerol increases the rate of decay of e_s^- and also reduces the yield of e_s^- observed by absorption spectroscopy. Typical data are shown in Figure 2e and f for pure glycerol and 0.2 *M* acetone, where the acetone causes a significant decrease in $G(e_s^-)$. To obtain the true value of $G(e_s^-)$ in the presence of added solutes, the decay of e_s^- was extrapolated back to the middle of the electron pulse. Figure 4 shows the effect of temperature and acetone concentration on the yield of e_s^- in glycerol. Very little effect of temperature from +30 to −197° is observed on the effect of acetone on reducing the yield of e_s^-.

Effect of Cadmium Ion on $G(e_s^-)$. Cadmium ions Cd^{2+} provide a particularly interesting case for the study of the effect of solute on $G(e_s^-)$, as the product of the reaction Cd^+ may be observed in the ultraviolet at 300 nm. Figure 5 shows the rate of decay of e_s^- in 0.42 *M* cadmium sulfate in a mixture of glycerol and 4% water at 300 nm[14] and the rate of appearance of the Cd^+. Both decay and growth are plotted as first-order kinetics and show identical rates. The inserts in Figure 5 show the decay of e_s^- at 550 nm in the presence of Cd^{2+} and the appearance of Cd^+ at 300 nm. This last picture clearly shows that a portion of Cd^+ appears at the same rate as e_s^- decays, while a large portion appears during the pulse with a time constant less than 2 nsec. About 45% of this rapid absorption is due to e_s^- which has a weak absorption at 300 nm, while 55% of the absorption is due to Cd^+. The cadmium ions also reduce the initial yield of e_s^- at

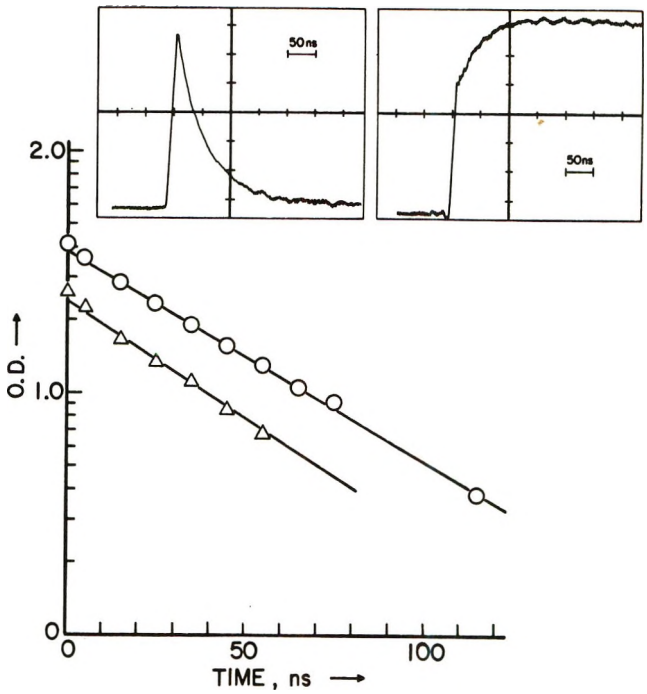

Figure 5. The decay of e_s^- in the presence of 5×10^{-2} *M* Cd^{2+}: ⊙, e_{aq}^- decay as OD; △, growth of Cd^+ as (OD_∞ − OD_+). Insets: (a) Decay of e_s^- λ 550 mμ and (b) growth of Cd^+ λ 300 mμ.

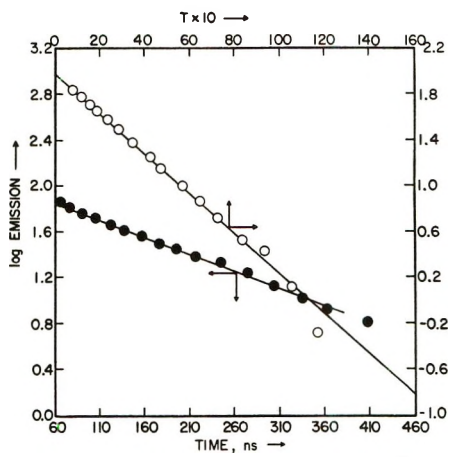

Figure 6. Decay of pyrene fluorescence in glycerol after laser excitation at λ 3471 Å: ○, 10^{-6} *M* pyrene; ●, 10^{-6} *M* pyrene, 0.5% nitromethane.

550 nm by 21%. It is concluded that Cd^{2+} reacts rapidly with a precursor of e_s^-, reducing the yield of e_s^-, this reaction leading to Cd^+, while a slower reaction of e_s^- with Cd^{2+} leads to a further development of Cd^+.

The increasing optical density (OD) of Cd^+ after the pulse is 0.060 and corresponds to a reaction of e_s^- with Cd^{2+} equivalent to an OD of e_s^- of 0.174. The OD of Cd^+ that is produced rapidly with the pulse is 0.056 and

(14) J. H. Baxendale, E. M. Fielden, and J. Keene, *Proc. Roy. Soc., Ser. A*, **286**, 320 (1965).

is equivalent to an e_s^- OD of 0.162. The total yield of Cd^+ is equivalent to an OD of 0.336 which is larger than that observed in the absence of Cd^{2+} which is 0.220. Hence some electrons must disappear rapidly compared to the response time of the system, while reacting with Cd^{2+} to produce the long-lived Cd^+.

Laser Excitation in Glycerol. Solutions of pyrene in deaerated glycerol were excited with pulses of 3471-Å light from a Korad laser, and the pyrene fluorescence was monitored with time. Typical data for pyrene are shown in Figure 6, the decay being exponential with a half-life <1 μsec. The addition of 0.093 *M* nitromethane quenches the fluorescence; typical data are shown in Figure 6. The difference in the slopes of Figure 6 gives the rate of quenching attributed to the nitromethane; a rate constant of $3.0 \times 10^7\ M^{-1}\ sec^{-1}$ is found for nitromethane interacting with the singlet excited state of pyrene in glycerol at room temperature (25°).

Discussion

It is concluded that the spectra presented in Figure 1 are due to solvated or trapped electrons. In the mobile liquid state at 30° the evidence is overwhelmingly in favor of this assignment. The position and broadness of the spectrum immediately suggests a solvated electron, while the geminate nature of the decay kinetics is also in agreement with the nature of electrons in alcohols. Finally the increase in the rate of decay of the absorption by the addition of the many electron scavengers, and in particular in the Cd^{2+} system the corresponding rise of Cd^+ while the red absorption decays can only be explained satisfactorily if the absorption is indeed due to e_s^-.

At lower temperatures the kinetic aspects of the foregoing discussion cannot be used as the e_s^- is not sufficiently mobile. However the blue shift with decreasing temperature of the spectrum is in accord with the behavior of solvated electrons,[2] and the reduction in yield of the absorption by the addition of typical electron scavengers confirms this assignment.

Previous work[5,15] has shown that at low temperatures the spectrum of the trapped electron shows a considerable blue shift. This is interpreted as trapping of the electrons in regions of the glass or liquid where orientations of the solvent molecules provide regions of low potential energy for the electron. This is subsequently followed by a further orientation of the molecules in the field of the electron to give a trap of deeper potential energy and a corresponding blue shift in the absorption spectrum. The rate-controlling step in this process may be the breaking of the hydrogen bonds of the alcohol followed by a very rapid relaxation of the free alcohol molecules around the electron.

Glycerol is extensively hydrogen bonded as exemplified by its high viscosity, yet the spectra observed at +30 and −197° are similar and do not show the relaxation effects illustrated by monohydric alcohols. It can only be suggested that even when the glycerol is hydrogen bonded many of the OH groups remain free to trap the electron. Subsequent breaking of the H bond then does not significantly improve the situation for the electron as although the breakage leads to more OH groups, a large number was initially available anyway. Some minor relaxation should be observed due to the packing of the glycerol molecules around the electron. This may occur rapidly at +30° but not at −197° in the stiff glycerol glass and may account for the broader nature of the spectrum at −197° compared to 30°.

The yield of the electron, $G(e_s^-) = 2.26$ is larger than that observed in any other alcohol, although it is often suggested that yields of e_s^- in excess of 4 exist at short times either as quasifree electrons,[16] or in spurs as solvated electrons. In the quasifree state the electron has a very high mobility and in a time short compared to 1 nsec either returns to the positive ion, finds a suitable arrangement of solvent molecules where it is trapped, or reacts with an added solute. If the electron is solvated in a spur or region of local high free-radical or ion concentration, then a rapid reaction may remove it again in a time short compared to 1 nsec. The addition of high concentrations of OH^- partly removes the positive ion *via* neutralization and eliminates the back reaction of the electron with the positive ion. This leads to a larger observed yield of solvated electrons as observed. The addition of a solute such as Cd^{2+} leads to competition between Cd^{2+}, the positive ion, and solvent trapping for the electron. The final yield of Cd^+ being the sum of electrons captured before solvation and those captured after solvation. The resultant yield of product equivalent to $G(e^-)$ is again larger than that observed directly as solvated electrons.

The peculiar decay characteristics of the electron, *i.e.*, a rapid initial decay over several hundred nanoseconds followed by an increasingly slower decay, suggests that the geminate recombination of e_s^- with a positive ion is being observed. The addition of NaOH removes the positive ion leading to a slower decay of e_s^- as observed. The reactions of solutes that affect either the yield or decay of the solvated electron may be divided into two classifications: reaction with the electron or precursor prior to observation in the solvated state and reaction with the solvated electron.

The data clearly show that the instantaneous yield of the electron observed at 10 nsec is decreased by the addition of many solutes. The data in Figure 4 show that temperature has very little effect on the efficiency of decreasing $G(e_s^-)$ as exemplified by a plot of percentage yield of e_s^- *vs.* solute concentration.

The most satisfying explanation of these data is that

(15) J. H. Baxendale and P. Wardman, *Chem. Commun.*, in press.
(16) G. Freeman, *J. Chem. Phys.*, **43**, 86 (1965).

the electron in its quasifree state prior to solvation may be captured by a solute molecule. Hence a competition exists between solvent and solute for the electron, and the yield of solvated electrons may be written as

$$G(e_s^-)/G(e_s^-)_0 = \frac{\alpha}{\alpha + \beta[S]}$$

where α and β are rate parameters applying to the capture of the electron by the solvent and solute, respectively, and $G(e_s^-)$ and $G(e_s^-)_0$ are the yields of solvated electrons in the presence and absence of scavengers. This type of simple relationship can explain the data in Figure 4, although the actual mechanism must be more complicated. However it can readily be seen that α, which is related to the number of solvent traps and the efficiency of trapping, is of prime importance in determining $G(e_s^-)$. At first sight it would seem that hydrogen bonding and hence availability of traps would depend on temperature, which is not borne out by the experimental data. However the extent of the hydrogen bonding in glycerol may be such that a large fraction of the OH groups are still free to trap the electron. This would then tend to indicate that the number of traps in glycerol does not depend on temperature.

The rates of reaction of the solvated electron in glycerol with several solutes, Table I, shows a striking difference to the corresponding rates measured in water. The most rapid reaction rate is $e_s^- + H^+$ which is $^1/_{20}$ that in water, while acetone with $k = 1.25 \times 10^8\ M^{-1}$ sec^{-1} is $^1/_{40}$ that in water. Other solutes show rates that vary from $^1/_3$ to $^1/_{10}$ that observed in water. Preliminary data show that the mobility of e_s^- in glycerol is $^1/_{50}$ that of e_s^- in ethanol.[17] The slower mobility and rates in glycerol are due to the viscosity of the glycerol which hampers the movement of the electron. If the electron rate followed the viscosity, then rates in glycerol should be $^1/_{624}$ those in water. The data in Table I show that the rate constants for $e_s^- +$ acetone vary as $1/\eta^{1/2}$ where η is the viscosity. This behavior has been noted previously[18,19] for the effect of viscosity on ionic reactions in hydrocarbons, and recently a theoretical background for this effect has been developed.[20]

The biggest difference in rate constants is observed for acetone where the rate in glycerol is $^1/_{40}$ that in water. For the proton reaction with e_s^- a difference of $^1/_{10}$ implies that the mobility of the proton is high in glycerol compared to e_s^- and controls the reaction rate. The smaller differences with chloroacetic acid and benzyl alcohol may be due to the fact that these solutes show slow rates of reaction even with the hydrated electron. If these reactions are not diffusion controlled, then the "cage effect" will predominate in these reactions. Hence we imply that for a diffusion-controlled rate where the species react at every collision, the rate constant in glycerol may be $^1/_{40}$ that in water as illustrated by the acetone rate data. If reaction does not occur on every collision, then the e_s^- and solute diffuse together and suffer many collisions in a solvent cage before diffusing apart. This effect applies to both the water and glycerol systems, and hence the lack of mobility of the e_s^- in glycerol compared to water is partially offset by the solvent cage effect. In an extreme case, for example, in going from the gas phase to water differences of 20× increase in rate constant have been predicted and observed for nondiffusion-controlled reaction.[21,22] We may also explain similarity of e_s^- rate constants in water and glycerol for the slower reactions in terms of a description by Waite.[23] He has described the rate constant for a bimolecular reaction k in terms of a rate constant of diffusion, k, and a rate constant of reaction of the species k_2 as

$$\frac{1}{k} = \frac{1}{k_1} + \frac{1}{k_2}$$

If $k_1 \gg k_2$ as in a nondiffusion-controlled reaction, then $k \simeq k_2$. Thus as k_1 varies with viscosity k is still mainly described by k_2, in agreement with data in Table I.

The laser data shows that the quenching of the excited singlet state of pyrene is $3 \times 10^7\ M^{-1}\ sec^{-1}$ in glycerol compared to $2 \times 10^{10}\ M^{-1}\ sec^{-1}$ in alcohol or cyclohexane. The ratios of the viscosities of these liquids to that of glycerol is about 1000, in fair agreement with the 700× ratio of the rate constants in these liquids. Thus for neutral reactions we may to a first approximation use the viscosity as a guide to the rate constant. The reactions rates of e_s^- are tenfold larger than those predicted by a direct viscosity correlation and seem to follow an inverse dependence on the square root of viscosity.

The initial rapid decay of the e_s^- in high concentrations of acetone may be partly explained in terms of the Smoluchowski equation[24]

$$k = k_0\left(1 + \frac{R}{\sqrt{\pi D t}}\right)$$

where k is the rate constant at time t, k_0 is the rate constant when t is ∞, R is the interaction distance, and D is the diffusion constant. This equation has also been derived for quenching in photochemical studies.[25]

For glycerol we may choose $R = 3 \times 10^{-8}$ cm and D as about 10^{-6} cm^2/sec. Then at $t = 2 \times 10^{-8}$ sec, k is $1.15k_0$ which indicates a faster initial decay of e_s^-.

(17) G. Beck and J. K. Thomas, unpublished data.

(18) J. A. Leone and W. H. Hamill, *J. Chem. Phys.*, **49**, 5294 (1968).

(19) J. Fuller, N. Petelski, D. Ruppel, and M. Tomlinson, *ibid.*, **74**, 3066 (1970).

(20) T. Sawai and W. H. Hamill, *J. Chem. Phys.*, in press.

(21) S. Benson, "Foundations of Chemical Kinetics," McGraw-Hill, New York, N. Y., 1960.

(22) J. P. Sweet and J. K. Thomas, *J. Phys. Chem.*, **68**, 1363 (1964).

(23) T. R. Waite, *J. Chem. Phys.*, **82**, 21 (1960).

(24) M. V. Smoluchowski, *Z. Phys. Chem. (Leipzig)*, **92**, 129 (1918).

(25) T. Förster, *Z. Naturforsch.*, **49**, 321 (1949).

The observed decay is larger than the 15% calculated, but the chosen time of 20 nsec is rather imprecise as the pulse is 10 nsec, and the diffusion constant may also differ from that chosen as 10^{-6}. It will be necessary to use shorter excitation periods, *i.e.*, pulse lengths, to reduce the span of time selected in t, in order to check the equation more thoroughly.

Acknowledgments. We would like to thank Mr. T. Deal and Mr. M. Kurtis for helping us with the Linac experiments and for excellent operation of this machine. We are also indebted to Mr. D. Schutt for aid in the design of our electronics, Mr. D Blessing for the glass blowing of our equipment, and Mr. S. Knapik for building much of the mechanical equipment.

Electron Spin Resonance Studies of Inorganic Radicals in Irradiated Aqueous Solutions. I. Direct Observation[1]

by D. Behar and Richard W. Fessenden*

Radiation Research Laboratories, Center for Special Studies and Department of Chemistry, Mellon Institute of Science, Carnegie-Mellon University, Pittsburgh, Pennsylvania 15213 *(Received December 13, 1971)*

Publication costs assisted by the U. S. Atomic Energy Commission

A search has been carried out for the esr spectra of radical intermediates present during steady-state, *in situ* radiolysis of aqueous solutions of inorganic salts. The technique used is capable of detecting radicals which react by diffusion-controlled recombination if the esr line widths are small (<1 G). In fact out of 15 systems studied, only four gave detectable esr signals. One is forced to conclude that the esr lines of the radicals formed in the other systems are broad. The radicals successfully studied are $\cdot SO_3^-$ (from $OH + SO_3^{2-}$, g = 2.00306), $\cdot PO_3^{2-}$ (from $OH + HPO_3^{2-}$, a^P = 567.6 G, g = 2.00154), $\cdot HPO_2^-$ (from $OH + H_2PO_2^-$, a^P = 480.4, a^H = 89.7 G, g = 2.00293), and $\cdot CS_2^-$ (from $e_{aq}^- + CS_2$, g = 2.00804). No esr lines were detected from solutions of HCO_2^-, CO_3^{2-}, S^{2-}, Se^{2-}, SeO_3^{2-}, Br^-, I^-, SCN^-, OCN^-, N_3^-, HO_2^-, NO_2^-, NH_2OH, or AsO_2^-. Steady-state measurements of radical concentrations have been used to determine rates of radical recombination for the species $\cdot SO_3^-$, $\cdot PO_3^{2-}$, and $\cdot HPO_2^-$.

Introduction

The present work (and that in the following paper[2]) represents an attempt to make use of the *in situ* radiolysis–esr technique[3-5] in furthering the understanding of the radiolysis of aqueous solutions of inorganic salts. The esr spectra of a wide range of inorganic radicals[6] have been studied in solids, where high concentrations of radicals can often be produced and detection is not generally a problem. With radicals in solution, on the other hand, concentrations are usually low because of diffusion-controlled recombination, and detection is possible only for radicals with narrow esr lines. (Those with relatively slow recombination reactions are, of course, also favored.) Among those known are $\cdot HO_2$,[7] $\cdot SO_2^-$,[8] and $\cdot CO_2^-$.[9,10] In the present work spectra were detected for $\cdot SO_3^-$, $\cdot PO_3^{2-}$, $\cdot HPO_2^-$, and $\cdot CS_2^-$ out of about 15 possible radicals studied. The relatively poor success in directly observing spectra of these radicals is generally a result of their having broad esr lines. This experience illustrates the difficulty in such studies.

The inorganic radicals under study were obtained by reaction of radiolytically generated OH or e_{aq}^- with various solutes. In most cases the desired radical could be produced by oxidation of an anion by electron transfer to OH (or O^-)

$$\cdot OH + X^- \longrightarrow \cdot X + OH^- \qquad (1)$$

(1) Supported in part by the U. S. Atomic Energy Commission.

(2) D. Behar and R. W. Fessenden, *J. Phys. Chem.*, **76**, 1710 (1972).

(3) R. W. Fessenden and R. H. Schuler, *J. Chem. Phys.*, **39**, 2147 (1963).

(4) K. Eiben and R. W. Fessenden, *J. Phys. Chem.*, **72**, 3387 (1968).

(5) K. Eiben and R. W. Fessenden, *ibid.*, **75**, 1186 (1971).

(6) See, for instance, the review by P. W. Atkins and M. C. R. Symons, "Structure of Inorganic Radicals," Elsevier, Amsterdam, 1967.

(7) E. Saito and B. H. J. Bielski, *J. Amer. Chem. Soc.*, **83**, 4467 (1961).

(8) See A. Reuveni, Z. Luz, and B. L. Silver, *J. Chem. Phys.*, **53**, 4619 (1970), and references therein.

(9) E. C. Avery, J. R. Remko, and B. Smaller, *ibid.*, **49**, 951 (1968).

(10) A. L. J. Beckwith and R. O. C. Norman, *J. Chem. Soc. B*, 400 (1969).

(where X^- represents ions such as SO_3^{2-} or CO_3^{2-}). Depending upon the exact pH (usually near 12), differing relative amounts of OH and O^- were present as a result of the equilibrium

$$OH \rightleftharpoons O^- + H^+ \qquad (pK = 11.9)^{11} \qquad (2)$$

With this method of radical generation, it was customary to saturate the solutions with N_2O to convert solvated electrons into O^- (or OH)

$$e_{aq}^- + N_2O \longrightarrow N_2 + O^- \qquad (3)$$

In the few cases where the radical under study was produced by reaction of e_{aq}^-, the solutions were deoxygenated with N_2.

The concentration with each of the solute systems was adjusted (taking into account known rate constants[12]) so that essentially complete scavenging of OH (O^-) or e_{aq}^- was achieved. In all cases, therefore, a new intermediate derived from the solute must have been produced. The absence of esr lines which occurred with a number of solutes cannot, therefore, be attributed to an inefficient production reaction.

Experimental Section

All solutions were prepared from analytical grade materials in doubly distilled water. The pH was adjusted with potassium hydroxide; no buffers were used. Solutions were deoxygenated by bubbling Baker nitrous oxide or Airco nitrogen without any purification. The irradiation was carried out in the esr cavity as previously described.[4,5] The irradiation cell of fused silica, with dimensions 0.5 × 10 × 40 mm, was mounted in the cavity and the solution was driven through the cell at flow rates of 50–150 ml/min. The solution was cooled prior to entering the cavity, and all measurements refer to about 15°. The electron beam current collected at an electrode in the solution was about 1 μA. For the measurement of line positions, second-derivative spectra were recorded by use of two modulation frequencies. In the experiments involving intercomparison of radical concentrations, only the 100-kHz modulation was used, and first-derivative spectra were taken in the usual way.

Results and Discussion

The best approach to the study of radicals in solution is, of course, the direct observation of the esr spectrum. However, as mentioned in the Introduction, only a few spectra are known of inorganic radicals in solution. A number of reasons for this lack can be cited, but an important one is that for many radicals rapid spin relaxation causes broad esr lines. Any atom or radical with the possibility of orbital angular momentum can have a large deviation of the g factor from the free-spin value. This orbital angular momentum is usually quenched in the solid, but in liquids the time dependence of the solvent interaction will provide a large modulation of the g factor and efficient spin relaxation. Radicals affected in this way include, for example, atoms in other than S states and OH. Radicals such as Br_2^- and related species possess large g factor and hyperfine anisotropies, and the tumbling in solution may not be rapid enough to average this anisotropy sufficiently to achieve a narrow esr line width. In addition, in these cases, solvent interactions may be able to significantly modulate the g factor and hyperfine constants, leading again to efficient relaxation. With radicals containing nuclei with spins greater than one-half (such as the halogens other than fluorine), the nuclear quadrupole interaction also provides a source of nuclear relaxation which affects the spectrum through the hyperfine interaction. For molecules with a small moment of inertia about one axis, spin–rotation interactions are important and in some cases can cause a significant increase in line width.[13] It is suggested that the very wide line for HO_2 radical (27 G)[7] is a result of this phenomenon. Finally, where the radical has acid–base properties, an exchange of protons can cause line broadening in certain pH regions. Other sources of excess relaxation also exist. With the limited radical concentrations available in systems where diffusion-controlled recombination occurs a line width of much more than 1 G will result in signals too weak for observation. In the radiolysis experiments, one can often be certain of both efficient radical production and of the recombination rate constant. Hence, a failure to detect the desired radical *must mean* that the esr lines are wide.

$\cdot SO_3^-$ Radical. The radical $\cdot SO_3^-$ has been identified in both pulse radiolysis[14,15] and flash photolysis;[15,16] the results in a recent paper[15] show that previous suggestions[16,17] regarding a product of $e_{aq}^- + SO_3^{2-}$ (such as $\cdot HSO_3^{2-}$) are incorrect and that no significant reaction occurs.

The esr spectrum of the $\cdot SO_3^{2-}$ radical has been measured in γ-irradiated single crystals of a number of compounds containing the sulfite group[18] (sodium dithionate, sulfamic acid, etc.), and has been characterized by a single line having a nearly isotropic g factor ($g = 2.0036$[18]). The isotropy of the g factor of the

(11) J. Rabani and M. S. Matheson, *J. Amer. Chem. Soc.*, **86**, 3175 (1964).

(12) See the table of rate constants compiled by M. Anbar and P. Neta, *Int. J. Appl. Radiat. Isotopes*, **18**, 493 (1967).

(13) For some comments on this effect in hydrocarbon radicals, see H. G. Benson, A. J. Bowles, A. Hudson, and R. A. Jackson, *Mol. Phys.*, **20**, 713 (1971).

(14) G. E. Adams, J. W. Boag, and B. D. Michael, *Proc. Chem. Soc., London*, 411 (1964).

(15) E. Hayon, A. Treinin, and J. Wilf, *J. Amer. Chem. Soc.*, **94**, 47 (1972).

(16) L. Dogliotti and E. Hayon, *J. Phys. Chem.*, **72**, 1800 (1968).

(17) G. E. Adams, J. W. Boag, and B. D. Michael, *Trans. Faraday Soc.*, **61**, 1674 (1965).

(18) G. W. Chantry, A. Horsfield, J. R. Morton, J. R. Rowlands, and D. H. Whiffen, *Mol. Phys.*, **5**, 233 (1962).

SO_3^- radical is favorable for detecting the esr spectrum of this radical in solution. No evidence was found in the solid state for the existence of $\cdot HSO_3^{2-}$.

In the present experiments, a solution 2×10^{-2} M in SO_3^{2-} (pH 12.5) and saturated with N_2O was irradiated. A single line was observed at $g = 2.00306$. When the solution was saturated with N_2, no other lines could be observed. This line is attributed to the $\cdot SO_3^-$ radical. Norman and Storey,[19] in work which was published after this present work was well along, have also found a line at $g = 2.0030$ in Ti^{3+}–H_2O_2 flow systems containing SO_3^{2-} and similarly attribute it to $\cdot SO_3^-$. The parameters for this radical and those following are summarized in Table I.

Table I: Hyperfine Parameters for Inorganic Radicals in Aqueous Solution[a,b]

Radical	Source	Line width	a	g
$\cdot SO_3^-$	SO_3^{2-}	0.1		2.00306
$\cdot PO_3^{2-}$	HPO_3^{2-}	0.5	$a^P = 567.65$	2.00154
$\cdot HPO_2^-$ [c]	$H_2PO_2^-$	0.35	$a^P = 480.44$, $a^H = 89.75$	2.00293
$\cdot CS_2^-$	CS_2	0.25		2.00804

[a] Hyperfine constants in gauss, g factors accurate to ±0.00005. [b] Parameters for $\cdot PO_3^{2-}$, $\cdot HPO_2^-$ calculated by the program EXCALIES.[21] Line positions measured to ±0.05 G in terms of nmr frequency, but because of the large splittings and a possible variation in the field difference between sample and nmr probe, the absolute accuracy of a^P may not be this good. [c] With a choice of like signs for a^P and a^H, lines fit with an rms error of ~0.02 G. Calculated parameters for unlike signs of a^H and a^P are not significantly different, although the degree of fit is slightly worse.

$\cdot PO_3^{2-}$ and $\cdot HPO_2^-$ Radicals. The species $\cdot PO_3^{2-}$ has been identified by its esr spectrum in a number of irradiated solids.[20] The phosphorus hyperfine constant varies somewhat,[20] but is usually between 500 and 600 G; the g factor for this radical in irradiated NH_4PF_6 is 2.0014.[21] The radical $\cdot HPO_2^-$ is also known from studies on crystals[22] and has the parameters $a^P = 520.7$, $a^H = 82.5$ G, $g = 2.0030$. Because of the large splittings in both cases, knowledge of the solid-phase spectrum was important for predicting the region of the spectrum to search for the lines. The rate constants for reaction of OH with HPO_3^{2-} and $H_2PO_2^-$ are high[23] and experiments with basic, 10^{-2} M solutions of the sodium salts did in fact yield the expected radicals

$$\cdot O^- + HPO_3^{2-} \longrightarrow \cdot PO_3^{2-} + OH^- \quad (4)$$

$$\cdot O^- + H_2PO_2^- \longrightarrow \cdot HPO_2^- + OH^- \quad (5)$$

The spectra consist of two and four lines, respectively; the parameters as calculated by the computer program EXCALIES[21] are given in Table I. Close examination of the exact calculations for $\cdot HPO_2^-$ show that a possibility exists for deciding whether or not a^H and a^P are of the same sign. With like signs, the separation of the low-field doublet corresponding to a^H should be smaller than that of the high-field doublet by 0.02 G. With unlike signs, the separation in the high-field doublet is the smaller (by a similar amount). Detection of such a small difference is difficult, but all measurements show the separation of the low-field doublet to be the smaller. The data, therefore, support the choice of like signs for a^H and a^P, as is found in the single-crystal study.[21] Calculated parameters for this case only are given in Table I. (Those for the other case are not significantly different in magnitudes.) The parameters found here for the radicals $\cdot PO_3^{2-}$ and $\cdot HPO_2^-$ in solution are similar to those obtained in studies on solids (as mentioned above), and the g factors are essentially identical.

The observation of $\cdot PO_3^{2-}$ and $\cdot HPO_2^-$ shows that the net result of reaction on the time scale of the esr experiments (hundreds of microseconds to milliseconds) is abstraction of a hydrogen bonded to phosphorus. It seems likely that the mechanism is as written in eq 4 and 5.

The CS_2 System. The reaction of e_{aq}^- with CS_2 is very fast[24] and is expected to give initially the $\cdot CS_2^-$ anion. On irradiating a saturated solution of CS_2 ($[CS_2] \cong 3 \times 10^{-2}$ M, pH 12.0), two esr lines at $g = 2.00518$ and 2.00804, respectively, were observed. Addition of 0.1 M NO_3^- as e_{aq}^- scavenger caused the disappearance of the line at $g = 2.00804$ and left the other unchanged in intensity. The former line is clearly the result of the reaction of e_{aq}^- while the latter must be produced by OH. Tentatively, the line at $g = 2.00804$ is identified as that of $\cdot CS_2^-$. It is not clear what species is responsible for the other line, but it clearly cannot be attributed to a secondary reaction product originating with $\cdot CS_2^-$. One obvious possibility is the radical $\cdot CS_2O^-$ which is related to $\cdot CO_3^-$ by two replacements of oxygen by sulfur.

Systems Not Giving Detectable Spectra. No detectable esr lines were observed when OH was allowed to react with the following anions: HCO_2^-, CO_3^{2-}, S^{2-}, Se^{2-}, SeO_3^{2-}, Br^-, I^-, SCN^-, OCN^-, N_3^-, HO_2^-, NO_2^-, NH_2OH, and AsO_2^-. Most of these are not surprising in relation to the comments on esr line widths given above. However, the radicals $\cdot CO_2^-$ and $\cdot CO_3^-$

(19) R. O. C. Norman and P. M. Storey, *J. Chem. Soc. B*, 1009 (1971).

(20) See the references in F. G. Herring, J. H. Hwang, W. C. Lin, and C. A. McDowell, *J. Phys. Chem.*, **70**, 2487 (1966).

(21) R. W. Fessenden, *J. Magn. Resonance*, **1**, 277 (1969).

(22) J. R. Morton, *Mol. Phys.*, **5**, 217 (1962).

(23) G. E. Adams, J. W. Boag, and B. D. Michael, *Trans. Faraday Soc.*, **61**, 1417 (1965).

(24) S. Gordon, E. J. Hart, M. S. Matheson, J. Rabani, and J. K. Thomas, *Discuss. Faraday Soc.*, **No. 36**, 193 (1963); E. J. Hart, S. Gordon, and J. K. Thomas, *J. Phys. Chem.*, **68**, 1271 (1964).

do deserve special mention. The production of $\cdot CO_2^-$ by abstraction from formate is a well-known reaction, and $\cdot CO_2^-$ should have a single, narrow esr line at $g = 2.0006$.[25] Unfortunately, this position is exactly under the signal from the irradiated silica cell. A chemical modulation experiment using pulsed irradiation as described by Eiben and Fessenden[4] was also not successful, and from this result we must conclude that the line width is >1 G. Beckwith and Norman[10] have detected a line at 2.0003 which they assign to $\cdot CO_2^-$ but do not mention the line width. (Avery, *et al.*,[9] have indirectly mentioned detecting $\cdot CO_2^-$ and report a relatively broad line.) The only source of excess relaxation for $\cdot CO_2^-$ seems to be the spin–rotation interaction arising because of the small moment of inertia[26] about the axis parallel to the O–O direction.

The inability to observe a spectrum of $\cdot CO_3^-$ is particularly surprising. This radical is known from studies[27] on irradiated single crystals of $KHCO_3$ and has the g factor 2.0066. The electron resides mainly on the three oxygen atoms, as shown by the small ^{13}C hyperfine constant of 11 G. The carbonate system is well characterized,[28] and the reaction rate constants are favorable. The formation reaction, $OH + CO_3^{2-}$, is somewhat slow ($k \sim 10^8\ M^{-1}\ sec^{-1}$),[29] but should not present a problem at 0.1 M carbonate concentration. More importantly, the second-order disappearance reaction is slow,[30] $2k = 1.25 \times 10^7\ M^{-1}\ sec^{-1}$, so that high concentrations should be achieved. The absence of a detectable line suggests a line width >5 G. It is possible that the excess width is associated with the inequivalence of the oxygens reported by Chantry, *et al.*,[27] in that a rapid interchange of the roles of the different oxygens could occur. However, the situation regarding the symmetry of $\cdot CO_3^-$ and the related radical $\cdot NO_3$ is somewhat unclear.

Recombination Rate Constants. Because the production rates of radicals in different systems can be quantitatively interrelated, it is possible to use relative steady-state radical concentrations to determine relative radical recombination rate constants.

$$R\cdot + R\cdot \xrightarrow{2k} RR$$

The systems containing SO_3^{2-}, HPO_3^{2-}, and $H_2PO_2^-$ studied here are particularly suited to this method because it is possible to produce only one radical species, thus avoiding the problem of the various cross-combination reactions in multiple-radical systems. We assume that the observed radical is the only one produced and that other reaction paths which give radicals with broad esr lines are absent. In each case, therefore, the yield of radicals is equal to the combined yield of OH and e_{aq}^- (through the use of N_2O). We will neglect the small direct yield of H, although this may also result in radicals by abstraction (with HPO_3^{2-} or $H_2PO_2^-$) or conversion to e_{aq}^- by $OH^- + H \rightarrow e_{aq}^- + H_2O$. Because the absolute radical production rates cannot as yet be accurately measured, it is necessary to make a comparison with a radical having a known recombination rate. The radical $\cdot CH_2CO_2^-$, for which $2k = 1.0 \times 10^9\ M^{-1}\ sec^{-1}$,[31] was chosen for this purpose. As a check on the method, the radical $\cdot CH(CO_2^-)_2$ ($2k = 5.7 \times 10^7\ M^{-1}\ sec^{-1}$)[32] was also studied.

The experiments were carried out by irradiating the various solutions under constant conditions and recording the first derivative of one line of the spectrum.[33] The field-modulation amplitude was chosen so that negligible broadening of the lines occurred and a lower than usual microwave power was used to avoid any problems of saturation. The areas of the absorption curves were obtained by double integration and the total intensity computed from the known multiplicity. The total intensities, I (proportional to radical concentrations), were converted to rate constants by the equation $2k' = (I/I')^2 2k$, where $2k$ is value for the reference radical $\cdot CH_2CO_2^-$.

The results so obtained and the chemical conditions of the various experiments are given in Table II. The value of $6.9 \times 10^7\ M^{-1}\ sec^{-1}$ obtained for $\cdot CH(CO_2^-)_2$ is in excellent agreement with the optically measured[32] value of 5.7×10^7, considering the difficulty of measur-

Table II: Second-Order Recombination Rate Constants

Solute[a]	[Solute], M	Radical	pH	$2k$, $M^{-1}\ sec^{-1}$
$CH_3CO_2^-$	10^{-1}	$\cdot CH_2CO_2^-$	11.4	(1.0×10^9)[b]
$CH_2(CO_2^-)_2$	10^{-1}	$\cdot CH(CO_2^-)_2$	12.1	6.9×10^7
SO_3^{2-}	10^{-2}	$\cdot SO_3^-$	11.8	1.9×10^9 [c]
HPO_3^{2-}	10^{-2}	$\cdot PO_3^{2-}$	12.0	3.0×10^7
$H_2PO_2^-$	10^{-2}	$\cdot HPO_2^-$	12.2	9.4×10^8

[a] All solutions were saturated with N_2O. [b] This value[31] was taken as a reference for calculating all other rate constants. [c] This number should be compared with the value 1.8×10^9 obtained by Hayon, *et al.*,[15] for comparable ionic strengths. Their value for zero ionic strength is 1.3×10^9.

(25) D. W. Ovenall and D. H. Whiffen, *Mol. Phys.*, **4**, 135 (1961).

(26) Using the OCO angle given in ref 25 and an OC bond length of 1.19 Å one obtains a value of 1.8 atomic mass units times angstroms^2 for this moment. Such a value is comparable to that of a radical of type $\cdot CH_2X$, where X is an atom or linear substituent.

(27) G. W. Chantry, A. Horsfield, J. R. Morton, and D. H. Whiffen, *Mol. Phys.*, **5**, 589 (1962).

(28) D. Behar, G. Czapski, and I. Buchovny, *J. Phys. Chem.*, **74**, 2206 (1970).

(29) The reaction $O^- + CO_3^{2-}$ is slower than $OH + CO_3^{2-}$.[28] The effective rate constant near pH 12 is as given.

(30) J. L. Weeks and J. Rabani, *J. Phys. Chem.*, **70**, 2100 (1966).

(31) P. Neta, M. Simic, and E. Hayon, *ibid.*, **73**, 4207 (1969).

(32) M. Simic, P. Neta, and E. Hayon, *ibid.*, **73**, 4214 (1969).

(33) In the case of $\cdot CH_2CO_2^-$, the low- and high-field lines are not of the same intensity, reflecting nonequilibrium population of the spin levels. The central second-order doublet which is presumed not to show this effect to any significant degree was used for the measurement. No effects of this sort were observed for $\cdot PO_3^{2-}$ and $\cdot HPO_2^-$.

ing the integral of the absorption curve from the first-derivative spectrum and the fact that the measured signal areas are squared in the calculation of the rate constant. Errors in the values given of up to a factor of 2 are possible. The singly charged radicals $\cdot SO_3^-$ and $\cdot HPO_2^-$ are seen to have recombination rates comparable to those of $\cdot CH_2CO_2^-$ and $\cdot CO_2^-$ ($2k = 1.7 \times 10^9\ M^{-1}\ sec^{-1}$).[31] The rate constant for the doubly charged radical $\cdot PO_3^{2-}$ is considerably smaller and is rather similar to that of doubly charged organic radicals such as $\cdot {}^-OCHCO_2^-$ ($2k = 1.5 \times 10^7\ M^{-1}\ sec^{-1}$).[32] It is possible to conclude that these inorganic radicals with localized orbitals recombine much the same way as organic radicals and that the charge on the radical is a major factor determining the rate constant.

Acknowledgment. The authors wish to thank P. Neta for help with certain of the experiments regarding the rate constant determinations.

Electron Spin Resonance Studies of Inorganic Radicals in Irradiated Aqueous Solutions. II. Radical Trapping with Nitromethane[1]

by D. Behar and Richard W. Fessenden*

Radiation Research Laboratories, Center for Special Studies and Department of Chemistry, Mellon Institute of Science, Carnegie-Mellon University, Pittsburgh, Pennsylvania 15213 *(Received December 13, 1971)*

Publication costs assisted by the U. S. Atomic Energy Commission

Radical trapping of the *aci* anion of nitromethane ($CH_2{=}NO_2^-$) has been used in a study of the intermediates in irradiated aqueous solutions of a number of inorganic salts. Steady-state, *in situ* radiolysis was carried out with a 2.8-MeV electron beam. Two types of reaction with this reagent were observed: direct addition of the inorganic radical ($X\cdot$) to the CN double bond to form the adduct $XCH_2NO_2^-$ and an electron transfer from $CH_2{=}NO_2^-$ to $X\cdot$, which results in the formation of $\cdot CH_2NO_2$ (which in turn reacts with another nitromethane molecule to form $O_2NCH_2CH_2NO_2^-$). Variation of the nitrogen and methylene proton hyperfine constants of the adduct radicals, $XCH_2NO_2^-$, is sufficient that a number of different spectra could be distinguished. In some cases hyperfine splittings by magnetic nuclei in the substituent X were also observed (*e.g.*, where $X\cdot$ was $CN\cdot$ or HPO_2^-). The radicals were identified by reference to the expected radiation chemistry of the inorganic solute. Accurate spectral parameters are given for 14 adducts to $CH_2{=}NO_2^-$. The successful application of $CH_2{=}NO_2^-$ as a radical trap in these various cases demonstrates the potential for general use both in other studies of these same radicals and in studies of other radicals both inorganic and organic. The results contribute to the understanding of the radiation chemistry of a number of these inorganic systems. Of particular importance is the demonstration of the reaction $e_{aq}^- + S_2O_3^{2-} \rightarrow \cdot S^- + SO_3^{2-}$.

Introduction

The preceding paper[2] demonstrated the difficulty in directly observing by esr the radical intermediates present during radiolysis of aqueous solutions of inorganic salts. To enable further study of these intermediates, we have resorted to the method of radical trapping.[3,4] This indirect approach involves the use of a scavenger which when allowed to react with a radical yields a secondary radical of longer lifetime. This secondary species, because of its long life and consequent higher concentration, can then be more easily studied. The adduct radical should also have narrow esr lines. Among the scavengers used for this purpose are nitroso compounds and nitrones.[3,4] In this work we have used the *aci* anion of nitromethane ($CH_2{=}NO_2^-$) which exists in basic solutions ($pK = 10.3$).[5]

$$CH_3NO_2 + OH^- \rightleftharpoons CH_2{=}NO_2^- + H_2O \quad (1)$$

Use of this scavenger followed from the observation by Eiben and Fessenden[6] that radicals derived from alco-

(1) Supported in part by the U. S. Atomic Energy Commission.

(2) D. Behar and R. W. Fessenden, *J. Phys. Chem.*, **76**, 1706 (1972).

(3) See the review by E. G. Janzen, *Accounts Chem. Res.*, **4**, 31 (1971).

(4) C. Lagercrantz, *J. Phys. Chem.*, **75**, 3466 (1971).

(5) D. Turnbull and S. H. Maron, *J. Amer. Chem. Soc.*, **65**, 212 (1943).

(6) K. Eiben and R. W. Fessenden, *J. Phys. Chem.*, **72**, 3387 (1968).

hols added readily to this carbon–nitrogen double bond. Norman and Storey,[7] in work which was published after the present study was well along, have also used nitromethane as a radical trap. They investigated the radicals $\cdot S^-$, $\cdot SO_3^-$, and $\cdot S_2O_3^-$ formed by OH in flow systems.

The inorganic radicals in the present study were obtained by reaction of radiolytically generated OH or e_{aq}^- with various solutes. In most cases the desired radical was produced by reaction of OH (or O^-) with an anion.

$$\cdot OH + X^- \longrightarrow \cdot X + OH^- \qquad (2)$$

(where X^- represents ions such as SO_3^{2-}, SCN^-, CO_3^{2-}). In these experiments the solutions were saturated with N_2O to convert solvated electrons to O^- (or OH)

$$e_{aq}^- + N_2O \longrightarrow N_2 + O^- \qquad (3)$$

(The pK for the dissociation of OH to O^- is 11.9.[8]) In the few cases where the radical under study was produced by reaction of e_{aq}^-, the solutions were deoxygenated with N_2.

Two types of reactions with nitromethane were found to occur. In most cases an addition reaction to the C=N bond takes place

$$\cdot X + CH_2{=}NO_2^- \longrightarrow XCH_2\dot{N}O_2^- \qquad (4)$$

The resulting $XCH_2\dot{N}O_2^-$ radicals are generally long lived, and their esr spectra can be observed in the *in situ* radiolysis experiments quite easily. The basic spectrum of this kind of radical consists of three 1:2:1 triplets resulting from splittings by the one ^{14}N nucleus and the two equivalent protons in the β position. Typical magnetic parameters are those of the OH adduct which has $a^N = 25.2$ G, $a^H = 9.0$ G, and $g = 2.0050$. In certain cases where X contains magnetic nuclei, further splittings caused by the interaction of the unpaired electron with these nuclei are found. The second type of reaction involves an electron transfer from the nitromethane anion to the inorganic radical forming the $\cdot CH_2NO_2^-$ radical. This radical has not been observed as it reacts rapidly with $CH_2{=}NO_2^-$ to form $O_2NCH_2CH_2\dot{N}O_2^-$. Recently Edge, Norman, and Storey[9] have found that $\cdot SO_4^-$ also reacts with nitromethane in this fashion to produce ultimately O_2NCH_2-$CH_2\dot{N}O_2^-$ and have proposed the same reaction scheme.

In most experiments relatively high concentrations of nitromethane should be present in order to fully scavenge the radicals X· in competition with the second-order recombination of X·. However, the concentration of nitromethane cannot be made too high because of its efficient reaction with e_{aq}^- and OH

$$e_{aq}^- + CH_2{=}NO_2^- + H_2O \longrightarrow CH_3\dot{N}O_2^- + OH^- \qquad (5)$$

$$(k_5 = 6.6 \times 10^9\ M^{-1}\ \text{sec}^{-1})^{10}$$

$$OH + CH_2{=}NO_2^- \longrightarrow HOCH_2\dot{N}O_2^- \qquad (6)$$

$$(k_6 = 9 \times 10^9\ M^{-1}\ \text{sec}^{-1})^{11}$$

Reaction 5 can compete with the scavenging of e_{aq}^- by N_2O (reaction 3) (because of the limited solubility of N_2O, 2×10^{-2} M) and reaction 6 can compete with the generation of the radical X· (reaction 2). As a consequence of these various competitions, most spectra have contributions from the radicals $CH_3\dot{N}O_2^-$ and $HOCH_2\dot{N}O_2^-$ in addition to the spectra of the desired radical $XCH_2\dot{N}O_2^-$. Usually sufficient resolution is available that the appearance of lines from these two extra radicals do not seriously interfere with the detection and identification of the $XCH_2\dot{N}O_2^-$ radicals.

Experimental Section

The experimental details are essentially as reported in the previous paper.[2] All solutions were prepared from analytical grade materials in doubly distilled water. The nitromethane (Eastern, spectrograde) was used without further purification. During this work an improvement in magnetic field homogeneity was obtained by replacing the stainless-steel walls of the cavity[6,12] with a copper–nickel alloy (12% Ni) of poor electrical conductivity (to allow the 100-kHz modulation to enter). The cavity interior was then plated with silver for a high electrical conductivity for the microwaves and a thin layer of gold for chemical inertness. Without the perturbing effect of the residual magnetism in the stainless steel, the minimum esr line width in this magnet is ~0.07 G. Resolution of some of the smaller hyperfine splittings (*e.g.*, in the SCN and N_3 adducts) was dependent upon this improvement in resolution.

Results and Discussion

An integral part of the use of $CH_2{=}NO_2^-$ as a radical trapping agent is the development of a table of spectral parameters of known adducts and such rules as may exist which allow these parameters to be related to the nature and identity of the radical trapped. Because differences in parameters are often small, it is important that the parameters are as accurate as possible. It is for these reasons that the common adducts of such as OH·, $\cdot CO_2^-$, and $\cdot SO_3^-$ are discussed in

(7) R. O. C. Norman and P. M. Storey, *J. Chem. Soc. B*, 1009 (1971).

(8) J. Rabani and M. S. Matheson, *J. Amer. Chem. Soc.*, **86**, 3175 (1964).

(9) D. J. Edge, R. O. C. Norman, and P. M. Storey, *J. Chem. Soc. B*, 1096 (1970).

(10) K.-D. Asmus, A. Henglein, and G. Beck, *Ber. Bunsenges. Phys. Chem.*, **70**, 459 (1966). The rate for $e_{aq}^- + CH_3NO_2$ is 2.1×10^{10} M^{-1} sec^{-1}.

(11) K.-D. Asmus and I. A. Taub, *J. Phys. Chem.*, **72**, 3382 (1968). No significant change in this rate was observed up to pH 11.8, where nearly half of the OH is present as O^-. A somewhat different rate for O^- reaction with $CH_2{=}NO_2^-$ is possible, however.

(12) K. Eiben and R. W. Fessenden, *ibid.*, **75**, 1186 (1971).

Table I: Hyperfine Parameters for Adducts to $CH_2{=}NO_2^-$ [a]

Primary species	Source	Adduct	a_α^N	$a_\beta^H(CH_2)$		g
H, e_{aq}^- [b]		$CH_3\dot{N}O_2^-$	25.96	12.12		2.00495
OH[b]		$HOCH_2\dot{N}O_2^-$	25.23	9.04		2.00502
		$^-OCH_2\dot{N}O_2^-$	25.70	9.92		2.00496
$\cdot CO_2^-$ [c]	HCO_2^-	$^-O_2CCH_2\dot{N}O_2^-$	24.55	8.51		2.00496
$\cdot CO_3^-$	CO_3^{2-}	$^-O_2COCH_2\dot{N}O_2^-$	25.08	8.92		2.00504
$\cdot SO_3^-$ [d]	SO_3^{2-}	$^-O_3SCH_2\dot{N}O_2^-$	22.19	7.50		2.00498
$\cdot S^-$ [e]	S^{2-}	$HSCH_2\dot{N}O_2^-$	24.46	4.47	$a_{SH}^H = 1.15$	2.00602
		$^-SCH_2\dot{N}O_2^-$	24.36	6.64		2.00584
$\cdot S_2O_3^-$ [f]	$S_2O_3^{2-}$	$^-O_3SSCH_2\dot{N}O_2^-$	23.94	6.00		2.00551
$\cdot SCN$	SCN^-	$NCSCH_2\dot{N}O_2^-$	21.69	3.39	$a_\epsilon^N = 0.31$	2.00616
$\cdot CN$	CN^-	$NCCH_2\dot{N}O_2^-$	25.27	8.04	$a_\delta^N = 0.51$	2.00505
$\cdot N_3$	N_3^-	$NNNCH_2\dot{N}O_2^-$	24.74	5.46	$a_\gamma^N = 2.73$, $a_\delta^N = a_\epsilon^N = 0.27$	2.00513
$\cdot CS_2^-$	CS_2	$^-S_2CCH_2\dot{N}O_2^-$	25.71	8.78		2.00503
$\cdot PO_3^{2-}$	HPO_3^{2-}	$^{-2}O_3PCH_2\dot{N}O_2^-$	24.96	10.64	$a_\gamma^P = 31.04$	2.00496
HPO_2^-	$H_2PO_2^-$	$^-O_2(H)PCH_2\dot{N}O_2^-$	25.15	10.14	$a_\gamma^P = 28.96$, $a_\gamma^H = 1.47$	2.00501
$\cdot AsO_2$	AsO_2^-	$O_2AsCH_2\dot{N}O_2^-$	23.13	8.86	$a_\gamma^{As} = 73.55$	2.00489
$\cdot NO_2$ [g]	NO_2^-	$^-O_2\dot{N}CH\dot{N}O_2^-$	9.58	4.09		2.00559

[a] Hyperfine constants in gauss, accurate to ±0.05 G; g factors measured relative to the peak from the silica cell, accurate to ±0.00003. Second-order corrections have been made. [b] Values listed are somewhat different than in ref 3. The present values are more accurate as a result of somewhat improved instrumental conditions. [c] Values given by Zeldes and Livingston[15] are $a^N = 24.52$, $a^H = 8.10$ G, and $g = 2.00500$; those of Edge and Norman[16] are $a^N = 24.2$, $a^H = 8.3$ G, and $g = 2.0051$. [d] Values given by Norman and Storey[7] are $a^N = 22.0$, $a^H = 7.45$ G, and $g = 2.0051$. [e] Values given in ref 7 for $^-SCH_2\dot{N}O_2^-$ are $a^N = 24.2$, $a^H = 6.6$ G, and $g = 2.0057$. [f] Values given in ref 7 are $a^N = 24.0$, $a^H = 6.0$ G, and $g = 2.0051$. This latter g factor seems to be in error. [g] Values given by C. Lagercrantz, K. Torssell, and S. Wold, *Ark. Kem.*, **25**, 567 (1966), are $a^N(2) = 9.60$, $a^H = 4.10$ G.

detail below. With these identifications upon very firm ground, it is then possible to proceed with less well understood systems. The usefulness of this radical-trapping method is illustrated by the study[13] of the photolysis of $S_2O_3^{2-}$ which was based on much of the work reported here. The present paper represents the detailed description of the method.

As mentioned in the Introduction, the use of $CH_2{=}NO_2^-$ as a radical trap puts conflicting requirements on the concentrations of the various solutes. The concentration of nitromethane must be high enough to scavenge the desired radicals, but not so high as to interfere with the reactions of e_{aq}^- and OH which produce the radical under study. Because the rate constants for reaction of e_{aq}^- and OH with nitromethane are high, complete scavenging of these species by the other solutes is not obtained and some residual reaction to form $CH_3\dot{N}O_2^-$ and $HOCH_2\dot{N}O_2^-$ occurs. Most of the esr spectra in this work contain, therefore, the esr lines of these species. Unless otherwise specified, the concentration of nitromethane was 10^{-2} M. The hyperfine constants of $CH_3\dot{N}O_2^-$ and $HOCH_2\dot{N}O_2^-$ are summarized in Table I.

The hyperfine splittings in the spectrum of $HOCH_2\dot{N}O_2^-$ are significantly dependent on pH in the region pH >12.5. The most probable cause for this variation is the dissociation of the hydroxyl proton. The measured splitting by the methylene protons of $HOCH_2\dot{N}O_2^-$ as a function of pH is given in Figure 1. As is evident from the values given in Table I, there is also some change of a^N upon dissociation of the OH proton. From these data the pK for this dissociation is estimated to be 12.8 ± 0.2. No effect of ionic strength (0.1 M Na_2SO_4) on the hyperfine constants of $HOCH_2\dot{N}O_2^-$ was found.

The Radical $\cdot CO_2^-$. The reaction of OH with HCO_2^- to yield $\cdot CO_2^-$ is well known. The radiolysis of an N_2O-saturated solution 10^{-2} M in both sodium formate and nitromethane at pH 12 yielded an intense spectrum of nine lines (intensity ratio 1:2:1:1:2:1:1:2:1) which can be assigned to $^-O_2CCH_2\dot{N}O_2^-$ (see Table I). In this case and in the cases of the $\cdot SO_3^-$ and $\cdot S^-$ adducts (see below), the large signal intensity is evident from the fact that sufficient signal is available to be able to study the ^{13}C- and ^{33}S-containing radicals.[14] From this large signal intensity it can be concluded that the addition of $\cdot CO_2^-$ to $CH_2{=}NO_2^-$ is efficient and that the disappearance reactions for this doubly charged radical are relatively slow.

The radical $^-O_2CCH_2\dot{N}O_2^-$ has been reported by Zeldes and Livingston to be formed by the photolysis of NO_2^- in the presence of acetate.[15] We agree with their parameters except for a^H, which they report as

(13) D. Behar and R. W. Fessenden, *J. Phys. Chem.*, **75**, 2752 (1971).

(14) G. P. Laroff and R. W. Fessenden, to be published.

(15) H. Zeldes and R. Livingston, *J. Amer. Chem. Soc.*, **90**, 4540 (1968).

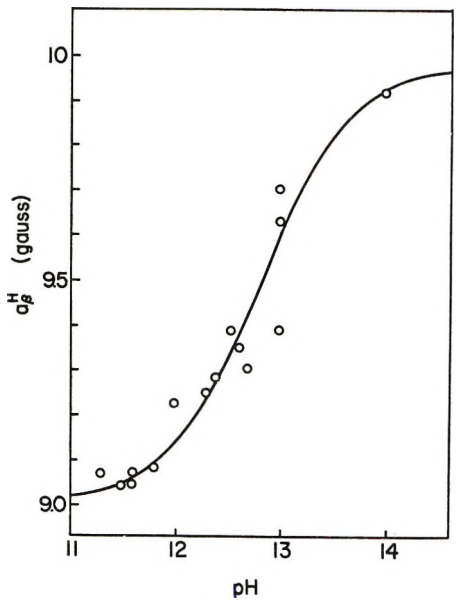

Figure 1. Variation of the hyperfine splitting of the methylene protons of $HOCH_2\dot{N}O_2^-$ as a function of pH. Solid curve is calculated for the equilibrium $HOCH_2\dot{N}O_2^- \rightleftarrows {}^-OCH_2\dot{N}O_2^- + H^+$ with $pK = 12.80$ and limiting values for $a_\beta^H(CH_2)$ of the undissociated and dissociated forms of 9.00 and 9.98 G, respectively.

8.10 G instead of the 8.50 G found here. Since this difference is far outside of the experimental errors in the two sets of measurements, there must be some unidentified environmental effect such as temperature or solute concentration which causes the difference. Edge and Norman[16] have also produced this radical by trapping $\cdot CO_2^-$ with nitromethane and their parameters (of somewhat poorer accuracy) are in reasonable agreement with ours.

The Radical $\cdot CO_3^-$. The failure to observe directly the esr spectrum of $\cdot CO_3^-$ (formed by the reaction of OH with CO_3^{2-}) has been detailed in the previous paper.[2] It has proved possible, however, to trap this radical with $CH_2{=}NO_2^-$. Radiolysis of a solution 2.5×10^{-2} *M* in carbonate (Na_2CO_3) and 10^{-3} *M* nitromethane at pH 12.3 yielded a spectrum which we attribute to $^-O_2COCH_2\dot{N}O_2^-$. The parameters are given in Table I and are seen to differ relatively little from those of the OH adduct to $CH_2{=}NO_2^-$. Because both species appeared in the same spectrum, there is no question of the existence of a new radical. (Five of the eight lines not obscured by the signal from the cell are fully resolvable into the contributions from OH and $\cdot CO_3^-$ adducts.) The intensities of the lines ascribed to $^-O_2COCH_2\dot{N}O_2^-$ are only comparable to those of $HOCH_2\dot{N}O_2^-$, in contrast to the large signals obtained for $^-O_2CCH_2\dot{N}O_2^-$. A number of reasons exist for this relatively low intensity. A primary reason is the inefficient scavenging of O^- (and OH) by carbonate in the presence of nitromethane (effective rate constant $\sim 10^8$ M^{-1} sec^{-1}).[17] Also contributing may be a slow reaction of $\cdot CO_3^-$ with $CH_2{=}NO_2^-$ to form the expected bond through oxygen and decomposition of the radical after formation. (The adduct is a carbonate ester.)

The small differences in the hyperfine constants of the OH and $\cdot CO_3^-$ adducts ($\sim$0.15 G) emphasize the importance of accurate measurements if an unknown radical is to be identified by its hyperfine constants. In the data of Table I all adducts can be distinguished by the magnitudes of their hyperfine constants. Any lesser accuracy such as that in the data of Norman and Storey[7] or Edge and Norman[16] makes confusion of the various adducts more likely.

The Oxalate System. Oxalate reacts with e_{aq}^- and OH presumably by

$$e_{aq}^- + C_2O_4^{2-} \longrightarrow \cdot C_2O_4^{3-} \quad (7)$$

$$OH + C_2O_4^{2-} \longrightarrow \cdot C_2O_4^- \text{ (or } \cdot CO_2^- + CO_2) \quad (8)$$

Esr experiments[12] have identified the radical $C_2O_4^{3-}$ and have shown that in the acid region the result of OH reaction is a reducing radical. The rate constants for reactions 7 and 8 are relatively small[18] so that it is difficult for the oxalate to compete with nitromethane. High oxalate and low nitromethane concentrations are needed, therefore. An experiment with 0.1 *M* oxalate and 10^{-4} *M* CH_3NO_2 showed a strong line of the radical $C_2O_4^{3-}$ ($g = 2.00407$) and the spectrum of one other adduct to $CH_2{=}NO_2^-$ besides that of the OH adduct. This other spectrum has parameters ($a^N = 24.60$, $a^H = 8.50$ G, $g = 2.00497$) which are essentially identical with those of the $\cdot CO_2^-$ adduct. At a nitromethane concentration of 1.0×10^{-3} *M*, a small signal of $C_2O_4^{3-}$ remains and again spectra of the OH and $\cdot CO_2^-$ adducts appear at comparable intensities. From the presence of a line from $C_2O_4^{3-}$ in the second experiment, it can be concluded that this radical does not react with $CH_2{=}NO_2^-$. (The signal of $C_2O_4^{3-}$ is weak because of competition for e_{aq}^- by $CH_2{=}NO_2^-$.) The intensity of the lines of the $\cdot CO_2^-$ and OH adducts are comparable but not as intense as those of $HOCH_2\dot{N}O_2^-$ in solutions with only nitromethane. It can be concluded, therefore, that reaction of OH with oxalate is occurring and that reaction 8 does not yield $\cdot CO_2^-$ in any direct way. (If reaction 8 did yield $\cdot CO_2^-$, then even after taking account of the competition for OH the lines of the $\cdot CO_2^-$ adduct would be very much more intense.) It must be concluded that an intermediate such as $\cdot C_2O_4^-$ is produced in reaction 8 and that this radical does not react with $CH_2{=}NO_2^-$.

The Radical $\cdot SO_3^-$. The formation of $\cdot SO_3^-$ from $OH + SO_3^{2-}$ has been discussed in the previous paper.[2]

(16) D. J. Edge and R. O. C. Norman, *J. Chem. Soc. B*, 1083 (1970).

(17) D. Behar, G. Czapski, and I. Buchovny, *J. Phys. Chem.*, **74**, 2206 (1970). The reaction $O^- + CO_3^{2-}$ is slower than $OH + CO_3^{2-}$. The effective rate constant near pH 12 is as given.

(18) See the table of rate constants compiled by M. Anbar and P. Neta, *Int. J. Appl. Radiat. Isotopes*, **18**, 493 (1967).

Figure 2. Second-derivative esr spectra of the $\cdot SO_3^-$ and $\cdot S^-$ adducts to $CH_2{=}NO_2^-$. Magnetic field increases to the right. The stick spectra show the lines assigned to the indicated species with the shift in the centers of the patterns corresponding to a difference in g factors of 0.00104. Also present to the right of center is the signal from the silica cell taken at the same gain setting. The values designated as a^N have been corrected for the different second-order shifts and so do not strictly correspond with the separation between the indicated lines. All figures have been made in this same way. Spectra were taken under the conditions $[SO_3^{2-}] = 2 \times 10^{-2}\ M$, $[CH_3NO_2^-] = 1 \times 10^{-2}\ M$, pH 12.1 and $[S^{2-}] = 2 \times 10^{-2}\ M$, $[CH_3NO_2] = 1 \times 10^{-3}\ M$, pH 13, respectively. In both cases the solutions were saturated with N_2O. Smaller lines are visible in the upper trace for $CH_3\dot{N}O_2^-$ and $HOCH_2\dot{N}O_2^-$ and in the lower trace for $^-O_3SCH_2\dot{N}O_2^-$.

When $\cdot SO_3^-$ reacts with nitromethane, addition to the C=N bond takes place. The resulting $^-O_3SCH_2\dot{N}O_2^-$ radical (see Figure 2) is relatively long lived (probably because of the double charge); its magnetic parameters are given in Table I.

The Sulfide System. In the pulse radiolysis of sulfide solutions, several radicals have been identified.[19] The primary $\cdot SH$ radicals formed from OH + H_2S or SH^- (depending on the pH) react at diffusion-controlled rates with the SH^- anion to form complexes of the type X_2^- ($(SH)_2^-$ and S_2H^{2-} were reported[19]) according to reactions 9 and 10.

$$\cdot SH + SH^- \rightleftharpoons (SH)_2^- \qquad K_{eq} = 2.5 \times 10^4\ M^{-1} \quad (9)$$

$$(SH)_2^- + OH^- \longrightarrow S_2H^{2-} + H_2O \quad (10)$$

Reaction 10 is followed by a fast decomposition of the S_2H^{2-}

$$S_2H^{2-} \longrightarrow S^- + SH^- \quad (11)$$

$k_{11} \sim 1.5 \times 10^7\ sec^{-1}$.

In the present work an N_2O-saturated, alkaline solution (pH 13) $2 \times 10^{-2}\ M$ in Na_2S and $10^{-3}\ M$ in nitromethane was irradiated and an intense esr spectrum of the $\cdot S^-$ adduct to the nitromethane $^-SCH_2\dot{N}O_2^-$ was observed (Figure 2). On lowering the pH to 9.3, an additional spectrum appeared which contained a further small splitting by a γ proton. This spectrum is attributed to the $HSCH_2\dot{N}O_2^-$ radical (see Table I and the figure in ref 13). The spectrum of the low-pH solution was about 100 times less intense than that at high pH. The high intensity of the $\cdot S^-$ adduct in comparison to the SH adduct seems to be caused by the double charge on the $^-SCH_2\dot{N}O_2^-$ radical, which has a much longer lifetime than the singly charged $HSCH_2\dot{N}O_2^-$ radical. The coexistence of both spectra indicates a relatively slow proton exchange on the SH group.

$$HSCH_2\dot{N}O_2^- + OH^- \rightleftharpoons {}^-SCH_2\dot{N}O_2^- + H_2O \quad (12)$$

Since the $\cdot SH$ radical reacts with the SH^- anion to form the $(SH)_2^-$ complex radical,[19] one might expect the reactive species toward the nitromethane to be $(SH)_2^-$ rather than $\cdot SH$ (or S_2H^{2-} rather than $\cdot S^-$). Therefore, the possibility of producing $^-(SH)_2CH_2\dot{N}O_2^-$ (or $^{2-}HS_2CH_2\dot{N}O_2^-$) instead of the above-mentioned adducts should be considered. The best way to check this is by producing the $\cdot SH$ or the $\cdot S^-$ radicals in a system where the complexing anions SH^- or S^{2-} are absent. The production of the above-mentioned radicals have been carried out by photolyzing alkaline thiosulfate solution containing nitromethane.[13] In that experiment the radicals $\cdot S^-$ and $\cdot SO_3^-$ were trapped by nitromethane to give the $^-SCH_2\dot{N}O_2^-$ and $^-SO_3CH_2\dot{N}O_2^-$ radical adducts with the same magnetic parameters as obtained in the radiolysis experiments. This photolysis experiment in which SH^- or S^{2-} were absent demonstrates clearly that the radical adduct does not contain the $(SH)_2^-$ or HS_2^{2-} fragments. In the radiolytic experiment one cannot exclude the existence of $(HS)_2CH_2\dot{N}O_2^-$ and $^{2-}HS_2CH_2\dot{N}O_2^-$ as the precursors of $HSCH_2\dot{N}O_2^-$ and $^-SCH_2\dot{N}O_2^-$. However, if such species exist they must be short lived and cannot be detected.

The Thiosulfate System. The behavior of thiosulfate under the influence of irradiation has not been extensively investigated. In the work of Adams, Boag, and Michael[20,21] the $\cdot S_2O_3^-$ radical was reported to be produced by the reaction of OH with the $S_2O_3^{2-}$ anion. This radical has an absorption band in the near uv region peaking at 375 nm.[20-22] Although it has been shown that $S_2O_3^{2-}$ is an efficient electron scavenger[23] the reaction of e_{aq}^- with the $S_2O_3^{2-}$ has not been considered in the pulse radiolysis of thiosulfate.[21] In the flash photolysis work of Dogliotti and

(19) W. Karman, G. Meissner, and A. Henglein, *Z. Naturforsch. B*, 22, 273 (1967).

(20) G. E. Adams, J. W. Boag, and B. D. Michael, *Proc. Chem. Soc., London*, 411 (1964).

(21) G. E. Adams, J. W. Boag, and B. D. Michael, *Trans. Faraday Soc.*, 61, 1674 (1965).

(22) L. Dogliotti and E. Hayon, *J. Phys. Chem.*, 72, 1800 (1968).

(23) R. Sperling and A. Treinin, *ibid.*, 68, 897 (1964).

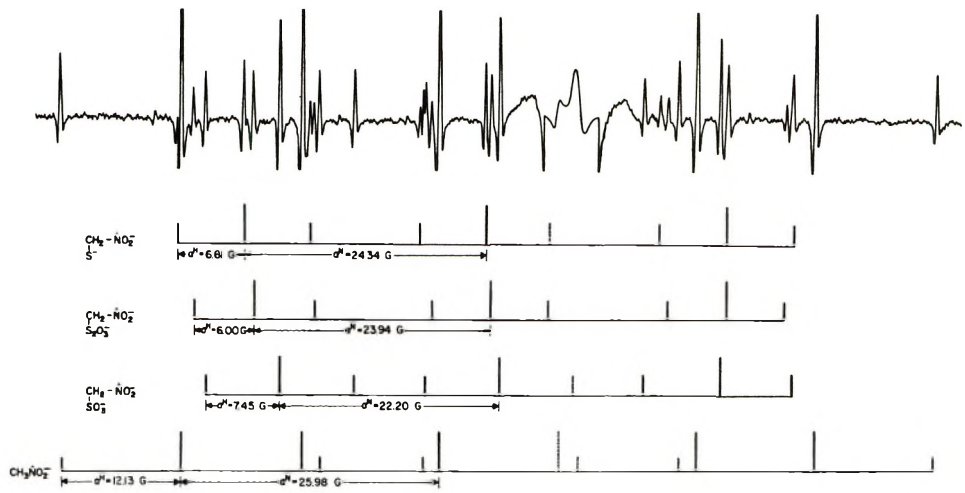

Figure 3. Esr spectrum taken during irradiation of an N_2-bubbled solution of 2×10^{-2} M $S_2O_3^{2-}$ and 3×10^{-3} M nitromethane at pH 12.5. Spectra of three adducts to $CH_2{=}NO_2^-$ are observed as indicated as well as that of $CH_3\dot{N}O_2^-$. The signal from the cell is taken at reduced gain. The hyperfine parameters given are those actually measured and so are slightly different than those in Figure 2 and Table I.

Hayon,[22] no transient species produced from the reaction of e_{aq}^- with $S_2O_3^{2-}$ was observed, although it was mentioned there[22] that reaction could occur to produce SH and SO_3^{2-}. In the γ irradiation of single crystals of $Na_2S_2O_3 \cdot H_2O$ esr spectra of two different radicals have been observed.[24] One of the spectra was assigned to the $\cdot S_2O_2^-$ radical while the other species has not been identified.

Irradiation of an N_2O-saturated solution of 2×10^{-2} M thiosulfate and 3×10^{-3} M of nitromethane at pH 12.5 yields an esr spectrum with contributions from two nitromethane adducts. The hyperfine constants and the g factor of one of the radicals are the same as for the $^-O_3SCH_2\dot{N}O_2^-$ radical obtained in the radiolysis of sulfite solution (see Table I). The other spectrum is assigned to $^-O_3S_2CH_2\dot{N}O_2^-$ which originates from the $\cdot S_2O_3^-$ radical formed in the reaction

$$S_2O_3^{2-} + OH \longrightarrow \cdot S_2O_3^- + OH^- \qquad (13)$$

The $\cdot SO_3^-$ adduct spectrum in this experiment was about 50 times less intense than the $\cdot SO_3^-$ adduct obtained in the radiolysis of sulfite solution. Therefore, we assume that the $\cdot SO_3^-$ radical produced in the radiolysis of the N_2O-saturated thiosulfite solution originates from a reaction between OH and SO_3^{2-} present as an impurity.

On irradiating the same solution but deoxygenated with nitrogen, an additional spectrum was observed whose hyperfine constants and g factor are the same as the $\cdot S^-$ adduct to the nitromethane (see Figure 3 and Table I). In addition the intensity of the spectrum of the $\cdot SO_3^-$ adduct increased by about a factor of 2. These results can be explained if one assumes a reaction between the solvated electrons and the thiosulfate

$$e_{aq}^- + S_2O_3^{2-} \longrightarrow \cdot S^- + SO_3^{2-} \qquad (14)$$

which produces $\cdot S^-$ directly. Because the irradiation was performed under steady-state conditions, the SO_3^{2-} produced in reaction 14 will react with OH to form $\cdot SO_3^-$ in addition to that formed from impurities and will, therefore, increase the $^-O_3SCH_2\dot{N}O_2^-$ steady-state concentration. The esr signal of the $\cdot S^-$ adduct to nitromethane is not as big as would be expected taking into account the stability of $^-SCH_2\dot{N}O_2^-$. A possible explanation for the loss of $\cdot S^-$ produced in reaction 14 is through abstraction of an electron from $S_2O_3^{2-}$

$$\cdot S^- + S_2O_3^{2-} \longrightarrow S^{2-} + \cdot S_2O_3^- \qquad (15)$$

The occurrence of reaction 14 explains the absence of an absorption by a product of e_{aq}^- reaction in the flash photolysis of thiosulfate. The product $\cdot S^-$ (or $\cdot SH$) is known to absorb only weakly[25,26] with a maximum at 384 nm and would, therefore, be obscured under the intense absorption band of the $\cdot S_2O_3^-$ radical.[20-22]

Halogenides and Pseudohalogenides. In previous pulse radiolysis and flash photolysis studies of halide ions in solution, it has been shown that the X_2^- complex radicals are formed from a reaction of halogen atoms with the halogenides.[27-30] In a recent publication by Marov and Symons[31] on γ-irradiated frozen

(24) J. R. Morton, *Can. J. Chem.*, **43**, 1948 (1965).

(25) J. Wendenburg, *Proc. 2nd Tihany Int. Symp. Radiat. Chem., Budapest*, 2, 225 (1967).

(26) J. Wendenburg, M. Mockel, A. Granzov, and A. Henglein, *Z. Naturforsch. B*, **21**, 632 (1966).

(27) L. I. Grossweiner and M. A. Matheson, *J. Phys. Chem.*, **61**, 1089 (1957).

(28) M. Anbar and J. K. Thomas, *ibid.*, **68**, 3829 (1964).

(29) J. K. Thomas, *Trans. Faraday Soc.*, **61**, 702 (1965).

(30) J. H. Baxendale, P. L. T. Bevan, and D. A. Stott, *ibid.*, **64**, 2389 (1968).

(31) I. Marov and M. C. R. Symons, *J. Chem. Soc. A*, 201 (1971).

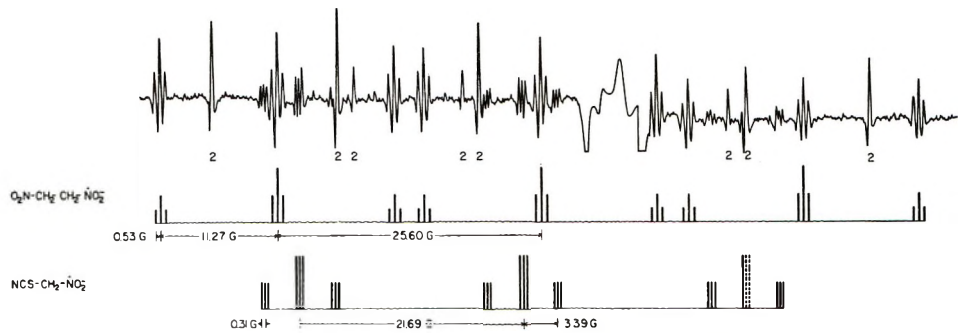

Figure 4. Esr spectrum taken during irradiation of an N_2O-saturated solution of 0.2 M SCN^- and 1×10^{-2} M nitromethane at pH 12.5. Radicals resulting from both addition to and oxidation of $CH_2{=}NO_2^-$ are evident as indicated. The central lines of the 11.27-G 1:2:1 triplets are less intense than expected and are about of same height as the outer lines of those triplets. The reduced intensity is believed to be caused by line broadening as a result of hindered internal rotation. The spectrum taken in the Br^- system, for example, which has only the lines of $O_2NCH_2CH_2\dot{N}O_2^-$ shows more clearly that this explanation if probably correct. The lines labeled by the number 2 are from $CH_3\dot{N}O_2^-$.

aqueous solutions of alkali metal halides, XOH^- radicals were detected and assumed to be the precursors to the X_2^- radicals. A confirmation of that assumption was found[32] in the pulse radiolysis of aqueous solutions of thiocyanate and iodide, where absorption spectra and kinetic evidence indicate the existence of $SCNOH^-$ and IOH^- as precursors of $(SCN)_2^-$ and I_2^-.

The radiolysis of alkaline solutions of Br^-, I^-, and SCN^- containing nitromethane yields in each case the same esr spectrum in the usual nine-line pattern for adducts to $CH_2{=}NO_2^-$ but with an additional small triplet splitting of 0.53 G (see Figure 4). Two pieces of evidence can be mentioned which help in the identification of this radical. It is obviously significant that the same radical is obtained in different chemical systems. In addition, the small triplet splitting is of similar size to those of γ protons in radicals such as $CH_3CH_2\dot{N}O_2^-$ (0.44 G)[15] and $^-O_2CCH_2CH_2\dot{N}O_2^-$ (0.66 G).[15] The radical is identified as O_2NCH_2-$CH_2\dot{N}O_2^-$ formed by the following reactions. First is the oxidation of $CH_2{=}NO_2^-$ by electron transfer

$$\cdot X_2^- \text{ (or } \cdot XOH^-) + CH_2{=}NO_2^- \longrightarrow \cdot CH_2NO_2 + 2X^- \text{ (or } X^- + OH^-) \quad (16)$$

followed by an addition reaction of the $\cdot CH_2NO_2$ radical to the nitromethane double bond

$$\cdot CH_2NO_2 + CH_2{=}NO_2^- \longrightarrow O_2NCH_2CH_2\dot{N}O_2^- \quad (17)$$

This same sequence of reactions but starting with $\cdot SO_4^-$ was reported by Edge, Norman, and Storey.[9] Hyperfine parameters for $O_2NCH_2CH_2\dot{N}O_2^-$ obtained with different oxidants are shown in Table II.

An attempt has been made to find which radical is the oxidizing species in reaction 16. If $\cdot XOH^-$ (or $X\cdot$) is the only reactive species, then by increasing the X^- concentration the signal intensity of the $O_2NCH_2CH_2\dot{N}O_2^-$ spectrum should decrease because of the competing reactions 18 and 19. On the other hand, if $\cdot X_2^-$ is the reactive species in reaction 16, the

$$\cdot XOH^- + X^- \rightleftarrows \cdot X_2^- + OH^- \quad (18)$$

$$(\text{or } \cdot X + X^- \rightleftarrows \cdot X_2^-)$$

$$\cdot XOH^- + CH_2{=}NO_2^- \longrightarrow X^- + \cdot CH_2NO_2 + OH^- \quad (19)$$

$$(\text{or } X + CH_2{=}NO_2^- \longrightarrow \cdot CH_2NO_2 + X^-)$$

intensity of the $O_2NCH_2CH_2\dot{N}O_2^-$ spectrum will increase or remain unchanged on increasing the X^- concentration. (This depends on the nature of the halide, since the equilibrium constant of reaction 18 is different for the different halides.) In our experiments with Br^-, I^-, and SCN^-, the intensity of the spectrum decreased with increasing X^- concentration. This decrease, however, was less than one would expect if $\cdot XOH^-$ were the only reactive species. Although a quantitative treatment could not be developed, it seems that both radicals $\cdot XOH^-$ (or $X\cdot$) and $\cdot X_2^-$ react with nitromethane. However, the decrease in the signal intensity demonstrates that $\cdot XOH^-$ is more

Table II: Hyperfine Constants and g Factors of the $O_2NCH_2CH_2\dot{N}O_2^-$ Radical Produced by Different Oxidizing Agents[a]

Electron-acceptor radical	a_α^N	a_β^H	a_γ^H	g
Br_2^-	25.59	11.31	0.55	2.00508
I_2^-	25.59	11.29	0.53	2.00508
$(SCN)_2^-$	25.60	11.27	0.53	2.00507
$(\cdot SO_4)^-$ [b]	(25.40)	(11.20)	(0.40)	(2.00500)

[a] Hyperfine constants in gauss, accurate to ±0.05 G; g factors accurate to ±0.00003. [b] Results in parentheses are those of Edge, Norman, and Storey.[9]

(32) D. Behar, P. L. T. Bevan, and G. Scholes, *Chem. Commun. D*, 1486 (1971).

reactive than $\cdot X_2^-$ in the electron-transfer reaction (reaction 18).

In addition to the electron-transfer reaction (reaction 16), the thiocyanate radical adds to the nitromethane double bond to form the thiocyanate adduct

$$(SCN)_2^- + CH_2{=}NO_2^- \longrightarrow N{\equiv}CSCH_2\dot{N}O_2^- + SCN^- \quad (20)$$

(The spectrum of $N{\equiv}CSCH_2\dot{N}O_2^-$, together with that of $O_2NCH_2CH_2\dot{N}O_2^-$, appears in Figure 4, the spectral parameters are given in Table I.) Reaction 20 is written involving $(SCN)_2^-$ because high concentrations of SCN^- are necessary in order to see the spectrum of this adduct. The bonding is believed to be through the sulfur, as shown, because of the esr parameters. Only those radicals with sulfur bonded to the CH_2 group have g factors significantly different than the usual value of ~2.0050 (see Table I); the value for the SCN adduct is 2.00616. In addition, the radical with bonding to the nitrogen of the SCN should have a considerably larger ^{14}N splitting as does the N_3 adduct (see below) with one splitting of 2.73 G. The small ^{14}N splitting of 0.31 G observed for the SCN adduct is similar in value to those of the distant nitrogens in the N_3 and CN adducts.

The Cyanide System. In the radiolysis of an alkaline cyanide solution (pH 13) containing nitromethane, an addition reaction of the cyanide radical or a derivative of the cyanide radical takes place. The spectrum of the adduct is characterized by a further 0.51-G triplet splitting caused by an interaction of the unpaired electron with the nitrogen of the cyanide group. Since the product of the reaction of O^- with CN^- has not been clearly identified, several alternatives for the active cyanide species exist. For instance

$$O^- + CN^- \xrightarrow{H_2O} \cdot CN + OH^- \text{ (or } \cdot CNOH^-) \quad (21)$$

Because very good evidence has been found for the formation of $\cdot XOH^-$ [31,32] (X = Cl, Br, I, SCN), it seems most probable that $CNOH^-$ is formed in the primary stage rather than $\cdot CN$. If the product of reaction 21 reacts with another CN^- ion in a reaction analogous to that occurring with the halides

$$\cdot CN \text{ (or } \cdot CNOH^-) + CN^- \longrightarrow (\cdot CN)_2^- \text{ or } [(\cdot CN)_2OH]^{2-} \quad (22)$$

then one of the radicals formed in reactions 21 or 22 might be the active species in the reaction with the nitromethane. Whatever intermediate is involved, only one nitrogen could be observed in the esr spectrum of the adduct, and the simplest adduct structure is $N{\equiv}CCH_2\dot{N}O_2^-$. It is also possible the adduct observed contains a group such as the suggested $CNOH^-$ and that any protons in this group do not give resolvable hyperfine splittings. The small nitrogen splitting is more consistent with a bond through the carbon of the CN group than through the nitrogen.[32a]

The N_3^- System. Upon the radiolysis of N_2O-saturated 5×10^{-2} M NaN_3 in the presence of 10^{-3} M nitromethane at pH 12.5, an addition reaction of the azide radical to nitromethane takes place

$$N_3^- + \cdot OH \longrightarrow \cdot N_3 + OH^- \quad (23)$$

$$\cdot N_3 + CH_2{=}NO_2^- \longrightarrow N_3CH_2\dot{N}O_2^- \quad (24)$$

Under moderate resolution, the spectrum of this adduct (given in Figure 5) can be described by three coupling constants: $a_\alpha^N = 24.74$, $a_\beta^H = 5.46$, and $a_\gamma^N = 2.73$ G. The 24.74- and 5.46-G values are typical of an adduct to $CH_2{=}NO_2^-$ and the 2.73-G coupling constant can be attributed to one of the nitrogens in the azide group. The latter constant is exactly one-half of the coupling constant of the two equivalent protons in the β position. By reducing the magnetic field modulation amplitude, each line of this spectrum could be further resolved into a 0.27-G quintet with intensity distribution of 1:2:3:2:1, indicating equal or nearly equal splittings by the other two nitrogens in the azide group. (One of these resolved lines is given in the top of Figure 5.) The equivalence of two out of three nitrogens in the azide group, as far as the esr spectum is concerned, raises the question of the structure of the $N_3CH_2\dot{N}O_2^-$ radical. Since the azide group in HN_3 is linear,[33] the azide radical would most probably be linear too.[34] One has to assume, therefore, a linear chain of the N_3 group in $N_3CH_2\dot{N}O_2^-$, where the major resonance forms of the molecule are probably I and II. The hyperfine constants of nitrogens

$$\overset{-}{N}{=}\overset{+}{N}{=}N{-}CH_2\dot{N}O_2^- \qquad N{\equiv}\overset{+}{N}{-}\overset{-}{N}{-}CH_2\dot{N}O_2^-$$

(3) (2) (1)

I II

2 and 3 are in this structure only fortuitously equal because the nitrogens are not equivalent. Another possibility is to assume structure III, where cyclization of the N_3 group takes place. This structure seems

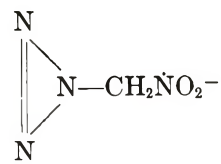

III

to be rather unlikely because of the very unnatural angles between the nitrogens in such a ring. The assignment in sections above of comparable ^{14}N hyper-

(32a) NOTE ADDED IN PROOF. Further studies have shown that the adduct found in CN^- solutions is $H_2NCOCH_2\dot{N}O_2^-$.

(33) M. Winnewisser and R. L. Cook, *J. Chem. Phys.*, **41**, 999 (1964).

(34) T. W. Archibald and J. R. Sabin, *ibid.*, **55**, 1821 (1971).

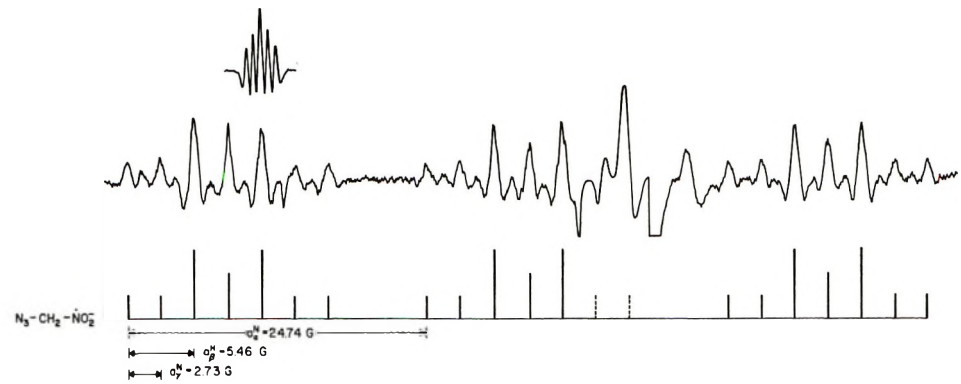

Figure 5. Esr spectrum of the adduct of $\cdot N_3$ to $CH_2{=}NO_2^-$ taken during irradiation of 5×10^{-2} *M* NaN_3 and 1×10^{-3} *M* nitromethane at pH 12.5 (N_2O saturated). The main spectrum is taken under relatively poor resolution with a large modulation amplitude. Above the main trace is an expanded recording of the line immediately below taken under better resolution conditions. Although this line is actually compound as a result of the 2:1 ratio of a_β^H and a_γ^N, all other lines show the same 1:2:3:2:1 structure. This fact demonstrates the exactness of this chance relationship between a_β^H and a_γ^N.

fine constants in $NCCH_2\dot{N}O_2^-$ and $NCSCH_2\dot{N}O_2^-$ makes not unlikely the former structure with the linear N_3 group and fortuitously equal hyperfine splittings.

The CS_2 System. Reaction products of both e_{aq}^- and OH with CS_2 have been detected through their esr spectra.[2] One of these radicals was tentatively identified as $\cdot CS_2^-$, and it was of interest to determine if this species could react with nitromethane. Radiolysis of an alkaline (pH 12.5) solution saturated with CS_2 to which 10^{-2} *M* nitromethane had been added produced the spectra of two adducts to $CH_2{=}NO_2^-$ in addition to the e_{aq}^- and OH adducts. Because of the high rate constant,[35] $k_{e_{aq}^- + CS_2} = 3.1 \times 10^{10}$ M^{-1} sec^{-1}, and CS_2 concentration ($\sim 3 \times 10^{-2}$ *M*), reaction of e_{aq}^- is predominantly with the CS_2. However, unless the rate constant for OH + CS_2 is very high, most of the OH radicals will be scavenged by the nitromethane. One of the adduct radicals obtained with this system is that previously identified as the $\cdot S^-$ adduct, namely $^-SCH_2\dot{N}O_2^-$. The other spectrum (whose lines were mostly masked by other lines) has the hyperfine constants $a_\alpha^N = 25.71$, $a_\beta^H = 8.78$ G, and $g = 2.00503$. This spectrum is attributed to the $\cdot CS_2^-$ radical adduct $^-S_2CCH_2\dot{N}O_2^-$. On repeating the experiment at pH 11.3, the spectrum of $^-SCH_2\dot{N}O_2^-$ disappeared and almost a full spectrum of the CS_2^- adduct could be observed. The source of $\cdot S^-$ which forms $^-SCH_2\dot{N}O_2^-$ seems most likely to be the reaction of OH with S^{2-} from the hydrolysis at high pH of CS_2.

$$CS_2 + 4OH^- \longrightarrow CO_2 + 2S^{2-} \qquad (25)$$

The S^{2-} formed in this reaction could be detected easily as H_2S by acidifying the alkaline solution.

The NO_2 Radical. $\cdot NO_2$ radicals were produced by reacting O^- with nitrite in N_2O-saturated alkaline solution

$$NO_2^- + O^- \xrightarrow{H_2O} NO_2 + 2OH^- \qquad (26)$$

In the absence of scavengers, the NO_2 hydrolyzes with a 300-sec^{-1} first-order rate constant.[36] To get a significant addition reaction in competition with the hydrolysis, it was necessary to use 10^{-2} *M* nitromethane. This concentration in turn necessitated a concentration of NO_2^- as high as 0.2 *M* in order that NO_2^- could compete with the nitromethane for O^- ($k_{O^- + NO_2^-} = 2.5 \times 10^8$ M^{-1} sec^{-1} [36] and $k_{O^- + CH_2=NO_2^-} = 9 \times 10^9$ M^{-1} sec^{-1} [11]).

The spectrum of the $\cdot NO_2$ adduct is composed of a 9.58-G quintet with intensity distribution of 1:2:3:2:1 where each line is further split into a 4.09-G doublet. This spectrum is different from all other nitromethane adducts in the sense that the typical nitrogen splitting of ~25 G is not observed. This spectral pattern indicates a radical with two equivalent nitrogens and one proton. Lagercrantz, *et al.*,[37] have reported an essentially identical spectrum formed by secondary reactions in the reduction of $C(NO_2)_3^-$ and identified it as $H\dot{C}(NO_2)_2^{2-}$. In the present work the primary stage seems to be addition of the NO_2 to the carbon nitrogen double bond

$$NO_2 + CH_2{=}NO_2^- \longrightarrow O_2NCH_2\dot{N}O_2^- \qquad (27)$$

This second nitro group seems to behave in the same manner as the nitro group in nitromethane in the sense of activating the protons on the carbon. Dissociation of a proton in alkaline environment is then possible

$$O_2NCH_2\dot{N}O_2^- + OH^- \rightleftharpoons (^-O_2N{=}CH{=}NO_2^-)\cdot + H_2O \qquad (28)$$
$$\text{IV}$$

The dinitromethane radical anion (IV) which has two equivalent nitrogens and one proton is consistent with

(35) S. Gordon, E. J. Hart, M. S. Matheson, J. Rabani, and J. K. Thomas, *Discuss. Faraday Soc.*, **36**, 193 (1963); E. J. Hart, S. Gordon, and J. K. Thomas, *J. Phys. Chem.*, **68**, 1271 (1964).

(36) A. Treinin and E. Hayon, *J. Amer. Chem. Soc.*, **92**, 5821 (1970).

(37) C. Lagercrantz, K. Torssell, and S. Wold, *Ark. Kem.*, **25**, 567 (1966).

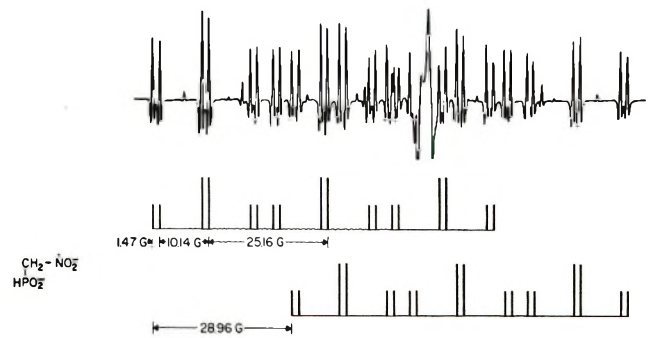

Figure 6. Esr spectrum of the adduct of $\dot{H}PO^{2-}$ to $CH_2{=}NO^{2-}$ taken during irradiation of 2×10^{-2} *M* $H_2PO_2^-$ and 1×10^{-2} *M* nitromethane at pH 12.5 (N_2O saturated). Also evident are small lines from $CH_3\dot{N}O_2^-$.

the observed esr parameters. Lagercrantz, *et al.*,[37] have discussed the electronic structure.

The spectrum of (IV) appeared only at pH ~12.5, and its intensity increased on increasing the pH up to ~13.5. No changes in the splittings or line widths were observed. The most obvious reason for this change in intensity is the equilibrium 28 with $pK >$ 12.5. However, at no pH in the range 10.7–13.5 could lines of the form $O_2NCH_2\dot{N}O_2^-$ be detected. No esr spectrum at all was observed at pH 10.7, where the nitromethane still reacts as a trap. Two explanations for the absence of a spectrum of $O_2NCH_2\dot{N}O_2^-$ can be advanced. Either the lifetime of this form is considerably less than that of IV or in $O_2NCH_2\dot{N}O_2^-$ an electron transfer occurs from one NO_2 group to the other at a rate which can cause broadening of the lines.

The Radicals $\cdot PO_3^{2-}$ *and* $H\dot{P}O_2^-$. The esr spectra of both $\cdot PO_3^{2-}$ and $H\dot{P}O_2^-$ have been observed in solution.[2] In the presence of nitromethane these radicals could be trapped forming the nitromethane adducts

$$\cdot PO_3^{2-} + CH_2{=}NO_2^- \longrightarrow {}^{2-}O_3PCH_2\dot{N}O_2^- \quad (29)$$

$$H\dot{P}O_2^- + CH_2{=}NO_2^- \longrightarrow {}^-O_2HPCH_2\dot{N}O_2^- \quad (30)$$

Splittings by ^{31}P of 31.04 and 28.96 G, respectively, are observed in these adducts, and in the case of the $H\dot{P}O_2^-$ adduct a splitting of 1.47 G by the HP proton is also present. The spectrum of this latter adduct is given in Figure 6. The magnetic parameters for both adducts are given in Table I. The radicals $\cdot PO_3^{2-}$ and $H\dot{P}O_2^-$ have previously been studied by radical trapping with *tert*-nitrosobutane.[4,38]

The Arsenite System. An experiment carried out with 10^{-2} *M* $NaAsO_2$ (Fisher) and 2×10^{-3} *M* CH_3NO_2 in N_2O-saturated solution (pH 12.7) yielded the spectrum of an adduct showing a large ^{75}As splitting of 73.55 G (see Figure 7). From this ^{75}As splitting, it is clear that bonding of the substituent is through the arsenic. Because some question exists as to the exact form of arsenic present in these solutions, we

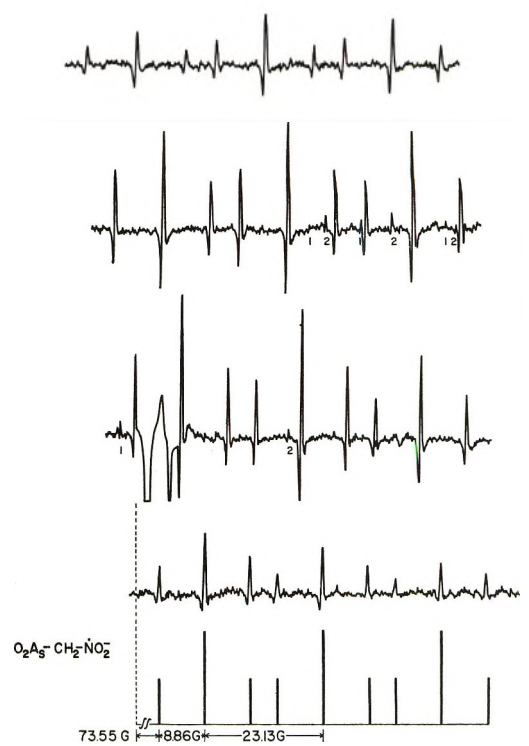

Figure 7. Esr spectrum of the adduct to $CH_2{=}NO_2^-$ taken during irradiation of 1×10^{-2} *M* sodium arsenite and 2×10^{-3} *M* nitromethane at pH 12.7 (N_2O saturated). The spectrum consists of four nine-line sets as a result of a 73.55-G splitting by ^{75}As (spin $^3/_2$) and is assigned as indicated. The total width of this spectrum is 285 G. The groups for $I_z = \pm^3/_2$ are broader and less intense and indicate some residual effect of the anisotropy of the ^{75}As coupling. The small lines labeled by the numbers 1 and 2 are from $HOCH_2\dot{N}O_2^-$ and $CH_3\dot{N}O_2^-$, respectively.

cannot be certain what radical is produced. If, as seems most likely,[39] the arsenic is present as AsO_2^-, then we expect to have produced $\cdot AsO_2$ by reaction of OH. From the signal intensity in Figure 7, the addition to $CH_2{=}NO_2^-$ must then be rather efficient. It is also possible that the radical is analogous to that in the phosphite system, namely $\cdot AsO_3^{2-}$.

The Hyperfine Constants of Adducts to $CH_2{=}NO_2^-$. All of the radicals discussed with the exception of $\cdot CH(NO_2^-)_2$ can be regarded as substituted nitromethane anions. Because substitution on the carbon (at the β position with respect to the main radical center) represents a minor change in the electronic structure of the radical, relatively small changes occur in the magnetic parameters with different substituents. At a finer level, a number of trends are observed which can be related to the nature of the substituent.

The major feature of the spectrum, the ~25-G nitrogen splitting, is affected significantly by substitution. If the value for $CH_3\dot{N}O_2^-$ (25.96 G, the highest

(38) G. Adevik and C. Lagercrantz, *Acta Chem. Scand.*, **24**, 2253 (1970); H. Karlsson and C. Lagercrantz, *ibid.*, **24**, 3411 (1970).

(39) G. Jander and H. Hofmann, *Z. Anorg. Allg. Chem.*, **296**, 134 (1958).

value in Table I) is taken as a reference, then the presence of a heavy atom in the γ position (bonded to the methylene carbon) lowers the nitrogen splitting by up to 4 G (as in the SCN adduct). This effect is seen for all of the radicals with sulfur in the γ position and also with arsenic. The two radicals with phosphorus in this position do not show this effect to any marked degree.

The hyperfine constant for the methylene protons potentially can be affected by the internal rotation about the CN bond. If this splitting obeys the relationship $a_\beta^H = A \cos^2 \theta$, where θ is the azimuthal angle between the CH bond and the axis of the p orbital on nitrogen, then a variation of from one-half to three-halves times the splitting in $CH_3\dot{N}O_2^-$ is possible (for equivalent CH_2 protons). The usual tendency for the splitting by β-methylene protons is to be below that of the CH_3 group at the same position.[40] In fact, several CH_2 splittings are below this lower limit ($\sim$6 G), so that additional factors appear to be important. There does not seem to be any correlation with size of the substituent, because while the $\cdot SO_3^-$ adduct has the value $a_\beta^H = 7.50$ G, the adducts of $\cdot PO_3^{2-}$ and $H\dot{P}O_2^-$ have values of 10.64 and 10.14 G. The very low values of a_β^H are associated with substituents which have some possibility of a direct interaction with the radical site. (This interaction is, of course, favored by the configuration with $\theta = 0$ for the substituent group and $\theta = 60°$ for the protons.) Examples are the adducts of $\cdot SO_3^-$, $\cdot S^-$, $\cdot SH$, $\cdot S_2O_3^-$, $\cdot SCN$, and $\cdot N_3$. Krusic and Kochi[41] have postulated such a direct interaction in radicals such as $\cdot CH_2CH_2SCH_3$ to explain similar low values for a_β^H. They find that the values of a_β^H can be explained by a tipping of the $-CH_2X$ group so that the X atom is closer to the radical site.

The other trend observed in the magnetic parameters is an increase in the g factor. Of the radicals observed in this study only those with divalent sulfur in the γ position show much effect. The adducts of $\cdot S^-$, $\cdot SH$, $\cdot S_2O_3^-$, and $\cdot SCN$ show this effect with increases in g factors by up to 0.0010. The most obvious reason for the increase in g factor is the involvement of the sulfur orbitals in the wave function for the unpaired electron. From the lack of effect on the g factor produced by the presence of sulfur in the $\cdot SO_3^-$ adduct, it must be that the sulfur lone-pair electrons are those interacting strongly with the radical site. It is not surprising that decreases in a^N and a_β^H also accompany the changes in g factor caused by the divalent sulfur. The results for the $\cdot SO_3^-$ and $\cdot AsO_2$ adducts, however, show that a decrease in a^N is possible without a significant effect on the g factor and that there may be more than one mechanism operable.

The structures assigned to the adduct radicals with respect to the bonding of the substituent are indicated in Table I. In many cases the bonding is obvious or is derived from the known structure of the substituent from solid-phase esr studies. Some cases have been discussed in the individual sections. Thus with $\cdot NO_2$, $\cdot CO_2^-$, $\cdot SO_3^-$, $\cdot PO_3^{2-}$, $H\dot{P}O_2^-$, and $\cdot AsO_2$, bonding is expected to be through the central atom. The hyperfine splittings by this central atom confirm this structure. With $\dot{C}O_3^-$ the unpaired electron is mainly in an orbital on the oxygens and bonding is expected to take place through an oxygen. The situation with $\cdot S_2O_3^-$ is similar, but a choice of bonding through either an oxygen or the outer sulfur is possible. From the large effect on both the g factor and a^N in the adduct, it seems evident that bonding is through the sulfur. By analogy with $\cdot CO_2^-$, it is expected that $\cdot CS_2^-$ should bond through the carbon. Although some question exists as to the presence of $\cdot CS_2^-$ in the CS_2 system, it is clear from the normal values of a^N and the g factor that the radical designated as the $\cdot CS_2^-$ adduct must have bonding to a carbon. The radical $-S_2C\dot{C}H_2NO_2^-$ has such bonding. The adducts formed from $\cdot CN$, $\cdot N_3$, and $\cdot SCN$ have been discussed in the individual sections.

The Reaction Path. Some comments are necessary on the path of reaction of inorganic radicals with $CH_2{=}NO_2^-$. Both addition and electron transfer (oxidation) are observed, and it is instructive to try to find the factors determining which reaction occurs. Clearly, the reduction potential of the radical reacting with $CH_2{=}NO_2^-$ determines if the electron transfer reaction is energetically possible or not. Lilie[42] has recently measured the reduction potentials of a number of radicals of concern here, and by comparison with the esr results has concluded that any radical with a reduction potential more positive than -0.8 V can oxidize $CH_2{=}NO_2^-$. The radicals successfully studied by him which fall into this category are Br_2^-, $(SCN)_2^-$, and I_2^-.

As we have seen, Br_2^- and I_2^- clearly oxidize $CH_2{=}NO_2^-$, while $(SCN)_2^-$ can react by both paths. Unfortunately, it was not possible for Lilie[42] to determine a potential for OH, but this species must be more strongly oxidizing than Br_2^- and should therefore react by oxidation of $CH_2{=}NO_2^-$. The esr results, however, show that the only reaction is addition. Another factor must be present which changes the path of the reaction. We believe this factor to be the strength of the new bond formed in the adduct. In the comparison of Br_2^- and OH, for example, the strengths of the (C–X) bonds in CH_3Br and CH_3OH are respectively 65 and 90 kcal mol^{-1}. Although one might hope to make a more quantitative comparison of the energy changes involved in the two reaction

(40) For example, the value of a_β^H in $CH_3CH_2NO_2^-$ is 9.75 G: L. H. Piette, P. Ludwig, and R. N. Adams, *J. Amer. Chem. Soc.*, **83**, 3909 (1961); **84**, 4212 (1962).

(41) P. J. Krusic and J. K. Kochi, *ibid.*, **93**, 846 (1971).

(42) J. Lilie, *J. Phys. Chem.*, in press.

paths for each of the radicals studied, the data available on electron affinities, ion solvation energies, and bond energies are not of sufficient accuracy to make such a comparison meaningful.

Conclusion

The use of the *aci* anion of nitromethane (CH_2=NO_2^-) as a radical trap has been shown to be a very effective method of studying inorganic radicals because of its high reactivity. Use of this agent extends the concept of a radical trap in the sense that the product radical is not completely stable. With any of a number of methods of continuous radical generation, complete stability is not necessary and sufficient radical concentrations for study are readily available.

Two types of reaction with CH_2=NO_2^- have been identified: addition and oxidation by electron transfer. Radicals reacting in the latter way obviously cannot be distinguished further. Fortunately, these radicals are limited to those of rather strong oxidizing power and are not numerous. A number of adducts to CH_2=NO_2^- have been identified in this work. The existence of their spectral parameters now makes possible identification of the same radicals in other chemical systems as has been done in the photolysis of $S_2O_3^{2-}$.[13] In a complementary sense, the finding of a spectrum of a new adduct in some system allows one to conclude that a new radical must be present. A number of the radiolytic reactions used to generate the initial radical seem to proceed in a straightforward way, allowing rather certain identification of the adducts. In other cases the generation reaction has been clarified. As an example, we can mention the elucidation of the reactions of $S_2O_3^{2-}$ with rather clear identification of $\cdot S^-$ as a product of reaction of e_{aq}^-. Also evident is the addition of N_3 as a unit to CH_2=NO_2^-. In this latter case, of course, we cannot be certain that intermediates such as N_6^- are not involved. Nevertheless, the net reaction is very clear. Some new information on the CS_2 and oxalate systems has also come from this work. Application of CH_2=NO_2^- as a radical trap in other radiation chemical and photochemical systems should be profitable.

Electron Spin Resonance Studies on Irradiated Heterogeneous Systems.

VIII. Radical Cation Formation from Toluene

by T. Komatsu,[1] A. Lund,* and P.-O. Kinell

The Swedish Research Councils' Laboratory, Studsvik, S-611 01 Nyköping 1, Sweden *(Received November 23, 1971)*

Publication costs assisted by the Atomic Research Council of Sweden

This investigation was initiated to resolve the question of whether positive or negative ions are formed from aromatic compounds irradiated in the adsorbed state. The predominant formation of molecular cations in the cases of toluene and toluene-α-d_3 adsorbed on silica gel and Vycor glass was demonstrated unambiguously by means of esr spectroscopy. Benzyl and tolyl radicals prepared by the radiolysis of the halides in the adsorbed state gave spectra which differ significantly from those obtained from toluene. Weak absorptions due to the cyclohexadienyl type of radical could occasionally be detected, but no spectrum attributable to the anion was found. The magnitudes of the isotropic coupling constants $|a_2|$ = 2.1 G, $|a_4|$ = 11.8 G, $|a_{CH_3}|$ = 18 G estimated by line profile simulations are in reasonable accord with theoretical estimates.

Introduction

It was previously shown that ionic species formed from aromatic compounds by irradiation remained stable in the adsorbed state at 77 K.[2,3] A comparison between the optical and the esr spectra and the influence of charge scavengers suggested that negative ions were formed from benzene adsorbed on silica gel as well as in the hydrocarbon glass. This is analogous to the free-radical formation in alkyl halides, which are known as electron scavengers, and in biphenyl and

(1) On leave from Department of Polymer Science, Hokkaido University, Sapporo, Japan.

(2) O. Edlund, P.-O. Kinell, A. Lund, and A. Shimizu, (a) *J. Chem. Phys.*, **46**, 3679 (1967); (b) *Advan. Chem. Ser.*, **No. 82**, 311 (1968).

(3) (a) P. K. Wong and J. E. Willard, *J. Phys. Chem.*, **72**, 2623 (1968); (b) P.-O. Kinell, A. Lund, and A. Shimizu, *ibid.*, **73**, 4175 (1969).

naphthalene, and this parallel behavior also favored the hypotheses that negative ions were formed.[3a] On the other hand, the coupling constants of the benzene and the biphenyl ions are slightly increased by comparison with the values for the negative ions generated in the solution, and this is usually the case for positive ions.[2] This alternative assignment is supported by the close similarity between the coupling constants of the positive naphthalene ion dimer and the radical species observed after γ irradiation of silica gel containing a small amount of the hydrocarbon.[3b] Ekstrom[4] attributes the species formed from benzene to the negative dimer, following comparison with a similar optical absorption in the trimethylpentane glass. However, this latter interpretation based on scavenger experiments has recently been questioned.[5]

The ambiguity in establishing the charge of the ionic radicals formed in radiation-induced processes arises because the difference in the optical or esr spectra between the positive and negative aromatic ion is small. An unambiguous assignment seems to be possible, however, when methyl-substituted benzenes such as toluene are used. In these molecules the degeneracy of the π-electron orbitals of the benzene nucleus is lifted.[6] Because of the electron-repelling substituent the e_{2u} level containing the odd electron in the negative toluene ion is split, and the lower energy is obtained when the spin density is that indicated by the first alternative (a).

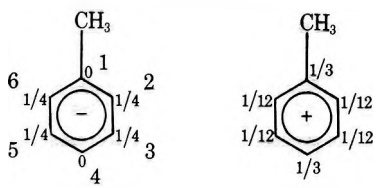

(a) (b)

In a similar manner the removal of an electron from the split e_{1g} level would leave the unpaired electron with a spin density distribution which is given approximately by (b). Completely different ring proton interactions are therefore expected to show up in the esr spectra from the positive and the negative ion. In addition the methyl protons should interact strongly in the positive ion but weakly in the negative species. A specific deuteration of the methyl group would thus affect the spectra to a different extent.

In the work reported here toluene and toluene-α-d_3 were adsorbed on silica gel, Vycor glass, and molecular sieves. The exclusive formation of positive ions could then be unambiguously proved, without the necessity of introducing other agents such as charge scavengers into the system. This corroborates the assignment of Nagai, *et al.*[7]

Experimental Section

The toluene had a stated purity of 99.9 mol %. The toluene-α-d_3 supplied from Merck Sharp & Dohme

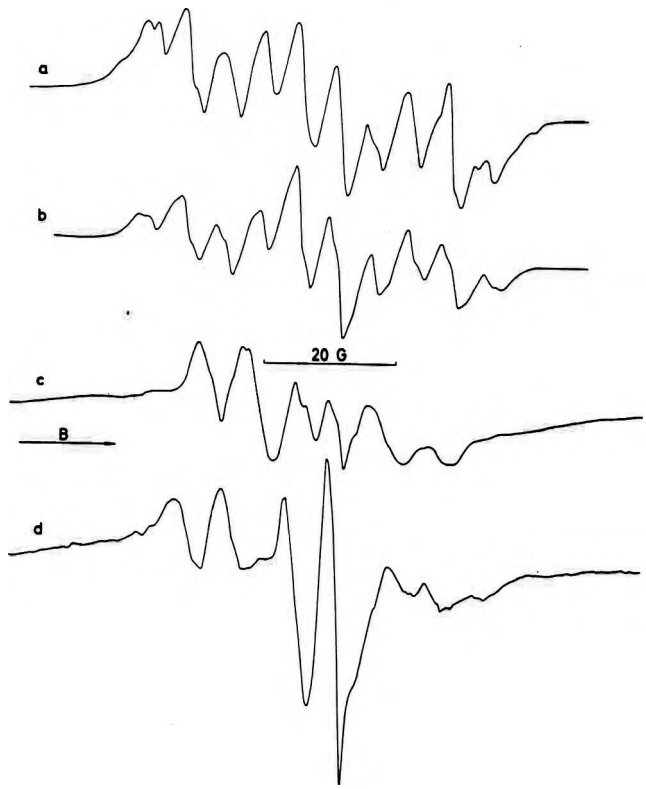

Figure 1. Esr spectra from silica gel samples previously degassed at 550° containing adsorbed material. Irradiation and recording were performed at 77 K: (a) with benzyl bromide adsorbed; (b) simulation of (a) due to $C_6H_5\dot{C}H_2$ with a_{CH_2} = 17.0 G, a_{ortho} = 5.0 G, a_{para} = 6.6 G, a_{meta} = 2.2 G, ΔH_{pp} = 2.2 G (Lorentzian shape); (c) with 2-iodotoluene adsorbed; (d) with 3-iodotoluene absorbed.

was used without further purification. Silica gel (667 m^2/g), porous Vycor glass (120 m^2/g), and molecular sieves in the hydrogen form HX (1000 m^2/g), HY (550 m^2/g) prepared from the NH_4^+ form by elimination of ammonia were used as adsorbents. The hydrocarbon was added on a vacuum line to the carefully degassed samples, which were kept in Suprasil tubes. The tubes (o.d. 4 mm) were sealed off in the vacuum and exposed to a dose of 1 Mrad with γ rays from ^{60}Co at 77 K. Esr spectra were observed at temperatures ranging from 77 to 300 K with the help of an instrument operating at 9.2 GHz.

Results

The spectrum observed at 77 K from a sample containing benzyl bromide adsorbed on silica gel previously degassed at 550° (Figure 1a) could be simulated with reasonable accuracy using the isotropic coupling constants given in Figure 1b. These values are in good

(4) A. Ekstrom, *J. Phys. Chem.*, **74**, 1705 (1970).

(5) B. Brocklehurst, *ibid.*, **75**, 1177 (1971).

(6) A. Carrington and A. D. McLachlan, "Introduction to Magnetic Resonance," Harper and Row, New York, N. Y., 1967, p 88.

(7) S. Nagai, S. Ohnishi, and I. Nitta, *Bull. Chem. Soc. Jap.*, **44**, 1230 (1971).

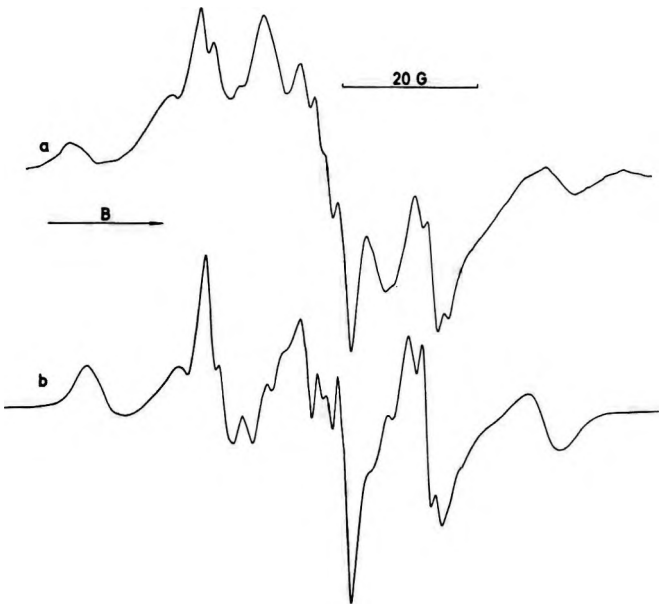

Figure 2. Esr spectra from silica gel samples containing toluene. Irradiation and recording were performed at 77 K: (a) with 1% toluene adsorbed on a sample previously degassed at 550°; (b) with 0.3% toluene adsorbed on a sample previously degassed at 300°.

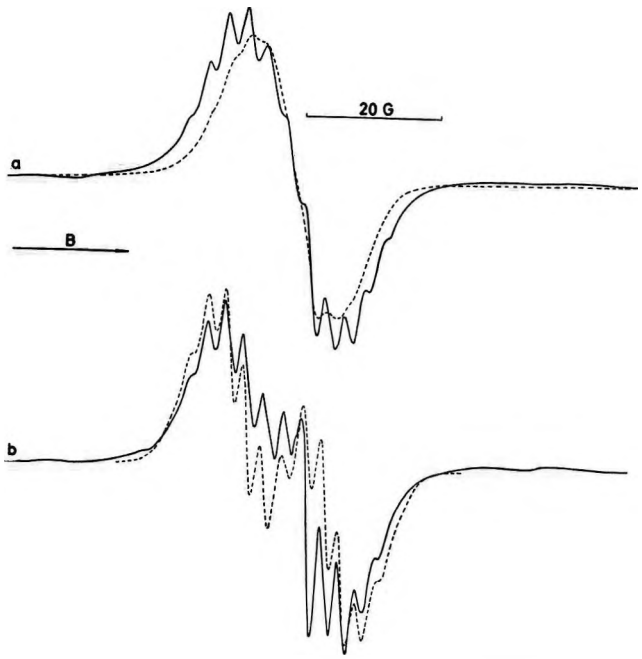

Figure 3. Esr spectra from silica gel samples containing toluene-α-d_3. Irradiation and recording were performed at 77 K: (a) with 1% toluene-α-d_3 adsorbed on a sample previously degassed at 550°; the dashed spectrum appeared after ir illumination ($\lambda > 1000$ nm); (b) with 0.3% toluene-α-d_3 adsorbed on a sample previously degassed at 250°; the dashed spectrum due to $C_6H_5CD_3^+$ is simulated with $a_{CD_3} = 2.75$ G, $a_{para} = 11.8$ G, $a_{ortho} = 2.1$ G, $a_{meta} = 0.75$ G, $\Delta H_{pp} = 1.9$ G (Lorentzian shape).

agreement with previous estimates for the benzyl radical in the solution.[8] The spectrum could be almost completely bleached by illuminating with filtered light ($\lambda > 1000$ nm). The absorptions generated by irradiating 2-iodotoluene (Figure 1c) and 3-iodotoluene (Figure 1d) under similar conditions exhibited unsymmetric line profiles. The apparent splitting constants previously estimated for the 2-tolyl radical[9] agrees with those measured from Figure 1c, $a_1 = 19.3$ G, $a_4 = a_6 = 7.3$ G.

The spectrum from a sample containing 1% toluene adsorbed on silica gel which had previously been degassed at 550° for 24 hr showed a rather complicated and asymmetric line profile (Figure 2a). It changed into a spectrum with a number of scarcely resolved lines separated by 7.4 G on warming or on illumination with infrared light ($\lambda > 1000$ nm). A similar spectrum was observed without any warming at a higher toluene content of 10%. These spectra differ significantly from the spectrum of Figure 1a. The spectra assigned to the 2-tolyl and 3-tolyl radicals (Figure 1c and d) as well as that from the 4-tolyl radical[9] are also all quite distinct from the line shape observed with toluene.

Better resolution was afforded with 0.3% toluene adsorbed on silica gel which had been degassed at a lower temperature of 250° (Figure 2b). In this case weak lines were observed on the wings of the main absorption. Comparison with the similar spectra observed from other aromatics under the same conditions[2,3b] showed that these were attributed to the cyclohexadienyl type of radical formed by hydrogen attachment to the benzene ring.

In the toluene-α-d_3 silica gel system the resolution into a number of components separated by 3 G achieved with the gel degassed at 550° was destroyed by the illumination with filtered light ($\lambda > 1000$ nm) (Figure 3a). Better resolution was obtained when the silica gel was treated at 250° before adsorbing a small amount (0.3%) of the hydrocarbon. In this case 11 components could be distinguished. Part of the asymmetry in Figure 3b is caused by a species formed in the gel.

The esr spectra of toluene and toluene-α-d_3 (Figure 4a and b) adsorbed on Vycor glass preheated to 300° are almost identical with those observed in the silica gel system. However, warming or illumination with infrared light had no significant effect on the line profile.

The esr spectrum of 1% toluene adsorbed on the molecular sieve (Figure 5a) HX was more complex than that observed in the toluene–silica gel or Vycor glass system. Some peaks may correspond to those from the benzyl radical as indicated by a comparison with the spectrum of Figure 1a. At a toluene content of 10% the spectrum of Figure 5b with an odd number of lines separated by 7.4 G was obtained. Most of the radicals had decayed at 150 K and only a single line at $g = 2.0029$, width 7 G, remained stable up to 273 K.

(8) W. T. Dixon and R. O. C. Norman, *J. Chem. Soc.*, 4857 (1964).
(9) S. Nagai, S. Ohnishi, and I. Nitta, *J. Phys. Chem.*, **73**, 2438 (1969).

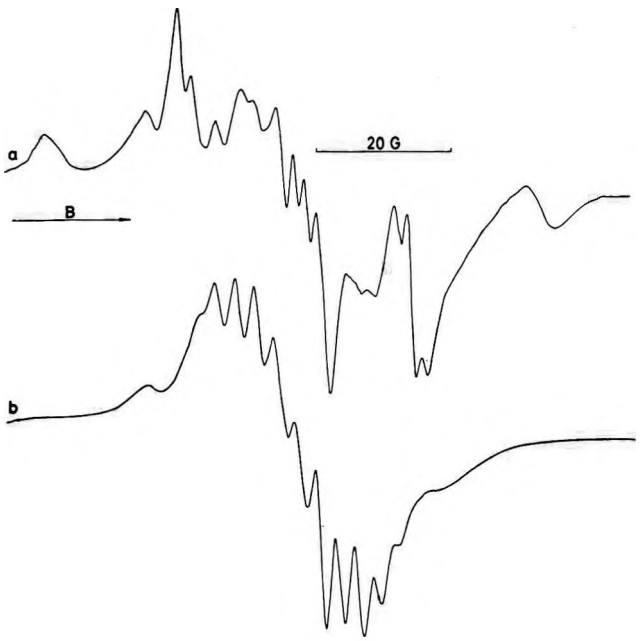

Figure 4. Esr spectra from (a) toluene and (b) toluene-α-d_3 adsorbed on Vycor glass previously degassed at 300°. Irradiation and recording were performed at 77 K.

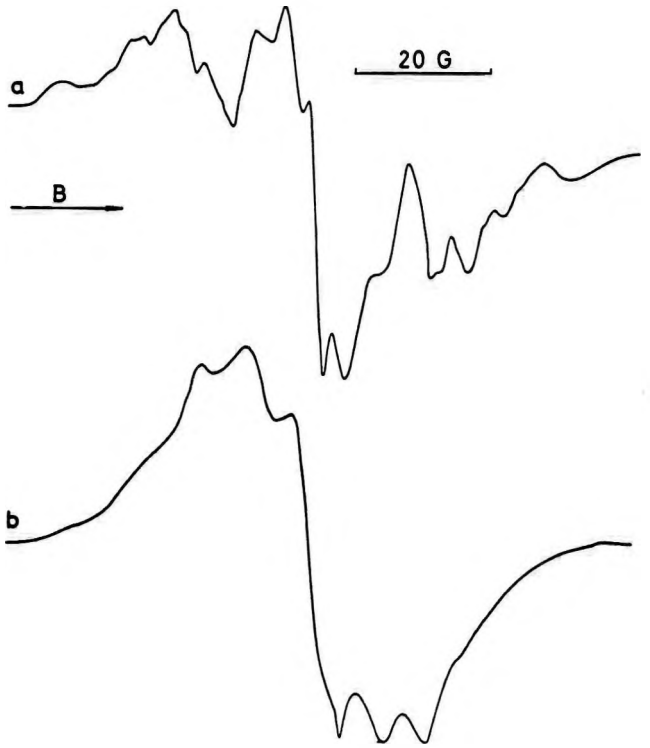

Figure 5. Esr spectra from toluene adsorbed on the molecular sieve HX previously degassed at 550°. Irradiation and recording were performed at 77 K: (a) with 1% toluene; (b) with 10% toluene.

The absorption from toluene on the molecular sieve HY had a line shape which resembled that found in the HX system. The signal intensity was lower than in the silica gel or Vycor glass systems.

Discussion

This study was initiated mainly to elucidate the nature of the ionic species formed in the γ-irradiated adsorbed systems containing aromatic compounds. For this reason most attention was paid to the analysis of the spectra from paramagnetic fragments stabilized on the silica gel preheated at 250° or Vycor glass. As will be discussed below, these absorptions are most probably due to toluene cations. With the other adsorbents more complex spectra were observed, indicating the simultaneous presence of neutral radicals formed by hydrogen abstraction or addition reactions.

Assignment of Coupling Constants. The change of spectral appearance when toluene-α-d_3 is used clearly demonstrates that the species present in the silica gel and Vycor glass system is due to the hydrocarbon. The experiments with benzyl bromide and iodotoluene exclude the possibility that the radicals formed are benzyl or tolyl. Neutral radicals of the cyclohexadienyl type are present only to a minor extent and could scarcely give rise to the strong central absorption. In agreement with the conclusion reached in previous studies[2,3] it appears most likely that the main spectrum can be assigned to an ionic species formed from the aromatic compound.

The assignment of the coupling constants was facilitated by a comparison with the spectra from samples containing toluene-α-d_3. Appropriate values for simulating the spectrum from the toluene-α-d_3 ion were $a_{para} = 11.8$ G, $a_{ortho} = 2.1$ G, (Figure 3b). In this case $a_{CD_3} = 2.75$ G is reduced by the factor $(g_D/g_H) = 0.153$, so that the methyl coupling is estimated to be $a_{CH_3} = 18$ G. The small coupling from the meta protons could not be resolved due to the excessive width $\Delta H_{pp} = 1.9$ G of the peak-peak derivative Lorentzian line.

Spin Densities and Hyperfine Couplings. Neither the methyl coupling nor the ring proton interactions are in accord with previous estimates[10] for the negative ion (Table I). To support the assignments some effort was made to theoretically estimate the hyperfine coupling constants of the toluene positive ion. Electron spin densities calculated from the simple theory are known to predict the experimental splittings of the ring protons rather well by the use of appropriate parameters[11] of the McConnell[12] or the Colpa–Bolton[13] relation. Suitable inductive corrections to the hyperconjugation model of the toluene anion have been previously reported.[14] The same parameters were employed here for the cation using the Hückel theory and

(10) J. R. Bolton and A. Carrington, *Mol. Phys.*, **4**, 497 (1961).
(11) I. C. Lewis and L. S. Singer, *J. Chem. Phys.*, **43**, 2712 (1965).
(12) H. M. McConnell, *ibid.*, **24**, 664 (1956).
(13) J. P. Colpa and J. R. Bolton, *Mol. Phys.*, **6**, 273 (1963).
(14) D. Lazdins and M. Karplus, *J. Amer. Chem. Soc.*, **87**, 920 (1965).

the method of McLachlan,[15] taking $\lambda = 1.0$. A detailed analysis of the spin distribution and hyperfine splittings of the toluene anion and cation radicals has previously been made.[16] In this instance the consequences of vibrational and thermal coupling of the near degenerate levels were considered. The deviations from the spin density distribution in the lowest electronic state, reproduced in Table II, were found to be small and were neglected here for simplicity. The methyl proton hyperfine splitting of 15 G calculated from the unpaired electron density in the pseudo-π orbital centered at the methyl protons of Table II could be reproduced with $Q = 44$ G in the relation $a_{CH_3}^{H} = Q \cdot \rho_1$. The couplings derived from the simple models in this manner are of comparable magnitude. A calculation which includes the interaction of all valence electrons was performed with the INDO method.[17] In this case the average methyl coupling calculated from the two geometries which differed by a rotation through 120° about the C_1–CH_3 bond is slightly larger than that predicted from the π-orbital models, while the magnitude of a_4 is smaller. The experimental couplings are somewhat closer to those predicted by the ASMO theory. In this case some parameters were optimized empirically[16] to produce good agreement with available experimental data. The INDO program[18] used did not permit the adjustment of the parameters.

Estimate of Anisotropic Parameters. The spectra shown in Figures 2b and 4a from the samples containing ordinary toluene could not be analyzed in terms of isotropic or axially symmetric anisotropic couplings. These absorptions do not contain any noticeable amounts of tolyl or bleachable benzyl; they represent rather pure spectra from the toluene positive ion. An attempt to estimate the anisotropy of the resonance parameters was carried out as follows. First the dipolar coupling between a proton and the unpaired spin density at each of the carbon atoms were calculated in a molecular coordinate system. The z axis is at right angles to the radical plane. The geometry of the benzene ring was adopted together with a C–CH_3 distance of 1.51 Å. The contribution from spin density at the nearest neighbor atom was evaluated empirically[19] and found to be $A_x = 14.0$ G, $A_y = -15.1$ G, $A_z = 1.1$ G. The interactions with spin density centered at distant carbon atoms were estimated by formulas given by McConnell and Strathdee.[20] Next the contributions were scaled to the appropriate π-electron spin density calculated by the ASMO method, added together, and brought into diagonal form in order to find the principal values and the direction cosines of the principal axes. The complete coupling tensors were derived, finally, by adding the appropriate isotropic splittings. The anisotropic g factors were evaluated using the theory of Stone.[21] A summary of the parameters derived is given in Table III. These data were used to simulate the line shape for randomly oriented radicals, employing a computer program written by Maruani.[22] Although a full account of all the spectral details could not be generally achieved, this treatment has proved useful for the assignments in a series of aromatic radicals.[19] The results obtained here showed that an isotropic coupling $a_{CH_3} = 18$ G was appropriate to reproduce the total width of the experimental spectrum. This corroborates the estimate derived from the deuteron splitting in the toluene-α-d_3 ion. The computed line profiles were sensitive to the values given to $a_3 = a_5$, but due to the rather poor agreement with the experimental spectrum neither the magnitude nor the sign could be established. The g factor anisotropy can probably be estimated more accurately from spectra recorded at a higher microwave frequency.

Table I: Calculated and Observed Coupling Constants (G) in the Toluene Cation

	Position			
	2,6	3,5	4	8
a	−2.9	−1.2	−12.7	+14.9[c]
b	−2.7	−1.1	−13.5	+14.9
INDO	−3.0	+0.3	−8.6	+24.8
$C_6H_5CH_3^-$ [d]	5.12	5.45	0.59	0.79
$C_6H_5CH_3^+$	2.1	...	11.8	18

[a] Ring proton couplings are calculated using the McConnell relation $a_i = 35.7 \times \rho_i$. Here the spin densities ρ_i are the ASMO values of Table II. [b] Ring proton couplings are calculated using the Colpa–Bolton equation $a_i = (-32.3 - 16\rho_i)\rho_i$. [c] Methyl proton couplings are calculated with $a_8 = 44\rho_1$. [d] Reference 10.

Table II: Toluene Cation π-Electron Spin Densities

	Position					
	1	2,6	3,5	4	7	8 = H_{CH_3}
HMO[a]	0.308	0.093	0.070	0.310	0.017	0.014
McL[b]	0.367	0.069	0.029	0.382	0.007	0.016
ASMO–CI[c]	0.339	0.081	0.033	0.355	0.010	0.068

[a] Hyperconjugative and inductive parameters according to ref 14. [b] Theory of McLachlan[15] with $\lambda = 1.0$. [c] Spin densities in the lowest electronic state. The effect of vibronic coupling considered in ref 16 is neglected.

(15) A. D. McLachlan, *Mol. Phys.*, **3**, 233 (1960).
(16) D. Purins and M. Karplus, *J. Chem. Phys.*, **50**, 214 (1969).
(17) J. A. Pople, D. L. Beveridge, and P. A. Dobosh, *J. Amer Chem. Soc.*, **90**, 4201 (1968).
(18) P. A. Dobosh, Program 141, Quantum Chemistry Program Exchange, Indiana University (1968).
(19) G. S. Owen and G. Vincow, *J. Chem. Phys.*, **54**, 368 (1971).
(20) H. M. McConnell and J. Strathdee, *Mol. Phys.*, **2**, 129 (1959).
(21) A. J. Stone, *ibid.*, **7**, 311 (1964).
(22) R. Lefebvre and J. Maruani, *J. Chem. Phys.*, **42**, 1480 (1965).

Table III: Hyperfine and g Tensor Components[a]

i[b]	k[c]	$a^{(i)}$, G	$A_k^{(i)}$, G	$l_x^{(i)}$	$l_y^{(i)}$	$l_z^{(i)}$
2	1	−2.1	−3.80	0.946	−0.323	0.0
	2		−3.03	0.0	0.0	1.0
	3		0.53	0.323	0.946	0.0
3	1	−0.8	−1.88	0.0	0.0	1.0
	2		−1.80	0.957	0.290	0.0
	3		1.27	−0.290	0.957	0.0
4	1	−11.8	−17.44	0.0	1.0	0.0
	2		−11.82	0.0	0.0	1.0
	3		−6.15	1.0	0.0	0.0
	1	g_k	2.0022	1.0	0.0	0.0
	2		2.0026	0.0	1.0	0.0
	3		2.0024	0.0	0.0	1.0

[a] The directions of the principal axes are specified by their direction cosines l_x, l_y, l_z in a common coordinate system with x along C_1–CH_3. The z axis is perpendicular to the molecular plane. [b] The subscript i indicates the position of the proton. [c] The subscript k designates the principal component $A_k^{(i)}$ of proton i.

Reactivity and Mobility. The spectrum observed at high toluene content is not sufficiently resolved to allow a detailed interpretation. The average splitting of 7.4 G between the scarcely resolved components suggests that dimeric radical cations of toluene are formed. In this case the splitting constant is approximately one-half that of the monomer.[2,11] The phenomenon of the species present initially at low toluene content changing into that typical for high concentrations on warming or on infrared illumination can be explained in terms of a monomer to dimer transformation. This behavior was previously observed[2] in the benzene–silica gel system.

The fact that the cation spectrum cannot be accurately reproduced either by isotropic or by axially symmetric parameters indicates that the reorientation rate is slow. This is in contrast to the observation of adsorbed benzene ions in which case a reorientation about the sixfold axis takes place even at 77 K. A similar motion for the toluene cation is rendered more difficult by the methyl group.

Conclusion

The exclusive stabilization of positive aromatic ions following γ irradiation at 77 K in the adsorbed state on silica gel or Vycor glass is supported by the following observations. (a) Deuteration of the methyl group in toluene has a large effect upon the observed spectrum which it would not have in the negative ion case. (b) The measured values of the coupling constants of the ring protons are in reasonable accord with those theoretically estimated for the positive ion but at variance with experimental data for the negative ion. (c) The formation of dimeric ions indicated has been previously confirmed only for positive species. Calculations indicate that the negative complex is less stable.[23] In view of the parallel behavior of all aromatics hitherto studied[2,3] it would appear that positive ions are preferentially stabilized on adsorbents such as silica gel and Vycor glass after irradiation at 77 K.

Acknowledgment. This work forms part of a project supported by Swedish Board for Technical Development and the Swedish Atomic Research Council.

(23) P.-O. Kinell and A. Lund, *Acta Chem. Scand.*, in press.

Electron Spin Resonance Studies on Irradiated Heterogeneous Systems. IX. Anisotropy of the *g* Factor and the Hyperfine Coupling Constant of the Benzene Cation in the Adsorbed State

by T. Komatsu and A. Lund*

The Swedish Research Councils' Laboratory, Studsvik, Fack, S-611 01 Nyköping 1, Sweden *(Received November 23, 1971)*

Publication costs assisted by the Atomic Research Council of Sweden

The esr spectrum of the benzene cation formed on the surface of a molecular HY sieve by γ irradiation at 77 K has been analyzed. At 203 K the axially symmetric proton couplings $|A_\perp| = 4.05$ G, $|A_{||}| = 5.00$ G, and $\Delta g = g_\perp - g_{||} = 1.8 \times 10^{-4}$ afforded a reasonable fit in a line shape simulation with a Lorentzian derivative line width $\Delta H_{pp} = 0.4$ G. A theoretical estimate of the dipolar coupling when rapid rotation takes place about the molecular sixfold axis agrees with the experimental value. At 77 K the line shape cannot be reproduced either with axially symmetric or completely anisotropic couplings indicating that the rotation frequency is comparable to the hyperfine coupling anisotropy.

In previous work the benzene cation has been studied by the esr method in a glassy matrix.[1] Ions can also be stabilized in the adsorbed state[2] following γ irradiation at 77 K. In the former case the line width was quite large (1.7 G), and deviations from the expected binomial intensities were noted. In the latter case a pronounced asymmetry of the line profile was observed as well as a variation in line width among the different components. The most probable cause for these observations is an incomplete motional averaging of the anisotropy of the hyperfine coupling and the *g* factor.[2] Accordingly, the reported splitting constants and the *g* factor are uncertain, to an extent determined by their anisotropy.

In the work reported here an enhanced resolution was achieved by using a molecular sieve of the Y type in H form as an adsorbent. In this case the monomeric ion is stable up to $-30°$. Temperature-dependent changes could thus be studied.

A small amount ($\sim$0.1%) of benzene was adsorbed on the HY molecular sieve which had been previously prepared from the NH_4 type by elimination of ammonia. The specific surface area was 550 m^2/g. The samples were sealed at 10^{-5} Torr following γ irradiation in a ^{60}Co source to a dose of about 1 Mrad. Esr measurement was made in the temperature range 77–243 K with a Varian E-9 spectrometer operating at a microwave frequency of 9.27 GHz, using the variable temperature accessory supplied with the instrument. The magnetic sweep was calibrated assuming $a_N = 13.0$ G for the coupling constant of Fremy's salt.

The spectrum obtained at 203 K (Figure 1a) was analyzed under the assumption of axial symmetry. The parameters $A_\perp = a - b = -(4.05 \pm 0.05)$ G, $A_{||} = a + 2b = -(5.00 + 0.05)$ G, $\Delta g = g_\perp - g_{||} = (1.8 \pm 1.0) \times 10^{-4}$ were estimated by visual comparison with a series of line profiles computed with a program which simulates esr spectra of amorphous samples.[3] To reduce the computation time, the high-field approximation was employed. This requires that the nuclear Zeeman term of the order 5.0 G at 9.27 GHz, should be large compared with $0.5A_{||}$ and $0.5A_\perp$. The peak-to-peak width of the Lorentzian derivative line used to obtain the dashed spectrum of Figure 1a was $\Delta H_{pp} = 0.4$ G. A Gaussian line profile yields a less satisfactory fit. From this analysis $a = -(4.37 \pm 0.05)$ G, $2b = -(0.63 \pm 0.10)$ G.

The magnitude of the isotropic coupling decreases slightly but significantly with increasing temperature. A rough estimate of the temperature coefficient $(da/dT) = -0.9 \times 10^{-3}$ G/K was obtained by measuring the displacement of corresponding features resolved on the high-field lines at 77 (Figure 1b) and 203 K. This value agrees with that found in the sulfuric acid glass.[1]

Dipolar interaction with the magnetic moment of the odd electron makes the proton splittings anisotropic. By following the treatment of McConnell, *et al.*,[4] the dipolar interaction between the unpaired electron density at each carbon atom in a π-electron radical and a specific proton may be calculated. The axes of the principal elements lie along the line joining the atoms

(1) M. K. Carter and G. Vincow, *J. Chem. Phys.*, **47**, 292 (1967).

(2) O. Edlund, P.-O. Kinell, A. Lund, and A. Shimizu, (a) *ibid.*, **46**, 3679 (1967); (b) *Advan. Chem. Ser.*, **No. 82**, 311 (1968).

(3) R. Lefebvre and J. Maruani, *J. Chem. Phys.*, **42**, 1480 (1965).

(4) (a) H. M. McConnell and J. Strathdee, *Mol. Phys.*, **2**, 129 (1959); (b) H. J. Silverstone, D. E. Wood, and H. M. McConnell, *J. Chem. Phys.*, **41**, 2311 (1964).

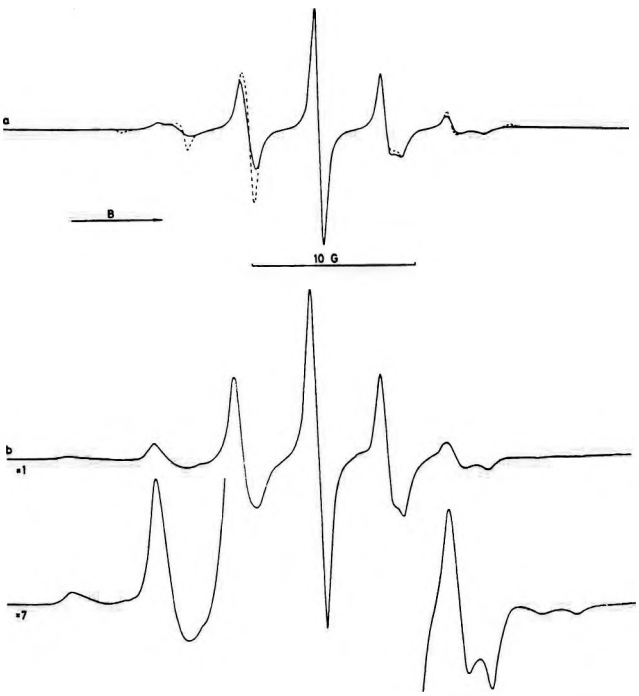

Figure 1. The esr spectrum from the benzene cation produced by γ irradiation at 77 K of the HY molecular sieve containing 0.1% benzene: (a) recorded at 203 K; the dashed spectrum is computed from the parameters $g_{||} = 2.00238$, $g_{\perp} = 2.00256$, $A_{||} = -4.99$ G, $A_{\perp} = -4.05$, $\Delta H_{pp} = 0.4$ G (Lorentzian shape); (b) recorded at 77 K.

(z), along the axis of the carbon $2p$ orbital (x) and perpendicular to x and z (y). The contributions from all carbon atoms were added after the transformation of the components to a common coordinate system. In this calculation a π-electron spin density $\rho^{\pi} = {}^1/_6$ was assumed at all carbon atoms. For the nearest neighbors, empirical estimates of the interaction corresponding to $\rho^{\pi} = 1$ are available;[5] contributions from nonadjacent carbon atoms were estimated with Slater orbitals having the exponent $\zeta = 1.59$.

This procedure yields a value $\mathbf{B} = (-0.79, -2.29, +3.08)$ G, which gives $2b = -0.79$ G if motional averaging occurs about the x axis. This is quite close to the experimental value $2b = -0.63$ G, suggesting that free rotation takes place preferentially about the molecular sixfold axis.

At a lower temperature the line shape cannot be reproduced accurately if axial symmetry is assumed. This indicates that at 77 K at least, the rotation frequency becomes comparable with the anisotropy in the radical plane corresponding to about 20 MHz. Proton relaxation studies of benzene on silica gel surfaces in the temperature range 133–343 K indicate[6] that anisotropic rotation takes place. At a coverage of less than 0.1 of a monolayer the molecules adsorb on sites where they possess a low degree of mobility. With an increasing benzene content other sites become occupied. Taking into consideration the activation energy of 2.3 kcal/mol[6] the correlation time τ (273 K) $= 5 \times 10^{-10}$ sec should increase at 77 K to an extent which would make anisotropic contributions to the esr line profile significant assuming that the ion and the molecule have a comparable degree of mobility.

The value of $g_{||} = 2.0024$ coincides with the theoretical value $g_{||} = 2.00238$ predicted from the theory of Stone.[7] On the other hand, $\Delta g = 1.8 \times 10^{-4}$ is an order of magnitude larger than the theoretical value. This deviation can be explained by the large error associated with Δg and the fact that the theory is valid only for radicals possessing a nondegenerate ground state.

The finding that the average hyperfine couplings and the g factors are the same in sulfuric acid glass[1] as in the adsorbed state indicates that matrix effects are small. In the adsorbed state on an HY molecular sieve the line width is reduced by comparison with that from the sulfuric acid matrix, possibly as a consequence of a less pronounced broadening due to unresolved hyperfine structure from the medium. Support for this view is obtained from saturation studies[8] which suggest that a homogeneous mechanism is at least partially responsible for the line broadening.

In contrast to other adsorbents such as silica gel, the molecular sieves possess crystalline regularity.[9] Consequently, the adsorption sites may be of a specific type having a defined structure. On the other hand, infrared studies[10] suggest that several types of sites are available for adsorption on the silica gel surface. This would tend to broaden the lines, since it is known that similar radicals adsorbed at different sites may possess slightly different coupling constants.[11] The line width of the benzene cation spectrum was about 0.8 G when silica gel was used as the adsorbent, that is about twice the width on the HY sieve.

Acknowledgments. This work forms part of a research project supported by the Board for Technical Development and the Atomic Research Council.

(5) G. S. Owen and G. Vincow, *J. Chem. Phys.*, **54**, 368 (1971).
(6) D. Michel, *Z. Naturforsch. A*, **23**, 339 (1968).
(7) A. J. Stone, *Mol. Phys.*, **7**, 311 (1964).
(8) T. Komatsu, unpublished results.
(9) D. W. Breck, W. G. Eversole, R. M. Milton, T. B. Reed, and T. L. Thomas, *J. Amer. Chem. Soc.*, **78**, 5963 (1956).
(10) L. R. Snyder and J. W. Ward, *J. Phys. Chem.*, **70**, 3941 (1966).
(11) G. A. Noble, R. A. Serway, A. O'Donnell, and E. S. Freeman, *ibid.*, **71**, 4326 (1967).

A Radical Cation Produced in a γ-Irradiated Single Crystal of dl-Methionine as Studied by Electron Spin Resonance and Optical Absorption Spectroscopy

by Shiro Kominami

Department of Chemistry, Faculty of Science, Kyoto University, Kyoto 606, Japan *(Received November 29, 1971)*

Publication costs borne completely by The Journal of Physical Chemistry

A photosensitive paramagnetic species was detected in a single crystal of dl-methionine γ-irradiated at 77°K, which was identified as a radical cation of dl-methionine with a hole in one of the nonbonding orbitals of sulfur, through the combined study of esr and optical absorption spectroscopy. The electronic structure of the radical cation is discussed in some detail based on the anisotropy in g factor and the optical absorption spectrum.

Introduction

A number of studies on the identity of radical ions produced in organic molecules γ- or X-irradiated at low temperature have been reported. Some of them have been carried out by esr spectroscopy on single crystals or polycrystals[1,2] and others by optical absorption spectroscopy mainly in the glassy state.[3,4] Both spectroscopic methods have shown that excess electrons or holes produced in sulfur-containing organic compounds by ionizing radiation are trapped predominantly in orbitals of the sulfur atoms.[1,3] Electronic structures of the radical ions produced in a disulfide compound have been discussed in some detail from the esr and the optical absorption study on a single crystal.[5] On the other hand, in sulfide compounds, radical cations with a hole in a nonbonding orbital of the sulfur atom have been identified from the esr studies in X-irradiated thiodiglycollic acid at 4.2°K[6] and in γ-irradiated *N*-acetyl dl-methionine at 77°K.[7] In these studies, however, no detailed information is obtained about the electronic structure of the radical cation.

In this investigation we have been able to identify the radical cation

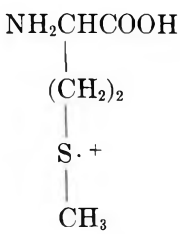

in the esr study of a single crystal of dl-methionine (β form) γ-irradiated at 77°K in the dark. It is also found that this radical cation is very sensitive to visible light and decays exponentially with time during illumination. Optical absorption spectra of the irradiated crystal were also measured at 77°K, which, together with the anisotropy of g factor in the esr spectra, have allowed us to discuss the electronic structure of the radical cation in some detail.

Experimental Section

Single crystals of dl-methionine were grown by slow evaporation of an aqueous solution. Mathieson found that dl-methionine crystallized in two monoclinic forms, namely the α form with space group $P2_1/a$ and the β form with the space group $I2/a$.[8] The crystals used for this study were shown by X-ray diffraction to be in the β form. Three orthogonal axes were chosen as reference, which were the crystallographic b and c axes and a' axis perpendicular to these two. Methionine with CD_3 substituted for the terminal CH_3 was synthesized by the methylation of homocysteine with methyl-CD_3 iodide in liquid ammonia according to the procedure of du Vigneaud, *et al.*,[9] followed by the refining processes of ion-exchange chromatography with an Amberlite IR-120 column and of recrystallizations. γ Irradiation was performed with ^{60}Co γ rays at 77°K to a total dose of about 10^6 R in the dark. Each crystal for the esr measurements was evacuated to about 10^{-5} mm for 1 hr in a quartz tube (Spectrosil) about 4 mm in diameter. The esr spectra were taken at 77°K with X-band spectrometers (JEOL P-10 and ME-X). The elements of g tensor were obtained by the least-squares method from the esr spectra taken by rotating every

(1) F. K. Truby, D. C. Wallace, and J. E. Hesse, *J. Chem. Phys.*, **42**, 3845 (1965); H. C. Box, H. G. Freund, K. T. Lilga, and E. E. Budzinski, *J. Phys. Chem.*, **74**, 40 (1970).

(2) J. W. Sinclair and M. W. Hanna, *ibid.*, **71**, 84 (1967); G. C. Moulton and B. Cernansky, *J. Chem. Phys.*, **53**, 3022 (1970).

(3) T. Shida, *J. Phys. Chem.*, **72**, 2597 (1968).

(4) W. H. Hamill in "Radical Ions," E. T. Kauser and L. Kevan, Ed., Interscience, New York, N. Y., 1968, p 321.

(5) K. Akasaka, S. Ohnishi, T. Suita, and I. Nitta, *J. Chem. Phys.*, **40**, 3110 (1964); K. Akasaka, S. Kominami, and H. Hatano, *J. Phys. Chem.*, **75**, 3746 (1971).

(6) H. C. Box, H. G. Freund, and E. E. Budzinski, *J. Chem. Phys.*, **49**, 3974 (1968).

(7) S. Kominami, K. Akasaka, H. Umegaki, and H. Hatano, *Chem. Phys. Lett.*, **9**, 510 (1971).

(8) A. M. Mathieson, *Acta Crystallogr., Sect. A*, **5**, 332 (1952).

(9) V. du Vigneaud, M. Cohn, J. P. Chandler, J. R. Schenck, and S. Simmonds, *J. Biol. Chem.*, **140**, 625 (1941).

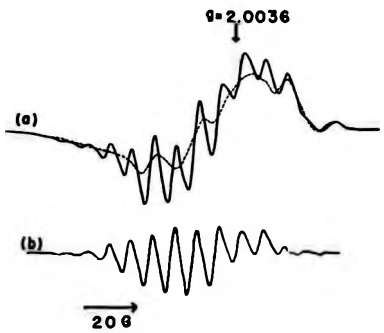

Figure 1. (a) Esr spectrum of a single crystal of DL-methionine γ-irradiated at 77°K in the dark (full line) and that after subsequent photoillumination in the visible range (broken line). These spectra are taken with the static magnetic field turned away from the a' axis towards the c axis by 75° in the $a'c$ plane. (b) The difference between the two spectra in (a).

10 or 5° about each of the three reference axes. Crystals for optical absorption measurements were about 10 × 10 × 1 mm in size with the main face (001). The optical absorption spectra at 77°K were taken with a Cary 14 R spectrophotometer equipped with a cryostat in which a crystal was supported with a copper holder cooled by liquid nitrogen.[10] Photoillumination in the visible range was performed with a collimated light from 150-W Xe lamp (HANOVIA compact arc or Hitachi) filtered by pure aqueous solution in a glass cell of 1-cm thickness.

Results

A typical first derivative esr spectrum of a single crystal of DL-methionine (β form) γ-irradiated and measured at 77°K in the dark is shown in Figure 1a (full line). It is obvious that a component with sharp lines is superimposed on some other components. This sharp component is very sensitive to light in the visible range and decays exponentially with the illumination time at 77°K. After sufficient exposure to the light (a few minutes), the esr spectrum of Figure 1a (full line) changes into that of Figure 1a (broken line). The difference between the two spectra in Figure 1a is presented in Figure 1b, which can be considered as the esr spectrum of the radicals that have decayed during the illumination. From the double integration of the spectra, it was found that the photobleached part amounted to about one-fifth of the total radicals produced. The main feature of this spectrum is determined by a component consisting of 13 hyperfine lines with an isotropic splitting of 8.3 G. This component shows considerable anisotropy in g factor, and the signal appears in duplicate related by the twofold axis of the crystal. The principal g values and their direction cosines for this component are tabulated in Table I. It may be important to note that there is a slight asymmetry in Figure 1b, which suggests that the spectrum might contain another component in the higher resonance field. This component does not appear to have

Table I: The Principal g Values and Their Direction Cosines for the Radical Cation Experimentally Obtained (Upper Part) and the Principal Directions Predicted through the Calculation of the Hybridization of Each Orbital around the Sulfur Atom in the Radical Cation (Lower Part)

Principal values	Direction cosines with respect to the a', b, and c crystallographic axis
$g_{min} = 2.002$	(0.362, ∓0.925, 0.121)
$g_{mid} = 2.013$	(0.589, ±0.327, 0.739)
$g_{max} = 2.022$	(−0.726, ∓0.196, 0.660)
g_{zz}	(0.393, ∓0.909, 0.140)
g_{xx}	(0.829, ±0.415, 0.373)
g_{yy}	(−0.392, ∓0.024, 0.920)

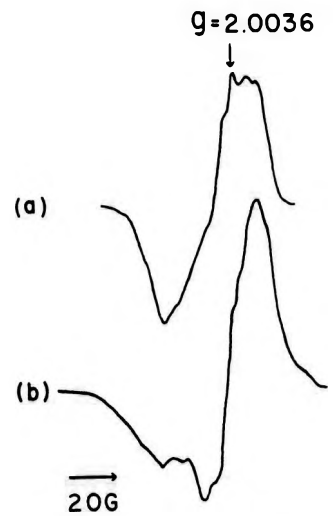

Figure 2. (a) Polycrystalline esr spectrum of the photosensitive radical species in methyl-deuterated methionine γ-irradiated at 77°K, obtained by subtracting the esr spectrum after photoillumination in the visible range from that before the illumination. (b) The same as (a), but undeuterated methionine is used.

a large anisotropy in g factor, although the detail is not clear because of the superimposition.

The corresponding esr spectra of the photosensitive species in the polycrystalline state are shown in Figure 2a and b, with methyl-deuterated and -undeuterated methionine, respectively. It is apparent that the esr spectrum of the photosensitive radicals in methyl-deuterated methionine is slightly narrower than, and different in shape from, that in undeuterated methionine. This indicates that the unpaired electron interacts with the methyl group, and the hyperfine splitting due to the methyl protons becomes smaller by the replacement of CH_3 with CD_3.[11]

The esr spectrum of Figure 1a (broken line) also depends critically on the crystal orientation with respect

(10) K. Ozawa, to be published.

(11) E. R. Andrew and R. G. Eades, *Proc. Roy. Soc., Ser. A*, 218, 537 (1953).

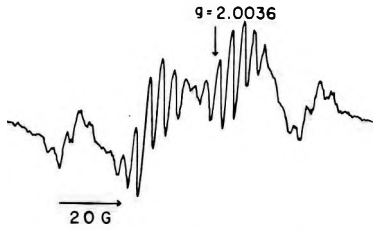

Figure 3. Esr spectrum of a single crystal of dl-methionine γ-irradiated at 77°K and subsequently photoilluminated in the visible range with the static magnetic field turned away from the a' axis towards the $-c$ axis by 20° in the $a'c$ plane.

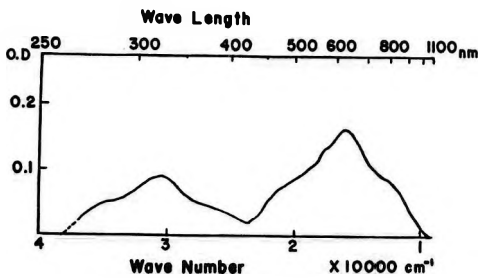

Figure 4. Optical absorption spectrum of the photosensitive species in a single crystal of dl-methionine γ-irradiated at 77°K, obtained by subtracting the spectrum after photoillumination in the visible range from that before the illumination.

to the magnetic field, and at a certain orientation appears as that of Figure 3, which is quite analogous to Figure 1 of ref 12, observed by Almanov, *et al.*, in the same crystal γ-irradiated at 77°K. They assigned the radical for this spectrum to R–$\dot{C}$H–S–CH_3. It is most probable that they observed a radical after the photosensitive species of Figure 1b had been bleached.

Single crystals of dl-methionine γ-irradiated at 77°K in the dark are colored blue and become pale yellow after photobleaching at 77°K. Figure 4 shows an optical absorption spectrum of the photosensitive species in a single crystal of dl-methionine γ-irradiated at 77°K, obtained by subtracting the spectrum after photoillumination in the visible range from that before the illumination. There are at least two absorption peaks, one around 600 nm and the other around 330 nm. The optical density at the absorption maximum at 600 nm is about 0.15 for the crystal of 1-mm thickness.

Discussion

Identification of the Radical Cation. The principal g values (2.002, 2.013, 2.022) and the isotropic 13 line hyperfine (hf) structure (8.3-G splitting) for the sharp component of Figure 1b are quite analogous to those observed in γ-irradiated *N*-acetyl dl-methionine,[7] although the hf splitting in dl-methionine is slightly larger than that in *N*-acetyl dl-methionine (6.3 G), indicating that both spectra originate from similar radical species. As discussed in the earlier paper,[7] these characteristic features of the esr spectrum can only be consistent with a cationic radical species in which a positive hole is trapped in one of the nonbonding orbitals of sulfur in a sulfide compound.

This identification is further supported by the present deuteration experiment of the terminal methyl protons (Figure 2); the narrowing and the shape alternation of the esr spectrum by the deuterium substitution clearly indicate that the unpaired electron interacts with the methyl group. Thus, the unpaired electron on the sulfur atom is expected to interact at least with five protons, three from the methyl and two from the methylene group next to the sulfur atom. The isotropic 13-line structure could therefore be constructed from the following assignment of coupling constants to these five β protons; 33.2 G to a set of two protons, 16.6 G to another proton, and 8.3 G to the last set of two. This assignment of coupling constants gives a theoretical intensity ratio of 1:2:2:2:3:4:4:4:3:2:2:2:1, which does not agree well with the observed intensity distribution (Figure 1b) that is excessively small in the wings of the resonance. If slight conformational differences exist among the radical cations distributed in the whole crystal, each of the radical cations should have slightly different coupling constants. Differences in the hf coupling constants would be accumulative in the outer portion of the resonance, and therefore should result in a pronounced broadening of hf lines in the wings of the resonance as compared with the lines near the central portion. In fact, in the case of the corresponding radical cation of *N*-acetyl dl-methionine, clearly distinguishable absorptions both in the esr and the optical spectra suggest existence of two or more different conformations.[13] It might also be possible that the involvement of hf interactions with nuclei belonging to surrounding molecules is responsible for the disagreement.[6]

In an earlier paper, Cadena, *et al.*, suggested that a room-temperature-stable radical in a single crystal of dl-methionine (α form) X-irradiated at 77°K, which shows an esr spectrum different from that of Figure 1b and has the direction for g_{max} parallel to the CH_3–S bond, should be assigned to the radical cation, CH_3–$\overset{+}{S}$–CH_2–R.[14] However, as will be discussed in a later part of this paper, the direction for g_{max} in such a radical cation should be parallel to the direction adjoining the two carbon atoms in the C–S–C′ group rather than to the CH_3–S bond. Moreover, the principal g values for their radical are greatly different from those obtained for our present radical and for the similar radical cations previously found in other sulfide compounds.[6,7]

(12) G. A. Almanov, P. U. Schastnev, and Yu. D. Tsvetkov, *Zh. Strukt. Khim.*, **10**, 986 (1969).

(13) S. Kominami, K. Akasaka, H. Hatano, K. Kawatsura, and K. Ozawa, to be published.

(14) D. G. Cadena, Jr., and J. R. Rowlands, *J. Chem. Soc. B*, 488 (1968).

Rather their values are closer to those of a bond-split, R–S· type radical.[15] Thus, it appears more reasonable to attribute the room-temperature-stable radical in DL-methionine (α form) to a radical of the R–S· type rather than to $CH_3\overset{+}{S}(\cdot)-CH_2-R$.

Assignment of the Optical Absorption Bands. Figure 4 shows the optical absorption spectrum of the photobleachable species which has an absorption maximum at 600 nm. *N*-Acetyl DL-methionine and polymethionine γ-irradiated at 77°K in the dark also show blue color (absorption around 600–700 nm) which is bleached by visible light.[7] This indicates that this common absorption band cannot be due to the electronic transitions in the carboxyl or amino group. Neither can this band be due to carbon radicals which show absorptions in a range of 240–360 nm.[16] Therefore, it is probable that the absorption around 600 nm is attributable to the radical cation $(RCH_2\dot{S}CH_3)^+$. The absorption spectrum of the corresponding radical cation in *N*-acetyl DL-methionine has two similar absorption bands, one around 600-700 nm and the other around 360 nm. The photoinduced hole transfer in *N*-acetyl DL-methionine, as evidenced by esr spectroscopy,[7] between an orbital of sulfur atom and that of –COOH accompanies the reversible optical absorption change in both of these two bands.[13] This clearly indicates that these two absorption bands are due to a trapped hole in a nonbonding orbital of the sulfur atom in *N*-acetyl DL-methionine. Although such a reversible hole transfer has not been observed in the DL-methionine system, it is quite natural to expect that the corresponding absorption bands (330 and 600 nm) in DL-methionine are also due to a trapped hole in a nonbonding orbital of sulfur.

The C–S–C′ group has strong absorptions below 250 nm which are assigned to 3p→4s and 3p→3d transitions.[17] In the case of radical cation additional transitions should arise between the occupied orbitals and the orbital with the unpaired electron which should be the higher nonbonding orbital of the sulfur atom, herewith designated as n_2 (the lower nonbonding orbital will be designated as n_1). The energetically lowest two of the additional transitions would be $n_1 \rightarrow n_2$ and $\sigma_{S-C} \rightarrow n_2$. The absorptions around 600 and 330 nm which are the lowest energy transitions observed should reasonably be attributed to $n_2 \rightarrow n_1$ and $n_2 \rightarrow \sigma_{S-C}$ hole transitions, respectively.

Electronic Structure of the Radical Cation. We will now discuss the electronic structure of the radical cation. If it is assumed that the unpaired electron should be in a $3p_{z'}$ orbital of the sulfur atom, where the Z' axis is chosen as the direction normal to the C–S–C′ bonding plane, the direction of g_{min} should be parallel to Z'.[18] However, the angle between the direction of Z' and that of g_{min} is about 20° which is out of the range of experimental error. This discrepancy suggests that

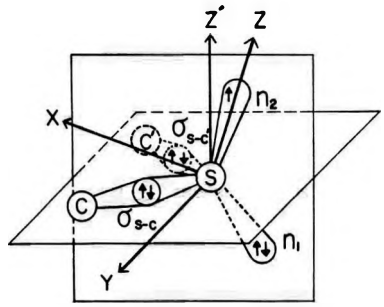

Figure 5. The coordinate system around the sulfur atom for the calculation of the electronic structure of the radical cation of DL-methionine. An assumption is made that σ_{S-C} and $\sigma_{S-C'}$ are equivalent, n_2 and n_1 being in the XZ plane which is perpendicular to the C–S–C′ bonding plane. The unpaired electron occupies n_2.

the orbital with the unpaired electron is made up of a hybridized orbital.

We consider now four orbitals made up of three 3p and one 3s atomic orbitals of sulfur, two of which form nonbonding orbitals and the other two make bonds with the carbon atoms. By choosing a coordinate system as shown in Figure 5, we can write these orbitals as

$$n_2 = \alpha(S)_s + (1 - \alpha^2)^{1/2}(p_z)_s$$

$$n_1 = \beta(S)_s - \left(\frac{1 - \alpha^2 - \beta^2}{1 - \alpha^2}\right)^{1/2}(p_x)_s - \left(\frac{\alpha^2\beta^2}{1 - \alpha^2}\right)^{1/2}(p_z)_s$$

$$\sigma_{S-C} = A\left[\frac{1}{\sqrt{2}}(1 - \alpha^2 - \beta^2)^{1/2}(S)_s + \left\{\frac{\beta^2}{2(1 - \alpha^2)}\right\}^{1/2}(p_x)_s + \frac{1}{\sqrt{2}}(p_y)_s - \alpha\left\{\frac{1 - \alpha^2 - \beta^2}{2(1 - \alpha^2)}\right\}^{1/2}(p_z)_s\right] + B\chi_C \quad (1)$$

$$\sigma_{S-C'} = A\left[\frac{1}{\sqrt{2}}(1 - \alpha^2 - \beta^2)^{1/2}(S)_s + \left\{\frac{\beta^2}{2(1 - \alpha^2)}\right\}^{1/2}(p_x)_s - \frac{1}{\sqrt{2}}(p_y)_s - \alpha\left\{\frac{1 - \alpha^2 - \beta^2}{2(1 - \alpha^2)}\right\}^{1/2}(p_z)_s\right] + B\chi_{C'}$$

where α and β are the parameters determining s characters in n_2 and n_1 orbitals, respectively, the orthonor-

(15) Y. Kurita and W. Gordy, *J. Chem. Phys.*, **34**, 282 (1961); E. Cipollini and W. Gordy, *ibid.*, **37**, 13 (1962).

(16) H. W. Shields, W. Marsh, and P. J. Hamrick, Jr., *ibid.*, **52**, 6437 (1970).

(17) S. D. Thompson, D. G. Carroll, F. Watson, M. O'Donnell, and S. P. McGlynn, *ibid.*, **45**, 1367 (1966).

(18) H. M. McConnell and R. E. Robertson, *J. Phys. Chem.*, **61**, 1018 (1967).

malization condition and symmetry being used for deriving these equations.[19] A and B are the coefficients determined by the S–C bonding scheme. χ_C and $\chi_{C'}$ are the orbitals of the carbon atoms adjacent to the sulfur atom. We expect that the unpaired electron occupies the higher nonbonding orbital, n_2, and that α for n_2 is smaller than β for n_1. It is also assumed that the bonding orbitals, σ_{S-C} and $\sigma_{S-C'}$, are energetically equal.

The elements of the g tensor of a radical can be calculated from the following equation[20]

$$g_{ij} = g_f\left\{\delta_{ij} - \lambda \sum_n \frac{\langle\psi_0|L_i|\psi_n\rangle\langle\psi_n|L_j|\psi_0\rangle}{\Delta E_n}\right\} \qquad (2)$$

where λ is the spin-orbital coupling constant, ψ_0 is the ground state wave function for the radical, ψ_n is an nth excited state wave function, and ΔE_n is the energy difference between the ground state and the nth excited state.

From eq 1 and 2, we obtain for the radical cation

$$\begin{aligned} g_{xy} &= g_{yz} = g_{zx} = 0 \\ g_{xx} &= g_f\left\{1 - \lambda\frac{A^2(1-\alpha^2)}{\Delta E_2}\right\} \\ g_{yy} &= g_f\left\{1 - \lambda\frac{1-\alpha^2-\beta^2}{\Delta E_1} - \lambda\frac{A^2\beta^2}{\Delta E_2}\right\} \\ g_{zz} &= g_f \end{aligned} \qquad (3)$$

where ΔE_1 and ΔE_2 are the energy difference between n_2 and n_1, and that between n_2 and σ_{S-C} or $\sigma_{S-C'}$, respectively, and λ is taken to be -382 cm^{-1}. Assuming that the C–S–C′ bonding angle of the radical cation in the single crystal is not much different from that of the original molecule (100°), we obtain 0.70 for $\alpha^2 + \beta^2$. Since it is obvious in eq 3 that g_{yy} is larger than g_{xx}, observed g_{min}, g_{mid}, and g_{max} should be equated to g_{zz}, g_{xx}, and g_{yy}, respectively. Following the assignment of the optical absorption bands, we put 16,600 (600 nm) and 30,300 cm^{-1} (330 nm) into ΔE_1 and ΔE_2 in eq 3, respectively, obtaining 0.80 for A, 0.57 for α, and 0.61 for β. Thus the s character of the orbital containing the unpaired electron (α^2) is estimated to be 0.33 in this approximation. The value 0.80 obtained for A is appreciably larger than the corresponding value ($1/\sqrt{2}$ or less) for the case of an equal distribution of bonding electrons on two atoms. This is quite reasonable because a positive charge on the sulfur atom will considerably increase the electronegativity of the sulfur atom.[21]

The results also predict the principal direction, X, Y, and Z of the g tensor with reference to the crystallographic data[8] (assuming all atom positions are unaltered from the original ones by irradiation), which are tabulated in the lower part of Table I. It is to be noted that the predicted principal directions for g_{xx}, g_{yy}, and g_{zz} are in fair agreement with the experimentally obtained ones for g_{mid}, g_{max}, and g_{min}, respectively. This indicates that our assumptions in the calculation of the electronic structure are largely valid. While the direction predicted for the orbital containing the unpaired electron (the direction of the Z axis) agrees closely with that experimentally obtained (the direction of g_{min}), the other predicted principal directions do not agree as well with the observed ones. This is not surprising, however, because these directions, as compared with that of g_{zz}, are easily susceptible to perturbations such as those coming from possible inequality in the σ_{S-C} and $\sigma_{S-C'}$ bonding orbitals due to the difference in electronegativity between the CH_3– and $-CH_2-CH_2-$ groups[22] and from the contribution of higher excited electronic configurations, through the nonzero value of g_{xy}. Additional disagreement in principal directions might arise from a slight conformational change around the C–S–C′ group as a result of γ irradiation at 77°K.

Concluding Remarks

By utilizing the optical absorption spectrum in addition to the esr spectroscopy, this paper has been able to show some detailed electronic structure of a sulfide cation radical in a γ-irradiated single crystal of dl-methionine. Mechanism of the photoinduced decay of the ionic species is another subject of interest, but this problem will be treated elsewhere.

Acknowledgments. The author should like to express his deep gratitude to Dr. K. Akasaka for his valuable discussions throughout the work. He also wishes to express his hearty thanks to Professor H. Hatano for his continual encouragement. The author is very grateful to Drs. K. Ozawa and K. Kawatsura of Japan Atomic Energy Research Institute, Tokai Research Establishment for their kind cooperation in optical measurements.

(19) I. Chen and T. P. Das, *J. Chem. Phys.*, **45**, 3526 (1966).
(20) M. H. L. Pryce, *Proc. Phys. Soc. (London)*, **A63**, 25 (1950).
(21) J. Hinze and H. H. Jaffé, *J. Amer. Chem. Soc.*, **84**, 540 (1962).
(22) M. S. Kharasch and R. Marker, *ibid.*, **48**, 3130 (1926).

Electron Spin Resonance Studies of the Electron-Transfer Equilibrium β-Ethyl Naphthalenide + α-Ethylnaphthalene ⇄ β-Ethylnaphthalene + α-Ethyl Naphthalenide

by G. Moshuk, H. D. Connor, and M. Szwarc*

Department of Chemistry, State University College of Forestry at Syracuse University, Syracuse, New York 13210 *(Received December 9, 1971)*

Publication costs assisted by the Petroleum Research Fund

The esr spectra of α- and β-ethylnaphthalene (α-EtN and β-EtN) were resolved and the validity of the pertinent coupling constants was confirmed by computer simulation. The equilibrium constant of the electron-transfer reaction proceeding in THF, α-EtN + β-EtN·⁻,K⁺ ⇄ β-EtN + α-EtN·⁻,K⁺, was determined over a wide temperature range. The results led to $\Delta H = 0.6$ kcal/mol and $\Delta S = -0.4$ eu.

In the course of our studies of electron-transfer processes it was shown that the esr technique could be applied in the investigation of the equilibrium

$$\beta\text{-EtN}\cdot^{-},K^{+} + \alpha\text{-EtN} \rightleftharpoons \beta\text{-EtN} + \alpha\text{-EtN}\cdot^{-},K^{+}$$

in THF as solvent, where α- and β-EtN denote 1- and 2-ethylnaphthalene, respectively, and α-EtN·⁻,K⁺ and β-EtN·⁻,K⁺ represent the potassium salts of the corresponding radical anions.

The radical anions were prepared by reducing the highly purified hydrocarbons with metallic potassium in tetrahydrofuran. Their esr spectra, shown in Figures 1 and 2, were obtained on a Varian V4504 esr spectrometer equipped with a 12-in. magnet. Their analysis leads to the coupling constants given in Table I, which agree well with those reported by Fraenkel, *et al.*,[1] for the corresponding methylnaphthalenes (see Table I). The computer-simulated spectra obtained from these coupling constants are included in Figures 1 and 2 below the respective experimental spectra.

The esr spectrum of the mixture of the two radical anions is shown in Figure 3. It reveals that the end lines of the spectra of the individual radical ions are well separated and therefore can be utilized to determine the relative concentrations of the two radical anions.

Separate solutions of α-EtN and β-EtN in THF were prepared and stored in evacuated ampoules equipped with break-seals. The concentration of hydrocarbon in each solution was determined by optical spectrophotometry (ϵ 0.605 × 10^4 at λ_{max} 280 nm for the α isomer and ϵ 0.500 × 10^4 at the same λ_{max} for the β isomer). Approximately 10% of each solution was treated with a potassium mirror and then mixed with the remaining hydrocarbon solution. The concentration of the resulting radical anions was determined by optical spectrophotometry (ϵ 0.55 × 10^4 at λ_{max} 380 nm for the α isomer and ϵ 0.38 × 10^4 at the same λ_{max} for the β isomer). However, this information was not required in calculation of the equilibrium constants of the investigated electron-transfer process. The two ampoules were then attached to a bulb containing an esr side arm. After evacuation of the unit, the break-seals were crushed and the solutions mixed. The esr spectra of the mixture were recorded then at temperatures ranging from 0 to −90°.

Two series of experiments were performed, one (A) at a total concentration of radical ions of about 4 ×

Table I: Coupling Constants (G) for K^+ Salts of the Naphthalenides in THF[a]

No.	α-EtN[b]	α-MeN[c]	β-EtN[b]	β-MeN[c]
1			4.56	4.58
2	1.57	1.42		
3	1.92	1.97	2.24	2.31
4	4.55	4.43	5.30	5.05
5	5.11	5.40	5.30	5.05
6	1.57	1.54	1.49	1.32
7	2.17	2.30	2.24	2.26
8	4.71	5.06	4.95	4.76
α-CH_2	3.12 (3.24[d])	3.87 (3.86[d])	1.12 (1.13[d])	1.71 (1.87[d])

[a] Note the decrease in the coupling constant of the protons in the CH_2 group of ethylnaphthalene when compared with the protons of the CH_3 group of methylnaphthalene. Such a decrease is expected when the most favorable conformation of the Et group places its C–CH_3 bond in the direction perpendicular to the nodal plane of the aromatic moiety. [b] −80°. [c] As reported by Fraenkel, *et al.*[1] [d] Reported by de Boer (private communication).

(1) R. E. Moss, N. A. Ashford, R. G. Lawler, and G. K. Fraenkel, *J. Chem. Phys.*, 51, 1765 (1969).

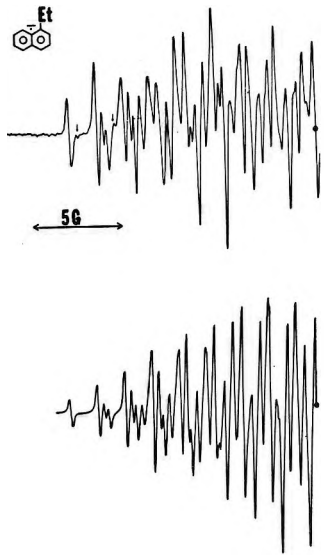

Figure 1. Esr spectrum of α-EtN·⁻,K⁺ in THF at −70°; below, the computer-simulated spectrum. The arrows denote the lines arising from the presence of a very small amount of the β isomer in the α compound.

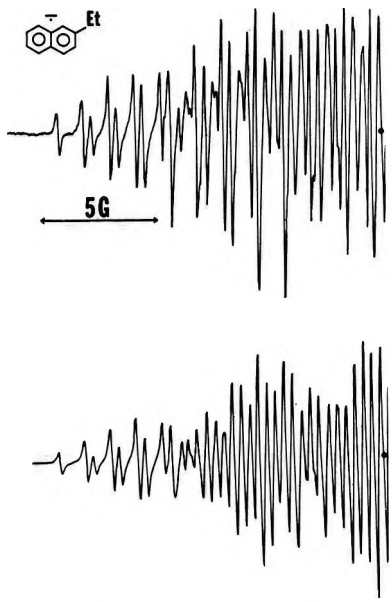

Figure 2. Esr spectrum of β-EtN·⁻,K⁺ in THF at −70°; below, the computer-simulated spectrum.

10^{-4} M and a concentration of hydrocarbons of about 3.4×10^{-3} M (α-EtN:β-EtN = 0.5) and the other (B) with concentrations 3.5×10^{-4} M and 4.2×10^{-3} M, respectively, and the initial ratio of α-EtN:β-EtN = 1.07. The end lines of the two superimposed esr spectra did not overlap at −80 and −60°, but the overlap became increasingly significant at higher temperatures. The increase in the overlap was due to two factors: (1) the separation of the end lines decreases at higher temperatures, and (2) the lines become broader because the spin–spin exchange is faster at higher temperatures. (The broadening of the lines due to the electron-transfer process is negligible at the concentration of hydrocarbons chosen in these experiments.) Hence, for the spectra obtained at −80 or −60°, the ratio [α-EtN·⁻,K⁺]/[β-EtN·⁻,K⁺] was determined by double integration of the two end lines, but at higher temperatures the double integration was performed on the unmerged halves of the pertinent lines. The calculated equilibrium constants are given

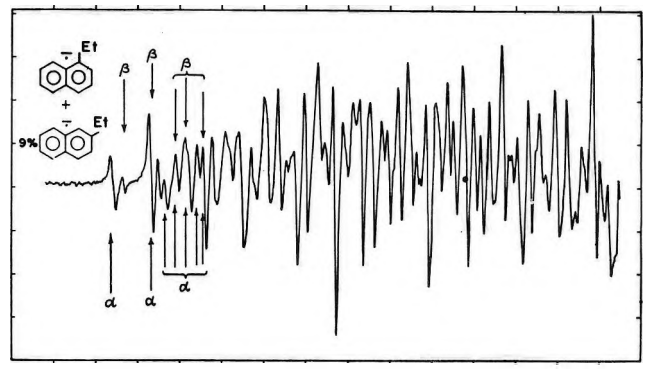

Figure 3. Esr spectrum of α-EtN·⁻,K⁺ containing 9% β-EtN·⁻,K⁺ in THF at −80°.

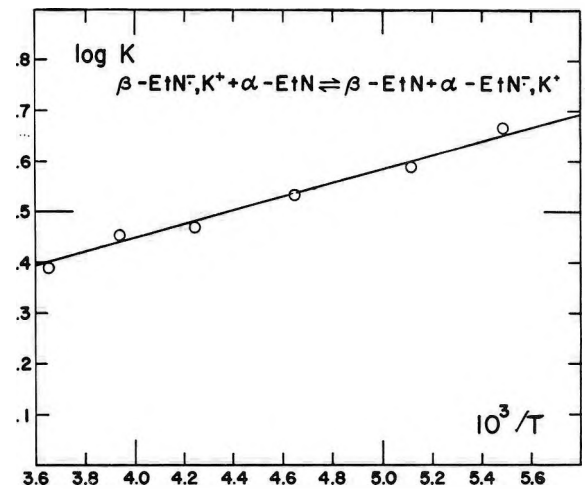

Figure 4. Plot of log K *vs.* $1/T$ for the equilibrium β-EtN·⁻,K⁺ + α-EtN ⇄ β-EtN + α-EtN·⁻,K⁺ in THF. $\Delta H = -0.6$ kcal/mol, $\Delta S = -0.4$ eu.

Table II: Equilibrium Constant, K, of the Electron-Transfer Reaction[a] β-EtN·⁻,K⁺ + α-EtN ⇄ β-EtN + α-EtN·⁻,K⁺

Temp °C	K	
	Series A	Series B
0	2.45 ± 0.5	
−20	2.85 ± 0.7	
−40	2.95 ± 0.5	2.45 ± 0.7
−60	3.40 ± 1.0	3.00 ± 0.6
−80	3.90 ± 1.0	3.85 ± 0.9
−90	4.55 ± 1.1	

[a] In THF.

in Table II and presented graphically by a van't Hoff plot in Figure 4. From this plot we calculate $\Delta H = -0.6$ kcal/mol and $\Delta S = -0.4$ eu; *i.e.*, within an experimental uncertainty of about 20% the electron transfer does not affect the entropy of the system.

The experimental uncertainties in the quoted equilibrium constants arise mainly from the double integration of the esr spectra from which the required ratios $[\alpha\text{-EtN}\cdot^-,K^+]/[\beta\text{-EtN}\cdot^-,K^+]$ were calculated. To improve the accuracy, the equilibrium constants were obtained by averaging the results derived from four to eight spectra recorded at each temperature. In series B, the overlap of the pertinent lines was too large at 0 and $-20°$ to allow a reliable integration and hence no K values are reported for these experiments.

The overlap of the lines in the esr spectra of the methylnaphthalenes is substantial, and therefore a similar study of the equilibrium

$$\beta\text{-MeN}\cdot^-,K^+ + \alpha\text{-MeN} \rightleftarrows \beta\text{-MeN} + \alpha\text{-MeN}\cdot^-,K^+$$

is not feasible. The overlap also prevented us from studying the equilibrium involving naphthalene and its methyl or ethyl derivatives.

Discussion

The above results clearly demonstrate that the electron affinity of α-ethylnaphthalene is higher than that of the β isomer, while consideration of the inductive effect of the alkyl group leads to the opposite conclusion. Our result agrees with the polarographic studies of Streitwieser and Schwager.[2] They found in dimethylformamide solution the half-wave potential of α-methylnaphthalene to be higher by 0.02 V than that of β-methylnaphthalene, although both potentials are more negative than that of the unsubstituted naphthalene. This anomaly was explained in terms of the conjugated effect of the alkyl group, which is more important for the α isomer than for the β one, and which opposes the inductive effect.

Acknowledgment. We wish to acknowledge the financial support of this investigation by the National Science Foundation and by the Petroleum Research Fund, administered by the American Chemical Society. Also, we thank Professor Streitwieser for drawing our attention to his paper on polarographic reduction of methyl-substituted aromatic hydrocarbons.

(2) A. Streitwieser and I. Schwager, *J. Phys. Chem.*, **66**, 2316 (1962).

Ultrasonic Studies of Proton Transfers in Solutions of Poly(lysine) and Poly(ornithine). Implications for the Kinetics of the Helix–Coil Transition of Polypeptides and for the Ultrasonic Absorption of Proteins

by R. Zana* and C. Tondre

C.N.R.S.—Centre de Recherches sur les Macromolécules, 67 Strasbourg, France *(Received January 21, 1972)*

Publication costs borne completely by The Journal of Physical Chemistry

Ultrasonic absorption measurements have been performed at pH ranging from 5 to 13 and in the frequency range 1–115 MHz on solutions of poly(L-lysine) and poly(DL-lysine) (PLL and PDLL) and of poly(L-ornithine) (PLO) in H_2O–0.3 *M* NaBr and of PLO in 85 parts H_2O–15 parts methanol–0.3 *M* NaBr. The curves absorption *vs.* pH go through a maximum at pH 11.4–11.5. From the study of the effect of pH on the excess ultrasonic absorption of these solutions it is concluded that the absorption maxima are due to proton-transfer reactions on the side-chain amino group of the polypeptides and not to the helix-coil transition because (1) PLL and PDLL give essentially identical absorption results and (2) methanol has only very little influence on the absorption of PLO solutions. The effect of frequency on the excess absorption of PLL and PLO solutions has enabled us to determine the rate constants and volume changes for the proton-transfer reactions. Finally, the implications of the results obtained in this study on the possibility of observing the helix-coil equilibrium using ultrasonic absorption in the megahertz range and on the interpretation of the ultrasonic absorption data obtained with protein solutions are examined.

I. Introduction

In a recent study, Chou and Scheraga[1] showed that if poly(L-lysine) (PLL) undergoes a helix–coil transition at pH 10.3, such a conformational change does not occur with poly(DL-lysine) (PDLL) over the whole pH range. This result prompted us to undertake new ultrasonic absorption measurements as a function of pH on both PLL and PDLL. It was hoped that the comparison of the curves absorption *vs.* pH relative to these two polymers would provide us with direct evidence as to whether the increase of absorption found at pH >9 by Parker, *et al.*,[2] for PLL is due to the helix–coil transition, as postulated by these authors, or to a proton-transfer reaction on the ϵ-NH_3^+ group of PLL, as was advanced in a recent paper.[3] If the first process prevails, one can readily predict that the increase of absorption at pH >9 will be strongly affected in going from PLL to PDLL. On the contrary, if this increase is due to a proton transfer, it should not be changed much in going from PLL to PDLL since our previous studies[4,5] have shown this process not to be greatly affected by the overall conformation of the molecule under study.

As part of this work, absorption measurements have also been performed on poly(L-ornithine) (PLO). This polypeptide is very similar to PLL, its side chain being one CH_2 shorter than that of PLL, and the pK_a values of the side-chain NH_2 groups of PLO and PLL are quite close (within 0.1–0.2 pH unit[1,6]). However, the shorter side chain of PLO results in lesser stability of its helical conformation: in water the maximum helical content of PLO found at high pH is 25%, as compared with a value close to 100% for PLL;[6] moreover, the midpoint of the helix–coil transition is found at pH 11 for PLO[6] and 10.3 for PLL.[1] A comparative study of the effect of pH on the absorption of PLL and PLO may therefore also provide some evidence as to whether proton transfer or helix–coil transition is responsible for the excess absorption observed with aqueous solutions of these two polymers.[2,7] PLO also gives a second manner to approach this problem: Chaudhuri and Yang[6] have shown that the helical content of PLO is greatly increased by relatively small additions of methanol. For instance, the helical content is increased from 25% in water to 60% in H_2O–methanol (85:15, v/v). This mixture is the solvent used by Hammes and Roberts[7] in their ultrasonic study of the helix–coil transition of PLO induced by pH changes. These authors interpreted their results in terms of a helix–coil equilibrium. As will be seen now, the com-

(1) P. Chou and H. A. Scheraga, *Biopolymers*, **10**, 657 (1971).

(2) R. Parker, L. Slutsky, and K. Applegate, *J. Phys. Chem.*, **72**, 3177 (1968).

(3) R. Zana and C. Tondre, *Biopolymers*, **10**, 2635 (1971).

(4) J. Sturm, J. Lang, and R. Zana, *Biopolymers*, **10**, 2639 (1971).

(5) J. Lang, C. Tondre, and R. Zana, *J. Phys. Chem.*, **75**, 374 (1971); R. Zana and J. Lang, *ibid.*, **74**, 2734 (1970).

(6) S. Chaudhuri and J. Yang, *Biochemistry*, **7**, 1379 (1968).

(7) G. Hammes and P. Roberts, *J. Amer. Chem. Soc.*, **91**, 1812 (1969).

parison of the results obtained in this work for PLL, PDLL, and PLO, the latter being studied both in H_2O and 85:15 H_2O–methanol leaves no doubt that the excess absorption found in PLL, PDLL, and PLO is entirely due to proton transfer on the side-chain amino group.

II. Experimental Section

Poly(L-lysine) and poly(L-ornithine) hydrobromides with polymerization degrees 480 and 540 were purchased from Pilot Chem. Co., while poly(DL-lysine) hydrobromide (polymerization degree 200) was obtained from Miles-Yeda, Israel. The three polymers were used without further purification.

The ultrasonic absorption measurements were carried out on solutions in H_2O–0.3 M NaBr (PLL, PDLL, and PLO) or in 85 parts H_2O–15 parts methanol–0.3 M NaBr (PLO), using the standard pulse technique[8] or the ultrasonic interferometer.[9]

While PDLL and PLO remained dissolved in the whole pH range, precipitation of PLL occured slowly at pH >10.3. To further slow down this process, the concentration of the PLL solution was brought down to 0.06 mol of monomer per liter (M in the following) as compared to 0.116 and 0.156 M in the study of Parker, *et al.*[2] It was then observed that the pH of the 0.06 M solution could be increased above 10.3 by addition of NaOH, with the solution remaining relatively clear during the time required for the measurement of its absorption coefficient α (15 min). Moreover, no effect of time on α could be measured during the hour which followed the increase of pH, although a considerable increase of turbidity occurred meanwhile. For further measurements the turbid solution was clarified by bringing its pH down to 9 by addition of concentrated HBr with stirring. The pH was then raised to the desired value and the measurement performed. Such a procedure was repeated for each of the experimental results at pH >10.3. These successive pH cycles increased the NaBr concentration, C_{NaBr}, of the solution. We found, however, that an increase of C_{NaBr} from 0.3 M (initial concentration) to 0.5 M (final concentration after six pH cycles) resulted in a negligible change of absorption. Similarly Parker, *et al.*,[2] found practically no effect of C_{NaCl} on the ultrasonic absorption of PLL solutions.

Optical rotation measurements were performed on 0.06 M PLL and PDLL solutions in H_2O–0.3 M NaBr using a Zeiss polarimeter at 589 nm. No change of optical rotation with pH was detected with PDLL, while the rapid change of optical rotation due to the helix–coil transition of PLL was observed at pH 10.5. The values 10.3 and 10.4 have been reported by other workers for PLL in H_2O–0.1 M KCl[1] and H_2O–0.2 M KCl,[6] respectively. For PLO, the measurements were performed both in H_2O–0.3 M NaBr and in 85 parts H_2O–15 parts methanol–0.3 M NaBr at 365 nm. In both solvents the helix–coil transition was found to occur at pH close to 11.0, in good agreement with the findings of others.[7] Moreover, the change of optical rotation was two times smaller in water than in the H_2O–methanol mixture, thereby indicating a higher helical content in this mixed solvent, as previously reported.[6]

III. Effect of pH on the Excess Ultrasonic Absorption of PLL, PDLL, and PLO Solutions

Figure 1 depicts the curves α/N^2 *vs.* pH, N being the frequency of the ultrasonic radiation, for PLL and PDLL. The α/N^2 value for H_2O–0.3 M NaBr was found to be very close to that of water (horizontal dotted line on Figure 1) over the whole pH and frequency range. In their work on PLL, Parker, *et al.*,[2] did not observe the absorption maximum which appears on curve at pH 11.5 because their solutions were rather concentrated and PLL readily precipitated at pH >10.2. However, at pH 7 their results are in good agreement with ours when concentrations are taken into account. The results of Figure 1 demand the following remarks: (1) the absorption maximum for PLL occurs at pH 11.5 and not at pH 10.5, *i.e.*, at the midpoint of the transition as would be expected if it is assumed that this maximum is due to the transition;[10] (2) an absorption maximum is also observed at pH 11.5 with PDLL, which does not present any helix–coil transition when the pH is changed;[1] and (3) curves 1 and 2 on Figure 1 can be made coincident by a translation of 110×10^{-17} cm^{-1} sec^2 (the dotted curve, very

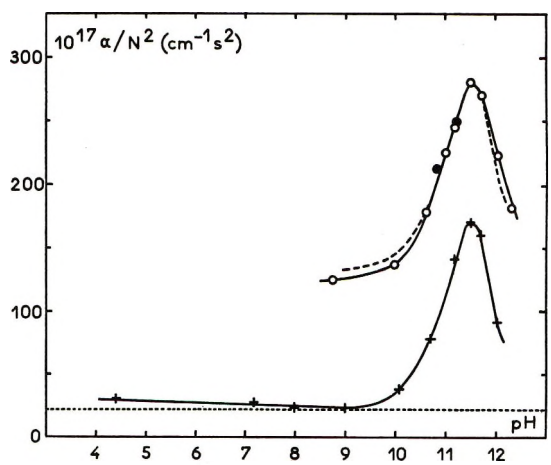

Figure 1. Variation of α/N^2 with pH at 6.49 MHz and 25° for 0.06 M solutions of PLL (+) and PDLL (○, direct titration; ●, reverse titration) in H_2O–0.3 M NaBr. The curve shown by the broken line practically coincident with the curve for PDLL was obtained by translating the curve relative to PLL. (. . . . .), α/N^2 for water.

(8) J. Andreae, R. Bass, E. Heasell, and J. Lamb, *Acustica*, **8**, 131 (1958).

(9) R. Musa, *J. Acoust. Soc. Amer.*, **30**, 215 (1958).

(10) G. Schwarz, *J. Mol. Biol.*, **11**, 64 (1965).

close to that for PDLL, was obtained by such a translation of the curve relative to PLL; the difference of 5–10 $\times$ 10^{-17} cm^{-1} sec^2 which then appears in the pH range where α/N^2 is almost constant is within the experimental accuracy). These results strongly suggest that the absorption maxima on Figure 1 are not due to the helix–coil transition but to proton transfer on the amino groups of PLL and PDLL. As will be seen now, the results obtained with PLO lead to the same conclusion. However, before considering these results some comments must be made on the shift of absorption which appears in Figure 1 between equimolecular solutions of PLL and PDLL. This shift is not modified when PLL undergoes the helix–coil transition at pH 10.5 and is practically constant over the whole pH range. Therefore, it cannot be due to the difference of conformation between helical PLL and randomly coiled PDLL, to suppress. We have tentatively assigned this shift to a small difference of composition between the PLL and PDLL samples used in this work. The two samples were of different origins. It is thought that an unknown but small percentage of residues of the PDLL sample may not have been decarbobenzoxylated in the process of preparation of this polymer [poly(lysine) is always obtained by decarbobenzoxylation of poly(ε-carbobenzoxylysine)]. Evidence for this may be found in the fact that the PDLL sample was not totally soluble in water at neutral pH; the insoluble part was removed by filtration. However, this fact affects in no way the conclusions which have been drawn from the results of Figure 1 because in this work PDLL was used as a nonhelical model compound for PLL.

Figure 2 shows the results obtained with PLO solutions. The α/N^2 value for the solvent 85 parts H_2O–15 parts methanol–0.3 M NaBr was found to be 2–5 $\times$ 10^{-17} cm^{-1} sec^2 over that for water in the whole pH and frequency range. As for PLL and PDLL, absorption maxima can be seen in Figure 1 at pH close to 11.5. The amplitude of the absorption maximum is slightly larger in water than in the mixed solvent in which the helical content of PLO is more than twice

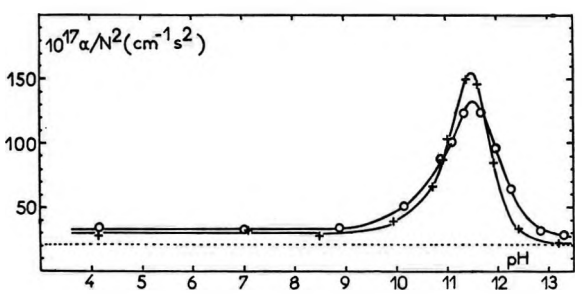

Figure 2. Variation of α/N^2 with pH at 6.49 MHz and 25° for 0.056 M solutions of PLO in H_2O–0.3 M NaBr (+) and in 85 parts H_2O–15 parts methanol–0.3 M NaBr (○). (. . . . .), α/N^2 for water.

that in water. In the assumption of the helix–coil equilibrium, one would have expected an opposite result.[10] The effect of methanol on the excess absorption of PLO is more thoroughly studied in the next paragraph. In addition to the effect of methanol, it is found that when plotted on the same graph the two curves α/N^2 *vs.* pH relative to PLL and PLO in H_2O–0.3 M NaBr are practically coincident at N = 6.49 MHz, despite the quite different stabilities of the helical forms of these two polymers. This also suggests that as for PLL and PDLL the absorption peaks in Figure 2 are not due to the helix–coil transition but to the proton-transfer reaction

$$NH_3^+ + OH^- \underset{k_B}{\overset{k_F}{\rightleftharpoons}} NH_2 + H_2O \qquad (1)$$

This assignment will now be substantiated in a quantitative manner.

IV. Study of the Kinetics of the Proton-Transfer Reaction in PLL and PLO Solutions

The expressions for the pH corresponding to the absorption maximum (pH_M), for the amplitude A of this maximum, and for the relaxation frequency characterizing the excess absorption associated with reaction 1 have been given in several papers[11–15] and will be used in what follows.

(*1*) *Position of the Absorption Maximum.* For a solution of simple base, pH_M is given by eq 2, where pK_a has its usual meaning and C is the concentration in

$$pH_M = (14 + pK_a + \log C)/2 \qquad (2)$$

moles per liter. For a solution of polybase a complication arises because pK_a depends on the state of ionization of the polybase.[16] However, both PLL and PLO are weak polybases with a degree of ionization of about 5% at pH 11.5. Therefore, in eq 2 pK_a can be replaced by the intrinsic pK_a, pK_0.

Chou and Scheraga[1] have reported the value pK_0 = 10.26 for both PLL and PDLL in H_2O–0.1 M KCl. Our work was performed at a higher ionic strength (0.3 M NaBr), but the change of pK_0 with ionic strength is expected to introduce in the calculation of pH_M an error well within the experimental accuracy on pH_M (±0.15 pH unit). The above value of pK_0 together with C = 0.06 M yields pH_M = 11.5 ± 0.1, in excellent agreement with the experimental result.

(11) K. Applegate, L. Slutsky, and C. Parker, *J. Amer. Chem. Soc.*, **90**, 6909 (1968).

(12) R. White, L. Slutsky, and S. Pattison, *J. Phys. Chem.*, **75**, 161 (1971).

(13) M. Hussey and P. Edmonds, *J. Acoust. Soc. Amer.*, **49**, 1309, 1907 (1971).

(14) H. Inoue, *J. Sci. Hiroshima Univ., Ser. A2*, **34**, 17 (1970).

(15) M. Emara, G. Atkinson, and E. Baumgartner, *J. Phys. Chem.*, **76**, 334 (1972).

(16) A. Katchalsky, N. Shavit, and H. Eisenberg, *J. Polym. Sci.*, **13**, 69 (1954).

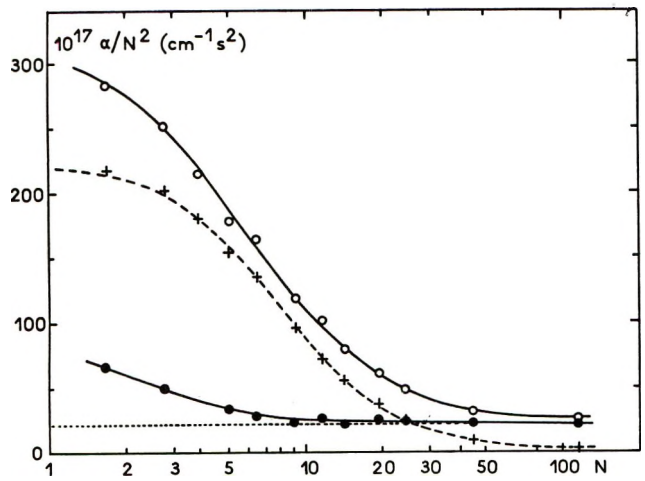

Figure 3. Ultrasonic absorption spectra of PLL in H_2O–0.3 M NaBr at 25° and at pH 7.0 (●) and 11.5 (○). The crosses show the values of $\delta\alpha/N^2$ (see text) and the broken line curve is the single relaxation time curve giving the best fit with the values of $\delta\alpha/N^2$. Concentration, 0.06 M. (. . . . .), α/N^2 for the solvent.

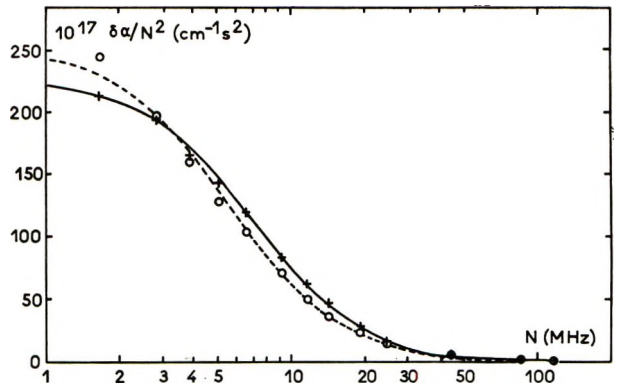

Figure 4. Variation of $\delta\alpha/N^2$ *vs.* N for 0.056 M solutions of PLO in H_2O–0.3 M NaBr (+) and in 85 parts H_2O–15 parts methanol–0.3 M NaBr (○) at 25°. The curves shown by the solid line and the broken line are single relaxation time curves giving the best fit with the results.

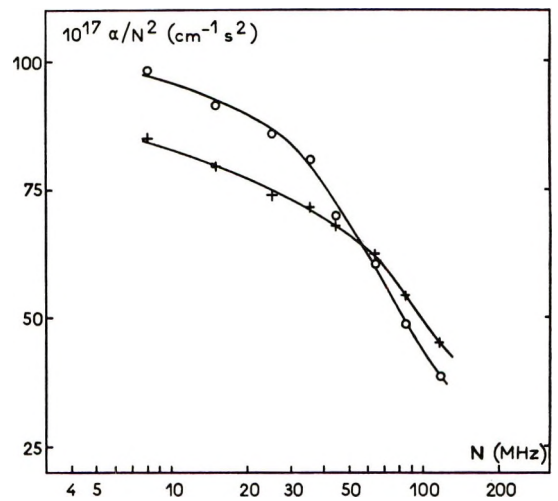

Figure 5. Ultrasonic absorption spectra of 0.1 M solutions of diethylamine in H_2O (+) and in 85% H_2O–15% methanol (○).

For PLO in H_2O–0.2 M KCl the "minimum value" $pK_0 = 10.1$ has been reported by Chaudhuri and Yang,[6] thus yielding pH_M 11.45 ± 0.05, in excellent agreement with the experimental result on Figure 2. On the other hand, the results compiled by Robinson and Stokes[17] indicate that the pK_a's of weak bases are increased by less than 0.2 pH unit in the presence of 15% methanol. If it is assumed that methanol has a similar effect on PLO, the maximum increase of pH_M would then be less than 0.1 pH unit, *i.e.*, practically within the experimental accuracy.

(2) Determination of the Rate Constants k_F and k_B and of the Volume Change Associated with Reaction 1. For this purpose the relaxation spectra of PLL and PLO solutions at pH 7.0 and 11.5 have been determined. The spectra relative to PLL are shown in Figure 3, in which are also given the values of $\delta\alpha/N^2 = (\alpha/N^2)_{pH\ 11.5} - (\alpha/N^2)_{pH\ 7.0}$. These values of $\delta\alpha/N^2$ have been obtained by drawing smooth curves through the experimental points at pH 11.5 and 7.0 and taking the difference between the values of α/N^2 at pH 11.5 and 7.0, read on these curves, at each of the frequencies where the absorption had been measured. This procedure averages the errors. The difference $\delta\alpha/N^2$ can be safely assumed to represent the contribution of reaction 1 since, as can be seen in Figure 2, the values of α/N^2 at pH 7.0 and 13.0 are practically identical. In Figure 3 the broken line curve represents the single relaxation time curve fitting the best with our results. This curve obeys the equation

$$\frac{\delta\alpha}{N^2} = \frac{A}{1 + (N^2/N_R^2)} + B \qquad (3)$$

The values of the relaxation parameters are given in Table I.

The ultrasonic absorption spectra of PLO at pH 7.0 and 11.5, in H_2O–0.3 M NaBr and in 85 parts H_2O–15 parts methanol–0.3 M NaBr have also been determined. The results are represented in Figure 4 in terms of $\delta\alpha/N^2$. The lines are single relaxation time curves fitting the results. The relaxation parameters characterizing these curves are given in Table I. The results in Figure 4 show that the introduction of methanol brings about a decrease of relaxation frequency from 7 to 5.5 MHz. A similar decrease of N_R upon addition of methanol can also be seen in Figure 5 for a 0.1 M solution of diethylamine. Thus, this slowing down of proton-transfer reactions upon introduction of methanol appears to be quite general. Our measurements also indicate that at neutral pH the α/N^2 value is smaller for PLO than for PLL, particularly at $N < 5$ MHz. At 1.6 MHz the α/N^2 of PLL and PLO were,

(17) R. Robinson and R. Stokes, "Electrolyte Solutions," 2nd ed, Butterworths, London, 1970, p 541.

Table I

Polypeptide (solvent)	N_R, MHz	$10^{17}A$, cm^{-1} sec^2	$10^{17}B$, cm^{-1} sec^2	$10^{-9}k_F$, M^{-1} sec^{-1}	$10^{-6}k_B$, sec^{-1}	ΔV_0, cm^3/mol
PLL (H_2O–0.3 M NaBr)	8	220	2	7.35	1.3	24
PLO (H_2O–0.3 M NaBr)	7	225	0	8.1	1.0	25.7
PLO (85 parts H_2O–15 parts methanol–0.3 M NaBr)	5.5	250	0	6.35	0.8	24

respectively, 60 and 40.10^{-17} cm^{-1} sec^2. This difference is to be compared to the increased excess absorption with increasing alkyl chain length observed in aqueous solutions of tetraalkylammonium salts.[18]

In the calculations of k_F, k_B, and ΔV_0 from the relaxation parameters A and N_R, the following equations were used[2]

$$pK_a = 14 + pK = 14 + \log (k_B/k_F) \quad (4)$$

$$\tau^{-1} = 2\pi N_R = k_F\left(\frac{c}{1 + Kc_{OH^-}} + c_{OH^-} + \frac{1}{K}\right) \quad (5)$$

$$A = \frac{2\pi^2\rho v}{RT}\frac{(Kc)c_{OH^-}}{Kc + (Kc_{OH^-} + 1)^2}\Delta V_0^2\tau \quad (6)$$

$$pH = 14 + \log c_{OH^-} \quad (7)$$

where τ is the relaxation time and ρ and v are, respectively, the density and velocity of ultrasound for the solvent. The activity coefficients were assumed to be unity. The results of these calculations are given in Table I. The values of the rate constants in Table I are the first ones reported for proton-transfer reactions on polymers. For PLL the value $\Delta V_0 = 24$ cm^3/mol obtained in this work compares well with that determined by Noguchi,[19] 22.9 cm^3/mol at ionic strength 0.2, using a dilatometric technique. On the other hand, some insight can be gained by comparing the value of k_F for PLL to that of the ϵ-amino group of its monomer, L-lysine. For this last compound two independent determinations of k_F have been reported.[13,14] The average value, $k_F = 1.9 \times 10^{10}$ M^{-1} sec^{-1} is larger by a factor of 2.5 than for PLL. This is a relatively small difference; one would have expected electrostatic effects to be of major importance in the case of PLL, as this polymer is also a polyelectrolyte. However, as stated above, only 1 out of every 20 residues is ionized at pH 11.5. This, together with the fact that the ϵ-amino side chain is more than 6 Å long, yields an average distance between charged residues over 30 Å. Therefore, in the vicinity of the polymer chain, the interaction of one OH^- ion with the chain can be approximated by the interaction of this ion with the closest $-NH_3^+$ group on the chain; the smaller the OH^-–NH_3^+ distance, the better this approximation. Another factor which must be taken into account in the comparison of the k_F values for lysine and PLL is the diffusion coefficient. The Debye–Eigen[20] equation giving k_F contains the sum of the diffusion coefficients of the reacting species. In going from lysine to PLL, the diffusion coefficient per $-NH_3^+$ group will decrease, thereby yielding a lower rate constant. Also, steric effects are likely to be more important with PLL than with its monomer because of the hindrance due to the polymer chain, thus resulting in a smaller rate constant. The three effects invoked above are difficult to take into account quantitatively. However, the results on lysine and PLL are to be compared with the findings of Atkinson, *et al.*,[15] for the effect of molecular weight on k_F for the four first oligomers of polyethylenimine. These authors observed a decrease of k_F with increasing molecular weight from 2.8×10^{10} M^{-1} sec^{-1} for ethylenediamine to 2.3×10^{10} M^{-1} sec^{-1} for tetraethylenepentamine.

At the end of this paragraph, it may be stated that proton-transfer reactions account quantitatively for the excess absorption observed in PLL, PDLL, and PLO solutions in the frequency range 1–155 MHz. This conclusion has important implications as regards the kinetics of the helix–coil transition in solutions of polypeptides and to the excess ultrasonic absorption of protein solutions.

V. Considerations on the Kinetics of the Helix–Coil Transition in Solutions of PLL and PLO

Unlike PLL and PLO, a small though measurable ultrasonic absorption associated with the helix–coil equilibrium has been found in aqueous solutions of poly(L-glutamic acid) (PLGA) in the megahertz range.[21,22] However, PLGA solutions in 2:1 (v/v) water–dioxane–0.2 M NaCl did not show any such excess absorption.[23,24] The first and, in our mind, most important reason for these differences is to be found in the value of nucleation parameter σ, characterizing the

(18) M. Blandamer, M. Foster, N. Hidden, M. Symons, *Trans. Faraday Soc.*, **64**, 3247 (1968).

(19) H. Noguchi, *Biopolymers*, **4**, 1105 (1966).

(20) M. Eigen and L. De Maeyer, *Tech. Org. Chem.*, **8**, 1032 (1963).

(21) T. Saksena, B. Michels, and R. Zana, *J. Chim. Phys. Physicochim. Biol.*, **65**, 597 (1968).

(22) R. Zana, *J. Amer. Chem. Soc.*, **94**, 3646 (1972).

(23) R. Zana, S. Candau, and R. Cerf, *J. Chim. Phys. Physicochim. Biol.*, **60**, 869 (1963).

(24) J. Burke, G. Hammes, and T. Lewis, *J. Chem. Phys.*, **42**, 3520 (1965).

helix–coil equilibrium,[25] which changes according to the nature of the polypeptide and of the solvent.[26,27] In fact, Schwarz[10] has shown that for the helix–coil transition

$$N_R = 2\sigma k_H/\pi \quad (8)$$

where k_H is the rate constant for the elementary step of growth of a helical region, *i.e.*, for the formation of a hydrogen bond. N_R has been found to be 0.15 MHz for aqueous solutions of PDGA[28] and PLGA.[29] If we assume that in water k_H is independent of the nature of the polypeptide, N_R will still depend on this parameter through σ. The values $\sigma = 3\text{–}5 \times 10^{-3}$, 10^{-3}, and 7×10^{-4} have been determined for aqueous solutions of PLGA,[30] PLO,[31] and PLL.[32] One can therefore expect smaller values of N_R for PLL and PLO than for PLGA, and in the megahertz range the condition $N^2/N_R^2 \gg 1$ to be fullfilled for these three polymers. Equation 3 then indicates that $\delta\alpha/N^2$ is proportional to AN_R^2, that is to $\Delta V_0^2 N_R$ since A contains the ratio $\Delta V_0/N_R$,[20] where ΔV_0 is the volume change associated with the helix–coil transition. Dilatometric measurements have shown[19,33] that in water ΔV_0 depends only little on the nature of the polypeptide. Therefore, to a first approximation $\delta\alpha/N^2$ is proportional to N_R, *i.e.*, to σ. For PLGA, $\delta\alpha/N^2$ has been found[34] to be 17 and 10×10^{-17} cm^{-1} sec^2 at 2.8 and 5 MHz, respectively. From the above one should expect for PLL and PLO excess absorptions three to seven times smaller than for PLGA, *i.e.*, $2\text{–}5 \times 10^{-17}$ cm^{-1} sec^2 at 2.8 MHz and $1\text{–}3 \times 10^{-17}$ cm^{-1} sec^2 at 5 MHz. Such excess absorptions would be barely detectable had the helix–coil transition been the only process giving rise to the absorption. That proton-transfer reactions contribute to the excess absorption in the same pH range as the helix–coil transition renders practically impossible the observation of this process. This is well illustrated by the following example: Figure 1 shows that at pH 10.5, midpoint of the helix–coil transition for PLL, the absorption due to reaction 1 is $40 \pm 5 \times 10^{-17}$ cm^{-1} sec^2; at the same pH, frequency, and concentration the helix–coil transition would contribute by about $1\text{–}2 \times 10^{-17}$ cm^{-1} sec^2.

Differences in σ values also permit us to explain the different behaviors of PLGA in H_2O[21,22] and in 2:1 H_2O–dioxane.[23,24] In these solvents σ has the values $3\text{–}5 \times 10^{-3}$ [30] and 1.2×10^{-3},[27] respectively. With the same assumptions as above, this would result in an excess absorption too small to be detected in the solvent mixture.

In addition to the larger value of σ, two other facts make the observation of the helix–coil equilibrium easier with aqueous PLGA than with PLL and PLO. First, the pH at the midpoint of the transition (5.1) is over two pH units higher than that at which the contribution of the proton transfer is maximum (2.8 for a 0.1 *M* PLGA solution), while the pH's characterizing both processes are 1 and 0.5 pH units apart for PLL and PLO, respectively. Second, the contribution of the proton-transfer reaction on a carboxylic group (reaction 9) such as that of PLGA is much smaller than that for reaction 1 in the megahertz range[5,13] and becomes quite small at the pH corresponding to the mid transition.

$$-CO_2H \rightleftharpoons -CO_2^- + H^+ \quad (9)$$

In conclusion, it appears that for aqueous solutions of polypeptides the helix–coil equilibrium gives rise to a measurable excess absorption in the megahertz range only when the cooperativity of the transition is low (high σ values) and when the pH's characterizing the transition and the proton transfer reactions are well separated on the pH scale (at least two pH units).

VI. Considerations on the Ultrasonic Absorption of Protein Solutions in the Alkaline Range

Studies of the ultrasonic absorption of protein solutions in the alkaline range have shown that the excess absorption goes through a well-defined maximum at pH 11.1–11.3.[5,35,36] We have shown[5] that this maximum is due to proton-transfer reactions which may involve all of the residues bearing on their side chains functional groups which titrate in the alkaline range, *i.e.*, lysine, arginine, histidine, and tyrosine. Thus, at first sight the situation appears quite complicated, since each type of residue is characterized by a different pK_0. However, upon examination of the pK_0 values,[37] histidine and tyrosine can be readily eliminated, as their pK_0's are such that they would result in calculated values of pH_M too different from the experimental ones. Moreover, the tables of the amino acid content of the proteins[38] whose ultrasonic absorption has been investigated reveal that lysine residues constitute 65–75% of the residues of interest. This led us as a first approximation to try to interpret the results obtained for protein solutions in the alkaline range in terms of reaction 1 involving only lysine residues. From the tables of the amino acid content and molecular weight

(25) B. Zimm and J. Bragg, *J. Chem. Phys.*, **31**, 256 (1959).
(26) O. Ptitsyn and A. Skvortsov, *Biofizika*, **10**, 909 (1965).
(27) G. Hagnauer and W. Miller, *Biopolymers*, **9**, 589 (1970).
(28) H. Inoue, *J. Sci. Hiroshima Univ., Ser. A2*, **34**, 37 (1970).
(29) A. Barksdale and J. Stuehr, *J. Amer. Chem. Soc.*, **94**, 3334 (1972).
(30) J. Rifkind and J. Applequist, *J. Amer. Chem. Soc.*, **86**, 4207 (1964); R. Snipp, W. Miller, and R. Nylund, *ibid.*, **87**, 3547 (1965).
(31) M. Gourke and J. Gibbs, *Biopolymers*, **10**, 795 (1971).
(32) G. Hagnauer, Ph.D. Thesis, University of Iowa, 1970.
(33) H. Noguchi and J. T. Yang, *Biopolymers*, **1**, 359 (1963).
(34) B. Michels and R. Cerf, *C. R. Acad. Sci. (Paris), Ser. D*, **274**, 1096 (1972).
(35) F. Dunn and L. Kessler, *J. Phys. Chem.*, **74**, 2736 (1970).
(36) I. Elpiner, F. Braginskaya, and O. Zorina, 7th International Congress on Acoustics, Communication 25 M7, Vol. II, Akademiai Kiado Ed., Budapest, 1971, p 153.
(37) C. Tanford, *Advan. Protein Chem.*, **17**, 69 (1962).
(38) C. Tristram and R. Smith, *ibid.*, **18**, 227 (1963).

of proteins,[38] one can calculate the concentration C of lysine residues which appears in eq 2 for a given weight–volume concentration of the protein solution. Then, using eq 2 together with the experimental values of C and pH_M, one can obtain the value of pK_0 which is to be used in the calculations of k_F and ΔV_0. The value 10.6 was thus obtained for bovine serum albumin (BSA). This value is close to the pK_0 for PLL, but it is higher than that obtained from potentiometric titration of BSA,[37] thus revealing the contribution of the arginine residues which have been completely neglected in this calculation. The ultrasonic absorption spectra of a 0.0116 g/cm³ solution of BSA have been determined at pH 7.0 and 11.3 (absorption maximum).[39] Here again, the curve $\delta\alpha/N^2 = (\alpha/N^2)_{11.3} - (\alpha/N^2)_{7.0}$ *vs.* N was found to be fitted by a single time relaxation curve with $N_R = 4.7$ MHz, $A = 225 \times 10^{-17}$ cm^{-1} sec^2, and $B = 0$. From these data and the above value of pK_0, we obtained $k_F = 0.7 \times 10^{10}\ M^{-1}$ sec^{-1} and $\Delta V_0 = 26$ cm³ mol^{-1}. These values are very close to those obtained for PLL (see Section III), thereby justifying *a posteriori* the above simplifications. Contrary to the opinion advanced by other workers,[11,14] the example of BSA shows that despite the complexity of proteins the ultrasonic absorption data in the alkaline range can be interpreted simply but also quantitatively by considering only lysine residues.

Acknowledgment. We gratefully acknowledge the technical assistance of M. Pister and M. Krauskopf in building the pulse equipment.

(39) R. Zana, J. Lang, C. Tondre, and J. Sturm, Proceedings of the Workshop on the Interactions of Ultrasound with Biological Tissues, Seattle, Nov 1971, in press.

Application of the m–6–8 Potential to Simple Gases[1]

by H. J. M. Hanley

Cryogenics Division, Institute for Basic Standards, National Bureau of Standards, Boulder, Colorado 80302

and Max Klein*

Heat Division, Institute for Basic Standards, National Bureau of Standards, Washington, D. C. 20234

(Received January 7, 1972)

Publication costs assisted by the National Bureau of Standards

The m–6–8 model potential function is applied to the gases argon, krypton, xenon, nitrogen, methane, and carbon dioxide and to the properties viscosity coefficient, self-diffusion coefficient, thermal conductivity coefficient, virial coefficient, and the isotopic thermal diffusion factor. The potential is shown to have a considerable advantage over previous simple analytic models in that it can satisfy two criteria: (a) it can be used to correlate a given property for all the gases studied over a wide temperature range with a single set of parameters, and (b) it can be used to correlate both transport and equilibrium properties for the monatomic gases with a single set of parameters. Reasons for the failure of polyatomic gases to satisfy (b) are suggested. A brief discussion on the relation of the potential to theory is given.

Introduction

A new model potential function, the m–6–8, was recently reported and shown to be successful when applied to the viscosity and second virial coefficients of argon.[2] The potential was a significant improvement over previous analytical models in that it satisfied two criteria: (1) the ability to correlate a given property over a wide temperature range with a single set of parameters; (2) the ability to correlate a property of one type (*e.g.*, a transport property) and a property of another type (*e.g.*, the equilibrium second virial coefficient) with a single set of parameters.

In this paper we extend the preliminary work given in ref 2 to other properties and other substances: our objectives are to investigate how the m–6–8 potential behaves when applied to data for simple gases and to see if that potential can be useful. We stress this latter objective because we are first interested in what we shall

(1) Work carried out at the National Bureau of Standards under the partial sponsorship of the Office of Standard Reference Data (for H. J. M. Hanley) and (for M. Klein), supported, in part, by the Air Force Command, Arnold Engineering Development Center, Tullahoma, Tenn. Delivery Order Number (40-600) 66-938 Program Element 61445014 AF Project 8951.

(2) M. Klein and H. J. M. Hanley, *J. Chem. Phys.*, 53, 4722 (1970).

term the "utility" of a potential. By utility we mean the ability of a potential to correlate particular kinds of data. This is a more realistic goal than seeking after the "validity" which we shall use to denote the ability of a potential to fit all possible kinds of data and, at the same time, to be compatable with independent fundamental ideas on the nature of the forces between molecules (*e.g.*, the results of *a priori* molecular calculation). The determination of the utility of a potential function is of importance both because the tests which are applied would also be needed for the determination of the validity of the function and because useful functions can generally be used for the production of tables of those properties which have successfully been correlated with them. It should be noted that valid functions form a subclass of useful functions since all requirements for utility must be satisfied for validity. It should also be noted that implicit in our use of utility is the assumption that the potential has a sufficiently small number of parameters to allow for the use of generalized reduced tables which need to be calculated only once for the potential.

In this work we are first concerned with the utility of the m–6–8 function and shall only examine its validity when the criteria of utility are satisfied. Needless to say we would hope to find the m–6–8 function a valid one for as many substances as possible.

The experimental data which have been used by us in these tests of the potential function were carefully selected from literature values in earlier studies of potential functions. The selections were made on the basis of consistency and, in the cases of the second virial coefficients and viscosities, on the basis of a careful study of the experimental papers.[3] In some cases, the data have been obtained from a new analysis of the quantities which were actually measured in the experiments. The state of the art accuracies (based on a combination of estimates by the experimentalists and intercomparisons between the results reported by different laboratories) are as follows: viscosity, ±2.0%; diffusion coefficient, ±5%; and second virial coefficient, ±2.0% (except near the Boyle temperature where the percentage increases). No such figure can be assigned to the thermal diffusion factor because of extreme experimental difficulties.

The m-6-8 Potential

The m–6–8 intermolecular potential function

$$\phi(r) = \frac{A}{r^m} - \frac{C_6}{r^6} - \frac{C_8}{r^8} \qquad (1)$$

has four parameters: m, a repulsive index, and A, C_6, and C_8 which are coefficients indicating the strengths of repulsion and attraction. The particular form of eq 1 used in our calculations is

$$\phi^*(r^*) = \frac{[6 + 2\gamma]}{m - 6}\left(\frac{d}{r^*}\right)^m - \frac{[m - \gamma(m - 8)]}{m - 6}\left(\frac{d}{r^*}\right)^6 - \gamma\left(\frac{d}{r^*}\right)^8 \qquad (2)$$

where $\phi^*(r^*) = \phi(r)/\epsilon$, $r^* = r/\sigma$, $d = r_m/\sigma$, and γ is the parameter which represents the inverse eight attraction and is related to C_8 through the relation $\gamma = C_8/(\epsilon r_m^8)$. Here σ is the distance parameter defined as the value of r when $\phi(r) = 0$, and r_m is the value of r at the maximum energy of attraction, $\phi(r_m) = -\epsilon$. The four parameters associated with this potential are m, σ (or r_m), ϵ, and γ. As a matter of interest we sketch eq 2 for two sample values of m and γ to illustrate the relationship between these two variables (see Figure 1). Figure 1a shows how the attractive part is affected by an increase in m, with $\gamma = 0.0$; Figure 1b shows how the attractive part is affected by increasing γ with m constant. Note that increasing γ at constant m has roughly the same effect as increasing m at constant γ. (We have not shown the associated small changes in the repulsive part of the potential because they are very small when compared to the changes in the attractive part.)

Collision Integrals and Second Virial Coefficients. Collision integrals and reduced second virial coefficients were computed for the m–6–8 potential with $9 \leq m \leq 18$ for values of γ such that $0 < [m - \gamma(m - 8)]$. The calculation procedure and generalized reduced tables are available in another publication.[4]

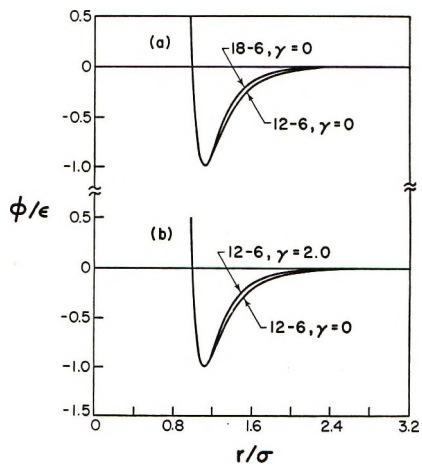

Figure 1. Plots of the m–6–8 potential determined from eq 2 shown to demonstrate how the attractive part varies with (a) an increase in m at fixed γ, and (b) an increase in γ at fixed m.

(3) (a) J. M. H. Levelt Sengers, M. Klein, and J. S. Gallagher, to appear in the "American Institute of Physics Handbook," McGraw-Hill, New York, N. Y. Also available as Report AEDC-TR-71-39, Arnold Engineering and Development Center, Tullahoma, Tenn. This report can be obtained from The Clearing House for Federal Scientific and Technical Information (CFSTI), Springfield, Va. 22151 as AD 719749. (b) See also H. J. M. Hanley and G. E. Childs, *Science*, **159**, 1114 (1968).

(4) M. Klein, F. J. Smith, H. J. M. Hanley, and P. M. Holland, NBS-NSRD Monograph, to be published.

Testing the m–6–8 Potential with the Rare Gases

As reported in ref 2, initial tests of the potential were made with argon using the viscosity and second virial coefficients. Theoretical expressions for these coefficients are[5]

Viscosity (to the first Chapman–Enskog approximation[6])

$$\eta = \frac{5}{16} \frac{\sqrt{\pi mkT}}{\pi\sigma^2\Omega^{(2,2)^*}(T^*)} \tag{3}$$

Second Virial

$$B = b_0 B^*(T^*) \tag{4}$$

where

$$b_0 = (^2/_3)\pi N\sigma^3 \tag{5}$$

In eq 3–5, the intermolecular potential function enters *via* $\Omega^{(2,2)^*}(T^*)$, the collision integral accounting for the dynamics of a binary collision in the viscosity process, and $B^*(T^*)$, the reduced second virial coefficient. For a given potential function, $\phi(r)$, both $\Omega^{(2,2)^*}(T^*)$ and $B^*(T^*)$ can be calculated as functions of T^*, where $T^* = T/(\epsilon/k)$. Also, in these equations, m is the mass of a molecule, N is Avogadro's number, k is Boltzmann's constant, and M the molecular weight.

The testing procedure followed was in two parts. First the viscosity coefficient was fitted separately at high *and* low temperatures and we sought correlations such that the same m–6–8 parameters were obtained in both cases. (We have previously discussed at length what we mean by a high and a low temperature[7]: it was pointed out that transport properties were insensitive to the potential function in a reduced temperature range of $2 \lesssim T^*_{12-6} \lesssim 5$. A correlation of the properties in this range can only give two parameters for a chosen potential. T^*_{12-6} is defined as $T/(\epsilon/k)_{12-6}$ with T the temperature in degrees Kelvin and $(\epsilon/k)_{12-6}$ the energy parameter for the Lennard-Jones, 12–6, potential.[8] By high temperatures is meant a temperature above $T^*_{12-6} \approx 5$ while a low temperature refers to a temperature below $T^*_{12-6} \approx 2$.) Second, the viscosity and second virial coefficients were fitted simultaneously over all temperatures and we required a single set of parameters which correlated the two properties to within their experimental error. The fitting procedures have been discussed in ref 9a and b and, in considerable detail, in ref 10 and so we do not have to repeat them in this paper. As mentioned above, the data selected for these initial correlations were chosen very carefully: second virial data, ref 3; viscosity data, ref 11–16. For argon, these two fitting procedures were successful and yielded a single set of m–6–8 parameters. The procedures were repeated for krypton and xenon with similar results.

Values of the m–6–8 parameters for the rare gases are given in Table I and graphs of the deviations between theory and experiment[3, 11–21] are shown as Figures 2–4. These graphs are self explanatory. They indicate that the m–6–8 is satisfactory and that the criteria listed in the Introduction are satisfied for argon, krypton, and xenon. It is interesting to note that these gases follow the corresponding-states law since the potential that applies to them differs only in the two parameters, σ and ϵ/k.

Table I: Values of the Parameters of the m–6–8 Potential Function Which Fit Both Transport and Equilibrium Properties

Gas	m	γ	σ, Å	ϵ/k, K
Ar	11	3	3.292	153
Kr	11	3	3.509	216
Xe	11	3	3.841	295

Further Checks on the Utility of the Potential

We examine three further statistical mechanical expressions.

Thermal Conductivity. The statistical mechanical expression for the thermal conductivity coefficient of a dilute monatomic gas, λ', involves the same collision integrals as does the viscosity coefficient

$$\lambda' = \frac{25}{32} \frac{\sqrt{\pi mkT}}{\pi\sigma\Omega^{(2,2)^*}(T^*)} \frac{c_v'}{m} \tag{6}$$

(5) J. O. Hirschfelder, C. F. Curtiss, and R. B. Bird, "Molecular Theory of Gases and Liquids," 2nd ed, Wiley, New York, N. Y., 1964.

(6) We have verified that our conclusions obtained by studying the relationship of the potential with the transport properties are not affected by taking the statistical mechanical expressions to the first approximation only.

(7) H. J. M. Hanley and M. Klein, *Nat. Bur. Stand. Tech. Note*, **No. 360** (1967).

(8) The particular choice of reducing T is made for convenience only; there is no special significance to the use of the 12–6 potential. This can be converted to a reduction by the Boyle temperature by dividing by the Boyle temperature for the 12–6 potential (*i.e.*, $T^*/B = 3.43$).

(9) (a) H. J. M. Hanley, *J. Chem. Phys.*, **44**, 4219 (1966); (b) M. Klein and H. J. M. Hanley, *Trans. Faraday Soc.*, **64**, 2927 (1968).

(10) H. J. M. Hanley and M. Klein, *Nat. Bur. Stand. Tech. Note*, in preparation.

(11) F. A. Guevara, B. B. McInteer, and W. E. Wageman, *Phys. Fluids*, **12**, 2493 (1969).

(12) M. Goldblatt, F. A. Guevara, and B. B. McInteer, *ibid.*, **13**, 2873 (1970).

(13) M. Goldblatt and W. E. Wageman, *ibid.*, **14**, 1024 (1971).

(14) A. G. Clark and E. B. Smith, *J. Chem. Phys.*, **48**, 3988 (1968).

(15) R. A. Dawe and E. B. Smith, *ibid.*, **52**, 693 (1970).

(16) J. Kestin, W. Wakeham, and K. Watanabe, *ibid.*, **53**, 3773 (1970); R. Dipippo and J. Kestin, Brown University Report NSF-GK 1305 (1967).

(17) H. L. Johnson and E. R. Grilly, *J. Phys. Chem.*, **46**, 948 (1942).

(18) J. A. Gracki, G. P. Flynn, and J. Ross, *J. Chem. Phys.*, **51**, 3856 (1969).

(19) D. L. Timrot, M. A. Sevednitskaya, and S. A. Traktueva, *Teploenergetika*, **16**, 83 (1969).

(20) A. O. Rankine, *Phys. Z.*, **11**, 745 (1910).

(21) J. Kestin and W. Leidenfrost, *Physica*, **25**, 1033 (1959).

or

$$\lambda' = \frac{15}{4}\frac{k}{m}\eta \qquad (7)$$

where $c_v'/m = (3/2)k/m$ is the translational specific heat per molecule. A check on the thermal conductivity thus serves as a cross check between the viscosity and thermal conductivity data and not necessarily as a check on the potential function. We show, however, a deviation curve for argon in Figure 5. (Data are from ref 22–33.)

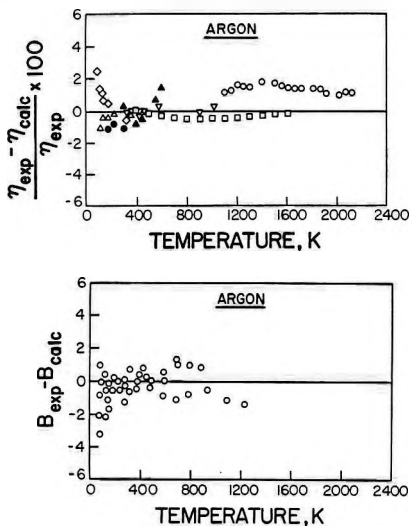

Figure 2. Second virial coefficients (top curve) and viscosity coefficients (bottom curve) of argon. Theoretical values determined from eq 3 and 4 using the m–6–8 potential with m = 11, γ = 3.0, σ = 3.292 Å, ϵ/k = 153 K. Experimental virials from ref 3. Experimental viscosities are from the references indicated in parentheses: ○ (12), △ (14), □ (15), ▽ (16), ◇ (17), ● (18), and ▲ (19).

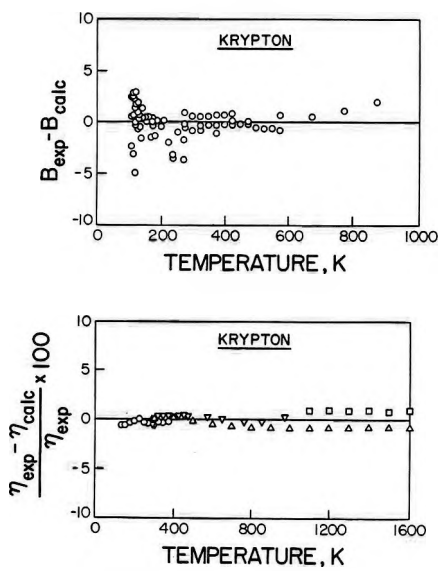

Figure 3. Second virial and viscosity coefficients of krypton; m = 11, γ = 3.0, σ = 3.509 Å, ϵ/k = 216 K. Virial data from ref 3. Viscosity data are from the references in parentheses: ○ (14), △ (15), ▽ (16), and □ (12).

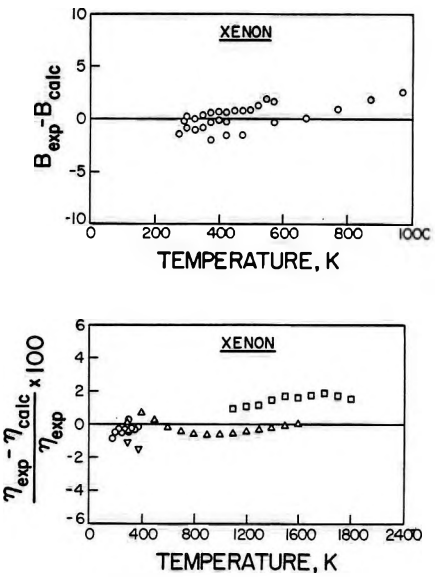

Figure 4. Second virial and viscosity coefficients of xenon; m 11, γ = 3.0, σ = 3.841 Å, ϵ/k = 295 K. Virial data from ref 3. Viscosity data are from the references in parentheses: ○ (14), △ (15), □ (13), and ▽ (20,21).

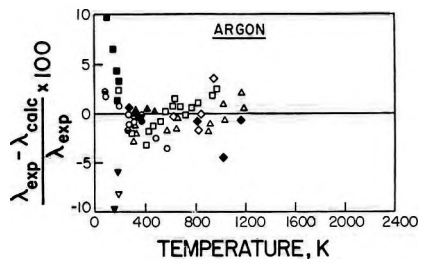

Figure 5. Deviation curve of experimental dilute gas thermal conductivity coefficients for argon compared to eq 6 with m–6–8 potential parameters as for the viscosity and second virial coefficients. Data are from references in parentheses: ◆ (22), ● (23), ▼ (24), ◒ (25), ■ (26), ▼ (27), ◇ (28), ○ (29), □ (30), △ (31), ◓ (32), and ▲ (33).

(22) F. G. Keyes and R. G. Vines, *J. Heat Transfer*, **87**, No. 2, 177 (1965).

(23) A. Michels, J. V. Sengers, and L. J. M. Van de Klundert, *Physica*, **29**, 149 (1963).

(24) A. Uhlir, *J. Chem. Phys.*, **20**, 463 (1952).

(25) A. Eucken, *Phys. Z.*, **12**, 1101 (1911).

(26) H. Ziebland and J. T. A. Burton, *Brit. J. Appl. Phys.*, **9**, 52 (1958).

(27) L. D. Ikenberry and S. A. Rice, *J. Chem. Phys.*, **39**, 1561 (1963).

(28) A. J. Rothman, *U. S. At. Energy Comm. Rep. UCRL* **2339**, 8 (1953).

(29) W. G. Kannuluik and E. H. Carman, *Proc. Phys. Soc. London Ser. B*, **65**, 701 (1952).

(30) B. Le Neindre, R. Tufeu, P. Bury, P. Johannin, and B. Vodar, Proceedings of the 8th Conference on Thermal Conductivity, Purdue University, Lafayette, Ind., 1968; B. Le Neindre, Thesis, University of Paris, 1970; B. Le Neindre, private communication.

(31) N. B. Vagaftik and N. Kh. Zimina, *Teplofiz. Vys. Temp.*, **2**, 716 (1964).

(32) W. Van Dael and H. Cauwenbergh, *Physica*, **40**, 165 (1968).

(33) J. W. Haarmann, Thesis, University of Delft, The Netherlands, 1969.

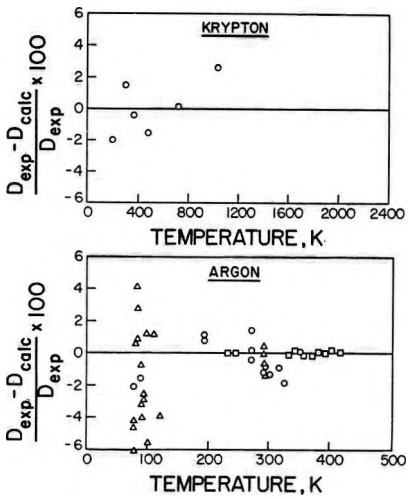

Figure 6. Self-diffusion of argon and krypton; deviation curves of experiment *vs.* theory, using the m–6–8 potential. Data: for argon (with references in parentheses): △ (34), □ (35), and ○ (36); for krypton: ○ (37). Note that the data from ref 35 are relative to the diffusion at 298.15 K. We used the calculated value for this reference point.

Self-Diffusion Coefficient, D. A collision integral other than $\Omega^{(2,2)^*}(T^*)$ is in the theoretical expression for this coefficient. The expression is to a first approximation

$$\rho D = \frac{5}{8}\frac{\sqrt{\pi mkT}}{\pi\sigma^2\Omega^{(1,1)^*}(T^*)} \tag{8}$$

where ρ is the mass density of the gas and $\Omega^{1(,1)^*}(T^*)$ is the collision integral for self-diffusion. Figure 6 gives deviation plots for argon and krypton[34-37] showing how self-diffusion data compare with the theoretical calculations based on eq 8 using the 11–6–8 ($\gamma = 3.0$) potential.

Isotopic Thermal Diffusion Factor, α_0. This coefficient is very sensitive to the potential function. The expression for the factor is, according to Kihara[38]

$$\alpha_0 = \alpha_0'(1 + \delta) \tag{9}$$

where

$$\alpha_0' = \frac{15(6C^* - 5)(2A^* + 5)}{2A^*(16A^* - 12B^* + 55)}$$

with δ given by

$$\delta = \frac{I^*}{9}\left\{\frac{2A^*}{(^{35}/_4) + 7A^* + 4F^*} \times \left[H^* + \frac{1}{2}\left(\frac{7(5 - 6C^*) + A^*I^*}{5 + 2A^*}\right) \times \left(\frac{(^{35}/_8) + 28A^* - 6F^*}{21A^*}\right)\right] - \frac{5}{7}\left[H^* - \frac{7}{5}\left(\frac{5 - 6C^*}{5 + 2A^*}\right) - \frac{3I^*}{10}\right]\right\} \tag{10, 11}$$

where

$$I^* = 7 - 8E^*$$

and

$$H^* = \frac{(^{35}/_4) - 3B^* - 6C^*}{5 - 6C^*} \tag{12}$$

The potential function enters into the equation for α_0 through ratios of collision integrals commonly designated by A^*, B^*, C^*, E^*, and F^* and given by

$$\begin{aligned} A^* &= \Omega^{(2,2)^*}/\Omega^{(1,1)^*} \\ B^* &= (5\Omega^{(1,2)^*} - 4\Omega^{(1,3)^*})/\Omega^{(1,1)^*} \\ C^* &= \Omega^{(1,2)^*}/\Omega^{(1,1)^*} \\ E^* &= \Omega^{(2,3)^*}/\Omega^{(2,2)^*} \\ F^* &= \Omega^{(2,3)^*}/\Omega^{(1,1)^*} \end{aligned} \tag{13}$$

Figure 7 shows a plot of α^0 determined from eq 9 compared to the data of Paul, *et al.*[39] Since thermal diffusion data are very difficult to obtain with any precision, we regard this curve as satisfactory.

Application of the m–6–8 Potential to Simple Polyatomic Molecules

The evidence presented in the previous section indicates that the m–6–8 potential is satisfactory for the monatomic molecules. This, alone, is a significant result but, obviously, this model function would be more important as a practical tool if it could be successfully applied to polyatomic molecules as well. Unfortunately, however, this extension is not straightforward because two very basic complications are then introduced.

1. In principle, the spherically symmetric m–6–8 potential (or any other spherical potential) can never properly depict the interaction between two polyatomic molecules; as the molecules collide, a number of orientation-dependent force laws are followed—one for each relative orientation.

2. Even if one has a potential which can account for orientation-dependent interactions, the statistical mechanical expressions used should allow for the fact that collisions between polyatomic molecules can be inelastic. The effect of the molecular internal degress of freedom in collisions has then to be considered.

These two problems have been discussed by many

(34) F. Hutchinson, *J. Chem. Phys.*, **17**, 1081 (1949); E. B. Winn, *Phys. Rev.*, **80**, 1024 (1950).

(35) H. F. Vugts, A. J. H. Boerboom, and J. Los, *Physica*, **44**, 219 (1969). Note that these values are relative measurements, relative to 298.15 K.

(36) M. De Paz, B. Turi, and M. L. Klein, *Physica*, **34**, 678 (1967).

(37) S. Weissman and G. A. Dubro, *Phys. Fluids*, **13**, 2689 (1970).

(38) H. J. M. Hanley and M. Klein, *J. Chem. Phys.*, **50**, 4765 (1969).

(39) R. Paul, A. J. Howard, and W. W. Watson, *ibid.*, **39**, 3053 (1963).

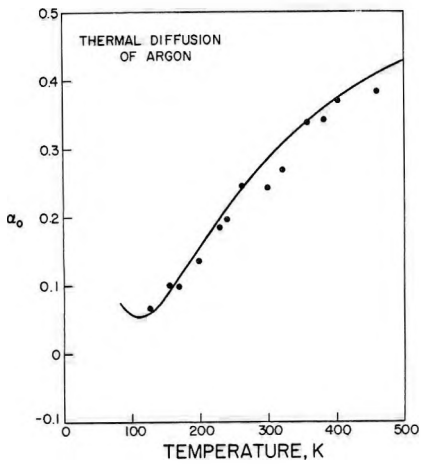

Figure 7. Thermal diffusion for argon: comparison of eq 9 using the m–6–8 potential with the data from ref 39.

authors but especially by Mason and his coworkers.[40] We summarize the principal conclusions and investigate how the m–6–8 potential applies to them.

Inelastic Collisions. It appears that allowances for inelastic collisions between polyatomic molecules make little or no difference in the expressions for the viscosity and diffusion coefficients. In fact, formal expressions for the latter are available[41] and are found to differ from the corresponding monatomic gas expression by a factor which is close to unity. On the other hand, the equation for the thermal conductivity, eq 6, has long been known to be incomplete for polyatomic gases. Several modifications to eq 6 have been proposed but the most satisfactory is that derived by Mason and Monchick,[40] who approximated the Wang-Chang, de Boer, Uhlenbeck theory for a dilute polyatomic gas to obtain (to a first approximation)

$$\lambda = \frac{5}{2}\eta\frac{c_v''}{m} + \rho D\frac{c_v''}{m} - \frac{2\eta}{\pi}\left(\frac{5}{2} - \frac{\rho D}{\eta}\right)^2\frac{c_v''}{mZ} \quad (14)$$

Here c_v'' is the internal specific heat and Z is the collision number for rotation, that is the number of collisions required for the interchange of rotational and translational energy. Finally, the expression for the thermal diffusion factor given by eq 9–13 is also very probably too simple for polyatomic gases.[42] Because of the complexity of the thermal diffusion phenomenon, however, it is not clear at this time how sensibly to modify eq 9. Consequently, eq 9 is used in practice.

Multiple Force Laws. Collision integrals and second virial coefficients for molecules which can interact with a multiple of force laws have been available for some time—particularly for polar molecules.[40,43] More recently, however, these quantities were computed for a potential applicable to the simple polyatomic molecules of interest to us.[44] The potential was a Lennard-Jones, 12–6, with a term added for the quadrupole–quadrupole interaction

$$\phi = \phi(12\text{-}6) + \phi(\text{quadrupole-quadrupole}) \quad (15)$$

Collision integrals calculated using eq 15 were found to be very close to the corresponding collision integrals for the 12–6 alone. [However, the combinations of the collision integrals, required for the thermal diffusion factor, are significantly different from their equivalents for the 12–6.] Second virial coefficients for several gases have also been determined from eq 15 [although, in this case, extra terms were added to account for other nonspherical effects. The quadrupole–quadrupole term still dominates, however.]. Unlike the collision integrals, the second virial coefficients were found to be substantially different from their counterparts calculated with the 12–6 alone.

One could conclude from the above that, even if our m–6–8 potential could be used to correlate the transport properties of a simple nonspherical gas successfully, a simultaneous fit of the viscosity and second virial coefficient would not be possible because of the absence of any quadrupolar term. These conclusions were indeed substantiated by us. We correlated the transport and second virial coefficients of nitrogen, oxygen, carbon dioxide, and methane. We found it possible to fit the viscosity data individually [and the thermal conductivity subject to the approximations in eq 14] at high and at low temperatures with the same set of parameters. Values are given in Table II. Although we were also able to correlate the second virial coefficients of these gases, it was not possible to obtain a satisfactory simultaneous fit of both viscosity and second virial coefficients.

Table II: Values of the Parameters of the m–6–8 Potential Function Which Fit Transport Data

Gas	m	γ	σ	ϵ/k
N_2	12	2	3.54	118
CH_4	11	3	3.68	168
O_2	10	1	3.437	113
CO_2	14	1	3.68	282

Detailed deviation curves are given in ref 10; here we show the viscosity and thermal conductivity of nitrogen with the parameter listed in Table II and shown in Figure 8. The viscosity data are from ref 11, 14–16, and 45–48 and thermal conductivity data from ref 25,

(40) For details and references, see article by E. A. Mason in "Proceedings of the 4th Symposium on Thermophysical Properties," ASME, New York, N. Y., 1968, p 21.

(41) E. A. Mason and T. R. Marrero in "Advances in Atomic and Molecular Physics," D. R. Bates and I. Estermann, Ed., Academic Press, New York, N. Y., 1970, p 156.

(42) L. Monchick, R. J. Munn, and E. A. Mason, *J. Chem. Phys.*, **45**, 3051 (1966).

(43) L. Monchick and E. A. Mason, *ibid.*, **35**, 1676 (1961).

(44) F. J. Smith, R. J. Munn, and E. A. Mason, *ibid.*, **46**, 317 (1967); T. H. Spurling and E. A. Mason, *ibid.*, **46**, 322 (1967).

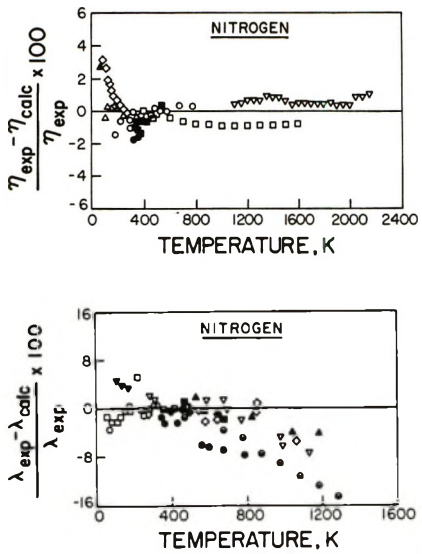

Figure 8. Viscosity and thermal conductivity deviation curves for nitrogen using $m = 12$, $\gamma = 2.0$, $\sigma = 3.54$ Å, and $\epsilon/k = 118$ K. Viscosity data are from the references indicated in parentheses: ▽ (11), △ (14), □ (15), ○ (16), ■ (45), ◇ (46), ▲ (47), and ● (48). Thermal conductivity data are from the references in parentheses: ○ (25), ▼ (26), ◆ (30), ◑ (33), △ (49), □ (50), ▽ (51), ◇ (52), ◒ (53), ● (54), ▲ (55), and ■ (56).

26, 30, 33, 49–56. Very similar results were found for oxygen, methane, and carbon dioxide.

Since it appears that the m–6–8 potential is an improvement over other analytical model potentials for the simple polyatomic gases—the first criterion, listed in the Introduction, is satisfied, for example—it would now be worthwhile to produce collision integrals and especially second virial coefficients for a modified version of our m–6–8 potential which included a quadrupole effect. There seems to be reason to believe that one might then be able to obtain a consistent set of parameters for both the transport and equilibrium properties for simple polyatomic gases.

Discussion

Our results indicate that the m–6–8 series of potentials seem a useful model of the intermolecular interaction. Our objective is largely achieved, therefore. In this section, we investigate briefly how valid the model is, restricting the discussion at this time to the repulsive part of the potential at small r and to the attractive part as represented by the coefficients C_6 and C_8 (eq 1). The discussion is also restricted to argon. Furthermore, we have avoided the inclusion of tests for validity which contain the unknown effects of potential nonadditivity.[57–59]

Repulsion: the Potential for $r < \sigma$. The repulsive part of the pair potential for argon at small separations has been estimated from molecular beam scattering data and we plot a composite curve obtained from these data as the heavy solid line[60] in Figure 9. The curve for the 11–6–8 ($\gamma = 3.0$), was calculated and is shown as a lighter solid curve. This curve begins to deviate at $r \sim 2.8$ Å or $\phi(r) \sim 0.1$ eV. Also shown as a matter of interest are the curves for the 12–6 function, long used as a good first approximation potential for the description of high-temperature argon data, and the 18–6 which is typical of all three-parameter potentials which can be used to describe low-temperature argon data.[3] Taken literally, this comparison indicates a need for a much softer potential at small r than the 11–6–8. While this conclusion is compatible with the notion that potentials for spherical molecules should reduce to a shielded coulomb potential for small r, it must be taken only with caution because pure repulsion is a poor approximation to these potentials even in the region of interest to scattering. For example, our potential for argon has a magnitude of approximately 1 eV at $r^* = 0.75$. For this value of r^*, the attractive inverse eighth term has a magnitude which is 38% of that of the inverse eleventh while the attractive inverse sixth term has a magnitude which is 2% of that repulsive contribution. Thus, if our potential for argon is at all valid, it follows that the analysis of scattering data in terms of pure repulsion can produce misleading results. The magnitude of the error introduced by the attraction in the use of an effective pure repulsion can be estimated as follows.

(45) R. Wobser and F. Müller, *Kolloid-Beih.*, **52**, 165 (1941).

(46) H. L. Johnston and K. E. McCloskey, *J. Phys. Chem.*, **44**, 1038 (1940).

(47) H. L. Johnston, W. R. Mattox, and R. W. Powers, *Nat. Adv. Comm. Aeronaut. Tech. Note*, No. 2456 (1951).

(48) F. Lazarre and B. Vodar, *Proc. Conf. Thermody. Transport Prop. Fluids*, 159 (1958).

(49) A. Michels and A. Botzen, *Physica*, **19**, 585 (1953).

(50) I. F. Golubev and M. V. Kal'sina, *Gazov. Prom.*, **9**, 41 (1964); translation available from SLA translation center, No. LA-TR-65-1.

(51) N. B. Vargaftik and N. Kh. Zimina, *High Temp.*, **2**, 782 (1964).

(52) A. A. Westenberg and N. de Haas, *Phys. Fluids*, **5**, 266 (1962).

(53) H. Geier and K. Schäfer, *Allg. Waermetech.*, **10**, 70 (1961).

(54) E. U. Frank, *Chem. Eng. Tech.*, **25**, 238 (1953).

(55) R. G. Vines, *Mass. Inst. Tech., Tech. Report MIT-20-P* (Sept 1958), DDC AD 205 694.

(56) R. L. Nuttall and D. C. Ginnings, *J. Res. Nat. Bur. Stand.*, **58**, 271 (1957).

(57) Examples of such tests are the third virial coefficient, Monte Carlo, and molecular dynamics calculations. A Monte Carlo calculation has, in fact, been carried out for argon with our potential for a reduced temperature which, based on the parameters obtained by us, corresponds to an isotherm at approximately twice the critical temperature.[58] Comparisons with the data of Michels, *et al.*,[59] naturally showed excellent agreement at low densities. At high densities, a significant difference was found between calculated values and experimental ones. The significance of this, particularly in relation to the validity of the potential function, must await a better understanding of the effect of nonadditivity on the equation of state at high densities. This relatively poor showing of the potential at high densities could have been anticipated since it is the inverse of the fact that the 12–6 function, which has been shown to predict experiment fairly well in purely additive theories at high densities, is totally inadequate at low densities.

(58) Max Klein and W. F. Streett, unpublished data.

(59) A. Michels, H. Wijker, and H. Wijker, *Physica*, **15**, 627 (1949).

(60) I. Amdur and J. E. Jordan, "Advances in Chemical Physics," Vol. 10, J. Ross, Ed., Interscience, New York, N. Y., 1966, Chapter 2.

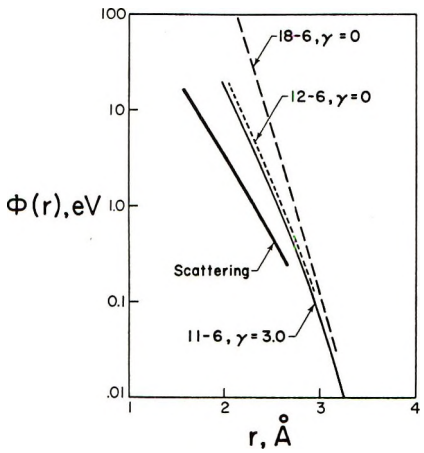

Figure 9. The repulsive potential for argon at small r. We compare the 11–6–8 ($\gamma = 3$) potential with the potential estimated from high energy scattering of neutral argon atoms.[58] Also shown as a matter of interest are the curves for the well known 12–6 and the curve for the 18–6. This latter is typical of all three parameter potentials which can fit argon data at low temperatures.

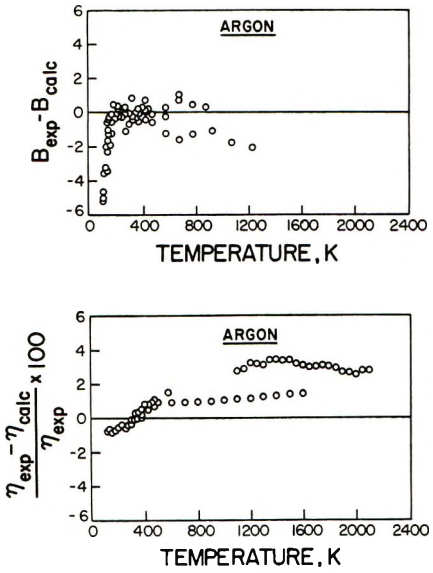

Figure 10. Second virial and viscosity curves for argon using an m–6–8 potential which has a reasonable value of the inverse sixth dispersion coefficient: $m = 11$, $\gamma = 2.0$, $\sigma = 3.356$ Å, and $\epsilon/k = 137$ K. Compare with Figure 2.

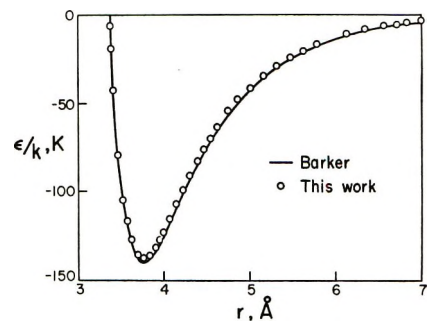

Figure 11. Plot of the $m = 11$, $\gamma = 2.0$ argon potential used in Figure 10 and the potential due to Barker and Bobetic.[62] We are grateful to Dr. Barker for allowing us to work with his potential before publication.

At each value of r^*, let us, in the style of the scattering experiments, represent our potential function by a pure inverse power repulsion. Thus

$$\phi(r^*) = A/r^{*m} \tag{16}$$

If this were a true representation of the function, an effective repulsive exponent could then be obtained simply by calculating

$$m = \frac{r^*}{\phi}\frac{d\phi}{dr^*} \tag{17}$$

Where this is only a local representation terms in dA/dr^* and dm/dr^* need to be added to the right side of eq 17. At $r^* = 0.75$, for example, using our potential, this leads to an effective value $m = 13$ while $m = 11$ in the potential itself. The further inadequacy of eq 16 as a representation of our m–6–8 function can be estimated by calculating m using eq 17 at each r^* and obtaining dm/dr^* from the result. For instance, by proceeding in that way, the value $dm/dr^* = 15$ is obtained at $r^* = 0.75$, clearly not negligible compared to the value of m obtained using eq 17 (*i.e.*, by neglecting dm/dr^*).

Attraction: a Comparison of the Dispersion Coefficient. The expressions for the dispersive coefficients C_6 and C_8 for the m–6–8 potential function are, from eq 2

$$C_6 = \frac{\epsilon}{(m-6)}[m - \gamma(m-8)]\sigma^6 d^6 \tag{18}$$

$$C_8 = \epsilon\gamma\sigma^8 d^8 \tag{19}$$

For argon we have $m = 11$, $\gamma = 3.0$, $\epsilon/k = 153$ K, and $\sigma = 3.292 \times 10^{-8}$ cm. d is then 1.114462. Using these values in eq 18 and 19 one obtains $C_6 \sim 21 \times 10^{-60}$ erg/cm^6 and $C_8 \sim 2000 \times 10^{-76}$ erg/cm^8. Semitheoretical quantum mechanical calculations,[61] however, indicate that $C_6 \sim 60 \times 10^{-60}$ erg/cm^6 and $C_8 \sim 120 \times 10^{-76}$ erg/cm^8. Since the coefficient C_6 is believed to be known quite accurately (within 5%), our 11–6–8 potential for argon is clearly not giving the correct value for the inverse sixth power coefficient C_6. Agreement for the coefficient C_8 is also poor although C_8 is known less accurately.

Let us now see what happens to the data correlation if the C_6 of our potential is *forced* to have a value approximately equal to 60×10^{-60} erg/cm. To do this, we effectively fix one of the four parameters. This we choose to do by fixing γ for a given m. A reasonable choice is[9b] $m = 11$, and $\gamma = 2$ which gives $C_6 \sim 55 \times$

(61) H. Margenau and N. R. Kestner, "Theory of Intermolecular Forces," Pergamon, New York, N. Y., 1959, p 32. See also the appropriate references quoted herein.

10^{-60} erg/cm, sufficiently close to the theoretical value. Corresponding best values of σ and ϵ/k are 3.356 Å and 137 K, respectively. Deviation curves for the second virial and viscosity using this 11–6–8 ($\gamma = 2.0$) potential are presented in Figure 10. One sees that these curves are not unreasonable; that is, the fit is within 3% (except for the second virial coefficient at very low temperatures). They do, however, show systematic deviations and are definitely much inferior to the curves given in Figure 2.

These results can be summarized in three remarks.

1. The numerical values of C_6 and C_8 for the m–6–8 potential are sensitive to the choice of m and γ because of the particular functional forms used, *e.g.*, eq 18. The quantity σ, which is also part of the expressions, is found from experiment and since σ is raised to the sixth or eighth power, uncertainty in it can introduce considerable uncertainty in C_6 and C_8.

2. A convenient argument says that our potential is not sufficiently flexible to fit data and give a good value for C_6 (and to a lesser extent C_8). That our potential is not flexible enough is obviously true—it is only meant to approximate the true potential. This argument, though necessary, is not sufficient, however, to justify the need for additional parameters. We can support this by referring to a recent potential function due to Barker.[62] According to Figure 11, our 11–6–8 ($\gamma = 2.0$) potential is very close to Barker's multiparameter potential for which C_6 is fixed at the correct value. Because of its additional parameters, Barker's potential is very flexible when compared with ours, especially with regard to the repulsive branch. It would thus appear that adding more parameters to our potential for additional flexibility would not necessarily remove the disagreement with theory even when additional parameters are added to the most uncertain part of the potential, the repulsive branch.

3. Since we regard the data we have fitted as reliable, the m–6–8 potential thus fails to be valid in that it cannot give the dispersion coefficients correctly. This failure must not be taken out of context, however. The m–6–8 potential, being a model function, can only be approximate. Its value is in its utility in the correlation of data and not necessarily in its ability to give correct theoretical predictions for the form of the potential itself—although it would obviously be a very powerful property of the potential if this were so. The extent of this utility needs to be determined by carrying out calculations of additional properties and of these same properties under different conditions. We now have calculations in progress to produce quantum mechanical collision integrals and second virial coefficients for this potential for use with quantum fluids.

Conclusion

We have shown that the m–6–8 potential is useful as a correlating tool.

(62) M. V. Bobetic and J. A. Barker, *Phys. Rev.*, *B*, 2, 4169 (1970)

Limiting Behavior of Alkylammonium Salts in Benzene

by O. Levy

Department of Chemistry, University of the Negev, Beer-Sheva, Israel *(Received June 21, 1971)*

Publication costs assisted by the Department of Chemistry, University of the Negev

The behavior of several alkylammonium salts ($(C_{12}H_{25})_3NHX$, where X = Cl, ClO_4, $FeCl_4$, and $FeBr_4$) at infinite dilution in benzene was studied by a molecular solution theory. Second virial coefficients were evaluated using a model which assumes two main contributions to the average potential between the particles: (i) repulsion due to their own molar volume and (ii) attraction resulting from dipole-dipole interactions. Good agreement was found between the calculated activity coefficient values and those obtained from vapor-pressure-lowering measurements. Several molecular distance parameters were evaluated and compared with those obtained from dielectric constant and conductivity data on the same systems.

I. Introduction

Previous dielectric[1] and osmometric[2,3] investigations on binary systems of long-chain alkylammonium salts in nonpolar organic solvents were interpreted in terms of deviation of the systems from ideal behavior due to the aggregation of the solute. It has been found that the extent (number) and degree (size) of the molecular associates depend considerably on the anionic part of the alkylammonium ion pair. Additionally, the osmometric data were also treated in terms of nonspecific nonideality expressed through the activity coefficients of the solutes *via* the Gibbs–Duhem relationship.[2-4] The curves representing the activity coefficient dependence on solute concentration indicate—as do the aggregation constants—a pronounced departure from ideal behavior, and again the extent of nonideality depends on the anion. The deviation from ideal behavior increases in the order[5] $Cl^- < Br^- < NO^-_3 < ClO_4^- \cong FeCl_4^- < FeBr_4^-$ in agreement with the increase of the anionic radii and other related properties.[6]

Various oligomerization models were tested for these systems. The choice of a certain model was dictated by the mathematical computation method, chemical intuition, and comparison with other literature data. In the case of trilaurylammonium salts with both simple and complex anions, the basic aggregation unit is the dimer. An angular shape can be inferred from dielectric constant measurements.[1]

An attempt is made here to treat such binary systems where the interactions are essentially physical in nature by a statistical mechanical approach in order to predict thermodynamic data useful in interpretation of systems having one polar component.

Virial coefficient calculations were made by Kozak, *et al.*,[7] for a large number of organic compounds. The effects of solute size were analyzed by using the lattice theory and the McMillan–Mayer theory for solutions. The intermolecular forces considered depend on the type of the system studied—self-association and structural changes for alcohol–water mixtures,[8] van der Waals and hydrogen-bond interactions for other mixtures[9] including those with hydrophobic bonding.[10] In alkylammonium salt–organic solvent systems a dipole interaction was considered as the main factor governing the self-aggregation in addition to a possible solute–solvent interaction.[11,12]

We choose now to treat the limiting behavior at infinite dilution of these solutions using a model based on the McMillan–Mayer theory[13] and to compare the predicted activity coefficients of the solutes with those determined experimentally.

II. Theory

For an imperfect gas the equation of state can be expanded to

$$p/kT = \rho + B_2(T)\rho^2 + B_3(T)\rho^3 + \ldots \qquad (1)$$

where p and T are the pressure and temperature of the

(1) O. Levy, G. Markovits, and A. S. Kertes, *J. Phys. Chem.*, **75**, 542 (1971).

(2) A. S. Kertes and G. Markovits, *ibid.*, **72**, 4202 (1968).

(3) O. Levy, G. Markovits, and A. S. Kertes, *ibid.*, **74**, 3568 (1970).

(4) A. S. Kertes and G. Markovits in "Thermodynamics of Nuclear Materials," I. A. E. Agency, Vienna, 1968, p 227.

(5) G. Markovits, Ph.D. Thesis, Jerusalem, 1969; O. Levy, Ph.D. Thesis, Jerusalem, 1970.

(6) A. S. Kertes, H. Gutmann, O. Levy, and G. Markovits, *Israel J. Chem.*, **6**, 643 (1968).

(7) J. J. Kozak, W. S. Knight, and W. Kauzmann, *J. Chem. Phys.*, **48**, 675 (1968).

(8) F. Franks and D. J. G. Ives, *Quart. Rev., Chem. Soc.*, **20**, 1 (1966).

(9) D. Stigter, *J. Phys. Chem.*, **64**, 118 (1960).

(10) G. Nemethy and H. A. Scheraga, *J. Chem. Phys.*, **33**, 3302, 3401 (1962).

(11) Y. Marcus and A. S. Kertes, "Ion Exchange and Solvent Extraction of Metal Complexes," Wiley-Interscience, London, 1969, Chapter 10.

(12) Yu. G. Frolov, A. V. Ochkin, and V. V. Siergievsky, *Atom. Energ. Rev.*, **7**, 71 (1969).

(13) T. Hill, "Introduction to Statistical Thermodynamics," Addison-Wesley, London, 1962.

gas, ρ is the number density of the particles, and k is the Boltzmann constant.

The virial coefficients $B_n(T)$ express the departure of the system from ideality. They are temperature dependent and often related to the various molecular interactions.

By defining the activity coefficient γ of the gas and using the virial expansion one obtains[13]

$$\ln \gamma = -\sum_{k \geq 1} \beta_k(T)\rho_k \qquad (2)$$

where β_k is defined as $\beta_k = -[(k+1)/k]\beta_{k+1}$.

According the the McMillan–Mayer theory for solutions, an analogy can be made between a dilute solution (solute in solvent) and "gas *in vacuo*," and consequently the virial expansion can be used for any suitable property of the solution.

The chemical potential (μ) will be expressed by

$$\mu^*/kT = \mu^{*0}/kT + \ln \rho + \ln \gamma \qquad (3)$$

μ^{*0} being the chemical potential in the standard state chosen.

Therefore, using the virial expansion, one obtains

$$\ln \gamma = +\sum_{k \geq 1} \left(\frac{k+1}{k}\right) B^*_{k+1}\rho^k \qquad (4)$$

In a very dilute solution, at a first approximation, all the terms in eq 4 can be neglected but the first with the second virial coefficient; then eq 4 becomes

$$\ln \gamma \cong +2B^*_2\rho \qquad (5)$$

Generally, the second virial coefficient is expressed in terms of $w(r, \Omega)$, the reversible work necessary to bring the molecules together from $r = \infty$ to r in the solvent of the given properties[13,14]

$$B^*_2(T) = -{}^1/_2\int_0^\infty \int \{\exp[-w(r, \Omega)/kT] - 1\} 4\pi r^2 dr d\Omega \qquad (6)$$

where the second intergrand expresses the angle-dependent contributions due to the interactions of dipoles.

For the hard-sphere hypothetical model

$$w(r, \Omega) = \infty \qquad r < a$$
$$= 0 \qquad r \geq a$$

and results in

$$B^*_2 = 2\pi a^3/3 \qquad (7)$$

where a is the distance of closest approach between centers of two spheres.

Now, as we deal with polar solutes, the average interaction energy between the solute molecules may be regarded as composed of (i) a repulsive energy component due to the molar volume of the solute particles (for $r < a$) and (ii) an attractive energy component which (neglecting the Lennard-Jones potential) includes the dipole–dipole interaction (for $r \geq a$). Equation 6 then becomes

$$B^* = -{}^1/_2\int_0^a (-1)4\pi r^2 dr - {}^1/_2\int d\Omega \int_a^\infty \{\exp[-w(r, \Omega)/kT] - 1\} 4\pi r^2 dr \qquad (8)$$

The repulsive term (integrand 1) can be equated with half the volume of the particle. In order to evaluate the attractive term (integrand 2), we have to look for an adequate expression for $w(r, \Omega)$.

According to Keesom,[14] for rigid spheres containing point dipoles

$$w(r, \Omega) = -\frac{\mu^2}{\epsilon r^3}[2 \cos \theta_1 \cos \theta_2 - \sin \theta_1 \sin \theta_2 \cos(\phi_2 - \phi_1)] \qquad (9)$$

where μ is the dipole moment of the solute, θ_1 and θ_2 are the angles between the direction of dipoles relative to their connecting line, ϕ_1 and ϕ_2 are the relative rotational angles, and ϵ is the dielectric constant of the solvent—the latter being introduced to account for the effect of the medium[12,14]

Now the expression for B_2^* can be written explicitly as

$$B^* = {}^1/_2\int_0^a 4\pi r^2 dr - {}^1/_{16\pi}\int_a^\infty 4\pi r^2 dr \int_0^\pi \sin \theta_1 d\theta_1 \int_0^\pi \sin \theta_2 d\theta_2 \int_0^{2\pi} \times d(\phi_2 - \phi_1)\{\exp[-w(r, \Omega)/kT] - 1\} \qquad (10)$$

where $w(r, \Omega)$ is expressed by eq (9) and ${}^1/_{16\pi}$ is a normalization factor.

III. Results and Discussion

The above integrands were calculated with a CDC 6400 computer using the trapezoidal rule and the experimental data obtained previously. Dipole moments were calculated from dielectric constant measurements,[1] and for the values of a (the closest approach between two molecules) we have some clues from dielectric,[1] conductivity,[6,15] and density data.[1,6] B_2^* was calculated by minimizing its value with respect to a. Parameter a was varied in steps of 0.1 Å till the minimum was reached, and the obtained values represent the "reversible work necessary to bring two solute molecules together from $r = \infty$ to $r = a$ in the given solvent"[13] (Table I).

(14) J. O. Hirschfelder, C. F. Curtis, and R. B. Bird, "Molecular Theory of Gases and Liquids," Wiley, New York, N. Y., 1964.

(15) R. M. Fuoss and F. Accascina, "Electrolytic Conductance," Interscience, New York, N. Y., 1959.

Table I: Dipole Moments, Virial Coefficients, Distance Parameters, and Molar Volumes of Alkylammonium Salts in Benzene

Salt	μ, D	$-B^*_2$	-0.5(slope) (exptl)	a^0, Å	r^*, Å	V^0, ml/mol	V^*, ml/mol
$(C_{12}H_{25})_3NHCl$	7.6	10	8	4.4	4.7	640	215
$(C_{12}H_{25})_3NHClO_4$	10.1	20	25	5.4	5.0	670	400
$(C_{12}H_{25})_3NHFeCl_4$	11.2	23	24	5.7	5.2[a]	662	470
$(C_{12}H_{25})_3NHFeBr_4$	12.3	34	37	6.1	5.4	705	573

[a] 5.5 Å from conductivity data.[5]

As stated before, ln γ *vs.* solute concentration curves were obtained from osmometric measurements using the Gibbs–Duhem relationship. The shape of these curves[2,3] indicates a high departure from ideal behavior in the systems, and this requires higher virial coefficients for a full treatment. We thus choose the limiting slope of the curves,[2,3] assuming that in the very dilute region the departure from ideality can adequately be treated by the second virial coefficient alone (*cf.* eq 5).

The limiting slope was evaluated by means of a least-squares program using polynomial expansions in terms of molality. The results agree with those obtained graphically.

The values in Table I show a fair agreement between the calculated virial coefficients and half the limiting slope (-0.5(slope)) of the experimentally determined-activity curves. The agreement between the calculated a values and those evaluated from dielectric constant measurement, r^*, are less satisfactory. One possible reason is that perhaps the r^* values refer to "dipole length," which as calculated from the dipole moment[3] does not include factors such as mutual polarization of the ions which are expected to have a positive contribution.

Similar arguments can account for the differences between the calculated "actual volume" of the particles (V^*) obtained from the first term in the integrand as twice the repulsive terms, and the apparent partial molar volumes computed from density data (V^0). ($V^0 = (1/m)\{([1000 + mM_2)/d] - (1000/d_0)\}$, where m = molality, M_2 = molecular weight of the salt, d = density of the solution, and d_0 = density of the solvent.) A mutual polarization between the molecules with large dipole moments (see Table I) can result in molecular deformations leading to closer approach than expected from the molar volume.

The use of the point dipole model assumes that in the case of bulky molecules, such as those studied here, the dipoles still remain separated even at small intermolecular distances.

As regards the application of the limiting slope, its use was proposed by Baes[16] for the solubility parameter calculation. In addition, the virial coefficients were proposed as analogs to the different aggregates[13] by the so-called "cluster diagrams."

Acknowledgment. The author is most indebted to Professor A. S. Kertes and Professor A. Ben-Naim for helpful discussions and suggestions.

(16) C. F. Baes, Jr., *J. Phys. Chem.*, **66**, 1629 (1962).

Hydrodynamic Interaction of Segmented Rodlike Molecules. A Comparison among Three Approximations

by Robert Ullman

Scientific Research Staff, Ford Motor Company, Dearborn, Michigan 48121 *(Received October 8, 1971)*

Publication costs assisted by the Ford Motor Company

A calculation of the intrinsic viscosity of rodlike molecules is performed in order to compare the Kirkwood–Riseman, Oseen–Burgers, and Rotne–Prager formulations of the hydrodynamic interaction tensor. Insofar as this model is capable of generalization, it appears that the simple Kirkwood–Riseman formulation is in good agreement with the other forms.

Introduction

The computation of flow properties of polymer solutions has been carried through with considerable success by treating the polymer as a solid object suspended in a continuous viscous fluid. The shape of a polymer molecule is usually time dependent and irregular, and the hydrodynamic boundary value problem becomes formidable. Kirkwood and his collaborators,[1-6] following earlier work by Kuhn,[7] Huggins,[8] Kramers,[9] and others, avoided the difficulties of the boundary value problem by treating the polymer as an array of resisting points which exert forces on the surrounding fluid. His method was derived from an adaptation of Burgers[10] of a solution to the linearized Navier–Stokes equations obtained by Oseen. This method has been extensively used, but normally in an oversimplified form because the perturbation of the velocity field in the neighborhood of a given polymer segment by all the other polymer segments cannot be accurately calculated without "preaveraging" the Oseen tensor if a polymer molecule is not of a simple shape. Pyun and Fixman[11-14] and also Imai[15,16] have developed techniques for reducing the error committed by preaveraging.

Another measure of the importance of preaveraging of the Oseen tensor can be obtained by using the same method on molecules of simpler geometry. Kirkwood and Auer[3] have demonstrated that the Oseen formulation without the simplification of preaveraging could be applied to the segmented rigid-rod polymer, and, indeed, this writer showed that the intrinsic viscosity calculated for a long segmented rigid rod was reduced at most by a factor of $^{15}/_{16}$ if the Oseen tensor was prematurely averaged.[17]

In an elegant analysis of the hydrodynamic interaction problem in macromolecular flow, Rotne and Prager[18] proposed a correction to the Oseen–Burgers formula. The RP result reduces to the Oseen equation when the chain segments are widely separated, or if the segmental friction constant is low. If a preaveraging procedure is applied to the RP hydrodynamic interaction tensor, the KR result is obtained. The KR result, as explained above, is the result of preaveraging the OB formula.

The intrinsic viscosity of a segmented rigid rod is more easily calculated than that of a random coil because of the simpler geometry and because the distance between beads on the chain is independent of time. All three formulations (RP, OB, and KR) of hydrodynamic interaction can be used and the results compared. This application is carried out in the following sections.

Formulation and Analysis

The intrinsic viscosity of a polymer solution is given in units of deciliters per gram by

$$[\eta] = -\frac{N_0}{100M\eta_0}\,\dot{\epsilon}\sum_{l=-n}^{n} y_l X_l \qquad (1)$$

Here N_0 is Avogadro's number, M is molecular weight in grams/mole, η_0 is the solvent viscosity in poises, and

(1) J. G. Kirkwood and J. Riseman, *J. Chem. Phys.*, **16**, 565 (1948).
(2) J. G. Kirkwood, *Recl. Trav. Chim. Pays Bas*, **68**, 649 (1949).
(3) J. G. Kirkwood and P. L. Auer, *J. Chem. Phys.*, **19**, 281 (1951).
(4) J. G. Kirkwood, *J. Polym. Sci.*, **12**, 1 (1954).
(5) J. J. Erpenbeck and J. G. Kirkwood, *J. Chem. Phys.*, **29**, 909 (1958).
(6) J. J. Erpenbeck and J. G. Kirkwood, *ibid.*, **38**, 1023 (1963).
(7) W. Kuhn, *Z. Phys. Chem. Abt. A*, **161**, 1 (1932).
(8) M. L. Huggins, *J. Phys. Chem.*, **43**, 439 (1939).
(9) H. A. Kramers, *J. Chem. Phys.*, **14**, 415 (1946).
(10) J. M. Burgers, "Second Report on Viscosity and Plasticity," North-Holland Publishing Co., Amsterdam, 1938, Chapter 3.
(11) C. W. Oseen, "Hydrodynamik," Akademische Verlagsgesellschaft, M.B.H., Leipzig, 1927, p 35, eq IIIc.
(12) M. Fixman, *J. Chem. Phys.*, **42**, 3831 (1965).
(13) C. W. Pyun and M. Fixman, *ibid.*, **42**, 3838 (1965).
(14) C. W. Pyun and M. Fixman, *ibid.*, **44**, 2107 (1966).
(15) S. Imai, *ibid.*, **50**, 2116 (1969).
(16) S. Imai, *ibid.*, **52**, 4212 (1970).
(17) R. Ullman, *ibid.*, **40**, 2422 (1964).
(18) J. Rotne and S. Prager, *ibid.*, **50**, 4831 (1969).

$\dot{\epsilon}$ is the velocity gradient in seconds^{-1}. x_l, y_l, and z_l are the components of the vector $\mathbf{r}_l$ designating the position of the lth segment with respect to the center of mass; X_l, Y_l, and Z_l are the components of the force $\mathbf{F}_l$ exerted by the lth bead of the fluid. It is assumed that Brownian motion is sufficiently active so that the individual molecules are randomly oriented. There are $2n + 1$ beads on the molecule numbered from $-n$ to $+n$. The force exerted by the lth bead is given by

$$\mathbf{F}_l = -\frac{\zeta\dot{\epsilon}}{2}(\mathbf{i}y_l + \mathbf{j}x_l) - \sum_{\substack{s=-n \\ s\neq l}}^{n} T_{ls}\cdot\mathbf{F}_s \qquad (2)$$

The friction constant of a single bead is designated by ζ. $\mathbf{i}$, $\mathbf{j}$, and $\mathbf{k}$ are unit vectors in the x, y, and z directions, respectively. T_{ls}, the hydrodynamic interaction tensor, takes the form

$$T_{ls} = \frac{1}{R_{ls}}\left[\mathbf{1}A_{ls} + \frac{\mathbf{R}_{ls}\mathbf{R}_{ls}}{R_{ls}^2}B_{ls}\right] \qquad (3)$$

$\mathbf{R}_{ls}$ is the vector connecting bead l to bead s, and R_{ls} is its magnitude. The quantities A_{ls} and B_{ls} take on different values depending on whether the Oseen approximation is used according to Burgers (OB), the prematurely averaged Oseen tensor following Kirkwood and Riseman (KR) is used, or the Rotne–Prager extension (RP) (see eq 21 of ref 18) is adopted. In short, one has

$$A_{ls} = B_{ls} = \zeta/8\pi\eta_0 \quad \text{(OB)} \qquad (4a)$$

$$A_{ls} = \zeta/6\pi\eta \qquad (4b)$$

$$B_{ls} = 0 \quad \text{(KR)}$$

$$A_{ls} = (\zeta/8\pi\eta_0)(1 + (2a^2/3R_{ls}^2)) \qquad (4c)$$

$$B_{ls} = (\zeta/8\pi\eta_0)(1 - 2a^2/R_{ls}^2) \quad \text{(RP)}$$

The radius of a bead is equal to a.

Calculated values of intrinsic viscosity can be obtained for finite chains by solving eq 2 and substituting the result in eq 1. This can be performed directly provided that the distances R_{ls} are fixed. In this paper we solve eq 2 for the rigid segmented rod using the representation of the hydrodynamic interaction tensor given in eq 4a–4c. The distance between adjoining beads is set equal to b. Therefore, $R_{ls} = b|l - s|$. The unit vector running in the positive direction along the macromolecule is $\mathbf{r}_0$, with components x_0, y_0, z_0. The friction constant is $\zeta = 6\pi\eta_0 a$, where a is the radius of the bead. The ratio of bead radius to bond length is designated by $f = a/b$. Note that $f = 0.5$ when the diameter of the bead is equal to the segment length. Because the rigid rod is centrosymmetric, $\mathbf{F}_l = -\mathbf{F}_l$. Using this relationship and defining φ_l as

$$\varphi_l = -\frac{6}{\zeta\dot{\epsilon}bl}\langle y_l X_l\rangle \qquad (5)$$

eq 1 becomes

$$[\eta] = \frac{N\pi b^3 f}{50M_0(2n+1)}\sum_{l=1}^{n} l\varphi_l \qquad (6)$$

Because of symmetry, only n of $2n + 1$ variables $\mathbf{F}_l$ are independent. The scalar product of $\mathbf{r}_0$ with $\mathbf{F}_l$ generates the set of simultaneous equations

$$\mathbf{Mq} = \mathbf{p} \qquad (7a)$$

$$p_k = k \qquad (7b)$$

$$q_k = 3\dot{\epsilon}kx_0y_0\langle(\mathbf{r}_0\cdot\mathbf{F}_k)\rangle_{\text{av}} \qquad (7c)$$

$$M_{jk} = \frac{A_{jk} + B_{jk}}{|j-k|} - \frac{A_{j,-k} + B_{j,-k}}{j+k}; \quad j \neq k \qquad (7d)$$

$$M_{kk} = 1 - (A_{k,-k} + B_{k,-k})/2k \qquad (7e)$$

The solution of this set of equations

$$\mathbf{q} = \mathbf{M}^{-1}\mathbf{p}$$

is substituted in eq 2 and the product y_0X_l is formed. This leads to a second set of simultaneous equations

$$\mathbf{N}\varphi = \mathbf{w} \qquad (8a)$$

$$\varphi_k = -(6/\zeta\dot{\epsilon}b)\langle y_0X_k\rangle \qquad (8b)$$

$$w_k = k + 0.2B_{k,-k}q_k/k - 0.4\sum_{s=1}^{n} q_s\left(\frac{B_{k,s}}{|k-s|} - \frac{B_{k,-s}}{k+s}\right) \qquad (8c)$$

$$N_{jk} = \frac{A_{jk}}{|j-k|} - \frac{A_{j,-k}}{j+k}; \quad j \neq k \qquad (8d)$$

$$N_{kk} = 1 - 0.2A_{k,-k}/k \qquad (8e)$$

Equation 8a, when solved, is substituted in eq 6 to yield the intrinsic viscosity.

Results and Discussion

Intrinsic viscosities of rigid-rod molecules were computed according to the above methods using a Fortran program on a Philco 212 computer. Several values of chain length and friction constant were considered, and the KR, OB, and RP methods compared. Numerical results are presented in Table I. Graphs of intrinsic viscosity *vs.* $n^2/\ln n$ are roughly linear for large n for $f = 0.3$ and 0.5, a result anticipated from the Kirkwood–Auer theory[3] for the long rigid rod. Agreement between the OB and RP methods was extremely close except at the largest value of the friction constant, $f = 0.5$, where deviations up to 2 or 3% become apparent. Since the difference between the OB and RP calculations is of the order of f^2, it is easy to see why the higher order terms of the RP formulation (see eq 4a) and 4c only play a significant role at higher values of f.

Table I: Intrinsic Viscosity of Segmented Rods[a]

Chain length	Friction constant, f	Intrinsic viscosity[b] RP	OB	KR
5	0.1	37.29	37.29	37.00
	0.2	73.73	73.73	72.59
	0.3	109.8	109.9	107.2
	0.5	184.9	190.5	176.4
7	0.1	70.61	70.61	70.38
	0.2	133.1	133.1	132.12
	0.3	190.0	190.1	187.6
	0.5	295.4	307.8	288.0
11	0.1	164.3	164.3	164.4
	0.2	293.0	293.1	292.4
	0.3	399.2	399.9	397.0
	0.5	572.7	609.5	566.5
15	0.1	292.4	292.4	293.0
	0.2	504.2	504.5	503.8
	0.3	669.0	670.7	666.6
	0.5	919.4	913.2	913.5
21	0.1	546.2	546.2	547.7
	0.2	911.5	912.2	911.0
	0.3	1,180.0	1,184.0	1,176.0
	0.5	1,562.0	1,598.0	1,553.0
41	0.1	1,897.0	1,897.0	1,902.4
	0.2	2,994.1	2,997.0	2,987.0
	0.3	3,727.0	3,741.0	3,702.0
	0.5	4,656.0	4,540.0	4,626.0
61	0.1	3,983.0	3,983.0	3,992.0
	0.2	6,114.0	6.121.0	6,087.0
	0.3	7,470.0	7,499.0	7.404.0
	0.5	9,101.0	9,262.0	9,019.0
81	0.1	6,772.0	6,773.0	6,784.0
	0.2	16,210.0	10,222.0	10,151.0
	0.3	12,332.0	12,381.0	12,200.0
	0.5	14,799.0	15,272.0	14,637.0

[a] The numerical values in this table are obtained by choosing Avogadro's number $N_0 = 6.02 \times 10^{23}$, $b = 10$ Å, and $M_0 = 100$. [b] The subheadings RP, OB, and KR refer to the use of the Rotne–Prager, Oseen–Burgers, and Kirkwood–Riseman approximations to the hydrodynamic interaction tensor.

If eq 1 and 2 are adjusted to apply to a two-bead dumbbell molecule, the intrinsic viscosity is easily calculated. The results are

$$[\eta]_{FD} = \frac{\pi b^3 f}{100 M_0} \tag{9a}$$

$$[\eta] = [\eta]_{FD} \Big/ \left(1 - \frac{f}{2}\right) \quad \text{(KR)} \tag{9b}$$

$$[\eta] = [\eta]_{FD} \left(1 + \frac{3f}{20(1 - {}^3/_4 f)}\right) \Big/ (1 - {}^3/_8 f) \quad \text{(OB)} \tag{9c}$$

$$[\eta] = [\eta]_{FD} \left(1 + \frac{3f\left(1 - \frac{f^{*2}}{2}\right)}{20\left(1 - {}^3/_4\left(1 - \frac{f^{*2}}{6}\right)\right)}\right) \Bigg/ \left(1 - {}^3/_8 f\left(1 + \frac{f^{*2}}{6}\right)\right) \quad \text{(RP)} \tag{9d}$$

Equation 9a is the so-called "free-draining" result obtained if the hydrodynamic interaction between the beads is neglected. The quantities f and f^* in eq 9d are both equal to a/b, the radius of the bead divided by half the length of the dumbell. The definition of f depends on the assumption that the friction constant per segment is that of a sphere, while f^* depends only on geometry. Since the hydrodynamic behavior of an individual segment is poorly defined, it is conceivable that f and f^* are quite different.

The intrinsic viscosity of an elastic dumbell has been calculated by Pyun[19] using the perturbation methods of Pyun and Fixman. He obtains two results, one which uses the preaveraged Oseen tensor (designated as PA) and one in which the preaveraging was not performed (PF). In the notation of this paper, these are

$$[\eta] = [\eta]_{FD}/(1 - 1.382f) \quad \text{(PA)} \tag{10a}$$

$$[\eta] = [\eta]_{FD}/(1 - 0.967f) \quad \text{(PF)} \tag{10b}$$

In Table II, comparative numerical results for the rigid dumbbell and elastic dumbbell are presented.

Table II: Intrinsic Viscosity of Dumbbell-Shaped Molecules

	$f = 0.3$	$f = 0.5$
KR	$1.176[\eta]_{FD}$	$1.333[\eta]_{FD}$
OB	$1.191[\eta]_{FD}$	$1.378[\eta]_{FD}$
RP ($f = f^*$)	$1.191[\eta]_{FD}$	$1.344[\eta]_{FD}$
PA	$1.69[\eta]_{FD}$	$3.23[\eta]_{FD}$
PF	$1.41[\eta]_{FD}$	$1.94[\eta]_{FD}$

If preaveraging of the hydrodynamic interaction tensor is numerically insignificant, the KR and OB computations should agree, which they do, and PA and PF should also agree, which they do not. The reason that the Gaussian dumbbell and rigid dumbbell molecules behave differently is unclear, but it should be noted that Pyun's calculations involve mathematical approximations which are unnecessary in the simpler problem of the rigid dumbbell molecule.

By taking the finite size of a polymer segment into account, Yamakawa[20] arrives at the Rotne–Prager modification of the Oseen tensor, which is valid for distances greater than the diameter of a chain segment. He finds the intrinsic viscosity of a Gaussian spring macromolecule to be insensitive to the RP corrective term. Also, the effect of preaveraging the Oseen tensor changes the intrinsic viscosity of these same models by 2% or less if the number of elements is greater than ten.[13] This is somewhat greater than the differences observed for the rigid segmented rod (Table I), but the effect of preaveraging is clearly minor.

(19) C. W. Pyun, *J. Chem. Phys.*, **49**, 2875 (1968).
(20) H. Yamakawa, *ibid.*, **53**, 436 (1970).

The Rotne–Prager improvements on the Oseen hydrodynamic interaction tensor were designed to deal with singularities in the intrinsic viscosity as noted by DeWames, *et al.*,[21] and Zwanzig, *et al.*[22] The singularities appear when the segmental friction constant is appreciably larger than that of a sphere obeying macroscopic hydrodynamics. It is evident that these same singularities arise in eq 9 and 10 at high values of f. It does not escape us that a further discussion of these singularities is in order in the light of our results, to which we hope to return in the future.

(21) R. E. DeWames, W. F. Holland, and M. C. Shen, *J. Chem. Phys.*, **46**, 2782 (1967).

(22) R. Zwanzig, J. Kiefer, and G. H. Weiss, *Proc. Nat. Acad. Sci. U. S.*, **60**, 381 (1968).

Liquid Junction Potentials and Single-Ion Activities by Computer Simulation. I. The Concentration Cell with Transference

by Robert N. Goldberg* and Henry S. Frank

Department of Chemistry, University of Pittsburgh, Pittsburgh, Pennsylvania 15213, and Mellon Institute of Carnegie-Mellon University, Pittsburgh, Pennsylvania 15213 *(Received December 3, 1971)*

Publication costs assisted by the University of Pittsburgh and the National Bureau of Standards

The liquid junction potentials in KCl, NaCl, and HCl concentration cells with transference have been evaluated by computer simulation, making use of Onsager flux coefficients tabulated by Miller, and of a convenient formalism for single-ion activity coefficients to make possible the representation of osmotic driving forces. Varying assumptions regarding single-ion activity coefficients lead to varying values of a computed steady-state junction potential, but these differences are canceled by corresponding differences in calculated electrode potentials, so that the computed overall cell potential remains unchanged—*i.e.*, measurement of the potential of a concentration cell with transference can give no information about single-ion activity coefficients. This expected result plus the agreement of computed cell potentials with experimental ones speaks both for the essential validity of the method and for the mutual self-consistency of the numerical values inserted for Onsager coefficients and for mean ionic activity coefficients. In contrast to the steady-state cell potential, the time rise of the calculated potential is sensitive to the choice made for the single-ion activity coefficient parameter. There would thus seem to exist a possibility for determining single-ion activities in an experiment, if the time rise of the cell potential, after the formation of the junction, could be measured on a nanosecond time scale.

Introduction

The liquid junction–individual ion activity problem remains, unsolved, as one of the classic problems of physical chemistry. Well-known thermodynamicists have at various times taken differing views on the problem. Guggenheim[1] has contended that individual ion activities and liquid junction potentials have "no physical reality," on the ground that there is and can be no way of measuring them, but is also identified with a convention for dealing with them.[2] Pitzer and Brewer[3] write that "single-ion properties are potentially measureable." Kirkwood and Oppenheim[4] have made an equivalent statement in pointing out that "it is possible to measure absolute single-electrode potentials (by non-thermodynamic methods)."

Frank[5] in advocating a return to the ascription of physical significance to single-ion activities, has defined (see below) a function useful for representing and manipulating individual ion activities. Unfortunately, there are to the best of our knowledge no data as yet available that lead rigorously to values of this function, although a number of ingenious proposals have been made. Most recently, Bates, Staples, and Robinson[6]

* Address correspondence to this author at the National Bureau of Standards, Washington, D. C. 20234.

(1) E. A. Guggenheim, *J. Phys. Chem.*, **33**, 842 (1929).

(2) D. A. MacInnes, "Principles of Electrochemistry," Dover Publications, New York, N. Y., 1961, p 242.

(3) G. N. Lewis and M. Randall (revised by K. S. Pitzer and L. Brewer), "Thermodynamics," McGraw-Hill, New York, N. Y., 1961, p 310.

(4) J. G. Kirkwood and I. Oppenheim, "Chemical Thermodynamics," McGraw-Hill, New York, N. Y., 1961, p 211.

(5) H. S. Frank, *J. Phys. Chem.*, **67**, 1554 (1963).

(6) R. G. Bates, B. R. Staples, and R. A. Robinson, *Anal. Chem.*, **42**, 867 (1970).

have assigned plausible values for single-ion activities in alkali halide solutions, derived on the basis of assumptions regarding single-ion hydration numbers, but these are not claimed to be either rigorous or unique.

It has long been recognized that if liquid junction potentials could be unambiguously evaluated, it would be possible to use this information in combination with data from readily accessible electrochemical cells to obtain individual ion activities. The customary numerical formulas[7] for liquid junction potentials depend, however, on prior assumptions regarding the individual ion activities, and so cannot be used to solve for them.

Another approach to this problem is through the calculation of the charge distribution in the junction arising from the differential mobility of the ions. Early attempts of this sort were made by Taylor[8] and Longsworth.[9] Recently, Hafemann[10] has carried out an improved calculation of this kind, making use of three developments not available to earlier workers; namely, the Onsager formulation of nonequilibrium thermodynamics, accurate transport data, and the availability of high-speed computational methods. In the present paper we have extended Hafemann's calculation, for a junction of the type MX(c), MX(c'), to include the cross coefficients in the Onsager equations, and have introduced a procedure to take more flexible account of individual ion activity behavior. These calculations display an internal consistency that lends support to the formalism adopted and to the numerical values of the transport coefficients employed. As will be seen, however, the calculation here reported cannot be used to obtain unique values for either single-ion activities or liquid junction potentials.

The Calculation

We are concerned with the calculation of the liquid junction potential for the simplest possible case, when two different concentrations of the same binary electrolyte are in contact with each other through an initially sharp boundary. Such a junction is represented by

$$\mathrm{MX}(c),\ \mathrm{MX}(c')$$

where we take M and X to be univalent cations and anions, respectively, and the end concentrations are c and c'.

The calculation considers the solutions to be infinite in extent in the y and z directions, so that all variations of composition and potential extend along the x direction. Representing the liquid junction potential as arising from a distribution of charged particles, the Poisson equation simplifies to

$$\partial^2\Phi/\partial x^2 = -\frac{\rho(x)}{\epsilon} \tag{1}$$

where Φ is the electrostatic potential in the interior of the solution, $\rho(x)$ is the charge density, and ϵ is the permittivity (mks units are used throughout this paper). If $c_1(x)$ and $c_2(x)$ are the concentrations, respectively, of cation and anion in particles per cubic meter and z_1 and z_2 are their signed charges, then $\rho(x) = z_1c_1(x) + z_2c_2(x)$. If a length from $x = 0$ to $x = l$ includes the whole of the region in which variations in c_1, c_2, ρ, or Φ are found, then the potential difference across the junction is given by the double integral

$$\Phi_l - \Phi_0 = -\int_0^l\int_0^x \frac{\rho(x)}{\epsilon}\mathrm{d}x\mathrm{d}x \tag{2}$$

This integral becomes essentially constant with time when it has adjusted itself so that over its length the differential pull, which $\Phi_l - \Phi_0$ exerts on the positive and negative ions, suffices to compensate the forces of diffusion which result from the differences in concentration.

The variation with time of the concentration of the ions is calculated by use of the Onsager phenomenological equations, using the formulation of Miller.[11] Assuming that bulk flow can be neglected, and choosing a solvent-fixed reference frame

$$\frac{\partial c_1}{\partial t} = -\frac{\partial J_1}{\partial x} \text{ and } \frac{\partial c_2}{\partial t} = -\frac{\partial J_2}{\partial x} \tag{3}$$

where the J's are fluxes given by

$$J_1 = -l_{11}\left[\left(\frac{\partial\mu_1}{\partial x}\right)_x + z_1F\left(\frac{\partial\Phi}{\partial x}\right)_x\right] - l_{12}\left[\left(\frac{\partial\mu_2}{\partial x}\right)_x + z_2F\left(\frac{\partial\Phi}{\partial x}\right)_x\right]$$

$$J_2 = -l_{21}\left[\left(\frac{\partial\mu_1}{\partial x}\right)_x + z_1F\left(\frac{\partial\Phi}{\partial x}\right)_x\right] - l_{22}\left[\left(\frac{\partial\mu_2}{\partial x}\right)_x + z_2F\left(\frac{\partial\Phi}{\partial x}\right)_x\right] \tag{4}$$

Here the l_{ij}'s are the Onsager transport coefficients, and his reciprocity relation states that $l_{12} = l_{21}$ (the applicability of the reciprocal relation to concentration cells with transference is assumed here in general and has been demonstrated in the case of the silver nitrate concentration cell[12]). $\partial\mu_i/\partial x$ is the gradient of the chemical potential of ion i. It, the l_{ij} terms, and the gradient of the electrostatic potential, $(\partial\Phi/\partial x)_x = -\int_0^x (\rho(x)/\epsilon)\mathrm{d}x$, are all to be evaluated at the appropriate position x. Miller[11] has given numerical values of l_{ij} for several aqueous systems as functions of concentration, derived from measured conductances, trans-

(7) See ref 2, Chapter 13.
(8) P. B. Taylor, *J. Phys. Chem.*, **31**, 1478 (1927).
(9) L. G. Longsworth, as quoted in ref 2, p 239.
(10) D. Hafemann, *J. Phys. Chem.*, **69**, 4226 (1965).
(11) D. G. Miller, *ibid.*, **70**, 2639 (1966).
(12) M. J. Pikal and D. G. Miller, *ibid.*, **74**, 1337 (1970).

ference numbers, and diffusion coefficients. We employ his tabulated values in our calculation.

The values of the $\partial\mu_1/\partial x$ and $\partial\mu_2/\partial x$ terms which appear in eq 4 are given by

$$\left(\frac{\partial\mu_i}{\partial x}\right)_x = RT\left(\frac{\partial \ln c_i}{\partial x}\right)_x + RT\left(\frac{\partial \ln y_i}{\partial x}\right)_x$$

$$\left(\frac{\partial\mu_i}{\partial x}\right)_x = RT\left(\frac{1}{c_i}\frac{\partial c_i}{\partial x}\right)_x + RT\left(\frac{\partial \ln y_i}{\partial \bar{c}}\right)\left(\frac{\partial \bar{c}}{\partial x}\right)_x \quad (5)$$

where $\bar{c} = (c_1 + c_2)/2$. To obtain numerical values for the gradients, use is made of Frank's[5] function, the mean ionic activity deviation, defined on the molarity scale by the equation $\ln \delta_\pm = (1/\nu)[\nu_+ \ln y_+ - \nu_- \ln y_-]$, where each ν is the appropriate ion number. For a 1–1 electrolyte, this becomes $\delta_\pm = [y_1/y_2]^{1/2}$, which complements the definition of the mean ionic (molar) activity coefficient, $y_\pm = (y_1y_2)^{1/2}$.

Introducing this function, the $\partial \ln y_i/\partial\bar{c}$ terms in eq 5 become

$$\frac{\partial \ln y_1}{\partial \bar{c}} = \frac{\partial \ln y_\pm}{\partial \bar{c}} + \frac{\partial \ln \delta_\pm}{\partial \bar{c}} \quad (6)$$

and

$$\frac{\partial \ln y_2}{\partial \bar{c}} = \frac{\partial \ln y_\pm}{\partial \bar{c}} - \frac{\partial \ln \delta_\pm}{\partial \bar{c}} \quad (7)$$

To perform the calculation, it is necessary to postulate a concentration dependence of $\delta_\pm$. For convenience, and on grounds of physical intuition, we have chosen a linear one for $\ln \delta_\pm$; namely

$$\ln \delta_\pm = B\bar{c} \quad (8)$$

Thus, if a value of the constant B is assumed and the experimental values of $\ln y_\pm$ are inserted, one can calculate the $\partial \ln y_i/\partial\bar{c}$ values which are needed for the determination of the $\partial\mu_i/\partial\bar{c}$ terms.

The integration of eq 2 is performed by what is essentially a computer simulation method where, beginning with the initial concentration profiles of the ions across the junction, $\Phi(x, t_0)$ the appropriate derivatives are computed and used to calculate the local fluxes and thence the changes over a sufficiently small period of time in the local concentrations of the ions. This gives a new distribution of the ions, to which there now corresponds a new $\Phi_t - \Phi_0$. By repeating this process as long as is necessary, one is able to obtain the time rise of the junction potential.

In order to perform the calculation on a digital computer, it is necessary to represent the analytical operations in terms of numerical approximations. In this regard, the $\Phi_t - \Phi_0$ integral (eq 2) is easily shown to reduce to Hafemann's[10] numerical expression for the junction potential. All derivatives were calculated by the method of central differences.[13] The l_{ij} data were taken from the critical evaluation of Miller,[11] and activity data from Wu and Hamer.[14] These data were then fitted to polynomial expressions in the concentration, using a least-squares fitting program from Oak Ridge National Laboratory.[15] Hafemann[10] has found that the value used for the permittivity affects only the time rise of the junction potential and not the final steady-state value. Our calculations confirmed this, and we have used a permittivity corresponding to a dielectric constant of 78.30, corresponding to that for pure water at 25.0°.[16] We have used a length increment of 10^{-10} m and a time interval of 10^{-10} sec in the calculation. All computations were performed on the CDC 1604 computer at Mellon Institute. Calculations performed using the more exact double-precision routine on the computer yielded the same results as a single-precision calculation, for which computation time was of the order of 3 min, to simulate a junction rise time of 10 nsec (*i.e.*, 100 "jumps"). It was found that the junction potential had largely leveled off by this time, and successive iterations yielded values linear in $1/t^3$. This dependence was therefore used to extrapolate to a virtual E_J at infinite time. This extrapolation correction was never more than a few per cent.

Results and Discussion

In Table I are presented the results of calculations for several junctions involving aqueous NaCl, KCl, and HCl as functions of the adjustable coefficients B. Also included are values of E_{JA} calculated, using the same B's, combined with experimental data from the appropriate concentration cells with transference, *e.g.*

Ag, AgCl, MCl(c), MCl(c'), AgCl, Ag
A

The measured emf of cell A is given by

$$E_A = \frac{RT}{F}\ln\frac{a_{Cl^-}}{a_{Cl^-}'} + E_{JA} = \frac{RT}{F}\ln\frac{y_{Cl^-}}{y_{Cl^-}'} + \frac{RT}{F}\ln\frac{c}{c'} + E_{JA} \quad (9)$$

$$E_A = \frac{RT}{F}\ln\frac{y_\pm}{y_\pm'} + \frac{RT}{F}\ln\frac{c}{c'} - \frac{RT}{F}\ln\frac{\delta_\pm}{\delta_\pm'} + E_{JA} \quad (10)$$

Turning eq 10 around and introducing the B coefficient, we obtain

(13) M. G. Salvadori and M. L. Baron, "Numerical Methods in Engineering," Prentice-Hall, Englewood Cliffs, N. J., 1961.

(14) Y. C. Wu and W. J. Hamer, National Bureau of Standards Report No. 9908, U. S. Government Printing Office, Washington, D. C., Sept 1968.

(15) L. H. Lietzke, ORNL-3132, Oak Ridge National Laboratory, Oak Ridge, Tenn., April 1961.

(16) C. G. Malmberg and A. A. Maryott, *J. Res. Nat. Bur. Stand.*, **56**, 1 (1956).

$$E_{JA} = E_A - \frac{RT}{F} \ln \frac{y_\pm}{y_\pm'} - \frac{RT}{F} \ln \frac{c}{c'} + \frac{RT}{F} B(c - c') \quad (11)$$

We thus have two ostensibly independent methods, one the computer simulation and the other eq 11, which are capable of yielding values for the liquid junction potential, both involving the same unknown coefficient B, but employing experimental data from entirely unrelated experiments. On the face of it, this would seem to afford a method of solving for B and thus obtaining values for the single-ion activities. As is obvious from an examination of Table I, however, the sets of values obtained by the two methods are in all cases quite close to each other, and by introducing slightly "juggled" input data into the calculations, it was confirmed that the values for E_{JA} (computer) agreed with those found by means of eq 11 within a reasonable assignment of the accuracy of the l_{ij} values. The two routes to the junction potential E_{JA} are therefore somehow tautological and furnish no basis for solving for anything.

Table I: Results of Liquid Junction Potential Calculations

Junction	Assumed B	E_{JA}(computer), mV	E_{JA}(eq 11), mV
KCl (0.10 M), KCl (1.0 M)	−4.0	93.40	93.51[a]
	0.0	1.17	1.02
	2.0	−44.95	−45.23
KCl (0.10 M), KCl (0.50 M)	−10.0	103.35	103.58[a]
	0.0	0.80	0.81
	10.0	−101.76	−101.96
KCl (0.10 M), KCl (0.20 M)	−10.0	26.01	26.05[a]
	0.0	0.34	0.36
	10.0	−25.34	−25.33
KCl (0.10 M), KCl (0.08 M)	−10.0	−5.24	−5.22[a]
	0.0	−0.11	−0.09
	10.0	5.03	5.05
KCl (0.10 M), KCl (0.0501 M)	−10.0	−13.13	−13.21[a]
	0.0	−0.33	−0.39
	10.0	12.47	12.43
KCl (0.10 M), KCl (0.04 M)	−10.0	−15.81	−15.91[a]
	0.0	−0.44	−0.49
	10.0	14.94	14.92
KCl (0.10 M), KCl (0.03 M)	−10.0	−18.47	−18.63[a]
	0.0	−0.58	−0.65
	10.0	17.32	17.34
KCl (0.10 M), KCl (0.01 M)	−10.0	−23.44	−24.23[a]
	0.0	−1.05	−1.11
	10.0	21.33	22.01
KCl (0.10 M), KCl (0.005008 M)	−10.0	−23.90	−25.83[a]
	0.0	−1.25	−1.42
	10.0	21.36	22.98
HCl (0.10 M), HCl (0.003447 M)	−10.0	30.51	29.12[b]
	0.0	51.58	53.92
	10.0	74.96	78.73
NaCl (0.09957 M), NaCl (0.049833 M)	−10.0	−16.49	−16.56[c]
	0.0	3.73	−3.78
	10.0	9.03	9.00

[a] E_A values from T. Shedlovsky and D. A. MacInnes, *J. Amer. Chem. Soc.*, **59**, 503 (1937). [b] E_A values from T. Shedlovsky and D. A. MacInnes, *ibid.*, **58**, 1970 (1936). [c] E_A values from A. S. Brown and D. A. MacInnes, *ibid.*, **57**, 1356 (1935).

That this sort of tautology should have been anticipated is to be understood in terms of the following argument. In the asymptotic limit in which the time rise of the junction potential has been completed, one has a condition of zero current flowing through the junction; that is

$$I = (z_1 J_1 + z_2 J_2)F = 0 \quad (12)$$

Miller[11] has shown that this condition leads to the classical expression for the liquid junction potential[7]

$$E_J = -\frac{RT}{F} \int_{\text{across junction}} \sum_i \frac{t_i}{z_i} \, \mathrm{d} \ln a_i \quad (13)$$

where t_i is the transference number of ion i. In the case represented by cell A, the integrand in eq 13 reduces to

$$t_{M^+} \mathrm{d} \ln a_{M^+} - t_{Cl^-} \mathrm{d} \ln a_{Cl^-} = \mathrm{d} \ln a_{Cl^-} + 2t_{M^+} \mathrm{d} \ln a_\pm \quad (14)$$

where use has been made of the identities

$$2 \ln a_\pm = \ln a_{M^+} + \ln a_{Cl^-} \quad (15)$$

and

$$t_{M^+} + t_{Cl^-} = 1 \quad (16)$$

Therefore

$$E_J = -\frac{RT}{F} \ln \frac{a_{Cl^-}}{a_{Cl^-}'} - \frac{2RT}{F} \int t_{M^+} \mathrm{d} \ln a_\pm \quad (17)$$

The value of E_J, the junction potential calculated in the computer, although arrived at by a seemingly independent route, is thus seen to contain implicitly the term $-(RT/F) \ln (a_{Cl^-}/a'_{Cl^-})$, which cancels the corresponding term in eq 9. This produces the result that the remaining part of the computed value of the junction potential at a virtual infinite time is fully represented by the last term in eq 17, which also represents the value of E_A, the total cell emf of cell A and contains no residue depending on the value of the parameter B. It is thus seen that after the time rise of the junction potential has been completed, the emf of cell A contains, and can furnish, no information about individual ion activities. This corresponds to our empirical finding that changes in the assumed values of the B parameter produce changes in the junction potential and in the electrode potentials that exactly cancel. The exactness of this cancellation, as evidenced by the agreement of our results in Table I, supports the essential correctness both of the simulation procedure and of the l_{ij} values as tabulated by Miller.[11]

The insensitivity of a computed junction potential to the assumed value of the permittivity ϵ presumably arises from a similar cancellation. While a rigorous analysis of this point would involve making ϵ a function of the position x in the liquid junction and therefore seems at present to be out of reach,[17] the qualitative features of the compensation seem clear enough. A smaller ϵ would result in stronger electrical forces, and thus a given concentration gradient would be accompanied by a smaller charge separation. In exactly the same proportion, however, a given charge separation would produce a larger potential difference, and the result is understandable that a given concentration gradient would give the same potential regardless of the value of ϵ.

An extension of the simulation procedure to the three-ion junction, *i.e.*, the Lewis and Sargent junction, was attempted by Hafemann.[10] The rigorous performance of such a calculation, however, requires not only more than one B parameter, but also a means of treating the mixed electrolyte solutions in the junction. An argument analogous to that given above leads to the expectation that the emf of the Lewis and Sargent junction will likewise prove incapable of yielding values for single-ion activities. A detailed analysis of this problem has been carried out by Chen and Frank.[19] We have also attempted to treat cells with liquid junctions containing four different ions, but to date have been unable to devise any interpretation which is both rigorous and useful for the emf values for cells of this type.

An additional result of the simulation calculations reported here is to suggest a novel thought experiment that might lead to a solution of the single-ion problem. This may be illustrated by reference to Figure 1, which illustrates the fact that only after the time rise of the junction potential is complete is the cell emf independent of the assumed B parameter. If, therefore, the time rise of the junction potential could be measured, an experimental basis might exist for assigning a numerical value to B and thence to the single-ion activities. Since the time rise is of the order of nanoseconds, such an experiment involves difficulties which are at present insuperable. Another possibly serious difficulty arises from the fact that the computed time rise for a given B is sensitive to the values of ϵ which underlies the computation, so that it might turn out that, if the variability of ϵ across the junction matters, the measured time rise might not fit any curve calculated for a constant ϵ. Insofar, however, as an extrapolation of E_A back to time $t = 0$ could be made, an estimate of B would seem feasible.

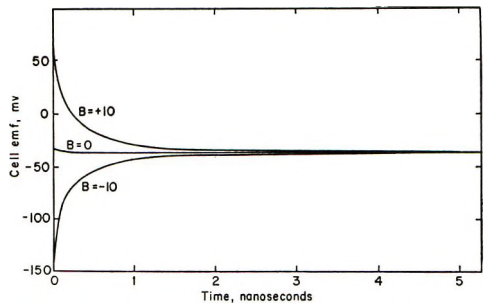

Figure 1. Computed values of cell emf, E_A, eq 9, as a function of time for the cell Ag, AgCl, KCl (0.10 M), KCl (0.50 M), AgCl, Ag. Computations are for three values of the parameter B, defined in eq 8.

Another thought experiment would involve the design of a cell in which the junction is far enough separated from the electrodes and well enough defined in extent to make possible a measurement of the dipole moment produced by its charge distribution. Here again, present experimental procedures fall far short of the sensitivity required for this measurement. Here also, medium or dielectric constant effects might present difficulties of interpretation.

Mention should also be made of Oppenheim's[20] development of Kirkwood's suggestion for direct measurement of an individual electrode potential. In that experiment, the electrode is brought into rapid oscillation and the intensity and angular distribution are measured of the quadrupole radiation produced. Oppenheim has derived equations that relate these quantities to the charge distribution at the electrode and thence to the individual electrode potential.

Acknowledgments. Grateful acknowledgment is made of the support of this work by the Office of Saline Water, U. S. Department of the Interior. We are also grateful to Dr. Donald G. Miller for helpful correspondence on a number of points in this paper.

(17) Related to the variability of ϵ with x is the position sometimes taken that since solutions of concentration c and c' are, properly speaking, different media, the difference in electrostatic potential which we have called $\Phi_l - \Phi_0$ is not, in a strict sense, a well-defined quantity. As was pointed out by Onsager, however,[18] there is no logical bar to the adoption of some convention for relating Φ_l to Φ_0. From this point of view eq 2 may be regarded as a postulate which, among other things, defines the convention on which the present discussion is based.

(18) L. Onsager, discussion at the H. S. Harned Memorial Symposium held by the Division of Physical Chemistry at the 160th National Meeting of the American Chemical Society, Chicago, Ill., Sept 4, 1970.

(19) C. H. Chen and H. S. Frank, manuscript in preparation.

(20) I. Oppenheim, *J. Phys. Chem.*, **68**, 2959 (1964).

Conductivity of Sodium Chloride and Potassium Chloride in Polymer Solutions and the Obstruction Effect

by P. H. Elworthy, A. T. Florence,*[1] and A. Rahman

Department of Pharmaceutical Chemistry, University of Strathclyde, Glasgow, C.1, United Kingdom
(Received November 23, 1971)

Publication costs borne completely by The Journal of Physical Chemistry

The conductivity of solutions of NaCl and KCl in the presence of the polymers poly(vinylpyrrolidone) 360,000, cetomacrogol 1000 (a nonionic surfactant), and poly(oxyethylene glycol) 6000 (κ) has been compared with the conductance of the solutions without these additives (κ_0). The lowering of the conductance by the polymer is due to the large solute molecules obstructing the movement of the ions in solution. For poly(oxyethylene glycol) and poly(vinylpyrrolidone) solutions, the conductivity of NaCl and KCl at infinite dilution can be calculated using Wagner's equation: $\kappa/\kappa_0 = (1 - \phi_h)/[1 + (\phi_h/2)]$, where ϕ_h is the volume fraction of solute including hydrating water, but this equation gives low values for the hydration of cetomacrogol micelles. The movement of the salts in micellar cetomacrogol solutions is explicable in terms of the model of Pauly and Schwan, which employs a nonconducting core (the hydrocarbon interior of the micelle) and an outer shell (the poly(oxyethylene glycol) layer) which has a conductivity 0.23 times that of the medium.

Introduction

When the viscosity of a solution is increased by the presence of large molecules the resistance encountered by small molecules and ions moving in the solution is also increased. Wang[2] has suggested that in viscous flow the solute molecules distort the streamlines of flow and therefore lengthen the effective paths of moving particles in conductance and diffusion. Because of this hindrance to flow—the obstruction effect—it is found that the specific conductivity of a suspension of nonconducting particles (κ) is less than that of the medium which surrounds the particles (κ_0).

As problems of steady current flow in conductors and lines of force in insulators are formally identical, the mathematical treatment of the dielectric behavior of suspensions and solutions is identical with that of specific conductance. The derivations of the dielectric constant of suspensions of low-dielectric particles can therefore be adapted for discussion of the conductivity of these systems.[3] The equations of Rayleigh,[4] Böttcher,[5] and Bruggeman,[6] which treat the dielectric constant of inhomogeneous media as a function of the volume fraction of the dispersed phase (ϕ) all reduce at low ϕ to

$$\epsilon/\epsilon_0 = 1 - 1.5\phi \quad (1)$$

or, in terms of specific conductance

$$\kappa/\kappa_0 = 1 - 1.5\phi \quad (2)$$

We became interested in the conductivity of NaCl and KCl solutions in the presence of nonelectrolyte additives when studying the dissolution of these salts by continuous monitoring of conductance in aqueous solutions of poly(oxyethylene glycol), cetomacrogol ($C_{16}H_{33}(OCH_2CH_2)_{22-24}OH$), and poly(vinylpyrrolidone). This necessitated the measurements described here, and as the systems differed in properties significantly from those systems, such as oil-in-water emulsions,[7] used previously to test the "obstruction" equations, we have attempted to explain our results on the basis of available obstruction models. The three polymers chosen have sufficiently different physicochemical properties to make a comparison of their obstruction effects pertinent (Table I).

Experimental Section

Materials. Poly(vinylpyrrolidone) (PVP), molecular weight 360,000, was obtained from Sigma. Poly(oxyethylene glycol) (PEG), molecular weight 6000, was obtained from B.D.H. Ltd., and Cetomacrogol 1000 B.P.C. (CMG) was obtained from Macarthy's Ltd. The glycol and cetomacrogol were deionized by passage of methanol–water solutions through a Biodemineralit column, followed by evaporation to dryness. Sodium chloride and potassium chloride were AnalaR grade (B.D.H.). Water was twice distilled from an all-glass apparatus.

Methods. Conductivities of solutions of NaCl and KCl in water and in aqueous solutions of the three

(1) To whom communications should be addressed.

(2) J. H. Wang, *J. Amer. Chem. Soc.*, **76**, 4755 (1954).

(3) R. H. Stokes and R. A. Robinson, "Electrolyte Solutions," 2nd ed, Butterworths, London, 1965, p 311.

(4) Lord Rayleigh, *Phil. Mag.*, **34**, 481 (1892).

(5) C. J. F. Böttcher, "Theory of Electric Polarization," Elsevier, New York, N. Y., 1952, p 419.

(6) D. A. G. Bruggeman, *Ann. Phys.*, **24**, 636 (1935).

(7) T. Hanai in "Emulsion Science," P. Sherman, Ed., Academic Press, London, 1968.

Table I: Physical Properties of the Polymeric Additives

Polymer	Mol wt	Partial specific volume, ml g^{-1}	Intrinsic viscosity $[\eta]$, ml g^{-1}	Hydration, g g^{-1}	Comments
Cetomacrogol	100,000[b]	0.917	7.3	1.9[a]	Above 0.006% exists as spherical hydrated micelles
PEG	6,000	0.835	18.0		Coiled hydrated molecule
PVP	360,000	0.802	174.0		Asymmetric particles, hydrated

[a] Calculated from Oncley's equation:[13] $[\eta] = 2.5(v_2 + \omega v_0)$, where v_2 = partial specific volume of solute, ω = hydration in grams per gram of solute, and v_0 = specific volume of water. [b] Micellar molecular weight (ref 10).

polymers were measured after equilibration at 25° using a Wayne–Kerr bridge (Universal Bridge B221) and autobalance adapter (AA221) and a Mullard conductivity cell (Type E7591/B). The cell constant (1.515 cm^{-1}) was determined using standard solutions of NaCl and KCl and the conductivity data of Chambers and Stokes[8] and of Shedlovsky.[9] Solutions of the salts and polymer were prepared by addition of salt solution to a known weight of polymer, so that κ_0 is the specific conductivity of the solvent surrounding the particles.

Densities were measured at ±0.01° with a Lipkin pycnometer which had been calibrated with water.

Viscosities were measured at 25 ±0.01° in a suspended-level dilution viscometer.

Results and Discussion

The specific conductivities of solutions of NaCl and KCl in water and in the presence of the additives were measured and the ratio κ/κ_0 calculated and plotted as a function of additive volume fraction, ϕ, for each salt concentration studied. Values of κ/κ_0 at each ϕ value corresponding to infinite dilution were then obtained by extrapolation. This procedure avoids complications arising from ion size and ion–ion interactions. Typical results are shown in Figure 1.

Polymer volume fractions were calculated from the concentration of solution (%, w/v) using the partial specific volumes obtained from density measurements (Table I). Further information on the physical properties of the polymers was obtained from viscosity measurements from which, in the case of the spherical micelles of cetomacrogol,[10] hydration values were obtained directly (Table I). As the molecules of PVP and PEG are asymmetric, hydration values cannot be obtained directly from viscosity measurements.

It became obvious from the results of the ratio κ/κ_0 plotted against ϕ that the simple eq 2 does not explain the obstruction effect caused by the three additives. The measured specific conductances are significantly lower than those predicted by this equation. It can be seen from Figure 2 that the asymmetric PEG and PVP molecules lower the conductance of the solutions more effectively than the spherical CMG micelles,

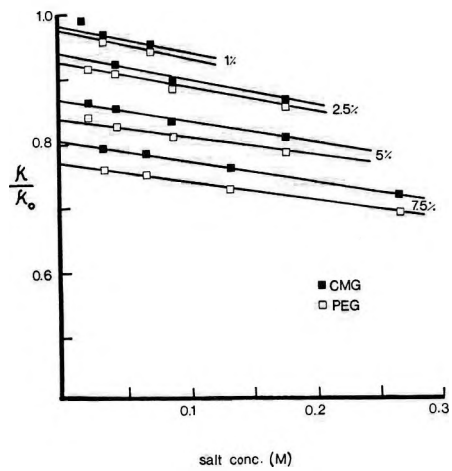

Figure 1. Plots of experimental specific conductivities of KCl, in the presence of cetomacrogol 1000 and poly(oxyethylene glycol), divided by the specific conductivity of the solution (κ/κ_0) as a function of additive concentration (%) and KCl concentration (M). Values extrapolated to zero salt concentration are the values used for comparison with calculated values of κ/κ_0 (see text).

in qualitative agreement with the theoretical predictions of Fricke.[11] The use of hydrated volume fractions (ϕ_h) can reasonably explain the measured conductances of the PVP solutions, although the results in this case are limited. ϕ_h is related to ϕ, the unhydrated volume fraction by

$$\phi_h = \phi\left(1 + \frac{\omega}{\bar{v}}\right) \tag{3}$$

where ω is the hydration in grams per gram of solute and $\bar{v}$ is the partial specific volume of the particle.

Because results with PVP are limited to a maximum concentration of 1% (w/v) (because of the high viscosity encountered), this system does not present a searching test of the obstruction equations. A hydration of 1.02 g g^{-1} results in a reasonable fit with the ex-

(8) J. F. Chambers and R. H. Stokes, *J. Phys. Chem.*, **60**, 985 (1956).

(9) L. Shedlovsky, *J. Amer. Chem. Soc.*, **54**, 1424 (1932).

(10) C. B. Macfarlane, *Kolloid Z. Z. Polym.*, **239**, 682 (1970).

(11) H. Fricke, *Phys. Rev.*, **24**, 575 (1924).

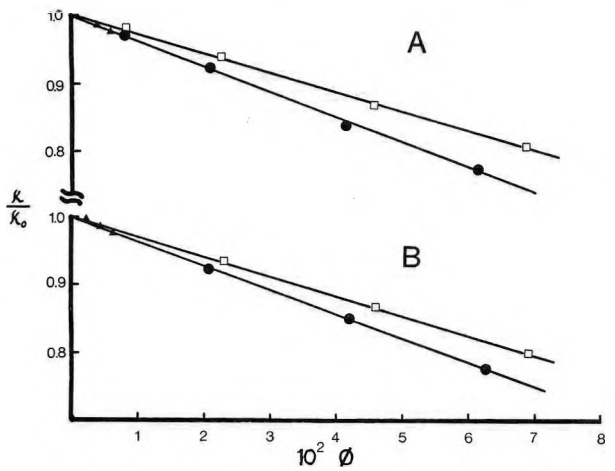

Figure 2. Experimental values of κ/κ_0 *vs.* ϕ for (A) KCl and (B) NaCl in PEG (●), CMG (□), and PVP (▲) solutions.

perimental data which can be represented by the equation (Table II) $\kappa/\kappa_0 = 1 - 3.4\phi$. Table II lists the equations which describe the conductivity ratios for the other systems studied. To obtain a fit with eq 2, hydrations of ~1.2 g g^{-1} are required for the PEG systems and 0.84 g g^{-1} for CMG. The assumption involved in the use of a hydrated volume in eq 2 is that the hydrated regions of the polymer or micelle are inaccessible to the moving ions. This is patently not so. Measured hydration values for cetomacrogol are in the region of 2 g g^{-1}. Other equations neglecting possible permeability of the particles give similar low results for hydration. Both eq 2 and Wagner's equation[12,13] for the case where κ_0 is much greater than the specific conductivity of the polymer particle, κ_p

$$\kappa/\kappa_0 = (1 - \phi)/[1 + (\phi/2)] \qquad (4)$$

give reasonable representations of the data for the PVP–salt systems when $\omega = 1$ g g^{-1}.

Table II: Experimental Conductivity Data. The Parameter α in the Equation $\kappa/\kappa_0 = 1 - \alpha\phi^a$

Additive	Salt	α	ω,[b] g g^{-1}
PEG	KCl	3.72	1.24
	NaCl	3.56	1.15
CMG	KCl	2.84	0.82
	NaCl	2.90	0.86
PVP	KCl	3.4	1.02
	NaCl		

[a] ϕ is the unhydrated volume fraction and ϕ_h is the hydrated volume fraction. [b] $\omega = (\alpha - 1.5)v/1.5$.

Conductivity ratios (κ/κ_0) were calculated with eq 4 for a series of hydration values in the range previously obtained for poly(oxyethylene glycols) (0.2 g–2.0 g g^{-1}).[14] The experimental results for PEG–NaCl fall

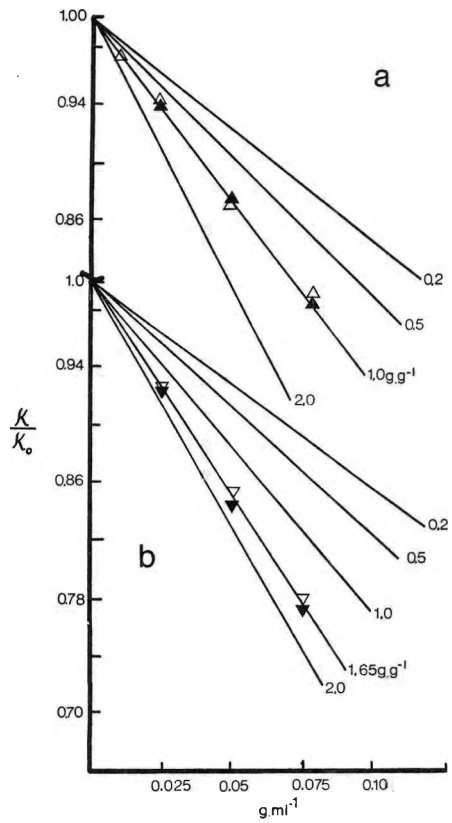

Figure 3. κ/κ_0 as a function of additive concentration, calculated by the equation $\kappa/\kappa_0 = (1 - \phi_h)[1 + (\phi_h/2)]$, with hydration values shown and with experimental points superimposed: (a) △, CMG–NaCl; ▲, CMG-KCl; (b) ▽, PEG–NaCl; ▼, PEG–KCl.

on the 1.65-g g^{-1} line, as shown in Figure 3. Similarly, the results for CMG–NaCl fall on the 1.0-g g^{-1} line, the deviation at low additive concentration being due to experimental error (Figure 3). This value is less than the 1.9 g g^{-1} established from viscosity measurements on cetomacrogol; therefore, this result led us to explore a further model, that of Pauly and Schwan.[15] This approach considers the dispersed particles to consist of a core surrounded by a shell, both core and shell having conductivities, κ_p and κ_s, respectively, differing from that of the medium (Figure 4). This model is more appropriate to the micellar systems of CMG studied, as the micelles consist of a hydrocarbon core surrounded by a heavily hydrated poly(oxyethylene) layer. The original derivation for systems of particles with shells was carried out on dielectric considerations by Pauly and Schwan, who obtained the following equation relating the dielectric constant of the system, ϵ, to ϵ_m, ϵ_s, and ϵ_p.

(12) K. W. Wagner, *Arch. Elektrochem.*, **2**, 371 (1914).
(13) J. L. Oncley, *Ann. N. Y. Acad. Sci.*, **41**, 121 (1940).
(14) P. H. Elworthy and A. T. Florence, *Kolloid Z. Z. Polym.*, **208**, 157 (1966).
(15) H. Pauly and H. P. Schwan, *Z. Naturforsch.*, **14b**, 125 (1959).

$$\frac{\epsilon_m - \epsilon}{2\epsilon_m + \epsilon} = \phi_h \frac{(\epsilon_m - \epsilon_s)(2\epsilon_s + \epsilon_p) + (\epsilon_m + 2\epsilon_s)(\epsilon_s - \epsilon_p)f}{(2\epsilon_m + \epsilon_s)(2\epsilon_s + \epsilon_p) + 2(\epsilon_m - \epsilon_s)(\epsilon_s - \epsilon_p)f} \quad (5)$$

In the analogous form for conductivities, this becomes

$$\frac{\kappa_0 - \kappa}{2\kappa_0 + \kappa} = \phi_h \frac{(\kappa_0 - \kappa_s)(2\kappa_s + \kappa_p) + (\kappa_0 + 2\kappa_s)(\kappa_s - \kappa_p)f}{(2\kappa_0 + \kappa_s)(2\kappa_s + \kappa_p) + 2(\kappa_0 - \kappa_s)(\kappa_s - \kappa_p)f} \quad (6)$$

where f is the fraction of inner-phase volume to the total volume of the dispersed particle. For cetomacrogol, f can be calculated from published data on core and micellar volumes[16] to be 0.08. κ_p can be considered to be negligible. Hence, the equation becomes

$$\frac{1 - \frac{\kappa}{\kappa_0}}{2 + \frac{\kappa}{\kappa_0}} = \frac{\phi_h}{2} \frac{(2 + f) - \frac{\kappa_s}{\kappa_0}(2 - f)}{2(2 + f) - \frac{\kappa_s}{\kappa_0}(f - 1)} \quad (7)$$

If the poly(oxyethylene) shell is considered to be nonconducting ($\kappa_s \rightarrow 0$), eq 7 reduces to the form of eq 2.

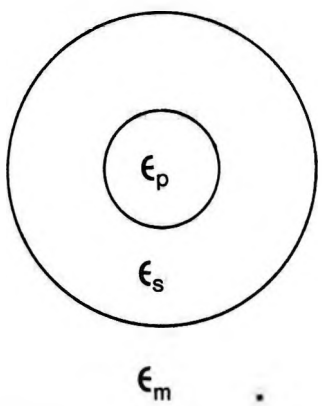

Figure 4. Model of Pauly and Schwan for particle with shell. ϵ is the dielectric constant of the suspension, ϵ_m is the dielectric constant of the medium, ϵ_p is the dielectric constant of the core, and ϵ_s is the dielectric constant of the shell.

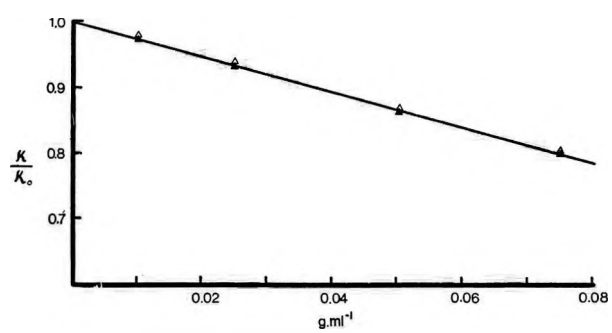

Figure 5. κ/κ_0 for cetomacrogol solutions calculated from eq 6 with $f = 0.08$ and $\kappa_s/\kappa_0 = 0.23$, using a hydration of 1.9 g g^{-1} to calculate hydrated volume fractions. Experimental points are for NaCl (▲) and KCl (△).

Using a hydration value of 1.9 g g^{-1} and f as stated, values of κ_s/κ_0 were chosen to obtain the best fit with the experimental data. Cetomacrogol micelles are monodisperse. As shown by Figure 5, the results for NaCl and KCl extrapolated to infinite dilution fall on the line generated using $\kappa_s/\kappa_0 = 0.23$, *i.e.*, the conductivity or permeability of the PEG layer to the salt ions is 0.23 times that of the solvent water (see Table III).

Table III: Experimental and Calculated[a] Conductivity Ratios at Infinite Dilution in Cetomacrogol

Salt	[Cetomacrogol], %	κ/κ_0(exptl)	κ/κ_0(calcd)	Deviation, ±%
NaCl	1.0	0.980	0.972	−0.82
	2.5	0.937	0.930	−0.75
	5.0	0.870	0.864	−0.69
	7.5	0.801	0.800	−0.12
KCl	1.0	0.982	0.972	−1.02
	2.5	0.940	0.930	−1.06
	5.0	0.869	0.864	−0.57
	7.5	0.806	0.800	−0.74

[a] Pauly and Schwan[15] equation, $\omega = 1.9$ g g^{-1}, $\kappa_s/\kappa_0 = 0.23$.

This significant conductivity in the poly(oxyethylene glycol) layer suggests that it is incorrect to consider the glycol molecules in the PEG–salt systems as being impermeable, which is the implication in eq 3. Hence we have attempted to fit our data for PEG–NaCl and PEG–KCl systems with the equation of Meredith and Tobias[17] which has terms accounting for both asymmetry (μ) and particle conductivity (κ_p)

$$\frac{\frac{\kappa}{\kappa_0} - 1}{\frac{\kappa}{\kappa_0} + \mu} = \phi_h \left[\frac{\frac{\kappa_p}{\kappa_0} - 1}{\frac{\kappa_p}{\kappa_0} + \mu} \right] \quad (8)$$

In this equation $\mu = 2$ for spheres and 1 for asymmetric particles. Using a value for hydration of 1.9 g g^{-1} as for cetomacrogol and $\mu = 1$, κ_p/κ_0 was found to be 0.20. There is no unique result for this system, as we have two variables in κ_p and ω, but nevertheless the result for the conductivity of the particles appears to be a reasonable one (see Table IV).

The additives studied here all increase the viscosity of the medium. The mobilities of ions in relation to viscosity is a problem which has attracted much attention. It is found that in solutions of sugars and relatively small nonelectrolytes, large ions obey Walden's rule, *i.e.*, that $\Lambda\eta$ = constant. Ion size is important; hydrogen ions, being small, are least

(16) D. Attwood, P. H. Elworthy, and S. B. Kayne, *J. Pharm. Pharmacol.*, **23**, 77s (1971).

(17) R. F. Meredith and C. W. Tobias, *J. Appl. Phys.*, **31**, 1270 (1960).

Table IV: Experimental and Calculated[a] Conductivity Ratios at Infinite Dilution in Poly(oxyethylene glycol) 6000

Salt	[PEG], %	κ/κ_0(exptl)	κ/κ_0(calcd)	Deviation, ±%
NaCl	1.0		0.969	
	2.5	0.925	0.920	−0.54
	5.0	0.854	0.846	−0.94
	7.5	0.778	0.769	−1.16
KCl	1.0	0.974	0.969	−0.51
	2.5	0.925	0.920	−0.54
	5.0	0.839	0.846	+0.71
	7.5	0.770	0.769	−0.13

[a] Meredith and Tobias[17] equation.

affected by an increase in viscosity. In the present work the differences in the volumes of NaCl and KCl in aqueous solution might cause them to be affected to a differing degree by nonelectrolyte addition, but different effects of these salts on water structure may compensate to some extent. There is an apparent increase in partial molal volume of the salts in the presence of the polymers which is perhaps the result of the effect of the additives on solvent structuring around the ions decreasing the electrostriction of water molecules.

Conclusions

The results presented here show that conductivity measurements can be used to give indications of the resistance offered to the movement of ions in polymer solutions at low concentrations ($\phi < 0.10$). It would be of interest to extend these studies to higher polymer concentrations, where the effects of particle shape of both ion and polymer are likely to be of greater importance. In both dilute and concentrated systems the problem of what value should be taken as the viscosity which the moving particle experiences has still to be resolved. The methods of measurement of the "microscopic" viscosity of polymer solutions and its relationship to their bulk viscosity have still to be worked out.

Acknowledgments. We thank the British Council (1968–1969) and Sandoz Ltd., Basel, Switzerland (1969–1971) for providing financial support for one of us (A. R.).

Interaction of Neighboring Groups in Maleic Acid Copolymers[1]

by Andrew W. Schultz and Ulrich P. Strauss*

School of Chemistry, Rutgers University, The State University of New Jersey, New Brunswick, New Jersey 08903
(Received July 12, 1971)

Publication costs assisted by the United States Public Health Service

Copolymers of maleic acids show pronounced deviations from normal polyelectrolyte titration behavior at degrees of neutralization above the halfway point. To find an explanation for this abnormality, two alternating copolymers of maleic acid, one with ethylene, the other with methyl vinyl ether as the comonomer, were investigated by potentiometric and viscosimetric titrations with tetramethylammonium hydroxide in a medium of 0.1 *M* tetramethylammonium chloride. It is shown that the special effects encountered in the titration results may be ascribed to the interactions between neighboring dicarboxylate groups. These interactions, which may be characterized by a single parameter, lead to a strong alternating tendency of singly and doubly charged dicarboxylate groups. The molecular origin of the phenomenon is ascribed to a local lowering of the effective dielectric constant near the doubly charged groups, caused by an extraordinarily large amount of bound water.

Introduction

It has been shown[2] that the pH in a solution of a poly(diprotic acid) may be given by the expression

$$\mathrm{pH} = \mathrm{p}K_1^\circ - \log\left\{{}^1/_2\left(\frac{1-\alpha}{\alpha}\right) + {}^1/_2\left[\left(\frac{1-\alpha}{\alpha}\right)^2 + \frac{4K_2^\circ}{K_1^\circ}\left(\frac{2-\alpha}{\alpha}\right)\right]^{1/2}\right\} + 0.434\phi \quad (1)$$

where K_1° and K_2° are the first and second intrinsic ionization constants of a diprotic acid unit, and α is the degree of neutralization (defined so as to be unity

(1) The support of this research by grants from the U. S. Public Health Service (Grant GM 12307) and from S. C. Johnson and Son, Inc., is gratefully acknowledged. This work constitutes a portion of a thesis presented by A. W. Schultz to Rutgers University in partial fulfillment of the requirements for the Ph.D. degree.

(2) P. L. Dubin and U. P. Strauss, *J. Phys. Chem.*, **74**, 2842 (1970).

at half-neutralization). The parameter ϕ is defined by the relation

$$\phi = \frac{1}{RT}\left(\frac{\partial G_{ion}}{\partial \alpha}\right) \quad (2)$$

where dG_{ion} is the differential change in the electrostatic and conformational free energy which accompanies a differential change in α. In the absence of conformational transitions ϕ may be approximated by the quantity $|e\psi/kT|$, ψ being the electrostatic potential at the binding site of the hydrogen ion whose charge is e.[3,4] No rigorous theoretical treatment for predicting the potential of a flexible polyelectrolyte coil is available. Nevertheless, by assuming the coil to be a rigid cylindrical rod, with its fixed charges uniformly distributed over its surface, it has been possible to calculate the potential by means of the Poisson–Boltzmann equation and to obtain fair correlation with experimental behavior in a number of instances, including the potentiometric titration and membrane equilibrium properties of polyacrylic acid under certain conditions.[5-9]

However, clear-cut deviations from these theoretical predictions were encountered in this laboratory in work dealing with potentiometric titrations of two alternating copolymers of maleic acid with tetramethylammonium hydroxide in the absence of metal ions.[10,11]

We have looked at this effect more closely with the aim of finding an explanation for the deviations. In the present paper we shall describe experimental work carried out with two 1–1 copolymers of maleic acid, one containing ethylene, the other methyl vinyl ether as the comonomer. We shall show that the results can be explained by considering nearest-neighbor interactions between dicarboxylate groups.

Experimental Section

Materials. The maleic anhydride–methyl vinyl ether copolymer (HVMEMA) was obtained from General Aniline and Film Corp. (their Gantrez An 139), and the maleic anhydride–ethylene copolymer (HEMA) was Monsanto Corp.'s Grade 31. Both these samples are high polymers with molecular weights of the order of 10^5. Hydrolysis of the anhydride units occurred spontaneously upon dissolution in aqueous media at room temperature.

Tetramethylammonium chloride (TMACl) and hydroxide (TMAOH) were reagent grades obtained from RSA Corp.

Potentiometric Titrations. Titrations of the polymer samples dissolved in 0.1 *M* TMACl were carried out potentiometrically at 24.5° under nitrogen. In all cases, 25 ml of 7×10^{-3} monomolar polymer solutions were used, where one monomole represents one maleic acid and one comonomer residue. The base, 0.260 *M* TMAOH, was added from a Gilmont 2-ml microburet. Blank titrations were carried out as usual.[2]

The potentiometric assembly was composed of the following Radiometer components: pH Meter Titrator TTT 1c, Scale Expander PHA 630 Ta, glass electrode Type G202C HF, and calomel electrode Type K4016 NK. The assembly was connected to the line through a Stancor 117V voltage stabilizer Model CV-500H.

Viscosity. Viscosities were measured at 25° in a Cannon–Ubbelohde dilution viscometer. The bath was controlled to within 0.01°.

Treatment of Interactions between Nearest-Neighboring Groups

The theory of neighboring group interactions in polyelectrolytes has been treated extensively.[12-15] For our purpose it is useful to express the final results of this theory in a phenomenological form which leaves the greatest possible freedom for the interpretation of the derived interaction parameters in terms of their molecular origins. As a point of departure, let us select the formulation developed by Lifson[15] for simple polyacids. Equation 35 of ref 15 can be written, in slightly altered form and notation, as follows

$$\mathrm{pH} + \log \frac{\alpha'}{1-\alpha'} = \mathrm{p}K_a + \log \frac{u_{11}}{u_{00}} + \log u - \log y^2 + 0.434|e\psi/kT| \quad (3)$$

where y is given by the expression

$$y = {}^1/_2(1 - R) + {}^1/_2[(1 - R)^2 + 4uR]^{1/2} \quad (4)$$

with $R = \alpha'/(1 - \alpha')$, and $u = u_{00}u_{11}/u_{01}u_{10}$. (We are using the primed symbol α' for the degree of neutralization to distinguish it from the unprimed symbol α used in eq 1.) Following Lifson's generalized treatment,[16] the quantities u_{AB} are related to F_{AB}, the free energies of interactions between two neighboring groups in states of ionization A and B, by the relation

$$u_{AB} = \exp(-F_{AB}/kT) \quad (5)$$

(3) J. Th. G. Overbeek, *Bull. Soc. Chim. Belg.*, **57**, 252 (1948).

(4) A. Katchalsky and J. Gillis, *Rec. Trav. Chim. Pays-Bas*, **68**, 879 (1949).

(5) R. M. Fuoss, A. Katchalsky, and S. Lifson, *Proc. Nat. Acad. Sci. U. S.*, **37**, 579 (1961).

(6) T. Alfrey, Jr., P. W. Berg, and H. Morawetz, *J. Polym. Sci.*, **7**, 543 (1951).

(7) L. Kotin and M. Nagasawa, *J. Chem. Phys.*, **36**, 873 (1962).

(8) Z. Alexandrowicz and A. Katchalsky, *J. Polym. Sci., Part A-1*, 3231 (1963).

(9) L. M. Gross and U. P. Strauss, in "Chemical Physics of Ionic Solutions," B. E. Conway and R. G. Barradas, Ed., Wiley, New York, N. Y., 1966, p 361.

(10) A. J. Begala, Ph.D. Thesis, Rutgers University, New Brunswick, N. J., 1971.

(11) A. J. Begala and U. P. Strauss, *J. Phys. Chem.*, **76**, 254 (1972).

(12) R. A. Marcus, *ibid.*, **58**, 621 (1954).

(13) F. E. Harris and S. A. Rice, *ibid.*, **58**, 725 (1954).

(14) T. L. Hill, *J. Polym. Sci.*, **23**, 549 (1957).

(15) S. Lifson, *J. Chem. Phys.*, **26**, 727 (1957).

(16) S. Lifson, *ibid.*, **29**, 89 (1958).

The symbols 0 and 1 denote the number of hydrogen ions bound by a given group. The parameter K_a is the acid dissociation constant of a hypothetical isolated group.

In the case of simple polyacids the conventional procedure is to extrapolate the left-hand side of eq 3 to $\alpha' = 0$ where ψ becomes zero. Inspection shows that the fourth term on the right-hand side of eq 3 also vanishes in this limit. The limit of the left-hand side, denoted by $pK°$, is then equal to the sum of the first three terms on the right-hand side of eq 3. Simplifying and anticipating that for the purposes of this paper $u_{01} = u_{10}$, we obtain

$$K° = K_a\left(\frac{u_{01}}{u_{11}}\right)^2 \tag{6}$$

which expresses the influence of the two adjoining groups on the acidity of the group under consideration when $\alpha' = 0$. We should like to point out in passing that on the basis of this analysis neither pK_a nor the individual u_{AB}'s can be rigorously determined from data obtained from polyacids alone. Only $pK°$ can be derived from such data; u can be calculated if, in addition, the dependence of ψ on α' is known or assumed. Further (but still incomplete) information about the individual u_{AB}'s would necessitate a knowledge of pK_a which might be estimated from the appropriate monomeric analog of the polyacid.

The method used to derive eq 3 for simple polyacids can, of course, be extended to poly(dibasic acids). However, because a dibasic acid unit can exist in three states of ionization,[17] a cubic equation results, leading to rather inconveniently complex relationships. Fortunately, the first and second ionization constants of the dibasic acid units in the polyacids treated here are far enough apart to limit the region where all three states exist simultaneously to a narrow interval around $\alpha = 1$. On each side of this interval the dibasic acid units exist in only two states which may be considered as the undissociated and dissociated forms of a simple polyacid whose behavior can be described by eq 3. Specifically, for the secondary dissociation region, on which our interest will be focused, eq 6 combined with eq 3 may be expressed in the form

$$\mathrm{pH} = pK_2° - \log\frac{\alpha^*}{1-\alpha^*} - \log y^{*2} + 0.434|e\psi/kT| \tag{7}$$

where $\alpha^* = \alpha - 1$, so that α^* and $1 - \alpha^*$ represent the fractions of completely dissociated and monoprotonated dicarboxylate groups, respectively. Relations linking y^* and α^* *via* R^* are defined as identical with those relating y and α' *via* R. Of course, the potential ψ does not vanish in the limit of $\alpha^* = 0$, but can be estimated by extrapolation from the primary region[2] or by other appropriate methods.

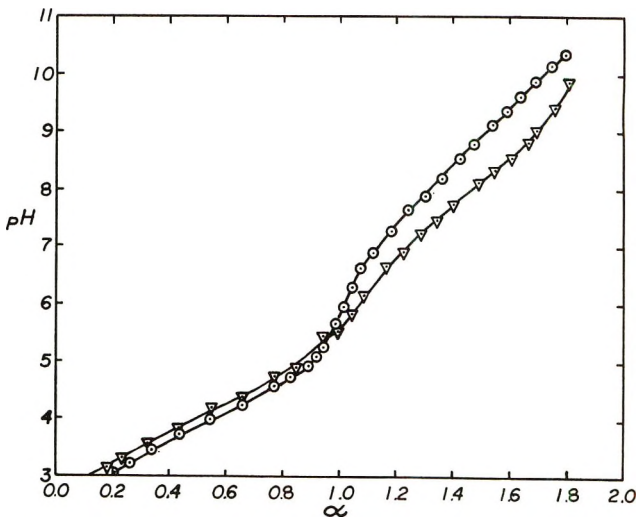

Figure 1. Potentiometric titrations of maleic acid copolymers with TMAOH in 0.1 M TMACl at 24.5°. The triangles refer to a copolymer with ethylene (HEMA), the circles to a copolymer with methyl vinyl ether (HVMEMA).

Results and Discussion

The potentiometric titration results for our samples of HVMEMA and HEMA are presented in Figure 1 where the pH is given as the function of the degree of neutralization, α. By the procedures described in ref 2, we obtain from these data $pK_1° = 3.0$, $pK_2° = 6.22$ for HVMEMA, and $pK_1° = 3.1$, $pK_2° = 5.86$ for HEMA. The observation that the differences between $pK_1°$ and $pK_2°$ are more than a unit larger than the corresponding difference for succinic acid[18] is in line with the conclusion reached previously on the basis of dilatometric titrations that upon hydrolysis of the anhydride units the two carboxylate groups are sterically restrained to remain in the cis position.[11] With these $pK°$ values eq 1 allows us to calculate the quantity 0.434ϕ which is presented in Figure 2 as a function of α for each of the two polyacids. For comparison, the theoretical function $0.434|e\psi/kT|$, calculated for a uniformly charged cylindrical rod model, with both the radius and the average distance between dicarboxylate groups taken to be equal to 5 Å,[9] is also given in Figure 2. The experimental curves are seen to differ from the theoretical curve in the secondary region in both magnitude and shape. At large α the observed values exceed the theoretical ones by almost two units, and the curvatures are clearly of opposite sign. As has been

(17) The monoprotonated condition is counted as only one state. The formal treatment provides for the possibility that the proton may be attached to either of two distinguishable carboxylate groups by permitting the pertinent interaction parameters u_{AB} to be interpreted as appropriately weighted averages taken over the possible proton positions. For the polyacids considered here dilatometric results provide evidence that the proton is bound to both carboxylate groups simultaneously;[11] thus, in this case there may, in fact, be only one monoprotonated state.

(18) J. J. Christensen, R. M. Izatt, and L. D. Hansen, *J. Amer. Chem. Soc.*, 89, 213 (1967).

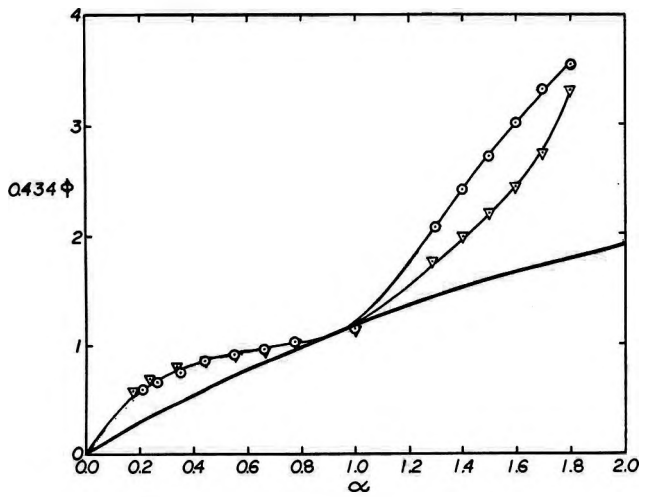

Figure 2. Comparison of experimental and electrostatic values of ϕ. The triangles refer to HEMA, values of ϕ calculated by eq 1 with $pK_1° = 3.1$, $pK_2° = 5.86$. The circles refer to HVMEMA, values of ϕ calculated by eq 1 with $pK_1° = 3.0$, $pK° = 6.22$. The thick curve gives the theoretical potential $0.434|e\psi/kT|$ for a uniformly charged cylindrical rod model (see text).[9]

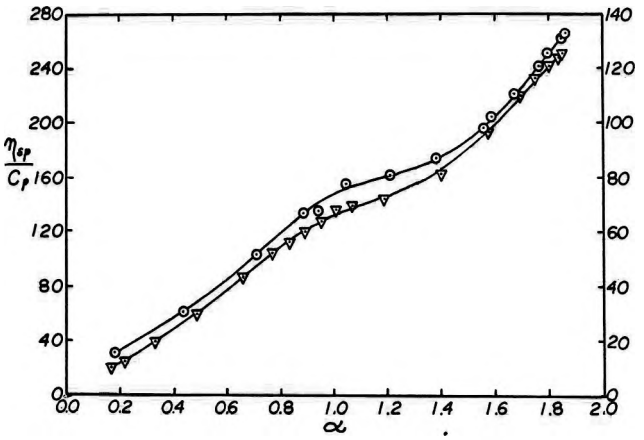

Figure 3. Reduced viscosity as a function of α. Polymer concentration, C_p, equals 7×10^{-3} monomol/l. Circles and left ordinate refer to HVMEMA; triangles and right ordinate refer to HEMA.

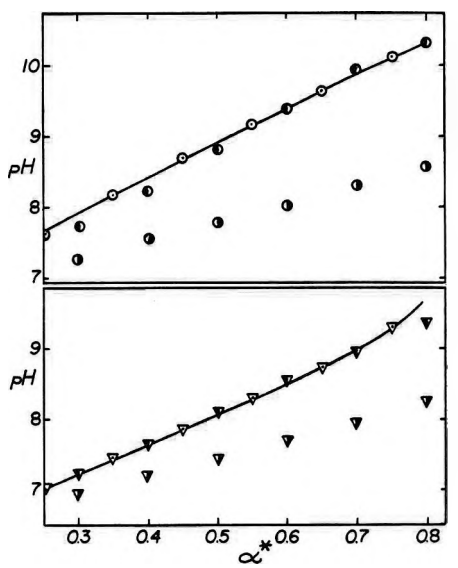

Figure 4. Test plot of eq 7. Upper diagram refers to HVMEMA, lower diagram to HEMA. Open symbols interpolated from experimental data. Left-shaded symbols, pH calculated from eq 7 with $u = 0.1$ for HVMEMA, and with $u = 0.22$ for HEMA. Right-shaded symbols, pH calculated from eq 7 with $u = 1$. See text.

alluded to in the Introduction, it is this striking divergence of the experimental findings from the theoretical expectations which is the focus of this paper.

It should be noted that while some arbitrariness might be ascribed to the choice of values for the parameters used in the theoretical model, the possible modification in these values would affect the theoretical curve in only minor ways and certainly would not affect its shape. Likewise, a small latitude in the choice of $K_2°$ values would produce no significant change in the magnitude and no change at all in the curvature of the experimental curve at α greater than 1.2 where eq 1 can be approximated by the simple form

$$\mathrm{pH} = pK_2° - \log \frac{\alpha^*}{1 - \alpha^*} + 0.434\phi \qquad (8)$$

To estimate qualitatively the possible effect of changing molecular dimensions on the electrostatic potential, we are presenting in Figure 3 the reduced viscosity, η_{sp}/C_p, expressed in liters per monomole, of each of the two samples as a function of α. The polymer concentration $C_p = 7 \times 10^{-3}$ monomol/l., was low enough to make this a reasonable approximation to the intrinsic viscosity. We note that the reduced viscosity increases by a factor of about 6 as α changes from 0.2 to 1.0, but increases by only a factor of 2 between $\alpha = 1$ and $\alpha = 1.9$. We would therefore expect that at low α where the polyacid molecules are strongly coiled the real electrostatic potential rises somewhat faster with increasing α than would be predicted on the basis of the rod model. Such an effect might indeed explain the small divergence between the experimental and theoretical curves in the primary titration region. However, as α increases and the macroion uncoils, one would expect the potential to rise more slowly and to approach the curve predicted by the rod model. It has been shown that the rod potential is a satisfactory approximation if the radius of curvature of the polymer chain is large compared to the characteristic Debye–Hückel length.[7,19] This criterion should be well satisfied in the secondary titration region to which the following treatment applies.

Having failed to find a clue to the observed anomaly from the examination of the molecular dimensions, we turn now to the consideration of nearest-neighbor inter-

(19) U. P. Strauss, *J. Amer. Chem. Soc.*, **80**, 6498 (1958).

actions between dicarboxylic acid groups. This hypothesis is tested in Figure 4 where the experimental pH values are compared with those calculated by means of eq 7 for the interval $0.3 < \alpha^* < 0.8$. The theoretical values of $0.434|e\psi/kT|$ used are those given in Figure 2. The parameter u was adjusted for best fit. It is seen in Figure 4 that quite good agreement between experimental and calculated pH was obtained with $u = 0.10$ for HVMEMA and $u = 0.22$ for HEMA. These small values of u indicate a strong alternating tendency for the distribution of singly and doubly ionized dicarboxylate groups along the polymer backbone. For comparison pH curves calculated by eq 7 with $u = 1$, *i.e.*, with neglect of neighbor interactions, are also included in Figure 4.

It is useful to speculate concerning the molecular origin of these results. From the definition of the u_{AB}'s we have

$$\Delta F/kT = -2.3 \log u \tag{9}$$

where $\Delta F = F_{00} + F_{11} - 2F_{01}$. Accordingly, the values of $\Delta F/kT$ for HVMEMA and HEMA are 2.3 and 1.5, respectively.

Let us examine the possibility that these free energies are simple electrostatic interactions. Then we can write

$$F_{AB}/kT = \frac{z_A z_B e^2 \exp(-\kappa r)}{DrkT} \tag{10}$$

where $z_A e$ and $z_B e$ are the charges on nearest-neighboring carboxylate groups, r is the distance between them, D is the dielectric constant of the medium, and κ is the Debye–Hückel parameter. Letting $D = 78$, the bulk dielectric constant of water, and $r = 5$ Å we obtain $\Delta F/kT = 0.86$, a value significantly smaller than those observed.

It might appear that better agreement can be obtained by arbitrarily choosing an effective dielectric constant lower than the bulk value. However, with any constant value for D, F_{00} is equal to $2F_{01}$, which will lead to the result that $\Delta F = F_{11}$; *i.e.*, ΔF will have the same predicted value for the primary as for the secondary titration region. The observations, on the contrary, indicate little unusual behavior in the primary region, pointing to a small value of ΔF there.

This difficulty would be overcome if different effective dielectric constants were to apply to the different interactions. A good case can indeed be made for the validity of such an assumption. From the observed volume changes resulting from the ionization of HVMEMA and HEMA it may be deduced that a doubly ionized dicarboxylate group carries more than 20 bound water molecules, practically all of which are released upon the binding of a hydrogen ion.[11] One may therefore surmise that the dielectric constant of the dense bound water surrounding a doubly charged group is significantly lower than the dielectric constant of the normal water surrounding a singly charged group.

To illustrate the consequences of this view, let us arbitrarily assume that the effective dielectric constant for the interactions between two doubly ionized groups is 50 which results in $F_{00}/kT = 5.40$. Using $D = 78$ for the interaction between two singly charged groups yields $F_{11}/kT = 0.86$. For the interaction between a singly and a doubly charged group it seems reasonable to choose the mean of the above values, *i.e.*, 64, for the effective dielectric constant, leading to $F_{01}/kT = 2.10$. In this way we obtain $\Delta F/kT = 2.06$ which is close to the experimentally obtained values.

These calculations should be considered as illustrative only. The uncertainties in specifying effective distances, dielectric constants, and shielding parameters for a polyion are well known. However, we have shown that with a choice of plausible values for these parameters we can provide a feasible molecular explanation for the nearest-neighbor interactions and thereby for the abnormalities encountered in the potentiometric titration behavior of poly(dicarboxylic acids).

Association of Crystal Violet in Aqueous Solutions

by W. H. J. Stork, G. J. M. Lippits, and M. Mandel*

The Gorlaeus Laboratories, Department of Physical Chemistry III, The University of Leiden, Leiden, The Netherlands
(Received July 16, 1971)

Publication costs borne completely by The Journal of Physical Chemistry

The association of crystal violet in aqueous solutions has been studied using spectroscopy in the visible region. For concentrations below 10^{-3} M this association can be described by a dimerization equilibrium characterized by an association constant $K_d = 6 \times 10^2$ l. mol^{-1} at 20°. At concentrations above 10^{-3} M, higher aggregates are formed. Degrees of association for crystal violet in aqueous solutions obtained from vapor pressure measurements were in qualitative agreement with the interpretation of spectroscopic data.

We wish to report some spectroscopic results on the association of crystal violet (CV, [4-[bis[*p*-(dimethylamino) phenyl] methylene]- 2,5- cyclohexadiene-1-yliden]ammonium chloride) in aqueous solutions, obtained during an investigation of the binding of this dye to poly(methacrylic acid).[1,2] A few papers on the association of CV have already been published. In some of them[3-5] it was concluded from the concentration dependence of the CV spectrum that several aggregation equilibria occur simultaneously, though Krasnov and Shilova[6] interpret their spectroscopic data by a simple dimerization equilibrium. The aggregation has also been investigated by polarographic measurements; high degrees of association were reported.[7,8]

The results of the present paper were obtained with CV of commercial origin (U.C.B.), purified by repeated crystallization from water. The purified and dried samples, dissolved in water at 20°, had an extinction coefficient ϵ 0.98 $\times$ 10^5 l. mol^{-1} at the absorption maximum 16,900 cm^{-1} (for a concentration of 10^{-4} M), in agreement with literature values.[4,6,9,10] Absorption spectra in the range between 14,000 and 23,000 cm^{-1} were measured with a Zeiss-PMQ-II spectrophotometer; very dilute solutions only were investigated with a Unicam SP 700 recording spectrophotometer. Adsorption of the dye, especially to ground surfaces and luted interfaces, was found to be a source of experimental error for the dilute solutions. A reduction of the influence of this effect was achieved by pretreating all glassware with solutions of adequate concentrations.

CV solutions at 26 different concentrations C_0 ranging from 2.5×10^{-7} to 2.5×10^{-2} M were investigated. For each concentration at least two independent measurements were performed. Some results are represented in Figures 1-3.

At $C_0 < 10^{-5}$ M the spectra are characterized by a peak at 16,900 cm^{-1} and a shoulder at 18,000 cm^{-1}. A decrease of the dye concentration results in an overall lowering of the intensity of the spectrum without change of its shape (Figure 1). The rise of the extinction coefficient in the uv region upon dilution, as reported by Schubert, *et al.*,[4] was carefully investigated but *not confirmed*. Buffered solutions (potassium acid phthalate, 0.005 M) of CV within the same concentration range also exhibited an analogous, although somewhat smaller, lowering of the intensity in the visible region with decreasing C_0. Therefore, we are rather inclined to ascribe this effect primarily to *adsorption phenomena* as has been done for other dyes (*e.g.*, ref 11) instead of to hydrolysis of the dye.[6] As a systematic study of the adsorption at these low concentrations is very difficult, no final conclusion can be reached, although it seems unlikely that *association* processes, of the kind to be discussed at higher concentrations, are involved in this concentration range. For $C_0 > 10^{-5}$ M, a peak at 18,500 cm^{-1} rises at the expense of the peak at 16,900 cm^{-1}. All spectra intersect in a small region near 18,000 cm^{-1} for $10^{-5} \leq C_0 \leq 10^{-3}$ M, where an *isosbestic point* may be assumed to occur. This is shown in Figure 2, where the extinction coefficients ϵ for 21 different concentrations are represented in the frequency region near 18,000 cm^{-1}. At $C_0 > 10^{-3}$ M, definite deviations from this isosbestic point are observed. The spectra shift to higher wave numbers with increasing C_0 (Figure 3), in accordance with the results reported by Schubert and Levine.[4] The presence of

(1) W. H. J. Stork, Thesis, Leiden, 1970.

(2) W. H. J. Stork and M. Mandel, to be published.

(3) T. P. Kravets, A. L. Peskina, and Z. V. Zhidkoya, *Izv. Akad. Nauk SSSR, Ser. Fiz.*, **14**, 493 (1950).

(4) M. Schubert and A. Levine, *J. Amer. Chem. Soc.*, **77**, 4197 (1955).

(5) L. V. Levshin and V. K. Gorshkov, *Opt. Spectrosc.*, **10**, 401 (1961).

(6) K. S. Krasnov and G. W. Shilova, *Izv. Vyssh. Ucheb. Zaved. Khim. Khim. Teknol.*, **8**, 915 (1965).

(7) P. J. Hillson and R. B. McKay, *Trans. Faraday Soc.*, **61**, 374 (1965).

(8) W. U. Malik and P. Chand, *J. Electroanal. Chem.*, **19**, 431 (1968).

(9) R. B. McKay and P. J. Hillson, *Trans. Faraday Soc.*, **61**, 1800 (1965).

(10) T. Soda and K. Yoshioka, *J. Chem. Soc. Jap.*, **86**, 1019 (1965).

(11) M. E. Lamm and D. M. Neville, *J. Phys. Chem.*, **69**, 3872 (1965).

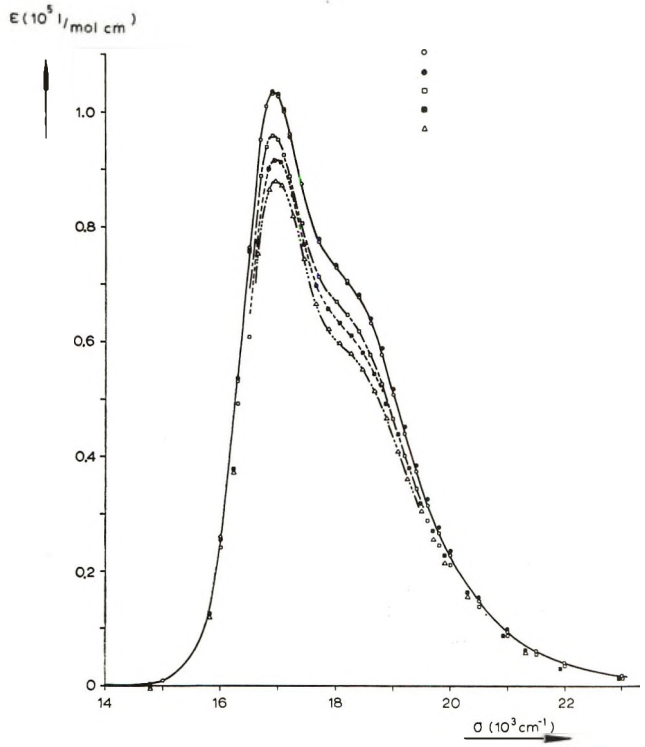

Figure 1. Absorption spectra of aqueous crystal violet solutions at various dye concentrations, $C_0 < 10^{-6}$ M: (○) 0.93×10^{-5}, (●) 4.89×10^{-6}, (□) 0.96×10^{-6}, (■) 4.90×10^{-7}; (△) 2.45×10^{7}.

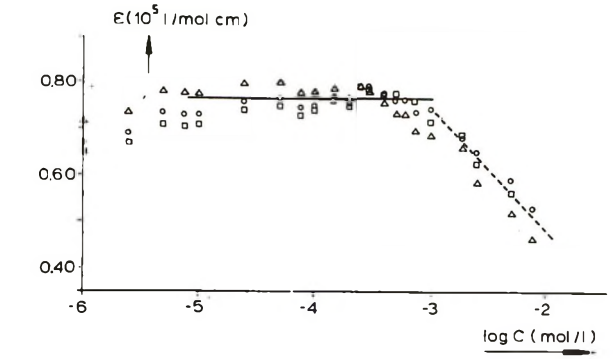

Figure 2. The extinction coefficient ϵ of aqueous crystal violet solutions as function of the concentration at σ = 17,800 (△), 18,000 (○), and 18,200 cm^{-1} (□).

NaCl, 2×10^{-3} M, has hardly any effect on the spectrum of a 10^{-4} M CV solution, indicating no influence of the counterion concentration. Assuming that an isosbestic point occurs near 18,000 cm^{-1}, the changes in the spectra observed for $10^{-5} \leq C_0 \leq 10^{-3}$ M may be interpreted by a single equilibrium (1) involving most likely a monomer and a dimer, in accordance with the conclusion reached by Krasnov and Shilova,[6] whereas

$$2(CV)^+ \rightleftharpoons (CV)_2^{2+} \qquad (1)$$

the particular features exhibited by the spectra at $C_0 > 10^{-3}$ M are probably due to the occurrence of higher aggregates. Therefore, the extinction coefficient of the dimer cannot be obtained by extrapolation of the apparent extinction coefficient ϵ to infinite concentration. A numerical approximation method was used to determine, from the spectral results at $10^{-5} \leq C_0 \leq 10^{-3}$ M, the dimerization constant K_d

$$K_d = (1 - x)/2C_0x^2 \qquad (2)$$

according to (1), x being the equilibrium fraction of monomer at each C_0 (deviations of the activity coefficients from unity were neglected at these low C_0's). This method, described by Lamm and Neville,[11] is a computerized version of the procedure derived by Bergmann and O'Konski[12] wherein K_d is assumed to have the value which yields the best fit, by a least-squares method, of the experimental points to the linear equation (at each wavelength)

$$\epsilon = E/C_0l = \epsilon_m x + {}^1/_2\epsilon_d(1 - x) \qquad (3)$$

Here E is the total extinction of the solution, l is the optical path length, ϵ_m and ϵ_d are the extinction coefficient of monomer and dimer, respectively, and x is calculated from (2) using arbitrary values for K_d. The uncertainty in K_d and ϵ_d was found to be rather large because the minima that are observed in the minimizing procedure of this method are rather broad (this may probably be explained by the fact that only

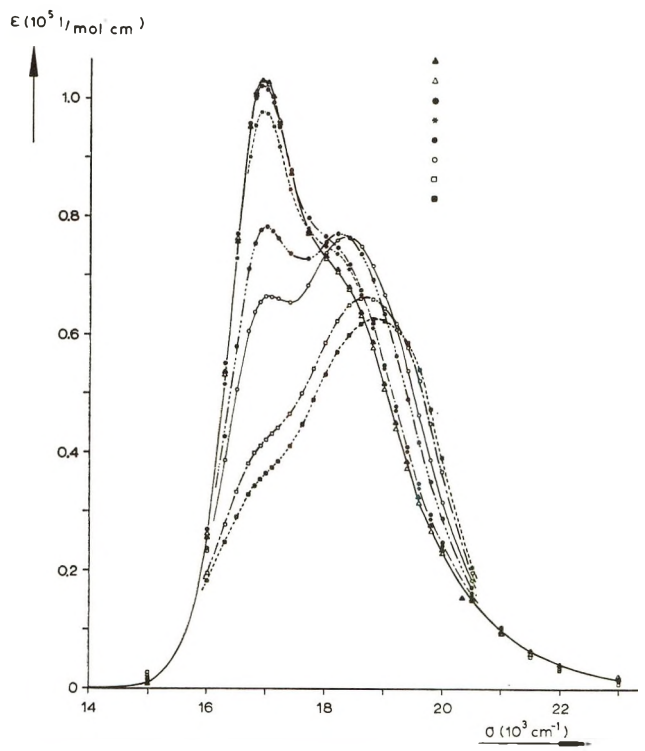

Figure 3. Absorption spectra of aqueous crystal violet solutions at various dye concentrations, $C_0 > 10^{-6}$ M: (▲) 4.89×10^{-6}, (△) 0.98×10^{-5}, (✱) 5.00×10^{-5}, (*) 0.98×10^{-4}, (●) 4.98×10^{-4}, (○) 0.99×10^{-3}, (□) 4.98×10^{-3}, (■) 0.99×10^{-2} M.

(12) K. Bergmann and C. T. O'Konski, *J. Phys. Chem.*, 67, 2169 (1963).

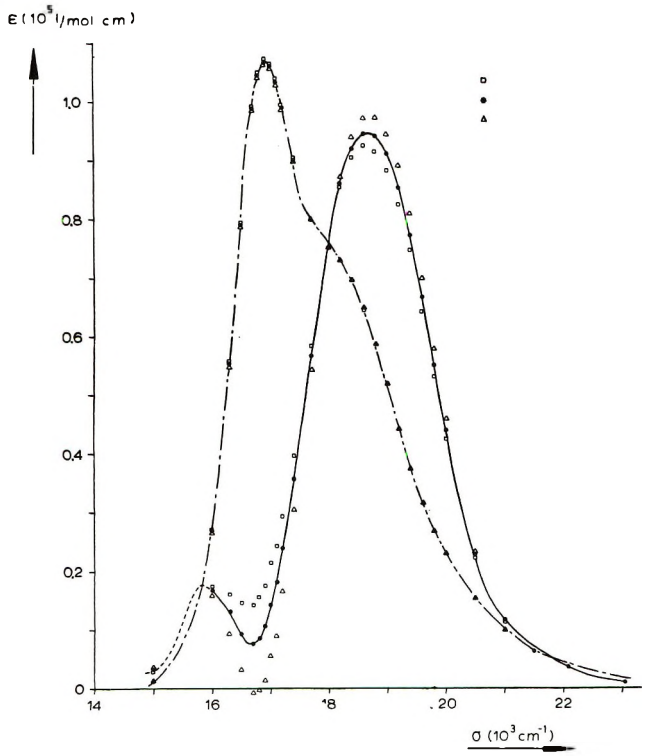

Figure 4. Absorption spectra of crystal violet monomer (- - -) and dimer (—) calculated for different values of K_d: (□) K_d = 7×10^2, (●) $K_d = 6 \times 10^2$, (△) $K_d = 5 \times 10^2$ l. mol^{-1}.

experimental results corresponding to low values of the degree of association can be used, data from more concentrated solutions being excluded in this method for fear of interference of higher aggregates).

From data at 17 wave numbers and all concentrations within the range $10^{-5} \leq C_0 \leq 10^{-3} M$, the value of K_d was estimated to be $(6 \pm 1) \times 10^2$ l. mol^{-1}, a value much lower than the one given by Krasnov and Shilova[6] ($K_d = 3 \times 10^5$ l. mol^{-1}). These authors assumed, however, that in a solution of $2 \times 10^{-3} M$ the dye is completely dimerized, an assumption which is not supported by the experimental results. With the help of the former K_d value, the monomer and dimer spectra were calculated, the results being shown in Figure 4 together with the influence of small deviations in the actual value of the dimerization constant. In Figure 5 experimental values of $\bar{\epsilon}$ and calculated values, using $K_d = 6 \times 10^2$ l. mol^{-1}, are compared at two wave numbers. The agreement is found to be satisfactory.

An attempt to analyze all spectra obtained within the range $10^{-5} \leq C_0 \leq 10^2 M$ by a computerized iteration procedure, including both a dimerization and a trimerization equilibrium, has failed due to lack of convergence.

Confirmation of the interpretation of the spectral results was sought by vapor-pressure measurements, using a Hitachi Perkin-Elmer 115 molecular weight apparatus, on aqueous CV solutions of concentrations $2 \times 10^3 \leq C_0 \leq 10^{-2} M$, although the observed vapor-

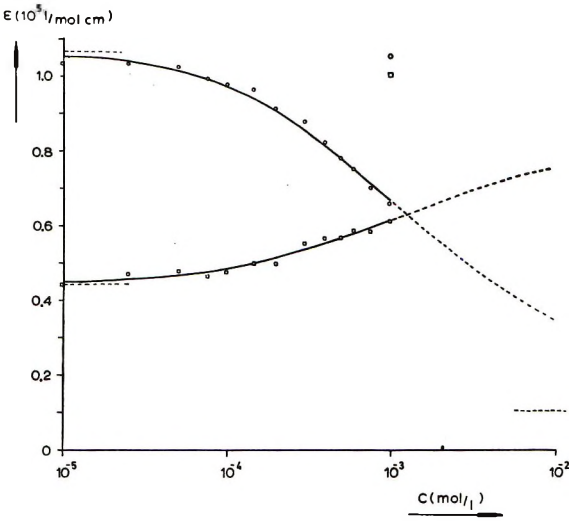

Figure 5. Comparison between experimental and calculated values of ϵ: (○) experimental points for σ = 16,900 cm^{-1}, (□) σ = 19.200 cm^{-1}; full curves are calculated with $K_d = 6 \times 10^2$ l. mol^{-1}.

pressure lowerings ΔP are at the limit of the possibilities of the instrument (the error in ΔP was estimated to be 7%). From ΔP the number-average degree of association Z of the dye was estimated with the help of Braswell's equation[13] (strictly valid only for a narrow distribution of aggregates[1] and if anions do not participate in the aggregation equilibrium). At the lowest concentration ($3 \times 10^{-3} M$) Z was found to be 1.8 ± 0.3, whereas at higher concentration Z increased to values larger than 3, in qualitative agreement with the interpretation of the spectroscopic data.

No evidence was found in this work for the high degrees of association at concentrations below $10^{-3} M$ which have been reported by Hillson and McKay[7] and Malik and Chand[8] using polarographic measurements. These results must, however, be considered with proper care. The aggregation number Z' was obtained from the square root of the diffusion coefficient D calculated from the limiting current i_d with the help of Ilkovic's equation and using a Cd salt of the same concentration as a standard and an empirical relation $D = AM^{-b}$ between molecular weight M and D (assuming A and b to be *constants* for $10^2 < M < 10^7$). It should be observed that, if several kinds of aggregates are present in the dye solution, the value of $D^{1/2}$ and Z' thus obtained will be averages (as is the case in our vapor-pressure measurements) which will depend on the actual distribution of aggregates according to the mechanism involved in the polarographic reduction yielding i_d. The authors did not analyze or investigate the exact nature of the averages obtained in their experiments. Furthermore, they calculated Z' assuming without further proof that the number of electrons n per monomeric

(13) E. Braswell, *J. Phys. Chem.*, **72**, 2477 (1968).

unit involved in the reduction of the dyes equals 2 in all cases. It is clear that if this assumption is not fulfilled the change of $D^{1/2}$ with C_0 as calculated from Ilkovic's equation will strongly be influenced by the eventual dependence of n on C_0. Also, the assumption of a single relation between D and M irrespective of the shape of the molecules is theoretically unsound. Finally, although the authors found the interfacial tension of mercury in the polarographic experiments to be reduced by the dyes, they did not investigate the possibility that the adsorption of the dyes may perturb the mechanism of the reduction leading to i_d.

Analyzing their polarographic measurements in such a way, Hillson and McKay found with unpurified CV for $10^{-5} < C_0 < 3 \times 10^{-5}$ M a constant Z' (although larger than unity) which increased at higher concentrations to $Z' = 5$ at 3×10^{-4} M. Malik and Chand,[8] using the same method, found even larger values for Z'. It is remarkable that for methylene blue the former authors claim their results to agree with these obtained from spectroscopic measurements by Bergmann and O'Konski[12] (who used the same approach as in the present work for CV) although they found at a concentration of 10^{-4} M a value of $Z' = 3$ instead of $Z' = 2$ as derived spectroscopically, this difference being "explicable by shape factors."

Coordination of Fluoride and Chloride Anions with Alcohol and Phenol[1]

by T. Kenjo, S. Brown,[2] E. Held,[3] and R. M. Diamond*

Lawrence Berkeley Laboratory, University of California, Berkeley, California 94720 *(Received November 29, 1971)*

Publication costs assisted by Lawrence Berkeley Laboratory

The extraction of tetraalkylammonium fluoride and chloride into solutions of benzyl alcohol and *p*-nonylphenol in toluene and in isooctane has been studied. In the organic-phase concentration regions studied, these species are associated to ion pairs. The results of slope analysis and of water determination by the Karl Fischer method suggest that the extracted fluoride species tend to involve a first-shell coordination number of four. For the extracted chloride species, the number seems less well defined, but the saturated limit may well be four also.

Introduction

In recent years, there has been renewed interest in the coordination or solvation of simple anions.[4-13] Most of these solvation studies of salts have been carried out by ir or uv spectroscopic methods.[4-10,12] A number of workers have studied the effect of alkylammonium halides on the X–H stretching frequencies of some protic solvents. Spectral shifts attributed to X—H···anion hydrogen bonding were observed, and their magnitude generally decreased in the order $F^- > Cl^- > Br^- > I^-$,[6] although some workers[9,12] found an anomalous position for F^-, that is, $Cl^- > F^- > Br^- > I^-$. Using pressure–composition isotherms at low temperatures, definite integral numbers of fluoroform or chloroform have been found to coordinate to some tetraalkylammonium halides,[11] but no definite fluoride complex could be found. The effect of the anions on the pmr chemical shifts of a number of alcohols has also been investigated,[14] and the chemical shifts decreased in the order $Cl^- > Br^- > I^-$, indicating a decreasing interaction with alcohol in the same order.

A recent paper[13] on the extraction of tetraalkylammonium fluoride[15] into toluene by alcohols and phenols indicated that definite numbers of extractant molecules

(1) Work supported under the auspices of the U. S. Atomic Energy Commission.

(2) Summer Visitor, NSF High School Teachers Program, 1967.

(3) Summer Visitor, Undergraduate Research Participation Program, 1968.

(4) J. Bufalini and K. H. Stern, *J. Amer. Chem. Soc.*, **83**, 4362 (1961).

(5) J. B. Hyne and R. M. Levy, *Can. J. Chem.*, **40**, 692 (1962).

(6) A. Allerhand and P. v. R. Schleyer, *J. Amer. Chem. Soc.*, **85**, 1233 (1963).

(7) H. Lund, *Acta Chem. Scand.*, **12**, 298 (1958).

(8) M. J. Blandamer, T. E. Gough, and M. C. R. Symons, *Trans. Faraday Soc.*, **60**, 488 (1964).

(9) S. C. Mohr, W. D. Wilk, and G. M. Barrow, *J. Amer. Chem. Soc.*, **87**, 3048 (1965).

(10) S. Singh and C. N. R. Ras, *Trans. Faraday Soc.*, **62**, 3310 (1966).

(11) R. M. Deiters, W. G. Evans, and D. H. McDaniel, *Inorg. Chem.*, **7**, 1615 (1968).

(12) Yu. G. Frolov, V. V. Sergievskii, and G. I. Sergievskaya, *Zh. Neorg. Khim.*, **13**, 1909 (1968); *Russ. J. Inorg. Chem.*, **13**, 994 (1968).

(13) D. J. Turner, A. Beck, and R. M. Diamond, *J. Phys. Chem.*, **72**, 2831 (1968).

were involved in the organic-phase species. These molecules were surely hydrogen bonded to the F^-, as little interaction would be expected with large quaternary ammonium cations. Four benzyl or decyl alcohol molecules were required, and with the phenols, two species were observed: a two-phenol and a higher, probably four-phenol, F^- complex. This suggested the stepwise complexing of the F^- by phenol, as is commonly observed with metal cations and simple ligands.

It was of interest to try to obtain better data on the higher F^-–phenol complex or complexes and to see if the F^-–alcohol data in toluene could be extended to more dilute alcohol concentrations so as to look for lower complexes. We were also curious to see whether the same alcoholation number would be obtained with a different diluent, and whether Cl^- would show the same behavior or indicate a different alcoholation and phenolation number. The Cl^- ion is larger and could accommodate a larger number of molecules around itself, but for the same reason it is less basic than F^- and so needs less solvation.

Experimental Section

Reagents. Stock solutions of tetraalkylammonium fluorides were prepared by titrating the hydroxide salts with hydrofluoric acid to pH 8. The hydroxide salts were obtained by shaking suspensions of the iodides (Eastman Organic Chemicals, White Label) in water with silver oxide. Completion of the conversion was checked by addition of silver fluoride solution. Hydrochloric acid was used instead of hydrofluoric acid for preparation of the chloride salts. The fluoride concentration was standardized by a spectrophotometric determination of the accompanying tetraalkylammonium cation as described below, and the chloride solutions were standardized against silver nitrate solution using fluorescein as indicator.

Benzyl alcohol (Eastman Organic Chemicals, White Label) and *p*-nonylphenol (Rohm and Haas, industrial grade) were distilled under reduced pressure, and the middle fractions dissolved in toluene (Baker Chemical Co., analytical reagent) to give stock solutions. Similarly, benzyl alcohol solutions in isooctane (Mallinckrodt spectro grade) were also prepared.

The 118-min $^{18}F^-$ tracer was obtained from the reaction $^{16}O(^4He,pn)^{18}F$ by irradiating distilled water with α particles at the Berkeley 88-in. cyclotron. The 35-min $^{38}Cl^-$ tracer was produced by neutron capture on LiCl in the Mark III Triga Berkeley research reactor.

The Karl Fischer reagent used for water determination was Matheson Coleman and Bell, stabilized, premixed, single solution.

Procedure. The aqueous solutions of fluoride, containing $^{18}F^-$ tracer, were shaken for 90 min with equal volumes of the organic-phase solutions of alcohol or phenol. The phases were then centrifuged and separated. Duplicate 3-ml aliquots were taken from the organic layer, and 100- or 200-μl aliquots were removed from the aqueous phase and then diluted to 3 ml. These samples were counted in a well-type scintillation counter with a 5 cm × 5 cm Na(Tl)I crystal. The concentration of fluoride in each phase was calculated from the distribution coefficients obtained and the initial concentration of fluoride in the aqueous phase.

The procedure for experiments with chloride was similar, except that the chloride was usually determined spectrophotometrically by means of its accompanying tetraalkylammonium cation.[16] Samples of the solutions were diluted to concentrations between 10^{-5} and 10^{-4} *M*. Then, 5 ml of the diluted solution was shaken with 5 ml of 0.010 *M* sodium picrate, 5 ml of saturated magnesium sulfate solution, and 5 ml of chloroform (for the aqueous-phase determination) or 5 ml of distilled water (for the organic-phase determination). Absorbance of the picrate in the organic layer was measured against reagent blank at the absorption peak in each solvent, using 1-cm cells. With isooctane solutions, 5 ml of dichloroethane was added to complete the extraction of tetraalkylammonium picrate. For samples less than 10^{-5} *M* in salt concentration, 10-cm cells were employed. The wavelengths used were 375, 362, and 372 mμ for chloroform, toluene, and isooctane–dichloroethane mixture, respectively. Interference by alcohol or by phenol was negligibly small when its concentration was less than 0.010 *M*.

The volume ratio of organic to aqueous phase was in most cases 1:1, although ratios of 1:2 and 1:5 were used when the distribution was high enough to cause a depletion of the salt in the aqueous phase.

Water coextracted with the salt into the organic phase was determined by the Karl Fischer method, using an electrometric end point. Since the water uptake depended somewhat on the room temperature, the amount of water extracted by the toluene alone and by the extractant–toluene solutions were always measured also at the same time. All experiments were done at room temperature, 23 ± 2°.

Results and Discussion

The process of handling the data by slope analysis is similar to that employed in earlier work,[13] but in the present study, computer least-squares fits to a polynomial expansion in the extractant concentration were also made, as well as the graphical fits. The equation

(14) R. D. Green, J. S. Martin, W. B. McG. Cassie, and J. B. Hyne, *Can. J. Chem.*, **47**, 1639 (1969).

(15) In ref 13, the fluoride salt used was stated to be tetraheptylammonium fluoride; from the present work and additional experiments that have been performed, it is clear that the salt was mislabeled and that it was tetrahexylammonium fluoride. This does not change the argument presented in that paper on the solvation of the fluoride ion.

(16) R. R. Grinstead and J. C. Davis, Annual Summary Progress Report, Dow Chemical Co., to the Office of Saline Water, 1966–1967, p 65.

for the extraction of a tetraalkylammonium salt as an ion pair into a dilute solution of a protic extractant in an inert solvent can be written

$$n\mathrm{ROH(org)} + m\mathrm{H_2O} + \mathrm{R_4N^+} + \mathrm{X^-} \longrightarrow \mathrm{R_4N^+\cdots F^-\cdot}m\mathrm{H_2O}\cdot n\mathrm{ROH(org)} \quad (1)$$

with the corresponding equilibrium constant

$$\mathcal{K}_n^a = \frac{(\mathrm{R_4N^+\cdots F^-\cdot}m\mathrm{H_2O}\cdot n\mathrm{ROH})_0}{(\mathrm{R_4N^+})(\mathrm{F^-})(\mathrm{H_2O})^m(\mathrm{ROH})_0^n} = \frac{[\mathrm{R_4N^+\cdots F^-\cdot}m\mathrm{H_2O}\cdot n\mathrm{ROH}]_0 y_0}{(\mathrm{R_4N^+})(\mathrm{F^-})(\mathrm{H_2O})^m[\mathrm{ROH}]_0^n y_{\mathrm{ROH}}^n} = K_n^a \frac{y_0}{y_{\mathrm{ROH}}^n} \quad (2)$$

We shall usually employ concentrations rather than activities for the tetraalkylammonium salts, but in the more concentrated aqueous solutions, measured or estimated activity coefficients are used. However, it should be remembered that the equilibrium concentrations of the different species must be used. This requires that the amount of extractant complexed by water be considered if that water–extractant complex involves more than one molecule of extractant. Previous work[13] has shown that in the concentration range under investigation, the benzyl alcohol–water complex in toluene does involve two molecules of alcohol per molecule of water and follows the expression

$$K_{\mathrm{H_2O}} = \frac{[\mathrm{H_2O}\cdot m\mathrm{ROH}]_0}{[\mathrm{ROH}]_0^m(\mathrm{H_2O})} \quad (3)$$

with $m = 2$. These values have been rechecked in the present work. A lower concentration, 0.1 M alcohol, was also done and found to have a higher value than that extrapolated from the higher concentrations, possibly suggesting the appearance of a 1:1 benzyl alcohol–water complex.

Figure 1 shows a log–log plot of organic-phase water *vs.* *p*-nonylphenol concentration in toluene; the water extracted by toluene itself, calculated as the solubility of water in toluene (0.024–0.026, depending upon the temperature, 23 ± 2°) times the volume fraction of toluene, has been substracted. It can be seen that the points essentially lie along a line of unit slope, indicating that only one molecule of phenol is involved in the water complex, as previously found for 1-naphthol. The value of $K_{\mathrm{H_2O}} = 0.11$ (with $m = 1$) is only slightly lower than that of 0.15 determined for the more acidic 1-naphthol. However, there is a slight trend upward in the nonylphenol data, which, if real, suggests that a higher phenol–water species is forming at the higher phenol concentrations. In all of these cases we are assuming, but have not proved, that only one water molecule is in the extracted complex.

With low-dielectric-constant diluents such as toluene (ϵ 2.38 at 25°)[17] and isooctane (ϵ 1.94 at 20°C),[17] one

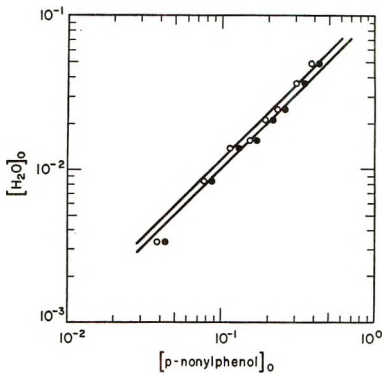

Figure 1. Variation of water content of organic phase (toluene diluent) with *p*-nonylphenol concentration: initial concentration of *p*-nonylphenol (●), equilibrium concentration of *p*-nonylphenol (○).

can expect the extracted complex to be an ion pair, and this can be checked by making a log–log plot of the organic-phase salt concentration, $[X^-]_0$, *vs.* the aqueous, $[X^-]$, holding the extractant concentration constant. A slope of two confirms the ion-paired nature of the extracted salt (with the reasonable assumption that it is dissociated in the aqueous phase). Then the complementary experiment of determining the slope of the log–log plot of $[X^-]_0$ *vs.* the equilibrium extractant concentration, $[ROH]_0$, holding the aqueous salt molarity constant, gives n, the coordination number of X^- toward the extractant.

In the previous paper, it was shown that the tetrahexylammonium fluoride–benzyl alcohol complex below $\sim 5 \times 10^{-3}$ M in toluene was indeed an ion pair.[13] Therefore, in Figure 2, which is an extension of the previous work to lower alcohol concentrations, the slope of the log–log plot of $[F^-]_0$ *vs.* [benzyl alcohol] indicates the average coordination number of F^- for alcohol at that point. The results at low alcohol concentration yield a slope of two; the curve at higher alcohol concentrations can be resolved into an additional component of slope four, the value previously found.[13] A least-squares fitting by computer to a power series expression in the alcohol concentration indicated the following equilibrium quotients for tetrahexylammonium fluoride and benzyl alcohol in toluene: $K_1^a = 3 \times 10^{-2}\ M^{-2}$, $K_2^a = 4\ M^{-3}$, $K_3^a = 3 \times 10^1\ M^{-4}$, $K_4^a = 3 \times 10^2\ M^{-5}$. This resolution of the curve is shown in Figure 2, and it can be seen that the 2:1 and 4:1 complexes predominate. A less complete study with tetraheptylammonium fluoride and benzyl alcohol yields, by graphical analysis, mainly 2:1 and 4:1 species, with $K_2^a = 2 \times 10^3\ M^{-3}$ and $K_4^a = 3 \times 10^5\ M^{-5}$.

Use of a chemically more inert diluent isooctane might be expected to change the magnitude of the extraction of F^- and possibly to affect the nature of the

(17) A. A. Maryott and T. R. Smith, "Table of Dielectric Constants of Pure Liquids," National Bureau of Standards Circular 514, U. S. Government Printing Office, Washington, D. C., Aug 1951.

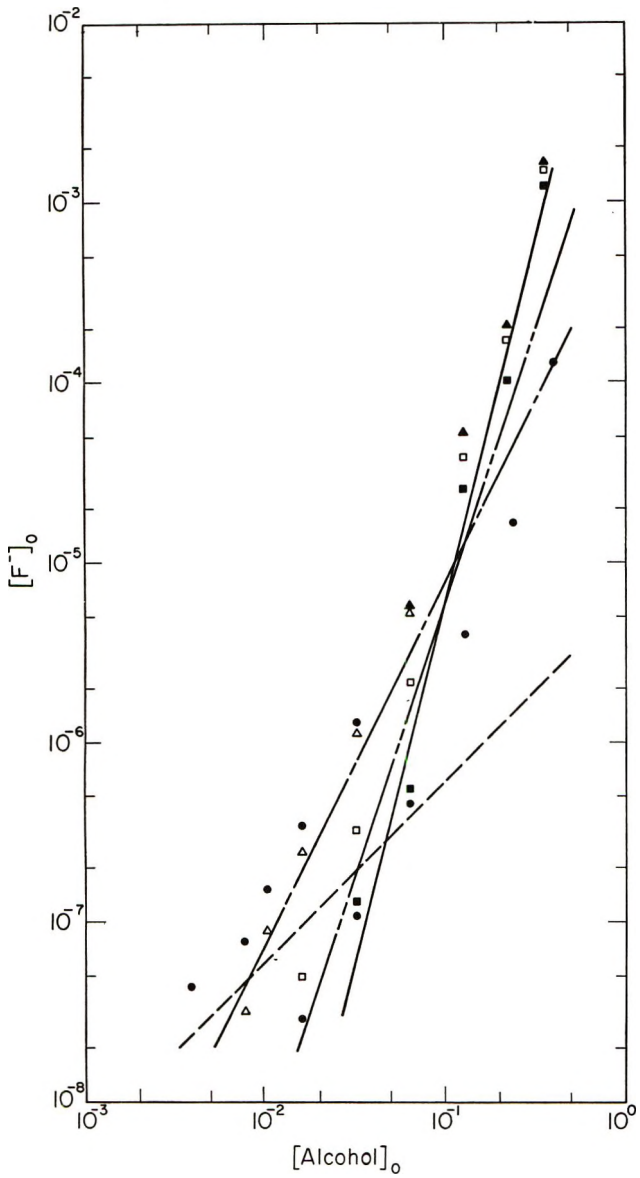

Figure 2. Dependence of tetrahexylammonium fluoride extraction on benzyl alcohol concentration in toluene at an initial aqueous fluoride concentration of 1.36×10^{-2} M (organic-phase blank of 1.00×10^{-7} M subtracted) and of 3.88×10^{-3} M (●); latter data corrected by factor of 11.8 to former data (▲). Monosolvate, by computer fit (– – –), total organic-phase fluoride minus monosolvate (△), disolvate (— – —), total fluoride minus mono- and disolvate (□), trisolvate (— – – —), total fluoride minus mono- di-, and trisolvate (■), tetrasolvate (—).

extracted species. Three experimental points (not shown) with varying benzyl alcohol concentration yield a slope of four, suggesting a tetrasolvate with the value $K_4^a = 2 \times 10^4$ M^{-5}. Little evidence for a disolvate appears in the limited concentrations region studied, 0.05–0.2 M alcohol, although equal amounts of the 4:1 and 2:1 species occur with ~0.1 M benzyl alcohol in toluene, and the latter species dominates at still lower alcohol concentrations. Probably the principal reason for the existence of the 4:1 complex in isooctane to lower alcohol concentration than in toluene is the greater chemical inertness of the aliphatic diluent relative to the aromatic. The alcohol's hydroxyl group can interact with the (basic) π-electron system of the latter solvent and so has a decreased effective concentration or activity compared to the same concentration in isooctane. The greater inertness of isooctane also means that the fluoride complex must obtain its solvation more completely from the alcohol and less from the diluent. Both of these effects enhance the proportion of (coordinatively) saturated 4:1 complex with respect to the lower complexes in isooctane compared to toluene for a given alcohol concentration. Finally, the lower dielectric constant of isooctane contributes to the 15-fold lower K_4^a of the ion pair than in toluene.

To confirm the higher (than two) solvate of phenol with F^- suggested earlier,[13] a study with nonylphenol in toluene was performed. Use of the more soluble phenol derivative, *p*-nonylphenol, rather than *p*-phenylphenol, makes possible an extension to higher phenol concentrations, as shown in Figure 3. The data have been taken at three aqueous salt concentrations, which have been normalized in the figure to the middle concentration. Resolution of the resulting curve appears more complicated than with benzyl alcohol, as no complex (slope) dominates over an appreciable concentration range. Computer least-squares fits yield equilibrium quotients of $K_1^a = 3.4$ M^{-2}, $K_2^a = 6.9 \times 10^3$ M^{-3}, $K_3^a = 2.2 \times 10^6$ M^{-4}, $K_4^a = 7.6 \times 10^7$ M^{-5}, showing a regular change as the number of phenols complexed increases. The ratios of these quotients show a steady decrease, a factor ~8 ($K_2/K_1 \sim 2000$, $K_3/K_2 \sim 300$, $K_4/K_3 \sim 35$), in contrast to the irregular behavior with benzyl alcohol ($K_2/K_1 \sim 133$, $K_3/K_2 \sim 7.5$, $K_4/K_3 \sim 10$). These patterns suggest that the process with phenol is the same type of reaction occurring over again in each step, *e.g.*, the replacement of a water molecule in the first coordination shell of F^- with a phenol molecule, while that with alcohol may involve a change in mechanism during the steps. It does seem, however, that four is the maximum number of alcohol or phenol molecules coordinated; allowance for a 5:1 complex did not improve the computer fits. It should also be noted that the more acidic, and so more strongly hydrogen bonding, phenol molecules increase the extraction of the tetrahexylammonium fluoride by three to five orders of magnitude over that with benzyl alcohol.

The behavior of chloride ion toward protic extractants may be different from that of fluoride. It is a bigger anion and so can sterically accommodate more solvating molecules. On the other hand, because of its larger size, it needs solvation less, and so might require fewer extractant molecules. A plot of tetrapentylammonium chloride concentration in the toluene phase *vs.* its concentration in the aqueous phase from 3 ×

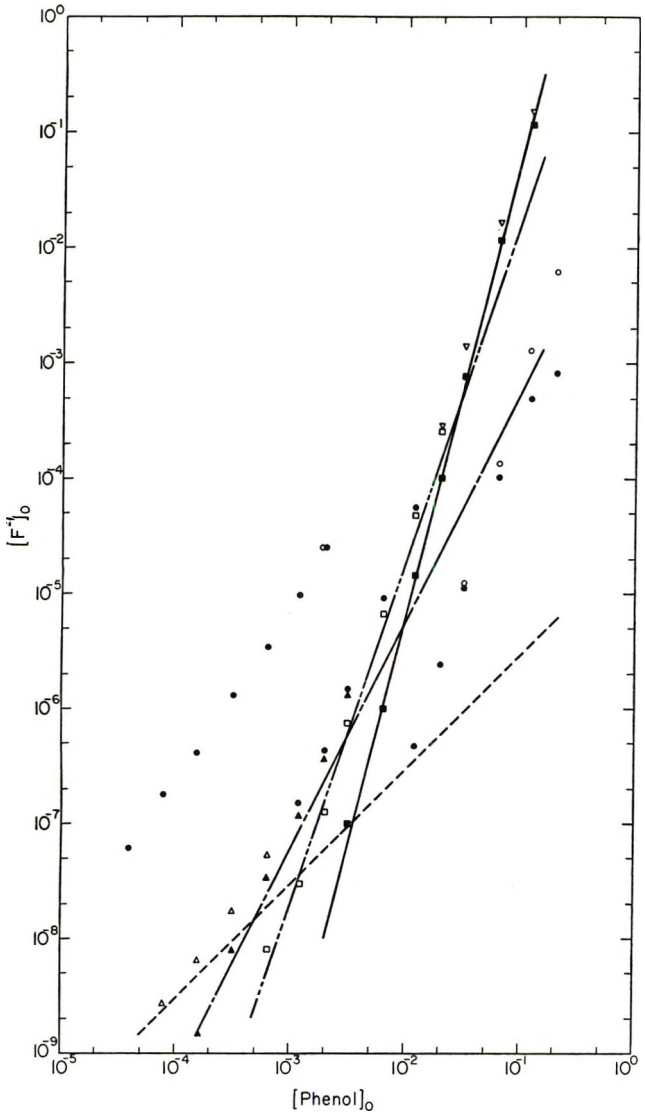

Figure 3. Dependence of tetrahexylammonium fluoride extraction on *p*-nonylphenol concentration in toluene at initial aqueous fluoride concentrations of 2.60×10^{-2}, 2.95×10^{-3}, and 2.60×10^{-4} M (●), corrected to constant (initial) equilibrium aqueous fluoride concentration (○). Data from 2.60×10^{-2} and 2.60×10^{-4} *M* curves normalized to fit 2.95×10^{-3} *M* points (△ and ▽, respectively). Monosolvate, by computer fit (— — —), total organic-phase fluoride minus monosolvate (▲), disolvate (— - —), total fluoride minus mono- and disolvate (□), trisolvate, (— - - —), total fluoride minus mono-, di-, and trisolvate (■), tetrasolvate (—).

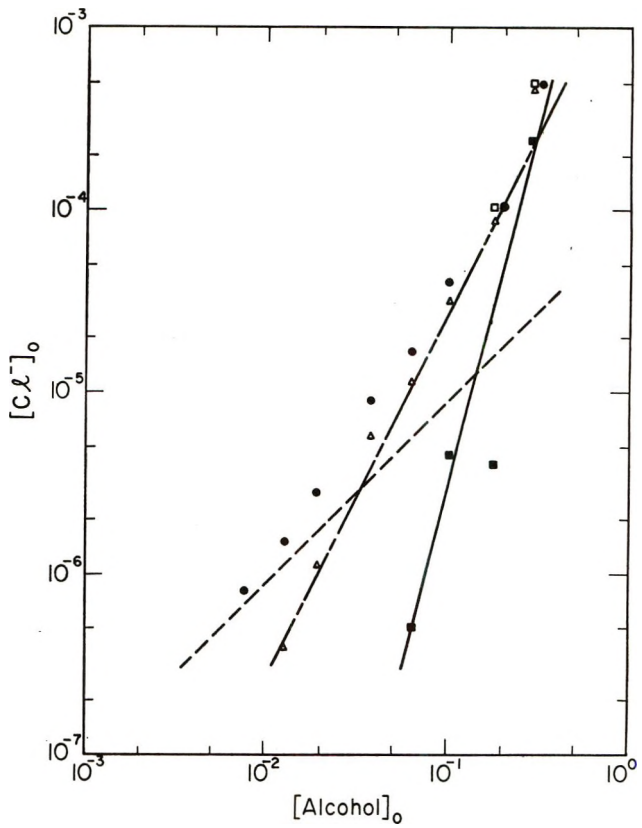

Figure 4. Dependence of tetrapentylammonium chloride extraction on benzyl alcohol concentration in toluene at an initial aqueous fluoride concentration of 2.19×10^{-2} *M* with blank (1.53×10^{-6} *M*) subtracted (●), correction for alcohol used up by water (□). Monosolvate, by computer fit (— — —), total organic-phase chloride concentration minus monosolvate (△), disolvate (— - —), total chloride minus mono- and disolvate (■), tetrasolvate (—). Resolution into mono-, di,- and trisolvates gives almost as good a fit.

10^{-4} to 4×10^{-2} *M* for 0.32 *M* benzyl alcohol gave a slope of two, indicating ion-pair formation under these conditions. Figure 4 shows a plot of extracted tetrapentylammonium chloride *vs.* benzyl alcohol concentration in toluene; the curve can be resolved into components representing 1:1, 2:1, and a higher complex. It can be seen that with the chloride anion the higher complexes occur at higher alcohol concentrations than with fluoride. This makes it harder to resolve the higher complexes in the range of alcohol concentrations available. In the present case, the computer fit for 1:1, 2:1, and 3:1 species is almost as good as for 1:1, 2:1, and 4:1 species, and both sets yield the values $K_1^a = 0.1\ M^{-2}$ and $K_2^a = 3\ M^{-3}$. But there simply are not enough data at high alcohol concentrations to unambiguously determine K_3^a and/or K_4^a. We can only say that there is at least one more higher complex, and we have shown it as a 4:1 complex in Figure 4, as this gives a somewhat better fit than the 3:1 complex. Also, the fact that a given complex with Cl^- occurs at a higher alcohol concentration than with F^- indicates, as do the larger values of K^a, that the most important difference between Cl^- and F^- is the less urgent need for hydration and solvation of the former anion.

With the more inert and lower dielectric constant diluent isooctane, a plot of extracted tetrahexylammonium chloride *vs.* benzyl alcohol concentration (not shown) indicates the existence of only a 4:1 complex from 0.20 to 0.05 *M* benzyl alcohol. The value of K_4^a obtained for tetrahexylammonium chloride in this case is $2.4 \times 10^3\ M^{-5}$, and again, as with F^-, the range of 4:1 species overlaps the region of alcohol concentration which with toluene as diluent yields lower solvates.

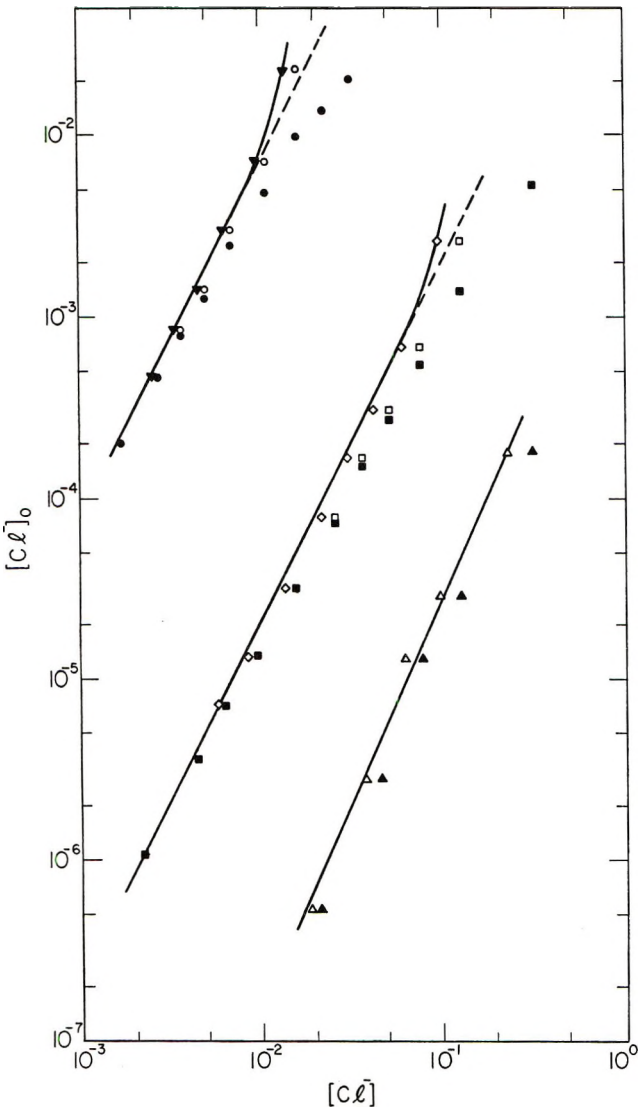

Figure 5. Dependence of tetrapentylammonium chloride extraction on aqueous chloride concentration: initial concentration of *p*-nonylphenol = 1.18 10^{-1} *M* (●), data corrected to a constant (initial) equilibrium concentration of *p*-nonylphenol (○), corrected to mean ionic activity of aqueous chloride (▼), initial concentration of *p*-nonylphenol = 1.05 × 10^{-2} *M* (■), data corrected to a constant (initial) equilibrium concentration of *p*-nonylphenol (□), corrected to mean ionic activity of aqueous chloride (◇); extraction by toluene alone (no phenol) (▲), corrected to mean ionic activity of aqueous chloride (△).

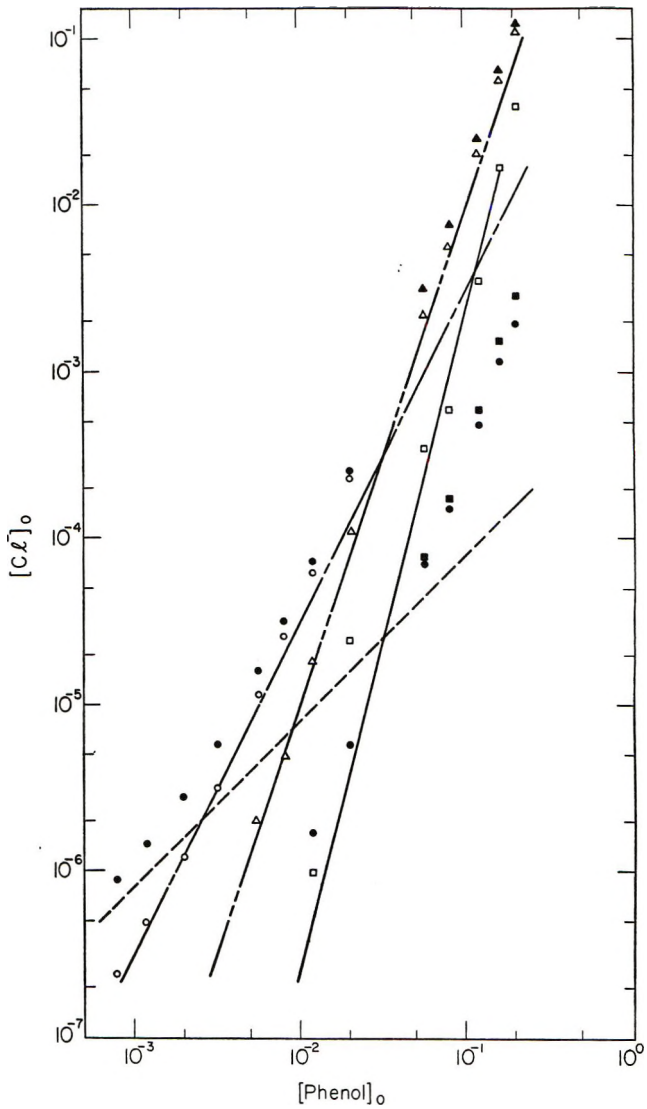

Figure 6. Dependence of tetrapentylammonium chloride extraction on *p*-nonylphenol concentration in toluene at fixed chloride concentrations: initial aqueous chloride concentration of 1.92 × 10^{-2} *M* (organic-phase blank of 1.68 × 10^{-6} *M* subtracted) and of 2.21 × 10^{-3} *M* (●), corrected to constant (initial) equilibrium aqueous chloride concentration (■); data from 2.21 × 10^{-3} *M* aqueous chloride normalized up (by factor of 43.6) to curve for 1.92 × 10^{-2} *M* aqueous chloride (▲); monosolvate by computer fit (— — —), total organic-phase chloride concentration minus monosolvate (○), disolvate (— - —), total chloride minus mono- and disolvate (△), trisolvate (— - - —), total chloride minus mono-, di-, and trisolvate (□), tetrasolvate (—).

Thus, with the relatively inert isooctane which cannot solvate either the alcohol or the extracted anion as well as can toluene, the extraction of the anion is hindered and it must achieve solvation in the organic phase more completely with the alcohol. The result is more complete formation of the saturated alcohol complex than with toluene as diluent and again this appears to be a 4:1 species.

Figure 5 shows a log–log plot of organic-phase tetrapentylammonium chloride concentration *vs.* the aqueous-phase salt concentration for two *p*-nonylphenol solutions in toluene, as well as for blank solutions containing no phenol. After correcting for the aqueous-phase activity coefficients, estimated from smooth curves drawn through the data of Lindenbaum and Boyd[18] above 0.1 *M* and from an evaluation of Poirier's expressions[19] below 0.01 *M*, it can be seen that over most of the range studied, straight lines of slope two are

(18) S. Lindenbaum and G. E. Boyd, *J. Phys. Chem.*, 68, 911 (1964).
(19) J. C. Poirier, *J. Chem. Phys.*, 21, 972 (1953).

obtained, showing the existence of ion pairs in the organic phase. However, the tops of both curves do deviate upward from the lines drawn with slopes of two; this may indicate an error in the increasingly large corrections applied, or that the species are really starting to aggregate beyond the ion pair. Thus, data for the log–log plots of tetrapentylammonium chloride extracted *vs.* the *p*-nonylphenol concentration at constant aqueous salt molarity should be taken below an organic-phase chloride concentration of a few times 10^{-3} *M*. In order to achieve this and to hold down the size of the corrections for changes in the aqueous-phase salt concentrations by extraction, the measurements shown in Figure 6 were taken in two sections, normalized together by overlapping points at 1.20×10^{-2} and 2.00×10^{-2} *M* phenol. The curve is complex; resolution by a computer least-squares-fit leads to 1:1, 2:1, 3:1, and 4:1 nonylphenol chloride complexes in the range of phenol concentrations studied. The values of the equilibrium quotients so obtained are: $K_1^a = 2.2$ M^{-2}, $K_2^a = 8.7 \times 10^2$ M^{-3}, $K_3^a = 2.7 \times 10^4$ M^{-4}, and $K_4^a = 7 \times 10^4$ M^{-5}, respectively, for this extraction of tetrapentylammonium chloride by *p*-nonylphenol in toluene. Again, as with F^-, the stepwise formation of the phenol complexes seems to be quite regular with the ratios of consecutive quotients, $K_2^a/K_1^a \sim 400$, $K_3^a/K_2^a \sim 30$, $K_4^a/K_3^a \sim 2.6$, decreasing each time by a roughly constant factor ($\sim$12). Again, we think this suggests that the same process is taking place at each step (although the factor of $\sim$12 is larger than the statistical factor for simple replacement, $\sim$2). Rather similar results have been obtained for the extraction of tetrabutylammonium chloride by 1-naphthol in toluene, except that extraction is a little higher (values of K^a somewhat larger) because of the greater acidity of 1-naphthol over nonylphenol.

Just as with benzyl alcohol as extractant, the concentration of phenol necessary to yield a particular average coordination number is higher with Cl^- than with F^-, again reflecting the former anion's less urgent need for solvation. Similarly, the higher values of K^a for Cl^- show that the weaker hydration of the Cl^- in the aqueous phase makes its extraction easier.

Additional information on the nature of the various complexes of F^- and Cl^- is furnished by the determination of the amounts of water coextracted with them, as given in Tables I–V. The water dissolved in toluene alone has been subtracted from the data shown in the $[H_2O]_{tot}$ column of the tables. The column labeled $\bar{n}$ lists the ratio of the average number of phenol or alcohol molecules complexed per halide ion, as determined from the slope of the appropriate plot at the corresponding free extractant concentration in Figures 2–6. The amount of water associated with the anion is obtained by subtracting the amount of water bound to uncomplexed phenol or alcohol from the total amount of water in the organic-phase $[H_2O]_{tot}$. After determining the amount of uncomplexed extractant by subtracting the appropriate multiple (the average coordination number, $\bar{n}$) of the anion concentration from the total extractant concentration, the water bound to the uncomplexed extractant is obtained by interpolation from additional experiments performed at the same time (and thus at the same temperature) using extractant–toluene solutions equilibrated with water alone.

Table I: Water Coextracted with Tetraheptylammonium Fluoride into 0.0971 *M* *p*-Nonylphenol in Toluene

$[THpAF]_0$	$\bar{n}$	$[phenol]_{free}$	$[H_2O]_{tot}{}^a$	$[H_2O]$	$[H_2O]/[THpAF]_0$
0.00912	3.5	0.065	0.0124	0.0059	0.6
0.0184	3.4	0.034	0.0148	0.0114	0.6
0.0329	2.8	0.005	0.0283	0.0278	0.9
0.0430	2.2	0.001	0.0818	0.0817	1.9

[a] Water dissolved in toluene alone subtracted.

Table II: Water Coextracted with Tetrapentylammonium Chloride into 0.115 *M* *p*-Nonylphenol in Toluene

$[TPAC]_0$	$\bar{n}$	$[phenol]_{free}$	$[H_2O]_{tot}{}^a$	$[H_2O]$	$[H_2O]/[TPAC]_0$
0.0114	2.8	0.0828	0.0153	0.0071	0.6
0.0180	2.7	0.0658	0.0158	0.0093	0.5
0.0277	2.6	0.0429	0.0173	0.0131	0.5

[a] Water dissolved in toluene subtracted.

Phenol is more acidic than water,[20] so that it should hydrogen bond more strongly to anions than does water. Thus with (small) strongly solvated anions where these molecules can be bound into a first-shell coordination sphere, it might be expected that phenol can displace water molecules from the first shell. From Table I, it can be seen that with F^- the 4:1 phenol complex has very little water associated with it and that the 2:1 complex has *ca.* two water molecules with it. We believe that the sum of the water and phenol numbers indicates that the higher phenol–fluoride complexes are essentially demonstrating a coordination number of four for F^-. These data are in agreement with the suggestion based on the equilibrium quotient ratios, that with phenol each step involves the replacement of a water in the first coordination shell with retention of a fixed coordination number. In this case the number is four.

The water uptake situation seems less clear with the chloride anion. Tables II and III indicate that, as the average number of complexed phenols increases from

(20) R. A. Robinson and R. H. Stokes, "Electrolyte Solutions," 2nd ed, Butterworths, London, 1959, Appendix.

Table III: Water Coextracted with Tetrahexylammonium Chloride into 0.0200 *M* *p*-Nonylphenol in Toluene

$[THxAC]_{tot}$	$[THxAC]_0$[a]	$\bar{n}$	$[H_2O]_{tot}$[b]	$[H_2O]_{blank}$[c] THxAC	$[H_2O]$	$[H_2O]/[THxAC]_0$
1.09×10^{-2}	1.04×10^{-2}	1.6	0.0136	0.0016	0.0117	1.1
8.48×10^{-3}	8.13×10^{-3}	1.75	0.0102	0.0011	0.0085	1.0
5.75×10^{-3}	5.47×10^{-3}	1.95	0.0072	0.0009	0.0054	0.9

[a] Tetrahexylammonium chloride extracting into toluene alone (no phenol) subtracted from first column. [b] Water dissolved in toluene alone subtracted. [c] Ratio of water with uncomplexed tetrahexylammonium chloride to uncomplexed tetrahexylammonium chloride concentration is 3.2.

Table IV: Water Coextracted with Tetrapentylammonium Chloride into 0.500 *M* Benzyl Alcohol in Toluene

$[TPAC]_0$	$\bar{n}$	$[H_2O]_{tot}$[a]	$[H_2O]_{alcohol}$	$[H_2O]$	$[H_2O]/[TPAC]_0$
8.78×10^{-3}	3.1	0.0513	0.0363	0.0150	1.7
2.00×10^{-2}	3.1	0.0716	0.0320	0.0396	2.0

[a] Water dissolved in toluene alone subtracted.

Table V: Water Coextracted with Tetraheptylammonium Chloride into 0.100 *M* Benzyl Alcohol in Toluene

$[THpAC]_0$[a]	$\bar{n}$	$[H_2O]_{tot}$[b]	$[H_2O]_{alcohol}$	$[H_2O]_{blank}$[c] THpAC	$[H_2O]$	$[H_2O]/[THpAC]_0$
4.57×10^{-3}	1.8	0.0140	0.0037	0.0010	0.0093	2.0
6.63×10^{-3}	1.8	0.0186	0.0034	0.0013	0.0139	2.1
9.43×10^{-3}	1.8	0.0239	0.0030	0.0016	0.0193	2.0

[a] Tetraheptylammonium chloride extracting into toluene alone (no alcohol) subtracted. [b] Water dissolved in toluene alone subtracted. [c] Ratio of water with uncomplexed chloride to uncomplexed chloride concentration is 3.2.

1.6 to 2.8, the average number of water molecules involved decreases only from 1.1 to 0.6. Thus, the sum of the number of phenol and water molecules is not a constant and is closer to three than to four in this concentration range. Certainly, because of the lower electric field around the larger Cl^- ion, one might expect its first-shell water molecules to be bound less tightly than with F^-. The higher limiting equivalent conductance in water of Cl^- than F^- (ref 20), although Cl^- has the larger crystallographic radius, indicates, indeed, that fewer water molecules are carried along by Cl^-. In addition, other work in this laboratory[21] shows that the extraction of Cl^- without any extractant present leads to ~3 mol of water per Cl^- (F^- extracts with more). Yet with enough phenol present, four molecules of phenol can be bound to a Cl^-; and although it is only our assumption that they are all hydrogen bonded to the anion to form its first coordination shell, this does seem plausible. Thus, in the organic phase, when the chloride anion goes from solvation by water to solvation by phenol, it appears to increase its average number of solvation molecules from *ca.* three to four.

The water uptake of the benzyl alcohol complexes follows a still different pattern, but may indicate the same general behavior. The 4:1 F^- complex with alcohol has been previously shown[13] to involve *ca.* two water molecules, and Tables IV and V suggest that the average 2:1 and 3:1 alcohol–chloride species both have *ca.* two water molecules also. Since benzyl alcohol is much less acidic than phenol and probably comparable to (even less acidic than) water, it may not be able to displace all the water from the first coordination shell around the anions as can phenols. Thus the 4:1 alcohol complex with both anions may retain two water molecules in the first coordination shell, with two alcohols also in that shell and two more bound, not directly to the anion, but to the water molecules, thus providing the latter with solvation to their rear side and acting as a buffer between them and the organic diluent. Such an arrangement might explain why the 3:1 species shows up poorly with alcohol and F^-, but is a major component with phenol, since with the latter extractant, each step is the same, namely replacement of a water with a phenol molecule (or *vice versa*). This alcohol complexing sequence is also in agreement with the observed feature that, when using the more inert diluent isooctane, the 4:1 complex occurs more readily for both F^- and Cl^- than with toluene; since the lower complexes would have water molecules on the anion exposed to the poorly solvating isooctane diluent, these complexes would be somewhat more disfavored with respect to the saturated alcohol complex than in toluene.

The results of this work indicate that the complexation of F^- and Cl^- by water-immiscible phenols and alcohols is a stepwise process similar to the complexa-

(21) T. Kenjo and R. M. Diamond, to be published.

tion of cations by ligands. With phenols the process seems a quite regular replacement of water by the more acidic and more strongly hydrogen-bonding organic molecules, as indicated by the regular decrease in the ratios of K_i/K_{i+1} and by the decrease in coextracted water as the number of coordinated phenols increases. With benzyl alcohol, the process may be different; especially with F^- there is a favoring of the 4:1 and 2:1 species. In addition, both anions seem to retain *ca.* two water molecules with the 4:1 (F^-) and 3:1 (Cl^-) complexes. It is suggested that perhaps the less acidic alcohol molecules cannot displace these two waters from the first shell of the anions, but merely hydrogen bond to them. For F^-, the 4:1 species with either alcohol or phenol could be made dominant, and there was no indication, in the concentration range studied, of a higher complex. With Cl^-, it was not possible to go to high enough extractant concentrations to say anything about the higher complexes.

Acknowledgments. The authors wish to thank Mr. J. Bucher for advice and assistance in many stages of the work.

Apparent Molal Volume of Glycine, Glycolamide, Alanine, Lactamide, and Glycylglycine in Aqueous Solution at 25° and High Pressures

by A. A. Yayanos

Physiological Research Laboratory, Scripps Institution of Oceanography, University of California, San Diego, La Jolla, California 92037 *(Received August 16, 1971)*

Publication costs borne completely by The Journal of Physical Chemistry

The volume of aqueous solutions of glycine and of its uncharged isomer, glycolamide, of D,L-α-alanine and of its uncharged isomer, lactamide, and of glycylglycine has been determined at 25° and at pressures to 1000 atm. The apparent molal volume of the dipolar amino acids increases, whereas that of the uncharged isomers decreases with pressure. The rate of change with pressure is concentration and pressure dependent. The electrostriction decreases with increasing pressure and appears dependent on the dipole moment of the amino acid. The Fuoss-Kirkwood theory of the solvation of amino acids does not appear to be adequate to explain the magnitude of the pressure effect on the electrostriction. The PV isotherms approximately fit a Mie-type equation of state from which an estimate of their tensile strength was made. The tensile strength increased with concentration and was higher in the case of the amino acid solutions than in that of corresponding uncharged isomers.

Values of the partial and apparent molal volume of electrolytes in aqueous solution evidently increase with increasing pressure if the concentration and pressures are not too great (see, for example, Gucker,[1] Owen and Brinkley,[2] or Hamann[3]). Amino acids are dipolar ions, albeit to varying degrees, in aqueous solution,[4-6] and the values of their apparent molal volumes, as in the case of other electrolytes, reflect the electrostriction which occurs due to their interaction with water. Bridgman and Dow[7] determined the volume of aqueous solutions of three amino acids at pressures to about 10,000 atm. They stated that after a run their solutions were visibly and chemically contaminated. Consequently, partial molal volumes cannot be calculated with confidence from their data. Indeed, data reported here on glycine differ systematically from those in their paper. Cohn and Edsall[4] referenced some unpublished work of Gibson's which claimed that glycine behaved like other electrolytes in that its partial molal volume increased with pressure. The work of Gucker, *et al.*,[8] shows that glycine and β-alanine have negative

(1) F. T. Gucker, *Chem. Rev.*, **13**, 111 (1933).

(2) B. B. Owen and S. R. Brinkley, Jr., *ibid.*, **29**, 461 (1941).

(3) S. D. Hamann, "Physico-Chemical Effects of Pressure," Butterworths, London, 1957.

(4) E. J. Cohn and J. T. Edsall, "Proteins, Amino Acids and Peptides as Ions and Dipolar Ions," Reinhold, New York, N. Y., 1943.

(5) J. P. Greenstein and M. Winitz, "Chemistry of the Amino Acids," Vol. 1, Wiley, New York, N. Y., 1961.

(6) J. W. Larson and L. G. Heppler in "Solute-Solvent Interactions," J. F. Coetzee and C. D. Ritchie, Ed., Marcel Dekker, New York, N. Y., 1969.

(7) P. W. Bridgman and R. B. Dow, *J. Chem. Phys.*, **3**, 35 (1935).

apparent molar adiabatic compressibilities at 1 atm. The electrical contact method for determining PV isotherms was first extensively used by Amagat[9] with liquids and gases, by Michels and Michels[10] and others[11] with gases, and more recently by Eduljee, Newitt, and Weale[12] with liquids. The construction, use, and a new calibration method of an electrical contact piezometer is here described. An error analysis of the method is also given. Data are reported on aqueous solutions of glycine and of its uncharged isomer glycolamide, of D,L-α-alanine and of its uncharged isomer lactamide, and of glycylglycine. These data show that, up to 1000 atm at 25°, the apparent molal volume of the above dipolar amino acids increases with pressure and suggest that the magnitude of the increase with pressure is dependent on the dipole moment of the amino acid. The apparent molal volumes of glycolamide and of lactamide decrease with increasing pressure.

The PV isotherms have been fit to a Mie-type equation of state

$$P = A/V^4 - A/V_0V^3 \qquad (1)$$

where P is the pressure at volume V, V_0 is the volume at zero pressure, and A is a constant. The procedure of using this kind of equation to evaluate the tensile strength of a liquid is described by Hamann[3] and more recently by Yayanos.[13] It is used here to evaluate the tensile strength of the solutions.

Experimental Section

The electrical contact piezometer shown in Figure 1 was used. This method as well as Amagat's[9] *méthode des regards* give values of the volume of a fluid at high pressures independently of the compressibility of mercury. Another advantage of this method is that one filling of the piezometer serves to obtain about 8–11 data points. The piezometer shown in Figure 1 consists of a 98-cm long Pyrex glass stem and a Pyrex bulb which in the assembled state is joined by a ground-glass connection to the stem. Most of the measurements in this paper were done with a 60-cm long bulb with a volume of 11.952 cm³ at 25°. The volume of the bulb was determined several times at 1 atm by filling it with mercury at a known temperature. The volume was determined to ±0.001 cm³. Eleven platinum wires penetrate the wall of the capillary stem and are spaced along the length of the stem. Each wire was imbedded in a small bead of blue glass which in turn was imbedded in the Pyrex. Outside of the capillary, each of the platinum wires was joined to its neighbor by a nichrome resistance wire (not shown in Figure 1 for the sake of clarity). The volume of the stem between its open end and each of the contacts was determined at 1 atm by coupling the open end of the stem to a micrometer buret[14] which was filled entirely with mercury. Mercury was delivered with this buret into the stem of the piezometer. The volume of mercury needed to fill

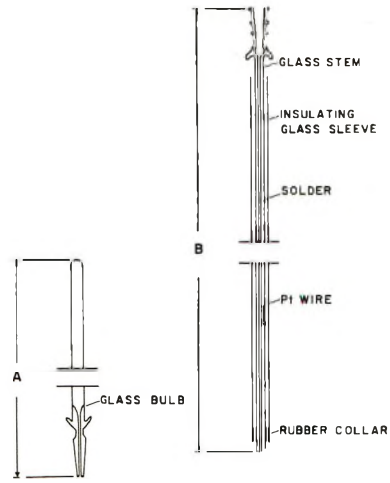

Figure 1. The piezometer. The bulb used here has a length, A, of 60 cm and the stem a length, B, of 98 cm.

the stem from the first contact to each of the other contacts was determined from the product of the difference in the readings of the micrometer and the calibration factor. The micrometer was read with an accuracy of ±0.002 mm. The calibration factor in cubic centimeters per millimeter was determined by weighing mercury which was delivered by a known displacement in millimeters of the micrometer spindle. The calibration factor for the micrometer (having a 0–25-mm graduated thimble) varied from 0.036945 ± 5 × 10^{-6} cm³/mm at the 0-mm end to 0.036855 ± 10 × 10^{-6} cm³/mm at the 25-mm end at 23°. The volume between the first contact and each successive contact was determined on many separate occasions over a period of 1 year. For example, buret displacements of 4.053, 4.056, 4.059, and 4.052 mm were obtained when filling with mercury the space between the first and fourth contacts at various times of the year. The values found in four separate trials were averaged and are (cm³) at 25°, 0.01714_4, 0.04199, 0.08575, 0.12479, 0.16678, 0.20803, 0.15131, 0.33344, 0.41458, 0.49386, 0.57537 for the volume between the open end and contacts 1 through 11, respectively. Although it has not been yet attempted, the errors associated with the stem volume determination possibly could be reduced (1) by the use of a better micrometer or (2) by constructing the open end of the stem with an opening smaller than the existing one of a 1-mm diameter. The volume of the piezometer

(8) F. T. Gucker, Jr., F. W. Lamb, G. A. Marsh, and R. M. Haag, *J. Amer. Chem. Soc.*, **72**, 310 (1950).
(9) E.-H. Amagat, *Ann. Chim. Phys.*, **29**, 68 (1893).
(10) A. Michels and C. Michels, *Proc. Roy. Soc., Ser. A*, **153**, 201 (1936).
(11) J. Saurel, *J. Rech. C.N.R.S.*, **31**, 129 (1957).
(12) H. E. Eduljee, D. M. Newitt, and K. E. Weale, *J. Chem. Soc.*, 3086 (1951).
(13) A. A. Yayanos, *J. Appl. Phys.*, **41**, 2259 (1970).
(14) P. F. Scholander, *Science*, **95**, 177 (1942).

from the 11th contact to the origin of the bulb in the ground-glass connection was determined by displacing water with the micrometer buret.

It should be remarked that the glass sleeve (10-mm o.d., 8-mm i.d.) which was slipped over the glass stem, as shown in Figure 1, serves to insulate the nichrome resistance wire from the wall of the pressure vessel and the mercury as well as to diminish the chance of breakage of the delicate glass stem.

The pressure vessel was made from a 6-ft length of 316 stainless-steel seamless tubing having a 1.5-in. o.d. and a 1-in. i.d. Each end of the tube was machined for an O ring closure,[15] and the closures were machined for connection to 0.25-in. o.d. high-pressure tubing. An electrical lead was passed through one of the caps. The electrical lead was made by first filling with epoxy (Conap. Inc., Allegany, N. Y.), which was delivered from a disposable syringe, a 3.5- to 4-in. length of high-pressure tubing (0.25-in o.d., 0.083-in. i.d.) which was threaded at one end for a high-pressure connection. Then a No. 16 enameled copper wire (Belden, Chicago, Ill.) was gradually worked through the tubing while the epoxy was still soft. The tubing was joined to a straight-through connector having a female high-pressure fitting on both ends. The epoxy was allowed to set overnight. The use of epoxy to make electrical leads for work to over 20,000 atm has been described by Davis, *et al.*[16] The one described here is not as sturdy as that of Davis, *et al.*, but has been used in our laboratory to 2500 atm. It was positioned so that an accidental failure (which has never been experienced) would be harmless. The water jacket was surrounded by a 2-in. layer of polystyrene foam. The pressure vessel was mounted vertically and pivoted at its center to allow easy loading. A cup of mercury was placed at the bottom of the vessel and a platinum wire kept the mercury in electrical contact with the pressure vessel. The piezometer, filled with a solution and at a lower temperature than that of the pressure vessel, was carefully slipped into the pressure vessel. The wire from the uppermost contact was joined to the wire which passed through the cover of the pressure vessel. At least 1 hr elapsed before pressure was increased to assure that the temperature of the contents of the piezometer was the same as that of the jacket around the pressure vessel. Just prior to increasing the pressure, the piezometer was lifted carefully so that its open end was slightly above the mercury, and then again placed beneath the mercury surface. This maneuver assured that the piezometer did not have a drop of solution trapped outside of its free end. The drop can form as the contents of the piezometer expand during the hour of thermal equilibration. Water at 25° was circulated through the jacket by means of a Haake Model FT constant-temperature circulator which was coupled to a Haake Model KR-30 refrigerated chiller (Polyscience Corp., Evanston, Ill.). The temperature of the contents of the pressure vessel was kept constant within 0.01°.

The electrical resistance between the pressure vessel (in electrical contact with the mercury) and the wire initially had a large value as measured with a Wheatstone bridge. The pressure was gradually increased with a screw piston pump (Ruska Instrument Co., Houston, Texas) until an abrupt change in resistance was detected. This indicated that the column of mercury had risen in the stem of the piezometer up to the first contact. The value of the pressure needed to make this contact was read on either a Bourdon gauge (Heise Bourdon Tube Co., Newton, Conn.) which has a 0–10,000-psi range with 10-psi divisions and was calibrated by the manufacturer to be within 10 psi of a deadweight gauge from 0 to 10,000 psi at 500-psi intervals, or one which has a 0–50,000-psi range calibrated to ±50 psi at 2500-psi intervals. The value of the pressure was noted and the pressure was decreased slightly (10–20 psi) so as to break the electrical contact between the platinum wire and the mercury column. After 10 min the pressure was again increased until the resistance changed abruptly. If the same pressure was not noted, then the pressure was decreased and another 10 min was allowed to pass. When two successive readings gave the same value of the pressure, then the pressure was gradually increased until the mercury column made an electrical contact with the next platinum wire. The volume, V^1_{PZ}, of the piezometer (bulb and stem) at any given temperature and at 1 atm is known from calibrations at 1 atm. The volume $V^1_{C,N}$, between the free end of the stem and the Nth platinum contact is also known from calibrations at 1 atm. The relative volume, V_R^P (also equal to 1 minus the compression[17]), of the liquid at a pressure, P, which was needed to bring the mercury–liquid interface to the Nth contact, is given by

$$V_R^P = (V^1_{PZ} - V^1_{C,N})(1 - k_g^P)/V^1_{PZ} \qquad (2)$$

where k_g^P is the compression of glass at the pressure P. The compressions which were used for Pyrex glass were those given in Tsiklis.[18] The relative volumes at a given temperature which were calculated with eq 2 from the data can be converted to specific volumes by multiplying them by the specific volume at 1 atm. The pressures read on the gauge when mercury is at a platinum contact were diminished by the amount of pressure which is needed to support the mercury column itself. At the eighth platinum contact, for example, this corresponds to about 0.4 atm.

(15) F. Gasche, *Ind. Eng. Chem.*, **48**, 838 (1956).

(16) L. A. Davis, R. B. Gordon, J. L. Tien, and J. R. Vaisnys, *Rev. Sci. Instrum.*, **35**, 368 (1964).

(17) The compression, k, is defined as $k = (V_0 - V)/V_0$, where V is the volume at the pressure P and V_0 is the volume at 1 atm.

(18) D. S. Tsiklis, "Handbook of Techniques in High-Pressure Research and Engineering" (translated from Russian), Plenum Press, New York, N. Y., 1968.

The experiments yield values of V_R^P as a function of pressure. The functional dependence of V_R^P on all of the experimental quantities is represented by

$$V_R^P = V_R^P(V^1_{PZ}, V^1_{C,N}, k_g^P, P, T) \quad (3)$$

Accordingly, the maximum deviation, ΔV_R^P, in V_R^P due to deviations in the experimental quantities is

$$\Delta V_R^P = \left|\frac{\partial V_R^P}{\partial V^1_{PZ}}\right| |\Delta V^1_{PZ}| + \left|\frac{\partial V_R^P}{\partial V^1_{C,N}}\right| |\Delta V^1_{C,N}| + \left|\frac{\partial V_R^P}{\partial P}\right| |\Delta k_g^P| + \left|\frac{\partial V_R^P}{\partial P}\right| |\Delta P| + \left|\frac{\partial V_R^P}{\partial T}\right| |\Delta T| \quad (4)$$

Equation 5 follows by a substitution in eq 4 of the corresponding values. These were determined from four repeated calibrations in the case of ΔV^1_{PZ} and $\Delta V^1_{C,N}$. The values for Δk_g^P, ΔP, and ΔT were estimated. The coefficients of thermal expansion and isothermal compressibility were used to estimate $\partial V_R^P/\partial T$ and $\partial V_R^P/\partial P$, respectively. The other partial derivatives were determined from eq 2. Thus, an estimate of the maximum error to be expected is

$$\Delta V_R^P \approx (1.7 \times 10^{-3})(2 \times 10^{-3}) + (8 \times 10^{-2})(1 \times 10^{-4}) + (0.9)(10^{-5}) + (40 \times 10^{-6})(0.68) + (26 \times 10^{-5})(0.01) \quad (5)$$

or 50×10^{-6} in the case of the piezometer shown in Figure 1. The greatest source of error is in the pressure determination.

Glycolamide and lactamide were purchased from Pfaltz and Bauer, Inc. (Flushing, N. Y.). Glycolamide was also purchased from the Sigma Chemical Co. (St. Louis, Mo.), as was glycylglycine. D,L-α-Alanine was purchased from Calbiochem (La Jolla, Calif.) and glycine from J. T. Baker (Phillipsburg, N. J.). All reagents were used without further purification. They were placed in a vacuum desiccator with Drierite for at least 1 day prior to use. The solutions were made with degassed singly distilled water and used immediately.

Results

The values of pressure and volume determined for water and all of the solutions at 25° are given in ref 19. Five sets of determinations were made with the piezometer volume at 12.8688 cm³. A comparison of the values from these replicate determinations establishes the precision of the pressure values (expressed as a standard error) at 0.6 atm for volumes determined at the first contact, and it increases to 1.5 atm for volumes at the eighth contact. The precision in the volume is within a few parts per million, which is expected from eq 2, and the small compressibility of glass. The pressure value in a given run appears to be determined with a precision of 0.14 atm, judging from a few cases in which the measurement was made at a given electrical contact over a period of days. It is likely that the variability in the determined P–V values from run to run is due to errors in the handling of the piezometer. Five possible operations for sources of such an error are: (1) a variability in the manner of seating in the ground-glass joint caused by varying amounts of stopcock grease; (2) an inconsistent filling of the piezometer, even though the raising of the piezometer above the mercury level is performed just prior to sealing the pressure vessel; (3) a drift in the temperature of the circulating fluid once a run has begun; (4) the inclusion of a small air bubble, especially near the loci where the platinum wires enter the bore of the glass capillary stem, on the initial filling of the piezometer; and (5) the trapping of variable amounts of liquid at the platinum wires by the mercury column. In brief, the precision is at about the same value as the predicted accuracy. P–V values were determined with the piezometer having a total volume of 8.8258, 12.8688, 14.7364, 25.7404, and 95.4551 cm³. A comparison was made between these PV values and those of Kell and Whalley.[20] The volumes in Table IV of their paper were linearly interpolated to arrive at the comparison values. The agreement between their values and those reported here is with a standard error ranging from 17 to 51 ppm in the case of individual PV runs, and with one of 42 ppm for all of the determinations.

The values for the specific volume of aqueous solutions of glycine and glycolamide at atmospheric pressure were taken from the papers of Gucker, Ford, and Moser[21] and Gucker and Ford,[22] respectively. The relative volume (the volume at a pressure P divided by the volume at 1 atm) of the solution is converted to the specific volume of the solution at P by multiplying the value of the specific volume at 1 atm by the value of the relative volume at P. The apparent molal volume at a given pressure was calculated from the expression

$$\phi_V = ((1000 + mM)v_s - 1000v_w)/m) \quad (6)$$

where ϕ_V represents the apparent molal volume of the solute, m the molality of the solution, M the molecular weight of the solute, v_s the specific volume of the solution, and v_w the specific volume of water. The values of v_w used in this calculation were taken from Table IV of Kell and Whalley by linear interpolation. The error in the values of ϕ_V ranges from ±0.04 to ±0.2

(19) Listings of the values of pressure, volume, apparent molal volume, and compressibility of water and all the solutions will appear immediately following this article in the microfilm edition of this volume of the journal. Single copies may be obtained from the Business Operations Office, Books and Journals Division, American Chemical Society, 1155 Sixteenth Street, N.W., Washington, D. C. 20036, by referring to code number JPC-72-1783. Remit check or money order for $3.00 for photocopy or $2.00 for microfiche.

(20) G. S. Kell and E. Whalley, *Phil. Trans. Roy. Soc. London*, **258**, 565 (1965).

(21) F. T. Gucker, Jr., W. L. Ford, and C. E. Moser, *J. Phys. Chem.*, **43**, 153 (1939).

(22) F. T. Gucker, Jr., and W. L. Ford, *ibid.*, **45**, 309 (1941).

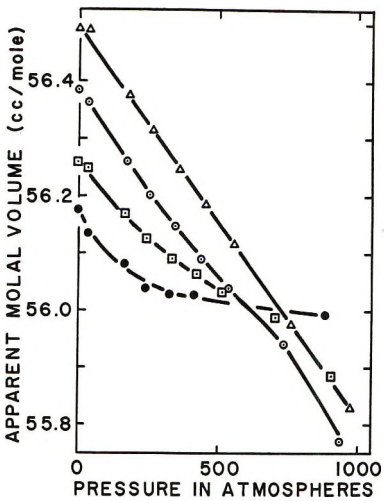

Figure 2. The apparent molal volume of glycolamide in aqueous solution. Concentrations are: (●) 0.5, (⊡) 1.0, (⊙) 2.0, and (△) 3.0 *m*. The temperature is 25°. The maximum error in the accuracy of the ϕ_V values for the 3 *m* solution is ±0.04 cm³/mol below 680 atm and ±0.12 cm³/mol above this pressure. This error with the 0.5 *m* solution was ±0.2 cm³/mol below 680 atm and ±0.6 cm³/mol above 680 atm.

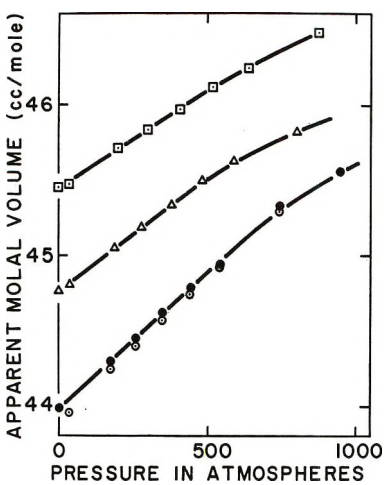

Figure 3. The apparent molal volume of glycine in aqueous solution. Concentrations are: (●, ⊙) 1.0, (△) 2.0, and (⊡) 3.0 *m*. The temperature is 25°. The maximum error in the accuracy of the ϕ_V values is ±0.1, ±0.06, and ±0.04 cm³/mol below 680 atm in the case of the 1.0, 2.0, and 3.0 *m* solutions, respectively. Above 680 atm, these errors are larger by a factor of 3.

cm³/mol. The error is largest in the case of the most dilute solutions at the highest pressures.

In Figure 2 (and Table II of ref 19) the apparent molal volume of glycolamide is seen to decrease with pressure, and in Figure 3 (and Table III of ref 19) that of glycine to increase with pressure. The difference between the apparent molal volume of glycine (1.0 *m*) and that of glycolamide (1.0 *m*) (the electrostriction)

$$\delta\phi V_{\text{isomer}} = \phi V_{\text{glycine}} - \phi V_{\text{glycolamide}} \qquad (7)$$

goes from 12.3 cm³/mol at 1 atm to 11.5 cm³/mol at 500

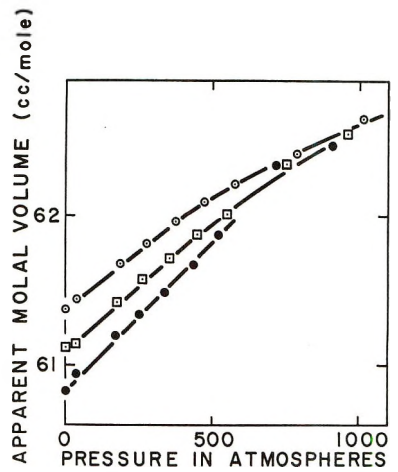

Figure 4. The apparent molal volume of D,L,-α-alanine in aqueous solution. Concentrations are: (●) 0.5, (⊡) 1.0, and (⊙) 1.5 *m*. The temperature is 25°. The maximum error in the accuracy of the ϕ_V values is ±0.2, ±0.1, and ±0.08 cm³/mol below 680 atm in the case of the 0.5, 1.0, and 1.5 *m* solutions, respectively. Above 680 atm, these errors are larger by a factor of 3.

atm and to about 10.2 cm³/mol at 1000 atm. The apparent molal volume of glycine increases with pressure, but the rate of increase with pressure (the apparent molal compressibility) is less the greater the concentration of the solution. The apparent molal compressibility of glycine is independent of pressure to about 500 atm and appears to be pressure dependent above 500 atm. Although the apparent molal volume of glycolamide decreases with pressure at a constant rate in a 3.0 *m* solution, a peculiarity is increasingly manifested as the solutions become more dilute. That is, the apparent molal volume changes with pressure until a certain value of the apparent molal volume (about 56 cm³/mole) is reached, where it ceases to change with increasing pressure over an interval of pressure which is longer with increasing dilution. This result is highly sensitive to errors in the high-pressure values of v_s and v_w. The sensitivity of the calculation with eq 6 to experimental errors has been discussed by Harned and Owen.[23] Although this electrical contact method is capable of the desired precision and accuracy, a device other than a Bourdon gauge must be used to determine the pressure. Thus, the inherent uncertainties in the pressure values determined here with Bourdon gauges preclude a firm statement on the pressure dependence of the apparent molal volume of the solutes, especially at pressures greater than 680 atm, where a 50,000-psi (3400 atm) gauge was used having an uncertainty in the accuracy of the value of a reading of ±50 psi (±3 atm). However, the similarity of the results with glycine and glycolamide to those with lactamide and D,L-alanine, discussed below, suggests that the effects observed are probably real.

(23) H. S. Harned and B. B. Owen, "The Physical Chemistry of Electrolyte Solutions," Reinhold, New York, N. Y., 1957.

Figure 4 (and Table IV of ref 19) shows the values of ϕ_V for D,L-alanine and Figure 5 (and Table V of ref 19) those for lactamide. The specific volumes at 1 atm were taken from the work of Gucker and Allen.[24] The comparison between ϕ_V values of D,L-alanine and those of lactamide results mostly in similar findings as the one between ϕ_V values of glycine and glycolamide.

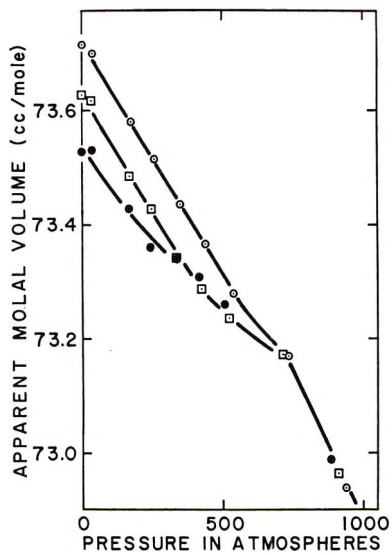

Figure 5. The apparent molal volume of lactamide in aqueous solution. The concentrations are: (●) 0.5, (⊡) 1.0, and (⊙) 1.5 m. The temperature is 25°. The maximum error in the accuracy of the ϕ_V values is ±0.2, ±0.1, and ±0.08 cm³/mol below 680 atm in the case of the 0.5, 1.0, and 1.5 m solutions, respectively. Above 680 atm, these errors are larger by a factor of 3.

Whereas the apparent molal volume of alanine (a dipolar ion) increases with pressure, that of lactamide (an uncharged isomer of alanine) decreases. The rate of increase with pressure of ϕ_V of alanine is constant to about 500 atm but pressure dependent above 500 atm. Unlike the ϕ_V of glycine and of glycylglycine (see below), the ϕ_V of alanine becomes independent of concentration at about 800 atm, with the slope of the ϕ_V *vs.* m curve becoming negative above 800 atm. The apparent molal volume of lactamide seems to be independent of concentration from 700 to 1000 atm but remains dependent on pressure. The value of $\delta\phi_{V_{isomer}}$ (eq 7) varies for 1 m solutions of D,L-alanine and lactamide from 12.5 cm³/mol at 1 atm, to 11.3 cm³/mol at 500 atm and to about 10.3 cm³/mol at 1000 atm. These differences are essentially the same as those found by comparing glycine with glycolamide.

The apparent molal volume of glycylglycine as a function of pressure is shown in Figure 6 (and Table VI of ref 19). The value of the specific volume at 1 atm was taken from Ellerton, *et al.*[25] ϕ_V for glycylglycine is seen to increase with pressure as it does for glycine and alanine, all three being dipolar ions in aqueous solution. The increment in ϕ_V between 1 and 1000 atm

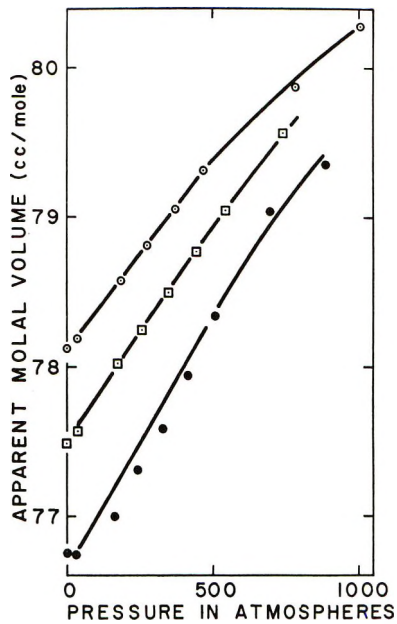

Figure 6. The apparent molal volume of glycylglycine in aqueous solution. The concentrations are: (●) 0.2, (⊡) 0.6, and (⊙) 1.0 m. The temperature is 25°. The maximum error in the accuracy of the ϕ_V values is ±0.5, ±0.2, and ±0.1 cm³/mol below 680 atm in the case of the 0.2, 0.6, and 1.0 m solutions. Above 680 atm, these errors are larger by a factor of 3.

for 1.0 m solutions of alanine, glycine, and glycylglycine is 1.4, 1.6, and 2.6 cm³/mol, respectively.

Discussion

These results are not in agreement with those of Bridgman and Dow,[7] but they are similar to those of Gucker, *et al.*,[8] who determined at 1 atm the adiabatic compressibility of aqueous solutions of glycine, glycolamide, D,L-α-alanine, β-alanine, and lactamide. They found that the apparent molal adiabatic compressibility increased with concentration. In the cases of lactamide and glycolamide it became more positive, and in the cases of the dipolar ions it became less negative. The negative value of the initial slopes in Figures 2–6 is the apparent molal isothermal compressibility, and it is seen to increase with concentration. Thus, our results are in qualitative agreement with those of Gucker, *et al.*[8] The value of the isothermal compressibility differs from that of the adiabatic one[26]

$$\beta_s = \beta_T C_V / C_P \qquad (8)$$

where β_s is the isentropic compressibility, β_T the isothermal compressibility, C_V the specific heat at constant volume, and C_P the isobaric specific heat. Of the latter two quantities, C_P is known but C_V is not. The coefficient of thermal expansion must also be

(24) F. T. Gucker, Jr., and T. W. Allen, *J. Amer. Chem. Soc.*, **64**, 191 (1942).

(25) H. D. Ellerton, G. Reinfelds, D. E. Mulcahy, and P. J. Dunlop, *J. Phys. Chem.*, **68**, 398 (1964).

(26) E. A. Guggenheim, "Thermodynamics," Wiley-Interscience, New York, N. Y., 1950.

known before a quantitative comparison can be made between the results of Gucker, *et al.*,[8] and those reported here.

It is on initial reflection unusual to think of an apparent molal volume as increasing with pressure, but this quantity is a composite one representing not only the intrinsic volume of the solute but also the change in volume arising from solute–solvent, solute–solute, and solvent–solvent interactions. The principal interactions with the dipolar amino acids are probably solvation and dipole–dipole interactions. The effect of pressure on solvation has been used by Hamann[3] to explain the increase with pressure to 10,000 atm of $\bar{V}_2$ (the partial molal volume) of NaCl in water. For example, Adams[27] found that $\bar{V}_2$ increased over the 1-atm value by 3.2 cm³/mol at 1000 atm. Hamann[3] calculated from the pressure derivative of the Born equation that the volume change associated with the solvation by water of NaCl at 1 atm is -22.2 cm³/mol and at 1000 atm is -19.6 cm³/mol. Hence, ΔV of solvation at 1000 atm is $+2.6$ cm³/mol greater than that at 1 atm and the 3.2-cm³/mol increase observed experimentally in the partial molal volume at 1000 atm appears largely accounted for by a change in the ΔV of solvation. Hamann's qualitative picture of this effect is that the structure of water is more and more broken down the greater the pressure. Hence, the transfer of water from the bulk phase (structured) to a solvated phase (equivalent to water at a great pressure) has a smaller effect at high pressures. This picture of solvated water as being like water at high pressures has been discussed, for example, by Zwicky.[28] Hamann[3] does not consider the role that ion–ion interactions might play in affecting $\bar{V}_2$. It is possible that ion association[29] could influence $\Delta_P\bar{V}_2$. If pressure caused an association of ions, there could be a diminution of the total amount of water hydrated by the pair in the region between the pair.[29] This would also contribute to an increase in the value of $\bar{V}_2$ at a high pressure over that at 1 atm. Similarly, if ion–ion association increased with concentration, then an increase with concentration in $\bar{V}_2$ would be expected, as has been suggested by others.[29]

Fuoss[30] and Kirkwood[31] have theoretically evaluated the effect on the free energy due to the interaction of dipoles with each other as well as the solvation of dipoles. Gucker, *et al.*,[8] have used these theories and find that the combined effect of solvation and of dipole–dipole interaction is insufficient to account for the difference between ϕ_V, $\bar{C}_P$, or ϕ_K (the apparent molal compressibility) of glycine and those of glycolamide. Equation 21 of Gucker, *et al.*,[32] estimates the volume change of solvation according to the Fuoss–Kirkwood approach. This equation is

$$(\Delta\bar{V}_2^0)_s = -\frac{3}{4}\frac{\mu^2 N}{b^3 D^2}(\partial D/\partial P)_T \qquad (9)$$

where $(\Delta\bar{V}_2^0)_s$ is the change at infinite dilution in the partial molal volume due to solvation, N Avogadro's number, b the radius of a sphere containing a dipole with a dipole moment μ, D the dielectric constant of the solvent, and P the pressure. At 1 atm $(\Delta\bar{V}_2^0)_s$ for glycine is calculated[32] to be about -4 cm³/mol and at 1000 atm it is here calculated to be about -3.5 cm³/mol. Thus this theory predicts a 0.5-cm³/mol increase in the value of $\bar{V}_2$ of glycine in an infinitely dilute solution at 1000 atm over that at 1 atm. Gucker, *et al.*,[32] pointed out that the 4 cm³/mol value for the electrostriction is less than the observed value of nearly 13 cm³/mol. It is difficult to arrive at an exact experimental value for $\bar{V}_2^0$ of glycine and glycolamide at 1000 atm from the data presented here. A rough estimate results in a value of 10.9 cm³/mol for the electrostriction in the case of infinitely dilute solutions at 1000 atm. Thus, an observed value of the change in electrostriction with pressure is about 2.1 cm³/mol (13 − 10.9), about four times larger than the calculated value, 0.5 cm³/mol. When PV data are available at more concentrations, the theory can be tested more fairly than was done here. Also, the insights of Whalley[33] into the theoretical approach to electrostriction have not been tried here but will be in a subsequent communication.

Considering amino acid solutions as composed of uncharged amino acid ($HN_2CH(R)COOH$) and charged amino acid ($^+NH_3CH(R)COO^-$), Edsall and Blanchard[34] and others have shown that the ratio, K_Z, of the amount of charged to uncharged amino acid is a large quantity. It is $10^{4.61}$ for glycylglycine, $10^{5.42}$ for glycine, and $10^{5.4}$ for alanine. Edsall and Blanchard showed that K_Z decreased with a decreasing dielectric constant of the solvent and with increasing temperature, which also decreases the dielectric constant of water. Since pressure increases the dielectric constant of water,[35,36] one might expect an increase in K_Z. However, this small effect of pressure on K_Z is probably not important to a consideration of the pressure effect on $\bar{V}_2$ at 25° of solutions of amino acids such as glycine, alanine, and glycylglycine, all of which have nonionizable side chains between the amino and carboxyl groups.

The apparent molal volumes of alanine, glycolamide,

(27) L. H. Adams, *J. Amer. Chem. Soc.*, **53**, 3769 (1931).
(28) H. M. Evjen and F. Zwicky, *Phys. Rev.*, **33**, 860 (1929).
(29) F. J. Millero, *Limnol. Oceanogr.*, **14**, 376 (1969).
(30) R. M. Fuoss, *J. Amer. Chem. Soc.*, **58**, 982 (1936).
(31) J. G. Kirkwood, *Chem. Rev.*, **19**, 275 (1936).
(32) F. T. Gucker, Jr., I. M. Klotz, and T. W. Allen, *ibid.*, **30**, 191 (1942).
(33) E. Whalley, *J. Chem. Phys.*, **38**, 1400 (1963).
(34) J. T. Edsall and M. H. Blanchard, *J. Amer. Chem. Soc.*, **55**, 2337 (1933).
(35) S. Kyropoulos, *Z. Phys.*, **40**, 507 (1926).
(36) B. B. Owen, R. C. Miller, C. E. Milner, and H. L. Cogan, *J. Phys. Chem.*, **65**, 2065 (1961).

and lactamide appear to lose their concentration dependence at pressures of 700–800 atm. Our data are not sufficient to definitively reveal either if this concentration independence persists at high pressures or if the apparent molal volume decreases with increasing concentration at higher pressures. It is not clear whether these phenomena are due to a mechanism common to the three solutes. The difference between alanine and glycine is that the former has a methyl group on its number two carbon where the latter has a hydrogen atom. This substitution makes alanine optically active. The alanine results could thus be due to an interaction between D and L forms, a hydrophobic interaction between methyl groups, an interaction between water and the methyl groups, or an interaction in water due to the presence of the methyl groups.

The pressure dependence of the partial specific volume ($\bar{v}_2$) of proteins is of interest to ultracentrifugal studies.[37-39] The value of $\bar{v}_2$ for a protein is difficult to determine, let alone its pressure dependence. This can be appreciated from a consideration of eq 6. Owing to the large molecular weight of a protein, m is a small number and consequently the specific volume of the solution must be determined with considerable accuracy. An ingenious high-pressure magnetic float densitometer has been constructed and used by Fahey, Kupke, and Beams[37] to determine the pressure dependence of $\bar{v}_2$ of ribonuclease and turnip yellow mosaic virus protein. There appears to be an uncertainty in their values of $\bar{v}_2$ of ± 0.0006 cm^3/g. The effects of pressure, if they exist on these proteins at pressures to 500 atm, are thus less than 0.0006 cm^3/g. From the data presented here it seems that pressure will cause an increase in the $\bar{v}_2$ of a protein due to the effect of pressure on the ΔV of hydration (electrostriction) caused by the electrostatic charges on the protein. On the other hand, it is evident that there will be a volume decrease due to the compressibility of the atoms themselves which make up the protein. An estimate can be made of this latter contribution from the data on lactamide and glycolamide. The 3.0 m glycolamide and 1.5 m lactamide solutions exhibited an apparent molal compressibility of about 0.68×10^{-3} and 0.82×10^{-3} cm^3/(mol atm), respectively. To a first approximation, these numbers can be taken to arrive at a value of the partial specific compressibility of the constituent atoms of a protein. From this, one obtains a contribution of -4.5×10^{-4} cm^3/g to the change in the partial specific volume of a protein when compressed to 500 atm. For a molecule the size of ribonuclease (mol wt = 13,686), the contribution is 6 cm^3/mol, which is indeed a small fraction of its total molal volume. The former contribution to the $\bar{V}_2$ of a protein is estimated from the pressure dependence of the values of the apparent molal volume of the amino acids. These are used for an estimate of the effect of pressure on the water which is solvated by the charged groups of a protein. A protein with 100 positively charged groups and 100 negatively charged groups is considered to a first approximation to be coated with 100 dipoles, as in Edsall's[40] work. Since these dipoles are situated on a surface, water molecules can only approach them from one side. Thus, a dipole like glycine on a surface might be expected to solvate water with an electrostriction one-half as great (~6 cm^3/mol) as that of free glycine (~12 cm^3/mol). The protein according to this model could cause an electrostriction of 600 cm^3/mol. It can be estimated from the glycine data that at 500 atm the electrostriction is diminished by 0.8 cm^3/mol of dipole or by 0.4 cm^3/mol of a surface-bound dipole. Thus, the $\bar{v}_2$ of the above protein would be increased by 100×0.4 cm^3/mol or 40 cm^3/mol of protein. If the protein had a molecular weight of 100,000, this amounts to a change of $+4 \times 10^{-4}$ cm^3/g in the partial specific volume. This quantity is almost exactly canceled by the volume decrease in the protein produced by the compressibility of its atoms. In the case of a smaller molecule such as ribonuclease, the pressure effect on electrostriction might not cancel out the compressibility effect on the protein. Indeed, the approximate calculations with the hypothetical protein with a 100,000 molecular weight might be very incorrect. This follows from the finding that the effect of pressure on the electrostriction is dependent on the dipole moment. Thus, the exact charge distribution on a protein might have to be known in order to assess the effect of pressure on the electrostriction. At any rate, these predicted changes in the partial specific volume of a protein are small and in agreement with the observations of Fahey, *et al.*[37] Even though small, these changes are important. Josephs and Harrington calculate that a small difference of 6×10^{-4} between the partial specific volume of monomer myosin and that of polymerized myosin is sufficient to account for the striking pressure effects which they observe on the polymerization equilibrium of myosin. Parenthetically, it should be noted that Brandts, *et al.*,[41] have an excellent discussion of the various contributions, and their pressure dependence, to the partial specific volume of a protein.

The values of apparent molal volumes and their pressure dependence can be used to evaluate what will happen to reactions at high pressures. Borsook[42] has considered the energetics of peptide bond formation. He gives the free energy of formation for the reaction

(37) P. F. Fahey, D. W. Kupke, and J. W. Beams, *Proc. Nat. Acad. Sci. U. S.*, **63**, 658 (1969).

(38) R. Josephs and W. F. Harrington, *ibid.*, **58**, 1587 (1967).

(39) G. R. Anderson, *Ark. Kem.*, **20**, 513 (1963).

(40) J. T. Edsall in "The Proteins," Vol. I, Part B, H. Neurath and K. Bailey, Ed., Academic Press, New York, N. Y., 1953, Chapter 7.

(41) J. F. Brandts, R. J. Oliveira, and C. Westort, *Biochemistry*, **9**, 1038 (1970).

(42) H. Borsook, *Advan. Protein Chem.*, **8**, 127 (1953).

$$2(\text{glycine}) \rightleftarrows \text{glycylglycine} + H_2O \qquad (10)$$

a value of −3590 cal at 37.5° (the equilibrium constant, K, is 2.99×10^{-3}). From eq 6, it follows that

$$\bar{V}_2 = \phi_V + \left(\frac{\partial \phi_V}{\partial m}\right)_{T,P} \qquad (11)$$

Using this expression, it is estimated that $\bar{V}_2$ for glycine in a 1 m solution is 44.9 at 500 atm and 25°. Similarly, $\bar{V}_2$ for glycylglycine in a 1 m solution is 79.7 cm³/mol at 500 atm and 25°. The volume change for eq 10 is thus smaller (+7.5 cm³/mol) at 500 atm than the 1-atm value (+8 cm³/mol). Although pressure is thus seen to inhibit glycylglycine synthesis, it does so to a lesser degree at 500 atm than at 1 atm.

Equation 1 has recently been found[13] to be an excellent equation of state for water and NaCl solutions. It fits the data of Adams[27] to 10,000 bars more closely than the Tait equation as used by Gibson.[43] More importantly, eq 1 is what might be expected as an equation of state for liquids in which the forces between molecules follow a Mie potential. The Tait equation has been given a theoretical basis.[44] Nevertheless, eq 1 is based on a simple physical model which has been thoroughly explored.[45,46] In short, the two principal advantages of eq 1 are: (1) its clear relationship to a physical model of a liquid and (2) its ease of use. This second advantage arises from the fact that a plot of PV^4 *vs.* V (or PV^3 as $1/V$) should result in a straight line. This equation reproduces the volume data in Table IV of the paper of Kell and Whalley with a standard error ($\times 10^6$) of 58, 85, 84, 81, 47, 67, 55, 48, 36, 27, and 17 at 0, 10, 20, 25, 30.1, 40, 50, 60, 70, 80, 90, and 100°, respectively. *A priori*, one would not expect a simple equation of state for a liquid like water because, for example: its atoms are compressible; the ionization constant of water changes with pressure[47] and the ionization occurs with a volume change;[48] hydrogen bonding is affected by pressure, the formation of a hydrogen bond occurring with a volume decrease;[3] and water has a structure which could undergo a pressure-dependent rearrangement with a concomitant volume change. Accordingly, it perhaps should be an expected fact that the isotherms of Kell and Whalley at the higher temperatures are fit exceptionally well to eq 1, for at these higher temperatures, events such as hydrogen bonding and structuring of water would be expected to a lesser degree than at lower temperatures.

Figure 7 shows some data on glycylglycine solutions plotted according to eq 1. The standard errors with which eq 1 fits all of the data reported here range from 17 to 132 ppm.[19] This equation was used to find the compressibility of the solutions and water as a function of pressure. Although the volumes of the solutions and of water were reproduced fairly well with this equation, the calculated values of compressibilities[19] of water at 1 atm were not in agreement with those found

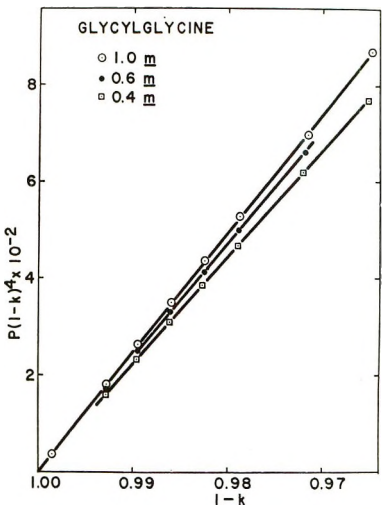

Figure 7. The PV isotherms of glycylglycine solutions plotted according to eq 1. The quantity $1 - k$ is equal to the volume of the solutions at a pressure, P, divided by the volume at zero pressure.

by several workers,[49] being higher than literature values by about $0.3–0.7 \times 10^{-6}$ atm^{-1}. It is hoped that modifications of eq 1, based on an improved model of the liquid, will lead to a better equation of state. Hamann has indicated that the value of the tensile strength of a liquid is derivable from an equation such as (1). $(\partial P/\partial V)_T$ will vanish at a value of the volume of $^4/_3V_0$, where V_0 is the volume of the liquid at zero pressure. That is, the maximum negative pressure (a metastable state) attainable in the liquid is $-27A/256V_0$.[4] The values of the tensile strength of a 1.0 m solution were −2487 (glycine), −2374 (glycolamide), −2522 (alanine), −2401 (lactamide), and −2619 atm (glycylglycine). These values are all higher than the −2270 atm for water and suggest that the calculated value for a solution is related to the nature of the solute. The reality of values calculated in this way is presently difficult to evaluate in the case of solutions, but not so in the case of liquids.[3,13] The aspects of tensile strength in liquids have recently been well reviewed.[50] Experimental values are, in general, one to two orders of magnitude less than those predicted theoretically. Further theoretical and experimental studies are needed to explain the disparity.

Acknowledgments. The author is indebted to Drs.

(43) R. E. Gibson, *J. Amer. Chem. Soc.*, **56**, 4 (1934).

(44) R. Ginnel, *J. Chem. Phys.*, **34**, 1249 (1961).

(45) J. E. Lennard-Jones and A. F. Devonshire, *Proc. Roy. Soc., Ser. A*, **163**, 53 (1937).

(46) J. E. Lennard-Jones and A. F. Devonshire, *ibid.*, **163**, 1 (1938).

(47) S. D. Hamann, *J. Phys. Chem.*, **67**, 2233 (1963).

(48) A. Bodanszky and W. Kauzmann, *J. Phys. Chem.*, **66**, 177 (1962).

(49) F. J. Millero, R. W. Curry, and W. Drost-Hansen, *J. Chem. Eng. Data*, **14**, 422 (1969).

(50) R. T. Knapp, J. W. Daily, and F. G. Hammitt, "Cavitation," McGraw-Hill, New York, N. Y., 1970.

P. F. Scholander, H. T. Hammel, and F. H. Fisher for stimulating discussions. This work was supported by National Science Foundation Grant No. GB-18749 and Public Health Service Research Career Development Award No. GM-47352 from the National Institute of General Medical Sciences.

COMMUNICATIONS TO THE EDITOR

Reversible Line Broadening in the Electron Spin Resonance Spectra of *tert*-Butyl Radicals in γ-Irradiated Crystalline *tert*-Butyl Isothiocyanate[1]

Publication costs assisted by the U. S. Atomic Energy Commission

Sir: We wish to report an unusual example of reversible esr line broadening which is understandable in terms of static and dynamic states of *tert*-butyl radical–thiocyanate anion pairs in γ-irradiated crystalline *tert*-butyl isothiocyanate. In addition, the esr results distinguish clearly between these two states of the radical–anion pair and the radical anion.

As shown in the upper spectrum of Figure 1, the esr spectrum of γ-irradiated *tert*-butyl isothiocyanate in the dark at 77°K consists of an even multiplet superimposed on a conspicuous central feature which henceforth will be referred to as a singlet. In the lower spectrum recorded while the sample was exposed to red light ($\lambda > 640$ nm), the singlet is virtually unchanged whereas the multiplet spectrum is much sharper and eight lines can be identified as the inner components of the 10-line spectrum of the *tert*-butyl radical produced during γ irradiation. After the light was turned off, the sharp spectrum of the *tert*-butyl radicals reverted to the original broad spectrum. There was no significant decrease in signal intensity, even after several cycles, showing that this effect of line sharpening is completely reversible.

On illuminating the γ-irradiated sample with unfiltered tungsten light, both the singlet esr spectrum and the color center responsible for the light brown appearance of the sample were bleached irreversibly. This change was accompanied by a large increase in the integrated intensity of the *tert*-butyl radical spectrum, as illustrated by a comparison of the lower spectrum in Figure 1 with the upper spectrum in Figure 2 recorded at a slightly lower gain. This photobleaching process is similar to that observed in γ-irradiated acetonitrile where the reaction involves the dissociation of either a monomer or dimer radical anion depending upon the crystalline phase.[2] Accordingly, the photobleachable esr singlet spectrum is assigned to the radical anion of *tert*-butyl isothiocyanate. After turning off the light, the lines of the *tert*-butyl radical spectrum broadened to yield the lower spectrum in Figure 2. Subsequent illumination of the sample with red light induced the reversible line-sharpening effect as observed for the *tert*-butyl radical spectrum before photobleaching. The relative increase in signal height was similar before and after photobleaching despite the greater intensity of the *tert*-butyl spectrum in the latter case. Therefore the phenomenon applies to the *tert*-butyl radicals produced by photodissociation of the radical anion as well as to the *tert*-butyl radicals formed during γ irradiation. This photodynamic effect was observed with samples which had been stored at 77°K for up to 40 days after γ irradiation and photobleaching.

Experiments with various combinations of color filters demonstrated that light in the near-infrared region ($\lambda > 1250$ nm) was required to bring about the effect. This suggested the possibility that absorption of near-infrared radiation might lead to bulk heating of the matrix. However, this is unlikely to be the case since it was found that the sharp spectrum obtained at 77°K by illumination could only be simulated thermally in the dark by warming the sample to 124°K, at which temperature there was no photoinduced line sharpening. The effect of temperature on the line width was also found to be reversible. At temperatures intermediate between 77 and 124°K, illumination resulted in a sharpening of the spectrum although, as expected, the magnitude of this effect diminished as the temperature was raised. Also from previous experience,[3] it seems most improbable that near-ir irradiation could raise the temperature in the bulk of the sample to about 50° above that of the surrounding

(1) This research was supported by the U. S. Atomic Energy Commission under Contract No. AT-(40-1)-2968, and this is AEC Document No. ORO-2968-73.

(2) (a) M. A. Bonin, K. Tsuji, and F. Williams, *Nature (London)*, **218**, 946 (1968); (b) K. Takeda and F. Williams, *Mol. Phys.*, **17**, 677 (1969); (c) K. Takeda and F. Williams, *J. Phys. Chem.*, **74**, 4007 (1970); (d) E. D. Sprague, K. Takeda, and F. Williams, *Chem. Phys. Lett.*, **10**, 299 (1971).

(3) E. D. Sprague and F. Williams, *J. Amer. Chem. Soc.*, **93**, 787 (1971).

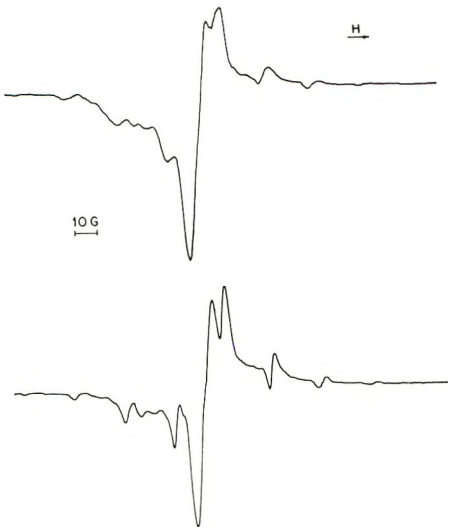

Figure 1. Esr first-derivative spectra of γ-irradiated crystalline *tert*-butyl isothiocyanate recorded under identical spectrometer conditions at 77°K before (upper spectrum) and during (lower spectrum) exposure of the sample to red light (Corning Filter No. 2030). The γ-irradiation dose was 0.65 Mrad.

Figure 2. Esr first-derivative spectra of γ-irradiated crystalline *tert*-butyl isothiocyanate recorded under identical spectrometer conditions at 77°K during (upper spectrum) and after (lower spectrum) exposure of the sample to unfiltered tungsten light. These spectra may be compared with those in Figure 1 since they refer to the same sample and the same spectrometer conditions except for a gain setting of 200 in this case instead of 250.

liquid nitrogen. Therefore it is much more likely that selective excitation is responsible for the observed photodynamic effect.

In typical experiments, the line width of the central components narrowed from 5 to 2 G and the signal height increased by more than a factor of 3 on illumination of the sample. As can be seen from Figure 2, there appear to be small line-width variations in the sharp spectrum which could be due to the small anisotropy of the proton hyperfine tensor. On the other hand, it is evident that the line broadening in the lower spectrum of Figure 2 is not markedly dependent on the nuclear quantum number, and the line shape is symmetric.

In contrast to the results reported here, a relatively sharp "isotropic" spectrum is generally observed for the *tert*-butyl radical in polycrystalline and glassy solids.[4] This is expected even for *tert*-butyl radicals which do not undergo a tumbling motion since the g anisotropy of alkyl radicals is small and the typical anisotropy of the β-proton hyperfine tensor measured in oriented radicals is only about 2.5 G for rotating methyl groups.[5] The possibility that the broadening originates from a hindered rotation of the methyl groups can be dismissed because this would destroy the equivalence of the isotropic hyperfine coupling to the nine β protons and thereby result in a much more complicated spectrum.

It is proposed that the line broadening is due to the interaction of the *tert*-butyl radical with the thiocyanate anion. These species represent the products from the irreversible photodissociation of the radical anion. Since the broadening is also observed for the *tert*-butyl radicals produced during γ irradiation, it is assumed that these radicals are formed directly by dissociative electron capture. The radiation- and photochemical processes can be represented as

$$(CH_3)_3C\text{–}NCS + e^- \rightarrow (CH_3)_3C\text{–}NCS\cdot^- \quad (1a)$$

$$(CH_3)_3C\text{–}NCS + e^- \rightarrow [(CH_3)_3C\cdots NCS^-] \quad (1b)$$

$$(CH_3)_3C\text{–}NCS\cdot^- \xrightarrow{h\nu} [(CH_3)_3C\cdots NCS^-] \quad (2)$$

Reaction 1b is analogous to the formation of methyl radical–halide ion pairs, for which definitive esr evidence has been obtained in the case of methyl bromide from the observation of bromine hfs.[6a] The resemblance between the halide and isothiocyanate system is further emphasized by the fact that the esr spectrum of the methyl radical–chloride ion pair is the familiar quartet spectrum of the methyl radical broadened by hyperfine coupling with the chloride ion.[6b]

The features of the magnetic resonance interaction responsible for line broadening in the present case are not directly evident. However, it is reasonable to assume that the reversible photodynamic and thermal behavior can both be attributed to motional effects involving the radical–anion pair. One way in which this motional narrowing could be brought about is through an averaging of the magnetic anisotropy which contributes to the line width in the polycrystalline sample. If this is so, then the anisotropy must reside in the g factor and/or in the hyperfine coupling to

(4) (a) B. Smaller and M. S. Matheson, *J. Chem. Phys.*, **28**, 1169 (1958); (b) P. B. Ayscough and C. Thomson, *Trans. Faraday Soc.*, **58**, 1477 (1962).

(5) P. B. Ayscough "Electron Spin Resonance in Chemistry," Methuen, London, 1967, p 228.

(6) (a) E. D. Sprague and F. Williams, *J. Chem. Phys.*, **54**, 5425 (1971); (b) E. D. Sprague and F. Williams, unpublished work.

^{14}N in the thiocyanate ion. However, the proton hfs of 22.4 G in both broad and sharp spectra is close to the isotropic splitting of 22.7 G for the free *tert*-butyl radical,[7] and this implies a very small transfer of spin density to the thiocyanate anion which is quite inadequate to give rise to anisotropic ^{14}N hyperfine broadening. On the other hand, *g*-factor anisotropy is admissible in this system owing to the large spin–orbit coupling constant of the sulfur atom as well as the possible nonlinearity of NCS^-.[8] The excitation of a rotational motion of the NCS^- could then give rise to an axially symmetric *g*-tensor with a reduction in the overall *g* anisotropy of the radical–anion pair. This explanation of line broadening in terms of *g* anisotropy attributable to the sulfur atom is consistent with our observation[9] of a sharp spectrum from the *tert*-butyl radical in γ-irradiated crystalline *tert*-butyl isocyanate ($(CH_3)_3C-NCO$) at 77°K and the fact that there was no significant change in the line widths (2.5 G for the central components) of this latter spectrum either on warming or illuminating the sample.

(7) R. W. Fessenden and R. H. Schuler, *J. Chem. Phys.*, **39**, 2147 (1963).

(8) (a) J. R. Saraf, *Sci. Light (Tokyo)*, **5**, 23 (1956); (b) F. A. Cotton and G. Wilkinson, "Advanced Inorganic Chemistry," 2nd ed, Wiley-Interscience, New York, N. Y., 1966, p 314.

(9) Y. J. Chung and F. Williams, unpublished work.

DEPARTMENT OF CHEMISTRY
THE UNIVERSITY OF TENNESSEE
KNOXVILLE, TENNESSEE 37916

YOON JIN CHUNG
FFRANCON WILLIAMS*

RECEIVED JANUARY 21, 1972

Need to know about...

The most advanced theory?

Then read such articles as: "Relation between Structure and Retention Time of Sterols in Gas Chromatography" and "Ion Association between Indicators and Indifferent Electrolytes".

The latest applications?

Then read such articles as: "Gas Chromatography of Volatiles from Breath and Urine" and "Identification of Dangerous Drugs by Isobutane Chemical Ionization Mass Spectrometry".

Newest chemicals and reagents?

Then read such articles as: "Clinical Test Kits for Enzymes, Phosphorus and Calcium Determinations, Narcotics Detection, Mercury and Lead Determinations" and "Ultrapure Chemicals: Enzymes, Refractory Metals, Organics, Other Metals".

All are found in ANALYTICAL CHEMISTRY.

Each month you receive information that is fresh, current and relevant to your needs. Brand new ideas are introduced. One of them might be the answer to one of your problems.

Two other good reasons for starting your ANALYTICAL CHEMISTRY subscription now are the 1971-72 LABORATORY GUIDE to Instruments, Equipment and Chemicals and the valuable ANNUAL REVIEWS issue.

The 500-page LABORATORY GUIDE gives you 20,000 separate entries with more than 1000 manufacturers selling over 600 products.

The special ANNUAL REVIEWS issue presents authoritative researchers reviewing the latest methodology and applications of analytical chemistry.

ANALYTICAL CHEMISTRY

American Chemical Society / 1155 Sixteenth Street, N.W., Washington, D.C. 20036

Please send me ANALYTICAL CHEMISTRY at the following subscription rate:

ACS members:	☐ U.S. $5.00	☐ Canada $ 9.00	☐ PUAS $ 9.00	☐ Other Nations $10.00
Nonmembers:	☐ U.S. $7.00	☐ Canada $11.00	☐ PUAS $19.00	☐ Other Nations $20.00

Note: Subscriptions at ACS Member Rates are for personal use only.

NAME _____ POSITION _____

ADDRESS _____

CITY _____ STATE/COUNTRY _____ ZIP _____

YOUR COMPANY _____ NATURE OF COMPANY'S BUSINESS _____

☐ **I am an ACS member** ☐ **I am not an ACS member** ☐ **Bill me for $**_____

☐ Payment enclosed in the amount of $_____ (payable to American Chemical Society)

AC72

what's happening on the frontiers of chemical research?

in short, critical articles that cover all areas *of chemical research.*

Whether you are a practicing chemist, professor or student, you want to keep up with the latest developments. Yet few of you have the time to read thoroughly all the journals of primary publications.

ACCOUNTS fills the gap.

Written by investigators active in the fields reviewed, ACCOUNTS' concise, brief articles place recent developments in perspective—and relate them to earlier work and their probable future significance.

Once you start relying on ACCOUNTS to keep you informed, you'll wonder how you got along without its monthly arrival.

Complete and mail back the form below. We'll prove how valuable this publication can be to you.

American Chemical Society / 1155 Sixteenth Street, N.W., Washington, D.C. 20036

Please send me ACCOUNTS OF CHEMICAL RESEARCH at the following subscription rates:

ACS members:	☐ U.S. $ 5.00	☐ Canada, PUAS $ 9.00	☐ Other Nations $10.00
Nonmembers:	☐ U.S. $15.00	☐ Canada, PUAS $19.00	☐ Other Nations $20.00

Name _____ Title _____

Employer _____

Address: ☐ Home ☐ Business _____

City _____ State/Country _____ Zip _____

Nature of employer's business? ☐ Manufacturing or processing ☐ Academic ☐ Government ☐ Other _____ (Please indicate)

Note: Subscriptions at ACS Member Rates are for personal use only.

☐ I am an ACS member ☐ I am not an ACS member

Payment must be made in U.S. currency, by international money order, UNESCO coupons, U.S. bank draft; or order through your book dealer.

323